Pacific Northwest
NATIONAL LABORATORY

PNNL-37506, Rev. 0
EWG-RPT-051, Rev. 0

# Direct Feed High-Level Waste APPS Model Glass Testing (DFHLW APPS) Matrix, Phase 2

March 2025

RL Russell, V Gervasio, X Lu, S Chong, JT Reiser, NL Canfield, JL George, NA Lumetta, J Neeway, LM Seymour, T Jin, MA Hall, ET Niehaus-Marcial, JD Vienna

U.S. DEPARTMENT of ENERGY

Prepared for the U.S. Department of Energy
under Contract DE-AC05-76RL01830

## DISCLAIMER



PACIFIC NORTHWEST NATIONAL LABORATORY
*operated by*
BATTELLE
*for the*
UNITED STATES DEPARTMENT OF ENERGY
*under Contract DE-AC05-76RL01830*

**Printed in the United States of America**

**Available to DOE and DOE contractors from**
**the Office of Scientific and Technical Information,**
**P.O. Box 62, Oak Ridge, TN 37831-0062**
**www.osti.gov**
**ph: (865) 576-8401**
**fox: (865) 576-5728**
**email: reports@osti.gov**

**Available to the public from the National Technical Information Service**
**5301 Shawnee Rd., Alexandria, VA 22312**
**ph: (800) 553-NTIS (6847)**
**or (703) 605-6000**
**email: info@ntis.gov**
**Online ordering: http://www.ntis.gov**

PNNL-37506, Rev. 0
EWG-RPT-051, Rev. 0

# Direct Feed High-Level Waste APPS Model Glass Testing (DFHLW APPS) Matrix, Phase 2

March 2025

RL Russell, V Gervasio, X Lu, S Chong, JT Reiser, NL Canfield, JL George, NA Lumetta, J Neeway, LM Seymour, T Jin, MA Hall, ET Niehaus-Marcial, JD Vienna

Prepared for
the U.S. Department of Energy
under Contract DE-AC05-76RL01830

Pacific Northwest National Laboratory
Richland, Washington 99354

# Summary

This report summarizes the data collected during the batching and melting of a second matrix of Direct Feed High-Level Waste (DFHLW) glasses generated using the preliminary enhanced waste glass models (EWG2.5) and the Britton and Anderson (2024)[1] preliminary DFHLW feed vector. The purpose of these glasses is two-fold:

1. Validate EWG2.5 glass calculations being used in the Aspen Process Performance Simulation (APPS) model.
2. Evaluate and ultimately improve the glass property models and formulation methods used for design of DFHLW glasses as part of an iterative process of data collection and model refinement.

Some of the 16 APPS2 glasses tested did not satisfy all target property constraints due to the limited data on DFHLW glass supporting the EWG2.5 models.

- One glass, APPS2-10, formed nepheline on canister centerline cooling (CCC) heat-treatment and failed the product consistency test (PCT) response limits. This glass also had high B and Cr release rates for the toxicity characteristic leaching procedure (TCLP). All other glasses were found to satisfy the PCT and TCLP constraints for both quenched and CCC samples.
- One glass, APPS2-08, had higher than acceptable viscosity due to magnetite crystallization.
- One glass, APPS2-09, formed greater than 2 vol% crystals at 950 °C. As the glass design criterion was that the temperature at 2 vol% crystal ($T_{2\%}$) be less than 950 °C, only one glass failed the criteria. However, this criterion is being reevaluated. Four additional glasses formed crystal fractions between 1 and 2 vol% at 950 °C (APPS2-03, -08, -12, and -14).
- Four glasses – APPS2-01, -02, -04, and -16 – failed the Monofrax K-3 refractory neck corrosion ($k_{neck}$) design limit of 0.04 in. at 1208 °C for 6 d. This is another criterion being reevaluated. Four additional glasses (APPS2-05, -06, -11, and -13) exhibited $0.025 \leq k_{neck} \leq 0.04$ in.
- All 16 glasses passed the sulfur solubility and TCLP constraints.

The measured property values were compared to predicted values using EWG2.5 and a selection of other existing models. A few models (e.g., electrical conductivity, TCLP) were found to be adequate for designing DFHLW glasses in the near future, while others require refits or offsets. It is recommended that new property models be developed for EWG3.0, as a large amount of DFHLW glass property data (> 14 × existing data) is expected to be collected in the compositional spaces where no data was previously available. To enable near-term calculations and formulations for designing DFHLW glasses and processing rate estimations, a formulation algorithm with minor modifications will be developed, EWG2.6.

[1] Britton MD and Anderson CK. 2024. *Direct-Feed High-Level Waste Feed Vectors Assessment*. RPP-RPT-64878 Rev. 0. Washington River Protection Solutions, Richland, WA.

# Acknowledgments

The authors gratefully acknowledge the financial support provided by the U.S. Department of Energy Hanford Field Office Waste Treatment and Immobilization Plant Project, with technical oversight by Albert Kruger. The following Pacific Northwest National Laboratory (PNNL) staff members are acknowledged for their contributions: Luke Campbell for data analysis, Aaron Sachs and David MacPherson for quality assurance, Chrissy Charron, and Cassie Martin for programmatic support during the conduct of this work, Will Eaton for project management, and Matt Wilburn for his editorial support.

Bechtel National, Inc. staff supported glass selection, including Bob Hanson, Danny Bauer, Steven Barnes, and John Julyk.

All of the other PNNL staff helping in the laboratory to complete this work are greatly appreciated and acknowledged: P Metheny, M Torres, DA Cutforth, JM Westman, JM Oshiro, JV Crum, J Kroll, S Choi, J Marcial, P Huynh, A Zwoster, ML Blazon, J Bai, and D Wang.

# Acronyms, Abbreviations, and Symbols

| | |
|---|---|
| 3TS | three-time saturation melt method |
| APPS | Aspen Process Performance Simulation (WTP steady-state flowsheet model) |
| ASTM | American Society for Testing Materials |
| BOF | balance of facilities |
| CCC | canister centerline cooling |
| CF | crystal fraction |
| DFHLW | Direct Feed High-Level Waste |
| DOE | U.S. Department of Energy |
| DWPF | Defense Waste Processing Facility |
| EA | Environmental Assessment (glass) |
| EC | electrical conductivity |
| EPMA | electron probe microanalysis |
| EWG | enhanced waste glass |
| EWG2 | second iteration of enhanced waste glass |
| GFC | glass-forming chemical |
| HLW | high-level waste |
| HTWOS | Hanford Tank Waste Operations Simulator |
| ICP-OES | inductively coupled plasma-optical emission spectroscopy |
| LAB | WTP Laboratory |
| LAW | low-activity waste |
| micro-CT | micro-computed tomography |
| MV | model validity |
| NC | normalized concentration by 7-day PCT |
| NL | normalized loss by 7-day PCT |
| NQAP | Nuclear Quality Assurance Program |
| PCT | product consistency test |
| PNNL | Pacific Northwest National Laboratory |
| PT | Pretreatment |
| Pt/Rh | platinum/rhodium |
| PTHLW | pretreated high-level waste |
| Q | quenched |
| $r_a$ | product consistency test normalized element release |
| RCRA | Resource Conservation and Recovery Act |
| RPD | relative percentage difference |
| SSM | sulfur-saturated melt |
| $T_{2\%}$ | temperature at 2 vol% spinel |

| | |
|---|---|
| TCLP | toxicity characteristic leaching procedure |
| $T_L$ | liquidus temperature |
| $T_L$-Zr | liquidus temperature for zirconium-containing phases |
| $T_M$ | melting temperature |
| UTS | Universal Treatment Standards |
| VFT | Vogel-Fulcher-Tammann |
| WC | tungsten carbide |
| $w_{SO3}$ | sulfur solubility |
| wt% | weight percent |
| WTP | Waste Treatment and Immobilization Plant |
| XRD | X-ray diffraction |
| ε | electrical conductivity |
| $\eta_{1150}$ | viscosity at 1150 °C |
| $\eta_T$ | viscosity at temperature T |
| ρ | density |
| σ | standard deviation |

# Contents

# Figures

# Tables

# 1.0 Introduction

The U.S. Department of Energy (DOE) Hanford Field Office is responsible for the safe storage, treatment, and immobilization of wastes stored in underground tanks at the Hanford Site. The Waste Treatment and Immobilization Plant (WTP) is the cornerstone of the tank waste treatment and immobilization strategy at Hanford. This plant includes, as primary components, the Low-Activity Waste (LAW) Facility, the High-Level Waste (HLW) Facility, the Pretreatment (PT) Facility, the Laboratory (LAB), and the balance of facilities (BOF). The current strategy is to stage the startup of the facilities with LAW starting first followed by HLW (DOE 2013; Bernards et al. 2020). The commissioning of the LAW Facility along with the needed components of the LAB and the BOF is underway.

An analysis of alternatives for startup and operations of the PT and HLW facilities was conducted to identify the most likely alternatives along with the upper-level implication of each (Parsons 2023). A total of 18 options were considered, including concurrent startup of the HLW and PT facilities and HLW Facility operations without the PT Facility. One of these options, alternative 18 (AoA-18), includes a Waste Transfer Vault that couples the HLW Facility with tank farms using a waste feed transfer vessel and an effluent collection vessel. The HLW Facility is planned to operate for a ~12-year period under a Direct Feed High-Level Waste (DFHLW) flowsheet while the HLW Pretreatment and Effluent Management Facilities are brought on-line. The general operating strategy laid out in AoA-18 serves as the reference case for DFHLW flowsheet development.

Effectively immobilizing HLW directly from the tank farm requires the use of enhanced waste glasses (EWG) (Vienna et al. 2022). Models and formulation approaches for EWG of pretreated high-level waste (PTHLW) were developed in 2016 (EWG1, Vienna et al. 2016). These models were sufficient to estimate the amount of glass expected from PTHLW. However, they were not sufficiently developed to identify specific glass compositions or to be used in plant operations. No glasses aimed at supporting DFHLW were included in model development or validation. The EWG1 models were used in evaluations of the DFHLW flowsheet until 2024 (Vienna et al. 2016, 2022, 2023; Lu et al. 2023). However, it was recognized that additional testing and modeling would be necessary to cover the glass composition space intended for DFHLW.

An iterative process was planned to expand the EWG property data and models to be applicable to DFHLW. The plan includes (1) identification of data gaps, (2) design of test matrices, (3) testing of matrix glasses to fill gaps, (4) development of models, (5) study of example DFHLW glasses formulated using models, and (6) improvements in modeling/formulation approaches. These steps would be iterated. Figure 1.1 represents that plan graphically.

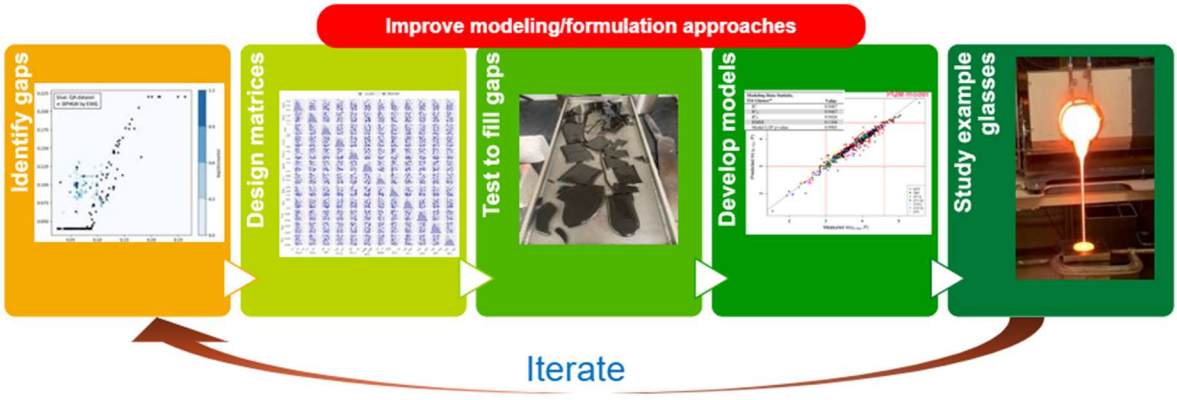


Figure 1.1. Iterative process to expand glass property models to cover DFHLW glass composition space.

The first iteration included gap analyses (Lu et al. 2023), design of a matrix of glasses to cover the high-alumina composition gap, testing of the high-alumina matrix glasses (Russell et al. 2025), study of an initial set of DFHLW glasses (Gervasio et al. 2024), and development of an initial model set aimed at DFHLW glasses. In 2024, an initial set of glass compositions was developed using EWG1 models and formulation methods (Gervasio et al. 2024). The resulting set of 15 glasses were compared to predicted values and used to develop the first iteration of EWG models specific to DFHLW glasses (EWG2.5, Vienna et al. 2024).

This report describes the results of the second set of DFHLW glass formulations that were developed with two purposes: (1) as a second iteration to expand the data and models for application of EWG to DFHLW and (2) to verify the results of EWG2.5 glass formulation methods used in the WTP Aspen Process Performance Simulation (APPS) tool used to perform the flowsheet calculations.

## 1.1 Quality Assurance

This work was performed in accordance with the Pacific Northwest National Laboratory (PNNL) Nuclear Quality Assurance Program (NQAP). The NQAP complies with DOE Order 414.1D, *Quality Assurance*, and 10 CFR 830, *Nuclear Safety Management*, Subpart A, *Quality Assurance Requirements*. The NQAP uses NQA-1-2012, *Quality Assurance Requirements for Nuclear Facility Application*, as its consensus standard and NQA-1-2012, Subpart 4.2.1, as the basis for its graded approach to quality.

The NQAP works in conjunction with PNNL's laboratory-level Quality Management Program, which is based on the requirements as defined in DOE Order 414.1D and 10 CFR 830 Subpart A.

The work described in this report was performed to a technology readiness level of 6. At this level, data is deemed appropriate to support design of a nuclear facility.

# 2.0 Test Methods

This section describes how the test matrix of 16 glasses was generated and data was obtained. The descriptions include the methods for (1) glass matrix generation, (2) glass fabrication and chemical composition analysis, (3) secondary phase identification from canister centerline cooling (CCC) treatment, (4) isothermal crystal fraction (CF) and liquidus temperature ($T_L$), (5) sulfur solubility measurement, (6) density (ρ) determination, (7) viscosity (η) measurement, (8) electrical conductivity (EC) measurement, (9) product consistency test (PCT) measurement, (10) toxicity characteristic leaching procedure (TCLP) measurement, and (11) K3 corrosion.

## 2.1 Matrix Design

This section describes how the glasses were formulated for representative DFHLW waste feed composition estimates using the current state-of-the-art glass property-composition models and constraint sets for DFHLW.

### 2.1.1 Waste Composition Estimates

Waste feed vectors from the southeast quadrant of Hanford tanks were provided by Washington River Protection Solutions (Britton and Anderson 2024), representing a range of DFHLW feed compositions. Glasses were formulated using the EWG2.5 method (Vienna et al. 2024). Glass compositions were optimized to have a maximum waste loading by varying the amount of glass-forming chemicals (GFCs), while satisfying a group of constraints. Property and compositional constraints are reported in Vienna et al. (2024). Formulation results are reported in Lu et al. (2024c).

### 2.1.2 Glass Composition Selection

Cluster analysis was performed to identify a modest number of representative glass compositions from a potential 126 DFHLW campaigns. These glass compositions were used to perform testing. Only 126 of the 214 DFHLW campaigns supplied by Britton and Anderson (2024) and formulated by Lu et al. (2024c) were used because their waste compositions satisfied the DFHLW waste acceptance criteria and process control limits (Voss 2024). The other 88 campaigns were developed specifically to fall outside of the current process control limits.

K-means cluster analysis was performed based on the glass composition factors of most interest (mass fractions of): NaK (= $Na_2O$ + 0.66 $K_2O$), $SO_3$, $Li_2O$, $B_2O_3$, $ZrO_2$, CaO, $Fe_2O_3$, $Al_2O_3$, ZnO, F, and $UO_3$. Figure 2.1 shows the within cluster sum-of-squares distance vs. number of clusters. This figure indicates a gradual elbow from 5 to 10 clusters with slower decreases for 11 and more clusters. There is a slightly larger decrease in distance between cluster 14 and 15. These results show that from a statistical standpoint, 5 compositions are too small and there are diminishing returns for compositions above 15. From a statistical point of view, 15 compositions can adequately represent the range of glass compositions in the dataset. Two-dimensional plots of key glass components for the 15 clusters showed that the concentration ranges of individual oxides (in particular, $K_2O$) could be better covered by including a 16$^{th}$ glass. A representative batch was selected for each of the 16 clusters, as summarized in Table 2.1. Figure 2.2 through Figure 2.4 show the distribution of the 126 glass compositions with different colors representing the glasses in each of the 16 clusters, with the selected representative glass numbered by the batch number in Table 2.2. The waste compositions, GFC masses, and glass compositions are given in Table 2.2, Table 2.3, and Table 2.4, respectively.

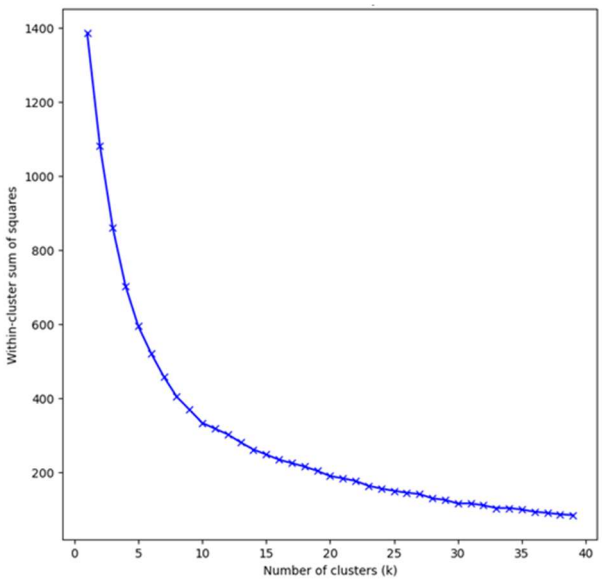


Figure 2.1. Within cluster sum of squares distance vs. number of clusters.

Table 2.1. Summary of represented batches from each of 16 clusters.

| Glass ID | Cluster # | Batch # | Feed Vector ID[(a)] | # in Feed Vector | Constraints[(b)] |
|---|---|---|---|---|---|
| APPS2-01 | 1 | 47 | B_120_120_100 | 12 | PCT, η, ε, $SO_3$, $k_{1208}$, $MV_{V2O5}$ |
| APPS2-02 | 2 | 15 | B_120_120_200 | 15 | η, ε, NP, $k_{1208}$ |
| APPS2-03 | 3 | 180 | B_120_105_100 | 25 | PCT, η, $MV_{B2O3}$, $MV_{ZnO}$ |
| APPS2-04 | 4 | 16 | B_120_120_150 | 1 | PCT, $SO_3$, $k_{1208}$, $MV_{V2O5}$ |
| APPS2-05 | 5 | 160 | B_120_105_100 | 5 | $MV_{ZrO2}$ |
| APPS2-06 | 6 | 146 | B_120_110_100 | 22 | η, $SO_3$, $P_2O_5$, NP, $MV_{V2O5}$ |
| APPS2-07 | 7 | 57 | B_120_120_100 | 22 | PCT, η, $SO_3$, $k_{1208}$ |
| APPS2-08 | 8 | 182 | B_120_105_100 | 27 | PCT, $SO_3$, $P_2O_5$, $MV_{Fe2O3}$ |
| APPS2-09 | 9 | 169 | B_120_105_100 | 14 | PCT, η, $P_2O_5$ |
| APPS2-10 | 10 | 175 | B_120_105_100 | 20 | NP, $MV_{B2O3}$ |
| APPS2-11 | 11 | 142 | B_120_110_100 | 18 | $MV_F$ |
| APPS2-12 | 12 | 176 | B_120_105_100 | 21 | η, NP, $MV_{B2O3}$, $MV_{ZnO}$ |
| APPS2-13 | 13 | 143 | B_120_110_100 | 19 | η, $P_2O_5$, $SO_3$, $k_{1208}$, $MV_{V2O5}$ |
| APPS2-14 | 14 | 170 | B_120_105_100 | 15 | $T_L$-Zr, $SO_3$, NP, $P_2O_5$, $k_{1208}$ |
| APPS2-15 | 15 | 33 | B_120_120_150 | 18 | η, ε, NP, $k_{1208}$ |
| APPS2-16 | 16 | 179 | B_120_105_100 | 24 | η, ε, NP, $k_{1208}$ |

(a) The numbering convention is B_xxx_yyy_zzz, where B stands for blend, xxx represents 100× the specific gravity of fluid used in retrieval, yyy represents 100× the specific gravity of fluid delivered to the HLW Facility, and zzz represents 10× the wt% of solids delivered to the HLW Facility.

(b) The glass formulations are subject to limiting constraints abbreviated as follows: PCT = product consistent test, NP = probability of nepheline formation, MVα = α component model validity, η = viscosity at 1150°C, ε = electrical conductivity at 1200°C, $SO_3$ = sulfur solubility, $T_L$-Zr = liquidus temperature of Zr-containing phases, $k_{1208}$ = k-3 refractory corrosion, $P_2O_5$ = probability of failing a phosphate constraint.

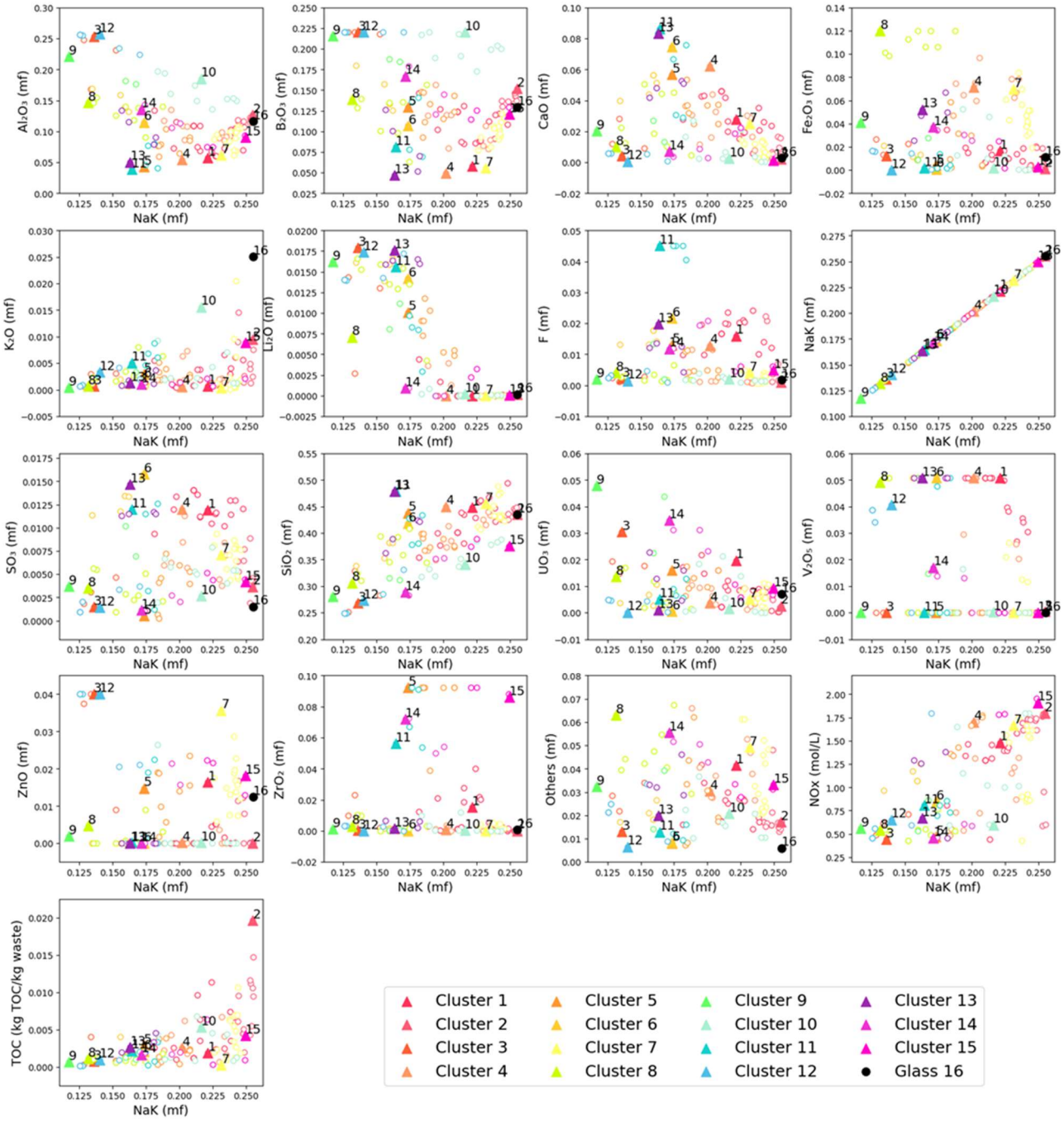


Figure 2.2. Major component concentrations for 126 (out of 214) glass compositions vs. NaK = $Na_2O$ + 0.66$K_2O$. Each color represents a cluster, and the numbered triangles show the selected batch to represent each cluster.

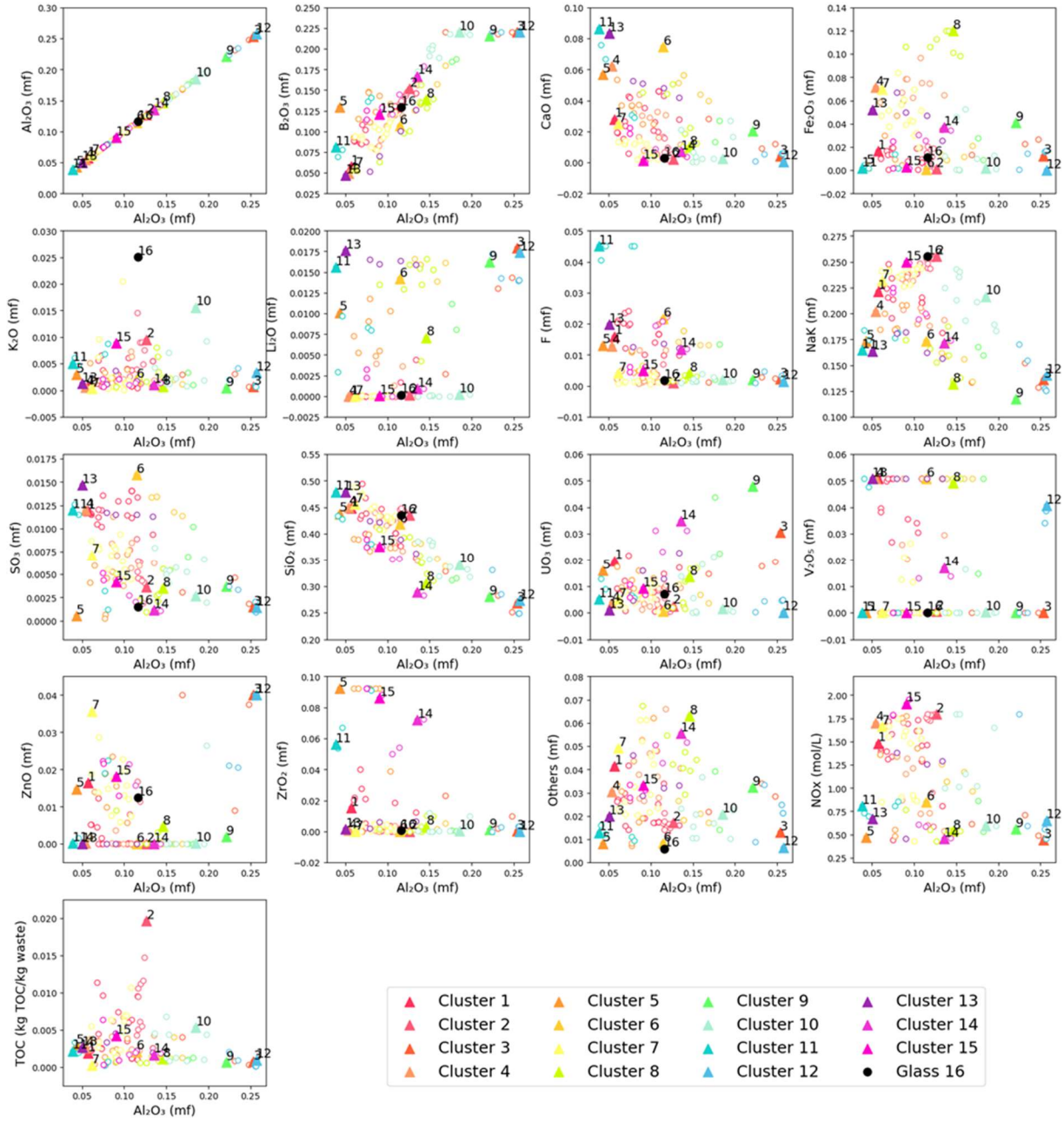


Figure 2.3. Major component concentrations for 126 (out of 214) glass compositions vs. $Al_2O_3$. Each color represents a cluster, and the numbered triangles show the selected batch to represent each cluster.

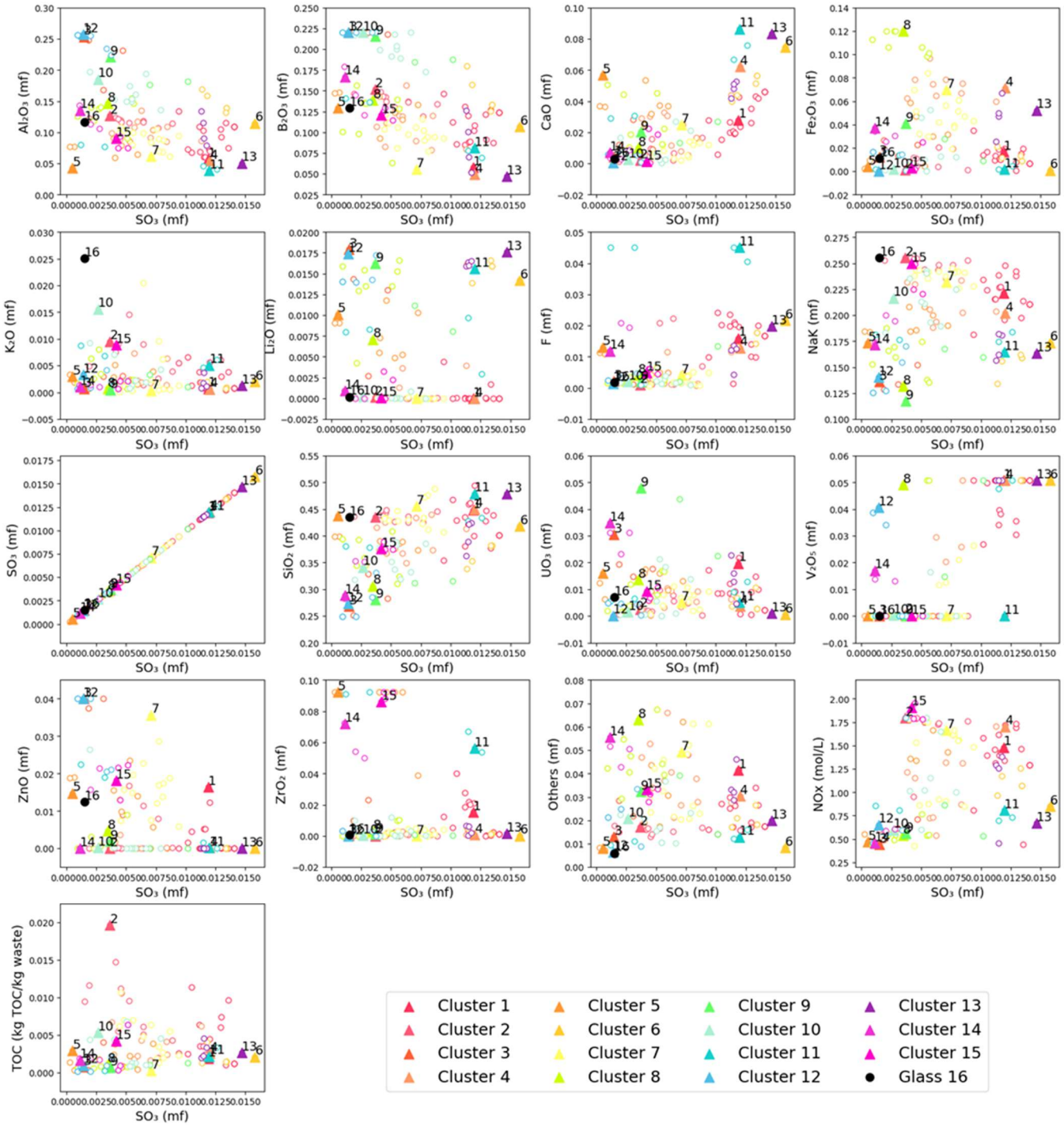


Figure 2.4. Major component concentrations for 126 (out of 214) glass compositions vs. $SO_3$. Each color represents a cluster, and the numbered triangles show the selected batch to represent each cluster.

Table 2.2. Waste compositions (mg/L waste) used for formulating the recommended glasses. Minor components have been removed but can be found in Lu et al. (2024c). Lanthanoids and actinoids are grouped into LN.

| Batch # | 47 | 15 | 180 | 16 | 160 | 146 | 57 | 182 | 169 | 175 | 142 | 176 | 143 | 170 | 33 | 179 |
|---|---|---|---|---|---|---|---|---|---|---|---|---|---|---|---|---|
| Al | 1.45E+04 | 3.37E+04 | 3.28E+04 | 2.05E+04 | 2.86E+03 | 2.86E+04 | 1.58E+04 | 1.80E+04 | 2.65E+04 | 2.34E+04 | 4.63E+03 | 3.68E+04 | 1.34E+04 | 1.71E+04 | 1.34E+04 | 1.23E+04 |
| B | 0.00E+00 | 2.01E+02 | 0.00E+00 | 1.36E+00 | 1.52E+01 | 7.61E+01 | 0.00E+00 | 0.00E+00 | 0.00E+00 | 2.18E+02 | 2.49E+02 | 1.02E+02 | 0.00E+00 | 0.00E+00 | 4.94E+02 | 1.55E+02 |
| Bi | 1.32E+01 | 9.66E+01 | 6.25E+01 | 4.87E+01 | 9.51E+01 | 9.10E+00 | 2.45E+03 | 3.23E+03 | 6.29E+01 | 1.65E+01 | 8.74E+01 | 9.61E+00 | 6.62E+00 | 2.32E+00 | 1.37E+02 | 1.49E+01 |
| Ca | 3.53E+03 | 9.67E+02 | 6.87E+02 | 2.41E+03 | 5.91E+02 | 1.27E+02 | 3.06E+02 | 1.65E+03 | 3.26E+03 | 4.28E+02 | 1.46E+02 | 8.86E+01 | 7.56E+02 | 1.21E+03 | 5.05E+02 | 4.94E+02 |
| Cl | 1.15E+03 | 1.65E+03 | 2.10E+02 | 1.61E+03 | 2.30E+02 | 6.93E+02 | 1.42E+03 | 2.71E+02 | 2.54E+02 | 4.61E+02 | 6.55E+02 | 4.67E+02 | 4.04E+02 | 2.23E+02 | 1.76E+03 | 3.85E+02 |
| Cr | 2.07E+02 | 8.61E+02 | 1.40E+02 | 1.47E+03 | 4.73E+02 | 2.55E+02 | 2.24E+02 | 2.59E+02 | 9.94E+01 | 1.67E+03 | 1.40E+03 | 2.96E+02 | 4.63E+02 | 2.59E+02 | 1.81E+03 | 4.52E+02 |
| Cs | 2.42E+00 | 1.43E+01 | 5.91E+00 | 4.82E-01 | 7.73E-01 | 5.29E-01 | 4.00E-01 | 1.08E+00 | 8.86E-01 | 6.59E+00 | 4.76E-01 | 4.12E-01 | 1.85E+00 | 4.52E-01 | 4.30E-01 | 1.05E+00 |
| F | 9.40E+03 | 7.53E+02 | 5.40E+02 | 9.37E+03 | 9.32E+03 | 1.03E+04 | 2.06E+03 | 9.66E+02 | 4.53E+02 | 4.87E+02 | 2.82E+04 | 3.96E+02 | 1.01E+04 | 2.83E+03 | 3.15E+03 | 4.38E+02 |
| Fe | 6.63E+03 | 3.39E+02 | 2.13E+03 | 3.60E+04 | 1.43E+03 | 5.23E+01 | 2.49E+04 | 1.96E+04 | 6.47E+03 | 2.80E+02 | 3.10E+02 | 3.26E+01 | 1.84E+04 | 6.17E+03 | 8.26E+02 | 1.90E+03 |
| I | 4.05E-01 | 1.25E-04 | 1.01E-01 | 3.26E-02 | 4.62E-02 | 4.94E-02 | 9.74E-01 | 3.03E-01 | 1.78E-01 | 2.64E-01 | 8.88E-02 | 4.78E-02 | 1.87E-01 | 5.35E-01 | 6.89E-02 | 6.51E-02 |
| K | 3.42E+02 | 6.02E+03 | 1.32E+02 | 3.54E+02 | 1.72E+03 | 7.89E+02 | 1.03E+02 | 1.29E+02 | 6.85E+01 | 3.10E+03 | 2.62E+03 | 7.47E+02 | 5.34E+02 | 1.93E+02 | 4.69E+03 | 5.30E+03 |
| LN | 1.77E+01 | 8.29E+02 | 7.23E+00 | 1.21E+03 | 3.99E+02 | 5.92E+01 | 6.72E+01 | 4.43E+01 | 1.43E+01 | 1.25E+02 | 1.14E+02 | 7.89E+01 | 1.05E+03 | 1.26E+01 | 2.09E+02 | 1.30E+02 |
| Li | 0.00E+00 | 4.14E+01 | 0.00E+00 | 2.96E-01 | 1.25E+01 | 1.02E+01 | 0.00E+00 | 0.00E+00 | 0.00E+00 | 2.56E+01 | 1.39E+00 | 1.37E+01 | 0.00E+00 | 0.00E+00 | 1.58E+01 | 1.92E+01 |
| Mg | 0.00E+00 | 4.14E+02 | 0.00E+00 | 2.38E+02 | 3.11E+02 | 2.95E+01 | 0.00E+00 | 0.00E+00 | 0.00E+00 | 6.21E+01 | 2.09E+02 | 3.94E+01 | 0.00E+00 | 0.00E+00 | 3.90E+02 | 1.27E+02 |
| Mn | 7.45E+02 | 4.09E+01 | 9.89E+02 | 3.65E+03 | 1.03E+03 | 4.85E+00 | 1.21E+03 | 1.29E+03 | 9.95E+01 | 2.74E+01 | 2.01E+01 | 3.93E+00 | 1.44E+03 | 1.39E+03 | 3.49E+02 | 5.27E+02 |
| Na | 9.64E+04 | 1.40E+05 | 1.95E+04 | 1.09E+05 | 3.59E+04 | 6.06E+04 | 8.80E+04 | 2.28E+04 | 1.97E+04 | 3.66E+04 | 7.43E+04 | 2.77E+04 | 5.77E+04 | 2.66E+04 | 1.15E+05 | 4.51E+04 |
| Ni | 2.39E+03 | 1.04E+02 | 3.45E+02 | 1.50E+03 | 7.20E+01 | 1.11E+01 | 7.48E+02 | 1.33E+03 | 1.68E+03 | 9.85E+01 | 2.41E+01 | 7.81E+00 | 8.94E+02 | 9.06E+02 | 6.50E+01 | 9.11E+01 |
| P | 4.64E+03 | 1.17E+03 | 2.85E+02 | 1.74E+03 | 2.36E+02 | 1.00E+03 | 5.37E+03 | 2.14E+03 | 1.51E+03 | 4.67E+02 | 1.04E+03 | 1.39E+02 | 9.06E+02 | 2.12E+02 | 5.40E+03 | 1.48E+02 |
| Pb | 5.10E+02 | 4.07E+02 | 1.57E+02 | 1.83E+03 | 7.14E+01 | 4.24E+01 | 2.45E+03 | 1.79E+03 | 7.81E+02 | 6.09E+01 | 1.74E+01 | 3.93E+01 | 4.79E+02 | 2.14E+02 | 2.84E+02 | 3.87E+02 |
| S | 2.80E+03 | 1.11E+03 | 1.40E+02 | 3.50E+03 | 1.39E+02 | 3.00E+03 | 1.46E+03 | 3.25E+02 | 3.34E+02 | 2.54E+02 | 3.00E+03 | 1.50E+02 | 3.00E+03 | 1.06E+02 | 1.06E+03 | 1.54E+02 |
| Se | 5.34E-02 | 1.29E+03 | 2.76E-04 | 9.75E+00 | 6.24E+01 | 2.95E+01 | 2.20E-03 | 2.48E-03 | 2.16E-03 | 6.21E+01 | 1.67E+00 | 3.94E+01 | 9.50E-03 | 2.97E-02 | 3.58E+01 | 3.74E+01 |
| Si | 1.51E+03 | 1.05E+03 | 5.37E+03 | 1.08E+04 | 1.02E+03 | 2.29E+02 | 5.19E+02 | 3.23E+03 | 1.49E+03 | 8.27E+02 | 4.80E+02 | 2.39E+02 | 1.25E+02 | 2.01E+03 | 7.63E+02 | 2.99E+02 |
| Sr | 6.48E+01 | 2.82E-01 | 3.27E+01 | 1.83E+02 | 4.12E+00 | 3.45E-01 | 6.31E+01 | 8.78E+01 | 1.17E+02 | 2.75E+00 | 3.62E-01 | 2.71E-02 | 6.52E+01 | 2.72E+01 | 3.14E+00 | 4.82E+00 |
| Tc | 1.54E+00 | 8.53E+00 | 4.20E-01 | 1.95E+00 | 4.20E-01 | 3.51E+00 | 5.33E-01 | 3.39E-01 | 4.88E-01 | 8.10E-01 | 9.59E-01 | 4.15E+00 | 1.11E+00 | 5.53E-01 | 2.98E+00 | 3.16E+00 |
| Th | 3.70E+03 | 2.26E+00 | 5.25E+01 | 9.43E+01 | 2.03E+01 | 2.52E-01 | 1.59E+02 | 9.82E+01 | 8.80E+01 | 5.15E-01 | 1.63E+00 | 2.61E-01 | 2.67E+02 | 7.13E+03 | 2.65E+00 | 9.58E+00 |
| Ti | 0.00E+00 | 4.14E+01 | 0.00E+00 | 3.03E+01 | 4.87E+00 | 2.95E+00 | 0.00E+00 | 0.00E+00 | 0.00E+00 | 6.21E+00 | 1.69E+00 | 3.94E+00 | 0.00E+00 | 0.00E+00 | 7.05E+00 | 5.09E+00 |
| U | 9.66E+03 | 1.63E+03 | 6.22E+03 | 2.23E+03 | 9.46E+03 | 1.93E+02 | 2.21E+03 | 2.62E+03 | 9.06E+03 | 2.85E+02 | 2.63E+03 | 2.99E+01 | 4.34E+02 | 6.93E+03 | 4.87E+03 | 1.50E+03 |
| V | 0.00E+00 | 2.07E+02 | 0.00E+00 | 3.56E+00 | 9.15E+00 | 1.48E+01 | 0.00E+00 | 0.00E+00 | 0.00E+00 | 3.11E+01 | 6.89E+00 | 1.97E+01 | 0.00E+00 | 0.00E+00 | 1.66E+01 | 7.22E+00 |
| Zn | 0.00E+00 | 4.58E+01 | 0.00E+00 | 7.76E+01 | 3.01E+01 | 1.77E+01 | 0.00E+00 | 0.00E+00 | 0.00E+00 | 3.31E+01 | 2.96E+00 | 2.36E+01 | 0.00E+00 | 0.00E+00 | 4.24E+01 | 5.26E+01 |
| Zr | 6.57E+03 | 6.47E+01 | 7.85E+01 | 4.15E+02 | 4.88E+04 | 2.40E+01 | 1.78E+01 | 5.21E+02 | 1.73E+02 | 2.73E+01 | 2.60E+04 | 3.62E+00 | 5.33E+02 | 1.28E+04 | 4.06E+04 | 1.20E+02 |
| $NO_2$ | 3.57E+04 | 4.16E+04 | 1.05E+04 | 4.04E+04 | 9.46E+03 | 1.93E+04 | 3.97E+04 | 1.14E+04 | 1.07E+04 | 1.33E+04 | 1.65E+04 | 1.41E+04 | 1.41E+04 | 1.12E+04 | 4.33E+04 | 1.28E+04 |
| $NO_3$ | 4.00E+04 | 5.45E+04 | 1.24E+04 | 4.45E+04 | 1.59E+04 | 2.54E+04 | 4.54E+04 | 1.69E+04 | 1.91E+04 | 2.25E+04 | 2.62E+04 | 2.06E+04 | 2.12E+04 | 1.24E+04 | 5.87E+04 | 2.58E+04 |
| TOC | 2.57E+03 | 2.63E+04 | 7.76E+02 | 2.67E+03 | 3.22E+03 | 1.80E+03 | 2.27E+02 | 1.15E+03 | 8.13E+02 | 5.35E+03 | 2.05E+03 | 8.03E+02 | 2.39E+03 | 2.08E+03 | 5.12E+03 | 9.02E+03 |

Table 2.3. Waste oxide loadings (mass fraction), and GFC masses (g/L simulant).

| Batch # | 47 | 15 | 180 | 16 | 160 | 146 | 57 | 182 | 169 | 175 | 142 | 176 | 143 | 170 | 33 | 179 |
|---|---|---|---|---|---|---|---|---|---|---|---|---|---|---|---|---|
| Waste oxide loading | 0.3961 | 0.3724 | 0.4719 | 0.4189 | 0.2139 | 0.3361 | 0.4217 | 0.5231 | 0.4992 | 0.4483 | 0.3105 | 0.4115 | 0.3103 | 0.5194 | 0.4353 | 0.3983 |
| Kyanite | 10.21 | 56.00 | 0.00 | 0.00 | 43.29 | 0.00 | 2.31 | 0.00 | 0.00 | 0.00 | 25.97 | 0.00 | 0.00 | 0.00 | 55.99 | 10.76 |
| Boric acid | 60.01 | 203.41 | 95.30 | 63.80 | 162.76 | 89.02 | 50.59 | 57.36 | 86.51 | 92.01 | 88.60 | 104.75 | 42.52 | 70.71 | 133.27 | 57.39 |
| Wollastonite | 24.22 | 0.44 | 0.00 | 88.21 | 83.21 | 73.95 | 25.93 | 0.00 | 0.00 | 0.00 | 113.20 | 0.00 | 87.24 | 0.00 | 0.00 | 0.00 |
| $Li_2CO_3$ | 0.00 | 0.00 | 10.91 | 0.00 | 17.88 | 16.68 | 0.00 | 4.12 | 9.14 | 0.00 | 24.27 | 11.62 | 22.38 | 0.53 | 0.00 | 0.00 |
| $Na_2CO_3$ | 0.00 | 0.00 | 11.83 | 0.00 | 126.32 | 0.00 | 0.00 | 0.00 | 0.00 | 0.00 | 0.87 | 0.00 | 8.66 | 8.66 | 0.00 | 0.00 |
| $V_2O_5$ | 30.09 | 0.00 | 0.00 | 37.19 | 0.00 | 24.23 | 0.00 | 11.58 | 0.00 | 0.00 | 0.00 | 11.00 | 26.10 | 4.10 | 0.00 | 0.00 |
| Zincite | 9.67 | 0.00 | 9.81 | 0.00 | 10.50 | 0.00 | 18.31 | 1.11 | 0.43 | 0.00 | 0.12 | 10.81 | 0.00 | 0.00 | 11.46 | 3.10 |
| Zircon | 0.00 | 0.00 | 0.00 | 0.00 | 0.00 | 0.00 | 0.00 | 0.00 | 0.00 | 0.00 | 0.14 | 0.00 | 0.00 | 0.00 | 0.00 | 0.00 |
| Silica | 244.87 | 306.42 | 54.34 | 260.57 | 251.00 | 160.81 | 219.13 | 65.04 | 60.76 | 80.27 | 231.73 | 73.66 | 200.24 | 64.94 | 215.37 | 106.19 |
| $Cr_2O_3$ | 3.26 | 0.00 | 0.00 | 2.24 | 0.56 | 0.00 | 2.78 | 0.00 | 0.00 | 0.00 | 1.63 | 0.00 | 1.60 | 0.83 | 1.19 | 0.88 |
| Sucrose | 24.28 | 0.00 | 7.29 | 27.76 | 2.24 | 13.45 | 33.59 | 8.38 | 9.65 | 1.26 | 11.81 | 11.77 | 8.19 | 4.51 | 28.18 | 0.00 |

Table 2.4. Glass compositions (mass fraction) recommended for testing based on the EWG2.5 formulation approach. These compositions were renormalized after removing minor components (Lu et al. 2024c list all tracked components). Lanthanoids and actinoids are grouped into $LN_2O_3$.

| Glass ID | APPS2-01 | APPS2-02 | APPS2-03 | APPS2-04 | APPS2-05 | APPS2-06 | APPS2-07 | APPS2-08 | APPS2-09 | APPS2-10 | APPS2-11 | APPS2-12 | APPS2-13 | APPS2-14 | APPS2-15 | APPS2-16 |
|---|---|---|---|---|---|---|---|---|---|---|---|---|---|---|---|---|
| Batch # | 47 | 15 | 180 | 16 | 160 | 146 | 57 | 182 | 169 | 175 | 142 | 176 | 143 | 170 | 33 | 179 |
| $Al_2O_3$ | 5.71E-02 | 1.27E-01 | 2.54E-01 | 5.42E-02 | 4.30E-02 | 1.15E-01 | 6.15E-02 | 1.46E-01 | 2.21E-01 | 1.85E-01 | 3.86E-02 | 2.57E-01 | 5.04E-02 | 1.36E-01 | 9.08E-02 | 1.16E-01 |
| $B_2O_3$ | 5.76E-02 | 1.53E-01 | 2.20E-01 | 4.96E-02 | 1.29E-01 | 1.07E-01 | 5.58E-02 | 1.38E-01 | 2.15E-01 | 2.20E-01 | 8.12E-02 | 2.20E-01 | 4.71E-02 | 1.67E-01 | 1.21E-01 | 1.30E-01 |
| $Bi_2O_3$ | 2.51E-05 | 1.42E-04 | 2.85E-04 | 7.47E-05 | 1.49E-04 | 2.14E-05 | 5.34E-03 | 1.54E-02 | 3.08E-04 | 7.70E-05 | 1.56E-04 | 3.96E-05 | 1.45E-05 | 1.08E-05 | 2.40E-04 | 6.53E-05 |
| CaO | 2.80E-02 | 2.12E-03 | 4.11E-03 | 6.23E-02 | 5.68E-02 | 7.46E-02 | 2.49E-02 | 9.94E-03 | 2.03E-02 | 2.53E-03 | 8.64E-02 | 6.43E-04 | 8.34E-02 | 7.09E-03 | 1.17E-03 | 2.77E-03 |
| Cl | 1.95E-03 | 2.18E-03 | 8.70E-04 | 2.22E-03 | 3.55E-04 | 1.46E-03 | 2.76E-03 | 1.16E-03 | 1.12E-03 | 1.93E-03 | 1.05E-03 | 1.73E-03 | 7.97E-04 | 9.37E-04 | 2.77E-03 | 1.52E-03 |
| $Cr_2O_3$ | 6.00E-03 | 1.66E-03 | 8.43E-04 | 6.01E-03 | 1.76E-03 | 7.90E-04 | 6.00E-03 | 1.62E-03 | 6.44E-04 | 1.02E-02 | 5.84E-03 | 1.60E-03 | 4.44E-03 | 5.03E-03 | 6.01E-03 | 6.01E-03 |
| $Cs_2O$ | 4.36E-06 | 2.00E-05 | 2.56E-05 | 7.04E-07 | 1.15E-06 | 1.18E-06 | 8.27E-07 | 4.88E-06 | 4.14E-06 | 2.92E-05 | 8.05E-07 | 1.62E-06 | 3.84E-06 | 2.00E-06 | 7.18E-07 | 4.36E-06 |
| F | 1.60E-02 | 9.94E-04 | 2.21E-03 | 1.29E-02 | 1.31E-02 | 2.17E-02 | 4.01E-03 | 4.13E-03 | 1.99E-03 | 2.04E-03 | 4.50E-02 | 1.47E-03 | 1.99E-02 | 1.18E-02 | 4.96E-03 | 1.72E-03 |
| $Fe_2O_3$ | 1.65E-02 | 1.29E-03 | 1.25E-02 | 7.14E-02 | 3.87E-03 | 8.59E-04 | 6.96E-02 | 1.20E-01 | 4.08E-02 | 1.75E-03 | 1.83E-03 | 2.36E-04 | 5.22E-02 | 3.69E-02 | 2.60E-03 | 1.11E-02 |
| I | 6.88E-07 | 1.65E-10 | 4.14E-07 | 4.48E-08 | 6.48E-08 | 1.04E-07 | 1.90E-06 | 1.29E-06 | 7.84E-07 | 1.10E-06 | 1.42E-07 | 1.77E-07 | 3.67E-07 | 2.23E-06 | 1.09E-07 | 2.56E-07 |
| $K_2O$ | 7.17E-04 | 9.58E-03 | 6.56E-04 | 6.00E-04 | 2.93E-03 | 2.02E-03 | 2.56E-04 | 6.74E-04 | 3.73E-04 | 1.56E-02 | 5.06E-03 | 3.34E-03 | 1.27E-03 | 9.81E-04 | 8.91E-03 | 2.52E-02 |
| $LN_2O_3$ | 3.52E-05 | 1.28E-03 | 3.46E-05 | 1.95E-03 | 6.57E-04 | 1.46E-04 | 1.54E-04 | 2.22E-04 | 7.40E-05 | 6.09E-04 | 2.15E-04 | 3.41E-04 | 2.42E-03 | 6.18E-05 | 3.86E-04 | 6.02E-04 |
| $Li_2O$ | 0.00E+00 | 1.18E-04 | 1.79E-02 | 8.78E-07 | 1.01E-02 | 1.42E-02 | 0.00E+00 | 7.08E-03 | 1.62E-02 | 2.30E-04 | 1.56E-02 | 1.74E-02 | 1.76E-02 | 8.88E-04 | 5.37E-05 | 1.63E-04 |
| MgO | 7.13E-05 | 9.50E-04 | 2.36E-05 | 6.75E-04 | 8.64E-04 | 2.65E-04 | 7.84E-05 | 2.49E-05 | 2.63E-05 | 4.59E-04 | 7.44E-04 | 2.69E-04 | 1.80E-04 | 2.33E-05 | 1.06E-03 | 8.70E-04 |
| MnO | 1.68E-03 | 7.03E-05 | 5.22E-03 | 6.60E-03 | 1.98E-03 | 1.69E-04 | 3.11E-03 | 7.10E-03 | 5.66E-04 | 1.48E-04 | 2.22E-04 | 1.94E-05 | 3.81E-03 | 7.49E-03 | 7.10E-04 | 2.68E-03 |
| $Na_2O$ | 2.21E-01 | 2.50E-01 | 1.36E-01 | 2.02E-01 | 1.72E-01 | 1.72E-01 | 2.31E-01 | 1.31E-01 | 1.17E-01 | 2.06E-01 | 1.61E-01 | 1.38E-01 | 1.62E-01 | 1.71E-01 | 2.44E-01 | 2.39E-01 |
| NiO | 5.16E-03 | 1.74E-04 | 1.80E-03 | 2.62E-03 | 1.29E-04 | 2.99E-05 | 1.86E-03 | 7.21E-03 | 9.40E-03 | 5.24E-04 | 4.89E-05 | 3.68E-05 | 2.23E-03 | 4.82E-03 | 1.30E-04 | 4.56E-04 |
| $P_2O_5$ | 1.80E-02 | 3.55E-03 | 2.66E-03 | 5.48E-03 | 7.58E-04 | 4.85E-03 | 2.40E-02 | 2.09E-02 | 1.52E-02 | 4.48E-03 | 3.80E-03 | 1.18E-03 | 4.07E-03 | 2.03E-03 | 1.95E-02 | 1.33E-03 |
| PbO | 9.33E-04 | 5.78E-04 | 6.91E-04 | 2.72E-03 | 1.08E-04 | 9.62E-05 | 5.14E-03 | 8.23E-03 | 3.70E-03 | 2.74E-04 | 2.99E-05 | 1.57E-04 | 1.01E-03 | 9.64E-04 | 4.82E-04 | 1.64E-03 |
| $SO_3$ | 1.19E-02 | 3.67E-03 | 1.47E-03 | 1.20E-02 | 5.24E-04 | 1.58E-02 | 7.12E-03 | 3.48E-03 | 3.70E-03 | 2.67E-03 | 1.20E-02 | 1.42E-03 | 1.47E-02 | 1.13E-03 | 4.19E-03 | 1.52E-03 |
| $SeO_2$ | 1.27E-07 | 2.39E-03 | 1.58E-09 | 1.88E-05 | 1.23E-04 | 8.75E-05 | 6.02E-09 | 1.49E-08 | 1.34E-08 | 3.65E-04 | 3.75E-06 | 2.05E-04 | 2.61E-08 | 1.74E-07 | 7.92E-05 | 2.07E-04 |
| $SiO_2$ | 4.48E-01 | 4.36E-01 | 2.68E-01 | 4.51E-01 | 4.38E-01 | 4.18E-01 | 4.56E-01 | 3.06E-01 | 2.81E-01 | 3.42E-01 | 4.79E-01 | 2.73E-01 | 4.78E-01 | 2.88E-01 | 3.76E-01 | 4.36E-01 |
| SrO | 1.29E-04 | 4.37E-07 | 1.54E-04 | 2.82E-04 | 6.70E-06 | 8.41E-07 | 1.42E-04 | 4.36E-04 | 6.08E-04 | 1.31E-05 | 6.58E-07 | 1.17E-07 | 1.42E-04 | 1.33E-04 | 5.77E-06 | 2.15E-05 |
| $Tc_2O_7$ | 4.10E-06 | 1.76E-05 | 2.69E-06 | 4.21E-06 | 9.23E-07 | 1.16E-05 | 1.63E-06 | 2.27E-06 | 3.36E-06 | 5.30E-06 | 2.40E-06 | 2.40E-05 | 3.40E-06 | 3.62E-06 | 7.34E-06 | 1.95E-05 |

| Glass ID | APPS2-01 | APPS2-02 | APPS2-03 | APPS2-04 | APPS2-05 | APPS2-06 | APPS2-07 | APPS2-08 | APPS2-09 | APPS2-10 | APPS2-11 | APPS2-12 | APPS2-13 | APPS2-14 | APPS2-15 | APPS2-16 |
|---|---|---|---|---|---|---|---|---|---|---|---|---|---|---|---|---|
| Batch # | 47 | 15 | 180 | 16 | 160 | 146 | 57 | 182 | 169 | 175 | 142 | 176 | 143 | 170 | 33 | 179 |
| $ThO_2$ | 7.15E-03 | 3.39E-06 | 2.44E-04 | 1.48E-04 | 3.24E-05 | 6.05E-07 | 3.52E-04 | 4.77E-04 | 4.41E-04 | 2.45E-06 | 2.96E-06 | 1.10E-06 | 5.94E-04 | 3.39E-02 | 4.75E-06 | 4.29E-05 |
| $TiO_2$ | 2.23E-04 | 8.00E-04 | 3.33E-05 | 1.48E-04 | 6.20E-04 | 9.24E-05 | 1.14E-04 | 4.17E-05 | 4.01E-05 | 9.37E-05 | 4.60E-04 | 6.52E-05 | 9.30E-05 | 4.07E-05 | 8.43E-04 | 4.67E-04 |
| $UO_3$ | 1.97E-02 | 2.59E-03 | 3.05E-02 | 3.69E-03 | 1.59E-02 | 4.89E-04 | 5.18E-03 | 1.35E-02 | 4.79E-02 | 1.43E-03 | 5.05E-03 | 1.33E-04 | 1.02E-03 | 3.48E-02 | 9.22E-03 | 7.08E-03 |
| $V_2O_5$ | 5.08E-02 | 4.88E-04 | 0.00E+00 | 5.09E-02 | 2.29E-05 | 5.08E-02 | 0.00E+00 | 4.92E-02 | 0.00E+00 | 2.32E-04 | 1.97E-05 | 4.06E-02 | 5.08E-02 | 1.70E-02 | 4.67E-05 | 5.07E-05 |
| ZnO | 1.64E-02 | 7.53E-05 | 4.00E-02 | 1.33E-04 | 1.48E-02 | 4.65E-05 | 3.56E-02 | 4.72E-03 | 1.89E-03 | 1.72E-04 | 1.90E-04 | 4.00E-02 | 0.00E+00 | 0.00E+00 | 1.81E-02 | 1.24E-02 |
| $ZrO_2$ | 1.51E-02 | 1.15E-04 | 4.33E-04 | 7.71E-04 | 9.25E-02 | 6.85E-05 | 4.70E-05 | 3.01E-03 | 1.03E-03 | 1.54E-04 | 5.63E-02 | 1.81E-05 | 1.41E-03 | 7.20E-02 | 8.63E-02 | 6.37E-04 |
| SUM | 1.00E+00 | 1.00E+00 | 1.00E+00 | 1.00E+00 | 1.00E+00 | 1.00E+00 | 1.00E+00 | 1.00E+00 | 1.00E+00 | 1.00E+00 | 1.00E+00 | 1.00E+00 | 1.00E+00 | 1.00E+00 | 1.00E+00 | 1.00E+00 |

### 2.1.3 Recommended Glass Compositions

Table 2.5 presents the glass compositions generated from the 16 waste cluster compositions. The glass compositions were simplified for testing, where minor components were removed and renormalized (except PdO and $Rh_2O_3$ were replaced by $RuO_2$, $ThO_2$ was replaced by $ZrO_2$, and $UO_3$ was replaced by $Nd_2O_3$ based on equal cation molar basis). For simplicity, these clusters are relabeled APPS2-01 to -16 in order of batch number and are referred to as such in the remainder of this report. The following process and quality product properties were measured: crystal formation during CCC and isothermal heat treatment (CF, $T_L$), sulfur solubility, density, viscosity, EC, product consistency via PCT, and toxicity via TCLP. Refractory corrosion test results will be reported separately.

Table 2.5. DFHLW glass compositions recommended for testing based on EWG2.5 formulation approach in mass fraction.

| Matrix ID | APPS2-01 | APPS2-02 | APPS2-03 | APPS2-04 | APPS2-05 |
|---|---|---|---|---|---|
| $Ag_2O$ | 0 | 0.00005 | 0 | 0.00009 | 0.00031 |
| $Al_2O_3$ | 0.05778 | 0.12748 | 0.25694 | 0.05428 | 0.04336 |
| $B_2O_3$ | 0.05833 | 0.1533 | 0.22289 | 0.04975 | 0.13015 |
| $Bi_2O_3$ | 0.00003 | 0.00014 | 0.00029 | 0.00007 | 0.00015 |
| CaO | 0.02833 | 0.00213 | 0.00416 | 0.06249 | 0.05722 |
| Cl | 0.00197 | 0.00219 | 0.00088 | 0.00222 | 0.00036 |
| $Cr_2O_3$ | 0.00608 | 0.00167 | 0.00085 | 0.00602 | 0.00177 |
| F | 0.01616 | 0.001 | 0.00223 | 0.01293 | 0.01317 |
| $Fe_2O_3$ | 0.0167 | 0.0013 | 0.01266 | 0.07156 | 0.0039 |
| $K_2O$ | 0.00073 | 0.00963 | 0.00066 | 0.0006 | 0.00296 |
| $Li_2O$ | 0 | 0.00012 | 0.01815 | 0 | 0.0102 |
| MgO | 0.00007 | 0.00095 | 0.00002 | 0.00068 | 0.00087 |
| MnO | 0.0017 | 0.00007 | 0.00529 | 0.00661 | 0.002 |
| $Na_2O$ | 0.22369 | 0.2508 | 0.13735 | 0.2022 | 0.17292 |
| $Nd_2O_3$ | 0.01174 | 0.00217 | 0.01819 | 0.00328 | 0.00964 |
| NiO | 0.00522 | 0.00017 | 0.00182 | 0.00263 | 0.00013 |
| $P_2O_5$ | 0.01827 | 0.00357 | 0.0027 | 0.00549 | 0.00076 |
| PbO | 0.00094 | 0.00058 | 0.0007 | 0.00272 | 0.00011 |
| $RuO_2$ | 0 | 0 | 0 | 0.00037 | 0 |
| $SO_3$ | 0.01205 | 0.00369 | 0.00149 | 0.01206 | 0.00053 |
| $SiO_2$ | 0.45352 | 0.4383 | 0.27165 | 0.45197 | 0.44143 |
| $V_2O_5$ | 0.05144 | 0.00049 | 0 | 0.05101 | 0.00002 |
| ZnO | 0.0166 | 0.00008 | 0.04053 | 0.00013 | 0.01487 |
| $ZrO_2$ | 0.01865 | 0.00012 | 0.00055 | 0.00084 | 0.09317 |
| SUM | 1.00000 | 1.00000 | 1.00000 | 1.00000 | 1.00000 |

Table 2.5 (cont.)

| Matrix ID | APPS2-06 | APPS2-07 | APPS2-08 | APPS2-09 | APPS2-10 |
|---|---|---|---|---|---|
| $Ag_2O$ | 0.00002 | 0 | 0 | 0 | 0.00011 |
| $Al_2O_3$ | 0.11473 | 0.06171 | 0.14695 | 0.22569 | 0.18567 |
| $B_2O_3$ | 0.1066 | 0.05591 | 0.13935 | 0.21983 | 0.22063 |
| $Bi_2O_3$ | 0.00002 | 0.00535 | 0.01548 | 0.00032 | 0.00008 |
| CaO | 0.07461 | 0.02498 | 0.01001 | 0.02068 | 0.00254 |
| Cl | 0.00146 | 0.00277 | 0.00116 | 0.00114 | 0.00193 |
| $Cr_2O_3$ | 0.00079 | 0.00602 | 0.00163 | 0.00066 | 0.01025 |
| F | 0.02167 | 0.00402 | 0.00415 | 0.00204 | 0.00204 |
| $Fe_2O_3$ | 0.00086 | 0.06982 | 0.12059 | 0.04163 | 0.00175 |
| $K_2O$ | 0.00202 | 0.00026 | 0.00068 | 0.00038 | 0.01563 |
| $Li_2O$ | 0.01419 | 0 | 0.00713 | 0.01653 | 0.00023 |
| MgO | 0.00027 | 0.00008 | 0.00003 | 0.00003 | 0.00046 |
| MnO | 0.00017 | 0.00312 | 0.00714 | 0.00058 | 0.00015 |
| $Na_2O$ | 0.17235 | 0.23193 | 0.1319 | 0.11931 | 0.20668 |
| $Nd_2O_3$ | 0.00036 | 0.00305 | 0.00797 | 0.0288 | 0.00115 |
| NiO | 0.00003 | 0.00186 | 0.00726 | 0.0096 | 0.00052 |
| $P_2O_5$ | 0.00485 | 0.02408 | 0.02105 | 0.01554 | 0.00448 |
| PbO | 0.0001 | 0.00516 | 0.00828 | 0.00378 | 0.00027 |
| $RuO_2$ | 0 | 0 | 0 | 0 | 0 |
| $SO_3$ | 0.01581 | 0.00714 | 0.0035 | 0.00378 | 0.00267 |
| $SiO_2$ | 0.41813 | 0.45679 | 0.30826 | 0.28649 | 0.3422 |
| $V_2O_5$ | 0.05084 | 0 | 0.04948 | 0 | 0.00023 |
| ZnO | 0.00005 | 0.03574 | 0.00475 | 0.00193 | 0.00017 |
| $ZrO_2$ | 0.00007 | 0.00021 | 0.00325 | 0.00126 | 0.00016 |
| SUM | 1.00000 | 1.00000 | 1.00000 | 1.00000 | 1.00000 |

Table 2.5 (cont.)

| Matrix ID | APPS2-11 | APPS2-12 | APPS2-13 | APPS2-14 | APPS2-15 |
|---|---|---|---|---|---|
| $Ag_2O$ | 0.00019 | 0.00004 | 0 | 0 | 0.00034 |
| $Al_2O_3$ | 0.03867 | 0.25758 | 0.0506 | 0.14012 | 0.09123 |
| $B_2O_3$ | 0.08145 | 0.22029 | 0.04722 | 0.17265 | 0.12172 |
| $Bi_2O_3$ | 0.00016 | 0.00004 | 0.00001 | 0.00001 | 0.00024 |
| CaO | 0.08662 | 0.00064 | 0.08371 | 0.00733 | 0.00118 |
| Cl | 0.00105 | 0.00173 | 0.0008 | 0.00097 | 0.00279 |
| $Cr_2O_3$ | 0.00585 | 0.00161 | 0.00445 | 0.0052 | 0.00603 |
| F | 0.04513 | 0.00147 | 0.01992 | 0.01222 | 0.00498 |
| $Fe_2O_3$ | 0.00183 | 0.00024 | 0.05239 | 0.03817 | 0.00261 |
| $K_2O$ | 0.00508 | 0.00334 | 0.00128 | 0.00101 | 0.00895 |
| $Li_2O$ | 0.01563 | 0.0174 | 0.01768 | 0.00092 | 0.00005 |
| MgO | 0.00075 | 0.00027 | 0.00018 | 0.00002 | 0.00106 |
| MnO | 0.00022 | 0.00002 | 0.00382 | 0.00774 | 0.00071 |
| $Na_2O$ | 0.16144 | 0.13811 | 0.1629 | 0.17664 | 0.24504 |
| $Nd_2O_3$ | 0.00303 | 0.00025 | 0.0006 | 0.02116 | 0.00555 |
| NiO | 0.00005 | 0.00004 | 0.00223 | 0.00498 | 0.00013 |
| $P_2O_5$ | 0.00381 | 0.00118 | 0.00408 | 0.0021 | 0.01959 |
| PbO | 0.00003 | 0.00016 | 0.00101 | 0.001 | 0.00048 |
| $RuO_2$ | 0 | 0 | 0 | 0 | 0 |
| $SO_3$ | 0.01201 | 0.00142 | 0.01473 | 0.00117 | 0.00421 |
| $SiO_2$ | 0.48034 | 0.2735 | 0.47972 | 0.29813 | 0.37818 |
| $V_2O_5$ | 0.00002 | 0.0406 | 0.05098 | 0.01762 | 0.00005 |
| ZnO | 0.00019 | 0.04005 | 0 | 0 | 0.01818 |
| $ZrO_2$ | 0.05645 | 0.00002 | 0.00169 | 0.09084 | 0.0867 |
| SUM | 1.00000 | 1.00000 | 1.00000 | 1.00000 | 1.00000 |

## 2.2 Glass Fabrication

The glasses were batched using chemicals composed of single-metal oxides, single-metal carbonates, sodium salts, and boric acid in the appropriate masses to form the target composition for each glass. For each glass, a ~1-kg batch was prepared for general characterization and a ~2-kg batch for K-3 corrosion testing. Laboratory crucible-scale fabrication of glasses is not intended to mimic the actual melter process or feed processability; rather, it is intended to fabricate a glass sample with a controlled composition for property testing.

The batched powders were thoroughly mixed in a plastic bag for at least 30 s until a uniform color developed. The powders were then transferred to an agate milling chamber and milled for 4 min in a vibratory mill (Angstrom TE110). Once milled, the powders were transferred to a clean crucible for melting.

Glasses melted in the Deltech furnace (Deltech Model DT-31-RS, Denver, Colorado) were melted at least two times. First and second melts were performed at 1150 ± 10 °C for 1 h ± 10 min. After the first melt, the glass was air quenched on a stainless-steel pouring plate, ground to a fine powder for 5 min (+ 1 min if glass chunks were still present) in a tungsten carbide (WC) vibratory mill (AngstromTE110) and melted

a second time. After each melt, the glass was observed under an optical microscope and the presence of undissolved particles and/or salts was reported. When the glass presented a large amount of undissolved particles, a third melt was performed at 1200 °C for 1 h ± 10 min after the glass was reduced to powder as described above.

For the tilt-pour furnace (UltraMELT, TLT-2P, Ronkonkoma, New York), melting was performed by following EWG-OP-086, Rev. 1.0.[1] Melting with a tilt-pour furnace took about 1 h for charging glass powders at 1150 ± 50 °C, and the powder was melted for 1 to 1.5 h after charging. The melt was stirred every 10 to 15 min for < 1 min to obtain homogeneous distribution of precursors. After the first melt was air quenched on a pouring plate, the glass was observed under an optical microscope and the presence of undissolved particles and/or salts was reported. An additional second melt was performed for the glasses with large amounts of undissolved particles and/or salts.

The glasses' chemical compositions were validated by electron probe microanalysis (EPMA) as described in Section 2.4. Three glasses were re-batched: APPS2-14 (1-kg batch), APPS2-05 (2-kg batch), and APPS2-06 (2-kg batch). APPS2-14 (1-kg batch) showed substantially low $ZrO_2$ [-30% relative percentage difference (RPD)]. APPS2-05 (2-kg batch) had low $B_2O_3$ (-58% RPD). APPS2-06 (2-kg batch) had low $Na_2O$ (-18% RPD) and $SiO_2$ (-17% RPD). One of the glasses, APPS2-01 (1-kg batch), had a mis-batched amount of $Bi_2O_3$. The target mass of $Bi_2O_3$ was 0.03 g, but 0.3 g was added. In terms of wt%, mis-batched $Bi_2O_3$ was about 0.03% of the glass; however, the glass was not re-batched because a significant change in glass properties was not expected. Re-batched glasses were marked with a "-1" (i.e., first re-batch) after the sample ID (e.g., APPS2-14-1). The EPMA result of APPS2-14-1 (1-kg batch) showed a decrease in RPD values of $Bi_2O_3$, F, and $ZrO_2$ compared to the first batch, indicating the target and measured concentrations of components are closer. The EPMA results of APPS2-05-1 (2-kg batch) showed the smaller RPD value of $B_2O_3$ (11% from -58%) compared to the first batch. As for APPS2-06-1 (2-kg batch), the RPD values of multiple components, including $Al_2O_3$, CaO, F, $Na_2O$, $SO_3$, $SiO_3$, $V_2O_5$, and ZnO, were significantly lower compared to the first batch.

These results are discussed in Section 3.2. Optical images of the quenched (Q) APPS2 glasses (1-kg and 2-kg batches) are presented in Appendix A and measured compositions are listed in Appendix B.

## 2.3 X-ray Diffraction and Scanning Electron Microscopy for Secondary Phase Investigation

Powdered glass samples were prepared for X-ray diffraction (XRD) using roughly 5 wt% $CeO_2$ as an internal standard phase with between 1 and 2 g of powdered glass. A glass piece representative of the whole sample (in the case of the CF, half sample was used) was milled alone for 1 min and then homogenized with the $CeO_2$ for 30 s in a 10-$cm^3$ tungsten carbide disc mill. The homogenized samples were loaded into plastic holders and analyzed using a Bruker D8 Advance XRD (Bruker AXS Inc., Madison, Wisconsin) with Cu Kα emission. Samples were scanned at a 0.015° 2θ step size, 1.5-s dwell time, from 5° to 75° 2θ scan range. XRD spectra were analyzed with DIFFRAC.EVA (Bruker Corporation, Billerica, Massachusetts) for phase identification. Full-pattern Rietveld refinement using TOPAS 5 Software (Bruker AXS Inc., Madison) was performed to quantify the fraction of each crystal phase present. Comparing the quantified fraction by Rietveld refinement to the quantity of the crystalline internal standard used allowed for quantification of the crystalline phases and amorphous phase in the sample.

[1] Neeway, JJ. 2024. *Operating Procedure for Tilt-Pour Furnace*. EWG-OP-086, Rev. 1.0.

## 2.4 Electron Probe Microanalysis/Wavelength Dispersive Spectroscopy for Chemical Composition Analysis

To measure the concentration of elements in the glass with atomic numbers > 4 (which excludes Li, assumed to be on target), a representative sample of each glass was analyzed using EPMA/wavelength dispersive spectroscopy with a JEOL JXA-8530F Hyperprobe (JEOL USA Inc., Peabody, Massachusetts). The samples were prepared as 2-mm-diameter cylinders using a drill press, mounted into an aluminum stage with an array of holes so multiple samples could be inserted. The samples were ground with 1500 grit paper and polished to a finish of 1 µm using 9-, 3-, and 1-µm diamond pads and polishing compound. Samples were then coated with iridium to dissipate charging.

The EPMA instrument used a field-emission gun equipped with five wavelength dispersive spectrometers, each with a take-off angle of 40°. The microprobe data was collected at an accelerating voltage of 15 kV, beam current of 40 nA, and beam size of 100 µm.

Appropriate standards were used for each of the elements analyzed. Interferences were identified and corrected for by applying interference standards for each element. Wavescans were collected using arbitrarily chosen coupons to fit background functions for each glass composition. Oxygen and lithium were not directly analyzed. Instead, oxygen was calculated based on stoichiometry of the oxides analyzed. The presence of lithium was qualitatively confirmed with laser-induced breakdown spectroscopy and the "as-batched" values are reported in the results.

Each coupon was measured in 10 different locations in an approximate square grid with the intention of maximizing representation of the sample. The average of the 10 duplicates measured was used as the glass measured composition. Images were taken of the regions of the sample where data was collected, and observations of the morphology were recorded.

## 2.5 Canister Centerline Cooling

A portion (~150 g) of each test glass was subjected to the simulated CCC temperature profile shown in Table 2.6 and Figure 2.5.

Table 2.6. Canister centerline cooling profile for the DFHLW samples.

| Segment | Start Temp (°C) | Stop Temp (°C) | Rate (°C/min) |
|---|---|---|---|
| 1[(a)] | 1150[(a)] | 1150[(a)] | 0.000[(a)] |
| 2[(b)] | 1150 | 1050 | free fall[(b)] |
| 3 | 1050 | 980 | -1.556 |
| 4 | 980 | 930 | -0.806 |
| 5 | 930 | 875 | -0.591 |
| 6 | 875 | 825 | -0.388 |
| 7 | 825 | 775 | -0.253 |
| 8 | 775 | 725 | -0.278 |
| 9 | 725 | 400 | -0.304 |

(a) Segment 1 is a 30-minute dwell at 1150 °C (melting temperature).
(b) Segment 2 free fall is at an estimated rate of -12.5 °C/minute.

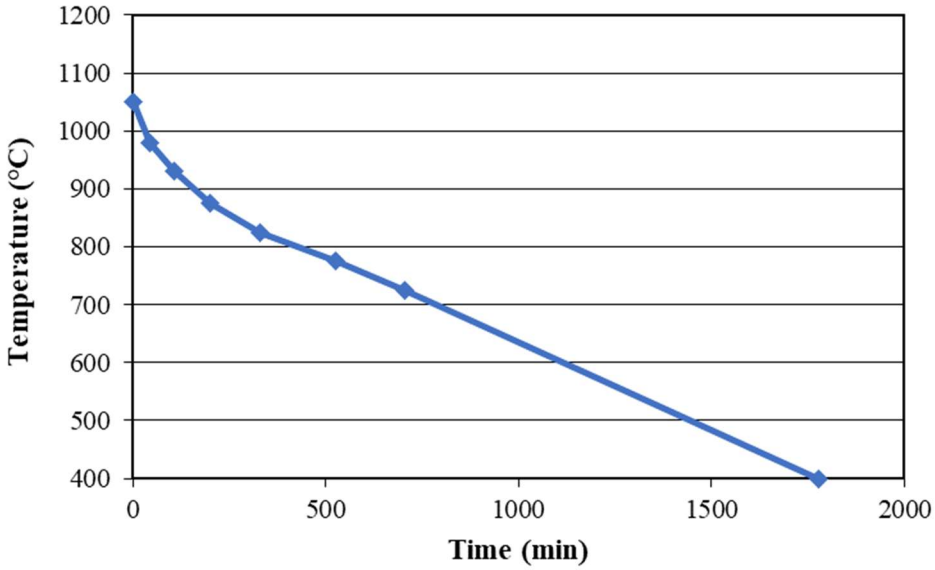


Figure 2.5. Plot of target temperature schedule during CCC treatment.

This profile is the temperature schedule of CCC treatment for Hanford HLW glasses planned for use at the WTP (Petkus 2003) and modified by PNNL to include a 30-min soak at 1150 °C before the cooling began. Pieces of Q glass, < 3 cm in diameter, were placed in a Pt-alloy crucible and covered with a Pt-alloy lid. The glass samples were placed in a furnace preheated to the $T_M$ = 1150 °C. After 30 min at $T_M$, the furnace temperature was quickly decreased to 1050 °C and the cooling profile started. It progressed down to about 400 °C based on seven cooling segments shown in Table 2.6. The starting temperatures for the seven segments of cooling were 1050, 980, 930, 875, 825, 775, and 725 °C.

The amounts and types of crystalline phases that formed during CCC treatment were analyzed by XRD according to Section 2.3. These results are discussed in Section 3.2.

## 2.6 Isothermal Crystal Fraction and Liquidus Temperature ($T_L$)

Isothermal CF as a function of temperature was measured in Pt-alloy crucibles with tight-fitting lids to minimize volatility according to the ASTM C1720. Prior to measuring the CF, the furnace temperature accuracy was verified using ARG-1 glass (Smith 1993).

Isothermal CF heat treatments were completed on each composition by selecting pieces of glass between 4 mm and 425 µm, washing with deionized water (three times) in a sonic bath, then performing a final wash with clean ethanol and drying in air for at least 12 h or by using an appropriate explosion-proof drying oven at 90 °C for at least 2 h. These pieces were loaded into a Pt-alloy crucible of roughly 1 $cm^3$ prepared following ASTM C1720. The crucible was first held for 30 min at melt temperature ($T_M$) prior to moving into a second furnace pre-heated to the desired temperature for the isothermal CF heat treatment. The heat treatment times and temperatures are reported in Table 2.7. The Pt-alloy crucibles were removed from the furnace and placed on a ceramic brick to cool. Due to the small size, water quenching was unnecessary to prevent crystal formation on cooling. The crystals that formed during heat treatment were determined by XRD according to Section 2.3.

Table 2.7. Heat treatment temperatures and durations used for CF measurements.

| Temp-Time | Glass IDs |
|---|---|
| 750 °C–72 h | All glasses except APPS2-03, -12, and -14-1 |
| 825 °C–48 h | APPS2-02, -06, -08, -10, -14-1, -15 and -16 |
| 900 °C–24 h | All glasses |
| 950 °C–24 h | APPS2-04 and APPS2-15 |
| 1000 °C–24 h | APPS2-10 and APPS2-15 |
| 1050 °C–24 h | APPS2-02, -03, -04, -06, -08, -09, -10, -11, -12, -13, -14-1 -15, and -16 |
| 1125 °C–24 h | APPS2-03, -08, -09, and -12 |
| 1200 °C–24 h | APPS2-08, -12, and -14-1 |
| 1400 °C–24 h | APPS2-14-1 |

Attempts were made to measure the $T_L$ of the test-matrix glasses using the CF extrapolation method in ASTM C1720, where $T_L$ is calculated by extrapolating CF as a function of temperature to zero crystals.

For glasses where a linear trendline did not fit well, a non-linear fit of the CF was calculated using a modified ideal-solution equation (Alton et al. 2002):

$$C_0 = C_{\max}\left\{1 - \exp\left[-B_L\left(\frac{1}{T} - \frac{1}{T_L}\right)\right]\right\} \tag{2.1}$$

where $C_0$ is the crystalline mass fraction at equilibrium, $C_{max}$ is the total solute mass fraction in glass, $B_L$ is crystal phase solubility temperature coefficient in K, T is temperature in K from isothermal heat treatment, and $T_L$ is glass liquidus temperature in K. The GRG Nonlinear Solver method in Excel was selected to adjust $C_{max}$, $B_L$, and $T_L$ to minimize the sum of squares difference between the measured and calculated CFs as a function of temperature. This works only if there is a $C_{max}$. Thus, if CF diminished when temperature increased, then this equation is valid.

The majority of the crystallization information from the HLW glass literature is presented in volume percentage (vol%); therefore, the model's constraint development uses vol% to represent the amount of crystals present. The conversion from weight percentage (wt%) to vol% was completed using the following equation:

$$vol\%_{crystal} = \frac{\rho_{glass}}{\left(\rho_{crystal} \times \left(100 \div wt\%_{crystal}\right) + \rho_{crystal}\right)} \times 100 \tag{2.2}$$

where the $vol\%_{crystal}$ = the amount of crystal present in volume percent, $wt\%_{crystal}$ = the amount of crystal present in weight percent, $\rho_{glass}$ = residual glass density (2.65 g/cm$^3$), and $\rho_{crystal}$ = crystal density (value from Table 2.8). This conversion assumed that the residual glass density is always 2.65 g/cm$^3$.

Table 2.8. Crystal density values used to convert weight percentage to volume percentage of crystals.

| Phases | Density ($g/cm^3$) | References |
|---|---|---|
| $ZnAl_2O_4$ | 4.60 | ICSD 94155 |
| $Cr_2O_3$ | 5.25 | ICSD 250078 |
| $NiFe_2O_4$ | 5.43 | ICSD 188487 |
| $Fe_3O_4$ | 5.24 | ICSD 84611 |
| $NdPO_4$ | 5.45 | ICSD 79750 |
| $Al_{1.898}Fe_{1.102}O_4$ | 4.31 | ICSD 95323 |
| $ZrO_2$ | 5.82 | ICSD 82544 |
| Residual glass | 2.65 | From Equation 4.1 in EWG-RPT-033, R1 |

The CF and $T_L$ results are summarized in Section 3.3.

## 2.7 $SO_3$ Solubility

The $SO_3$ solubility ($w_{SO3}$) was determined using the three-time saturation melt method (3TS) adapted from Jin et al. (2019). Fifty grams of the Q glass was crushed and mixed with ~3.82 g of $Na_2SO_4$ (equivalent to 4 wt% of $SO_3$ in glass if 100% is dissolved in the melt). The mixture was melted in a Pt/Rh crucible at 1150 °C for 1 h, Q on the stainless plate, and ground using a WC mill. The mixture was melted and crushed three times to ensure complete saturation of the sulfate into the glass. After the third melt, the concentrations of oxides in the glasses were analyzed using EPMA, including the concentration of $SO_3$ as discussed in Section 2.4. The excess $SO_3$ salt phase was washed from the monolith surface during the polishing steps of the EPMA sample, so only the $SO_3$ contained in the glass was measured.

These results are discussed in Section 3.4.

## 2.8 Density

Density of each glass was measured at room temperature using a MicroMeritics AccuPyc II 1340 gas pycnometer (MicroMeritics, Norcross, Georgia). Approximately 1 g of glass was loaded into a 1-$cm^3$ sample holder and placed within the instrument. The pycnometer was purged 10 times with He gas prior to volume measurement, and the volume of each glass was measured 10 times. The average of 10 volume measurements and the measured mass of the sample were used to calculate the glass density. The pycnometer calibration was verified before and after measurements for that day using a National Institute of Standards and Technology traceable standard tungsten carbide ball.

These results are discussed in Section 3.5.

## 2.9 Viscosity

The viscosity of each glass was measured as a function of temperature using the viscosity dependance to the shear stress and shear rate [Eq. (2.3)]:

$$\eta = \frac{\tau}{\gamma} \tag{2.3}$$

where $\eta$ is the viscosity, $\gamma$ is the shear rate, and $\tau$ is the shear stress.

A rotating spindle digital viscometer capable of measuring viscosities from 1 to 100 Pa·s (Brookfield Digital Model LVTD) was staged above a high-temperature Deltech furnace (Deltech Model DT-31-RS, Denver, Colorado) equipped with a Pt/Rh spindle to fit through a hole in the top of the furnace. A 50-mL glass sample was added to a 100-mL Pt/Rh alloy crucible with approximate dimensions of 5 cm diameter × 6 cm height. The crucible was placed into the furnace, which was set at 1150 °C, and the glass was left to melt for about 20 min. The spindle was then lowered into the molten glass in the center of the crucible with the lower end of the rod suspended 1 cm above the bottom of the crucible. The furnace was programmed to follow a set ramp schedule at the following temperatures: 1150, 1050, 950, 1150, 1200 °C, and back to 1150 °C. The soak time was 45 min at each temperature. This temperature profile allowed for the potential impacts of crystallization (at lower temperatures) and volatility (at higher temperatures) to be assessed (via reproducibility) at the repeated 1150 °C temperature. The viscometer was calibrated using the Defense Waste Processing Facility (DWPF) startup frit. At each target temperature, the maximum and minimum spindle torque values were recorded three times each at 3-min intervals. The average of the three measurements was used for data analysis. A secondary thermocouple was placed below the crucible and temperature was recorded continuously during measurement to ensure thermal equilibrium was reached before measurement.

Results are discussed in Section 3.6.

## 2.10 Electrical Conductivity

The EC (ε in S/m) as a function of temperature was calculated from the resistance (R' in Ω) and cell constant (K in $m^{-1}$) by:

$$\varepsilon = K/R_s \tag{2.4}$$

where $R_s$ is the solution resistance obtained for the KCl calibration solutions and K is the cell constant and is linked to the geometry of the system.

A Biologic VSP-3E potentiostat connected to a two-blade Pt/Rh probe staged above a high-temperature Sentrotech furnace (Sentrotech Model ST-1200-7812, Strongsville, Ohio) was used to measure the molten glass impedance. Data was recorded at 1200, 1150, 1050, and 950 °C after roughly 30-min soaks at each temperature, allowing the program to collect impedance data at an applied voltage of 100 mV, frequencies of 0.5 to $5x10^5$ Hz, measuring 25 data points per decade, and repeating the scan three times for a total of four measurements per glass per temperature.

Approximately 18 g of Q glass was added to an alumina crucible with the two-blade Pt/Rh probes attached perpendicular to one another 20 mm apart, and the assembly was loaded into the furnace at room temperature. The furnace was then slowly (~10 °C/min) ramped to 900 °C to prevent thermal shock to the crucibles and was successively fast ramped to 1200 °C to complete glass melting. The furnace was then held (~30 min) at 1200 °C to homogenize the glass before taking the first measurement. Each change in temperature was performed at a slow rate (~10 °C/min) and the glass was allowed to equilibrate at each temperature for ~30 min before the corresponding measurement was taken.

Solution resistance ($R_s$) was calculated by fitting the impedance spectra (i.e., Nyquist plots). A cell constant was determined using 0.1 M and 1.0 M KCl solutions measured at the same volume in the same alumina crucible and Pt/Rh probe apparatus. The conductivity is then calculated from Eq. (2.4).

These results are discussed in Section 3.7.

## 2.11 Product Consistency Test

The PCT responses were measured for Q and CCC samples of each glass using Method A of ASTM C1285, *Standard Test Methods for Determining Chemical Durability of Nuclear, Hazardous, and Mixed Waste Glasses and Multiphase Glass Ceramics: The Product Consistency Test (PCT)*. Tests were performed in triplicate for each Q and CCC glass. Alongside each triplicate, the Approved Reference Material-1 (ARM-1, Mellinger and Daniel 1984) glass was also tested in triplicate. Two blanks, which consisted of deionized water in a cleaned vessel without glass, were added with each set of tests. Glasses were ground, sieved to -100 +200 mesh, washed, and prepared according to Section 19.6 of ASTM C1285-21. Then, 1.5 g of the prepared glass was added to 15 mL of deionized water. Type 304L Parr stainless steel vessels with polytetrafluoroethylene gaskets were used. The vessels were closed, sealed, and placed into an oven at 90 ± 2 °C for 7 days ± 3 h.

After 7 days, the vessels were removed from the oven and allowed to cool until they were cool to the touch. The final mass of the vessel and the solution pH were recorded. The leachate from each test vessel was filtered through a 0.45-µm-size filter and acidified with concentrated, high-purity $HNO_3$ to 1 vol% before analysis. The leachates were analyzed using inductively coupled plasma-optical emission spectroscopy (ICP-OES) for Si, Na, Li and B at the Southwest Research Institute.

Normalized concentrations of element *i* ($NC_i$, g $L^{-1}$) were calculated with the following formula:

$$NC_{\mathrm{i}} = \frac{C_i}{f_i} \tag{2.5}$$

where: $C_i$ = the concentration of element *i* in solution ($g_i \cdot L^{-1}$)
$f_i$ = mass fraction of element *i* in the glass ($g_i \cdot g_{glass}^{-1}$)

Subsequently, the normalized mass losses of element *i* ($NL_i$, g $m^{-2}$) were calculated with the following formula:

$$\mathrm{NL}_i = \frac{NC_i}{S/V} \tag{2.6}$$

where: S = glass surface area ($m^2$)
V = volume of solution ($m^3$)

Assuming a spherical particle geometry and a density of 2.65 $g \cdot cm^{-3}$, the resulting glass surface area:solution volume ratio is approximately 2000 $m^{-1}$. Measured densities were not used in the calculations. Calculations of $NC_i$ and $NL_i$ were based on target glass compositions.

These results are discussed in Section 3.8.

## 2.12 Toxicity Characteristic Leaching Procedure

The TCLP based on EPA Method 1311 with some notable exceptions was performed on the Q and CCC glasses to measure the release of toxic elements present in the glasses (Cr, Ni, Pb, V, Zn) compared to their delisting limit concentrations provided in Table 2.9 and to predicted TCLP releases from various models discussed in the results.

Table 2.9. Waste Treatment and Immobilization Plant Delisting Limits, and Resource Conservation and Recovery Act (RCRA) Toxicity and Universal Treatment Standards (UTS) Limits for TCLP (40 CFR 268, 2015)

| Element | Ag | As | Ba | Cd | Cr | Hg | Ni | Pb | Se | V | Zn |
|---|---|---|---|---|---|---|---|---|---|---|---|
| WTP Delisting Limit (mg/L) | 3.07 | 0.616 | 100 | 0.48 | 4.95 | 0.2 | 22.6 | 5 | 1 | 16.9 | 225 |
| RCRA Toxicity Limit (mg/L) | 5 | 5 | 100 | 1 | 5 | 0.2 | -- | 5 | 1 | -- | -- |
| RCRA UTS Limit (mg/L) | 0.14 | 5 | 21 | 0.11 | 0.6 | 0.025 | -- | 0.75 | 5.7 | -- | -- |

The notable exceptions to EPA Method 1311 included glasses being size-reduced to pass through a sieve < 5.0 mm according to ASTM D6323-D19 rather than < 9.5 mm as described in EPA Method 1311. Additionally, the amount of glass tested was reduced from 100 g to 15 g and the corresponding extraction fluid volume was reduced from 2000 mL to 300 mL. These changes to the test method were agreed upon for application to Hanford HLW glasses between the Washington State Department of Ecology, DOE, Vanderbilt University, and PNNL (Kruger 2023). A pretest was performed on each Q and CCC glass to identify the extraction fluid used for testing according to EPA Method 1311. Glasses were tested in duplicate. Each campaign of tests was conducted for 18 ± 2 h in ambient temperatures of 23 ± 2 °C. One blank vessel for each extraction fluid used in a campaign was tested in parallel with tests in the campaign. After 18 ± 2 h, the TCLP leachate was filtered with 0.45-µm polytetrafluoroethylene filters, preserved with 100 µL Optima concentrated $HNO_3$, and refrigerated until the samples were ready for solution analysis. The solutions were analyzed at Southwest Research Institute using ICP-OES according to SW846-Method 6010D.

The normalized concentration of B (*NC(B)*) was calculated to compare with predicted normalized concentrations from models. *NC(B)* was determined using Eq. (2.7)

$$NC(B) = \frac{c_B}{f_B} \tag{2.7}$$

where $c_B$ is the TCLP leachate concentration of B and $f_B$ is the mass fraction of boron in the unaltered glass.

The TCLP results are discussed in Section 3.9.

## 2.13 Refractory Corrosion Test

The Monofrax K-3 refractory corrosion test was performed using a crucible-scale test method based on ASTM-C621-09 with minor modifications of crucible size and coupon size. The setup is shown in Figure 2.6. K-3 test coupons were cut from K-3 refractory slabs into 1-cm × 1-cm × 11-cm coupons. A notch was cut on the top end of the coupons to denote face 'A-A'. Each coupon was mounted with the crucible lid made by castable alumina (RESCOR™ CER- CAST CERAMIC 780, Cotronics Corp., Brooklyn, New York) with a 1-cm × 1-cm slot in the center. The test coupon was inserted into a Pt crucible with crushed glass. The loaded crucible was heated in a furnace and the K-3 test coupon was submerged into a static glass melt at 1150 °C or 1200 °C for 3 or 7 days. Following the 3- or 7-day test, the coupons were removed from the glass melt for characterization.

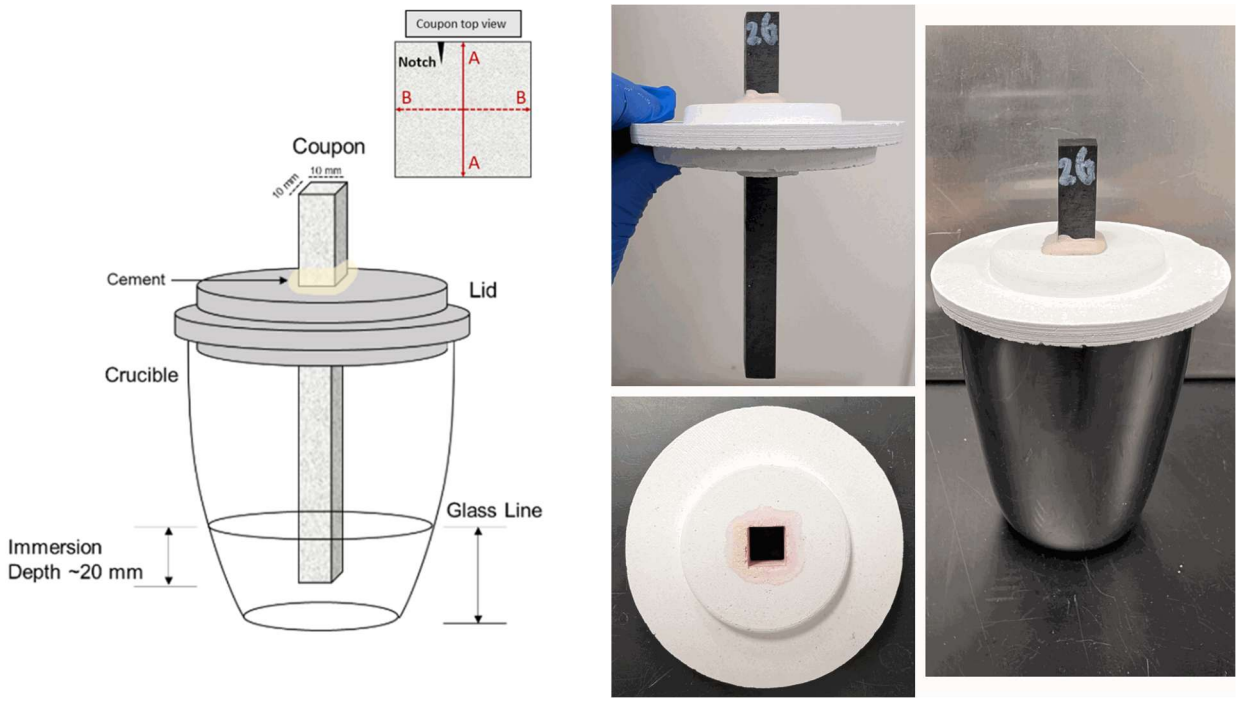


Figure 2.6. K-3 corrosion test setup in a static glass melt showing general measurements for coupon size and positioning, glass depth, and coupon immersion depth.

Both pre-test and post-test coupons were scanned by Zeiss Xradia Versa 610 micro-computed tomography (micro-CT) (Carl Zeiss Microscopy GmbH, Jena, Germany). As shown in Figure 2.7, the coupons were mounted in 3D printed plastic sample holders. Up to four coupons were bundled to fit in the scanning volume. Each single scan covers a cylindrical volume ~ 4-cm tall and 4-cm in diameter; three to five scans were conducted vertically to cover a 6-10 cm length. (Single scans must be partially overlapped for stitching.) Voxel size was set to 0.04 mm. A certified volume standard was used to verify the voxel size of the micro-CT measurement.

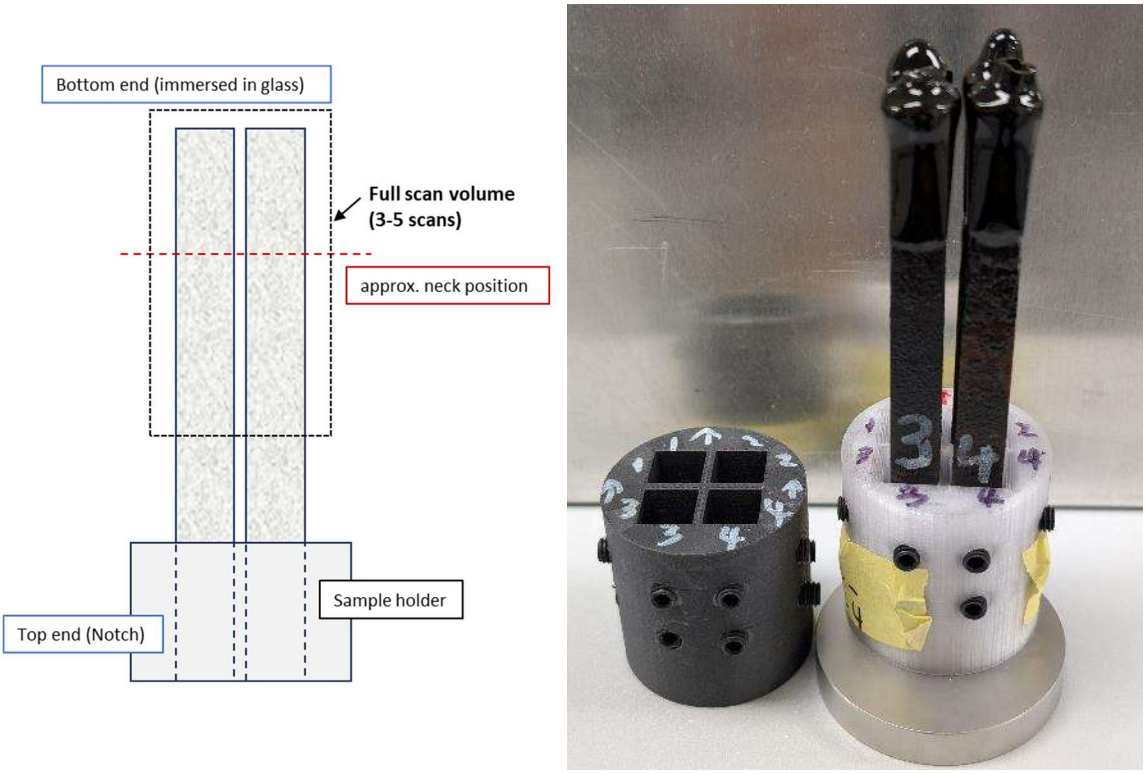


Figure 2.7. Samples for micro-CT scan.

The K-3 corrosion was calculated by dimension changes of the coupons after crucible tests in glass melts. As shown in Figure 2.8, the micro-CT scan produces a "stack" of X-ray images, which can be reconstructed to a 3D object for each sample. The 3D object can be sliced from different angles for analysis. Each coupon was scanned twice by micro-CT, pre-test and post-test. The data, two stacks of images, was adjusted and aligned for analysis. Each image stack contains a 50-mm-long section of coupon (1250 slices × 0.04 mm = 50 mm; each slice is one voxel thick, 0.04 mm), with each slice set to 12 mm × 12 mm (300 × 300 pixel, where pixel size is the same as voxel size for the 2D images). The pre-test and post-test image stacks of the same sample were aligned by matching the slices with visible features (grain sizes, pores, etc.), i.e., the same slice number in the pre- and post-test image stacks should have corresponded to the same position on the sample.

After adjusting and aligning, each slice was converted to a binary outline image and then a bounding rectangle of the outline. Adjustment of contrast of the X-ray images was necessary to draw the outline of the post-test coupons to separate the glass and the K-3, which are of different brightness in the X-ray images. After generating the stack of outlines from the X-ray image stack, a stack of bounding rectangles was generated from the stack of outlines (Figure 2.8). A data set was generated by measuring the dimensions of the A-A and B-B directions of the bounding rectangles: $G_A(i)$ and $G_B(i)$, the dimensions of the A-A and B-B directions of the *i*th slice of the pre-test stack; $g_A(i)$ and $g_B(i)$, the dimensions of the A-A and B-B directions of the *i*th slice of the post-test stack ($i$ = 1–1250). The dimension change or corrosion depth ($d_{corr}$) of each slice was calculated by:

$$d_{corr,_A}(i) = \frac{G_A(i) - g_A(i)}{2} \quad (2.8)$$

$$d_{corr,_B}(i) = \frac{G_B(i) - g_B(i)}{2} \quad (2.9)$$

The maximum corrosion depth along the coupon is the neck corrosion depth ($d_{neck,A}$ and $d_{neck,B}$) and the average neck corrosion ($d_{neck}$) of the A and B side were calculated by:

$$d_{neck,_A} = MAX[d_{corr,_A}(i)] = MAX[\frac{G_A(i) - g_A(i)}{2}] \quad (2.10)$$

$$d_{neck,_B} = MAX[d_{corr,_B}(i)] = MAX[\frac{G_B(i) - g_B(i)}{2}] \quad (2.11)$$

$$d_{neck} = \frac{d_{neck,_A} + d_{neck,_B}}{2} \quad (2.12)$$

The refractory corrosion results are discussed in Section 3.10.

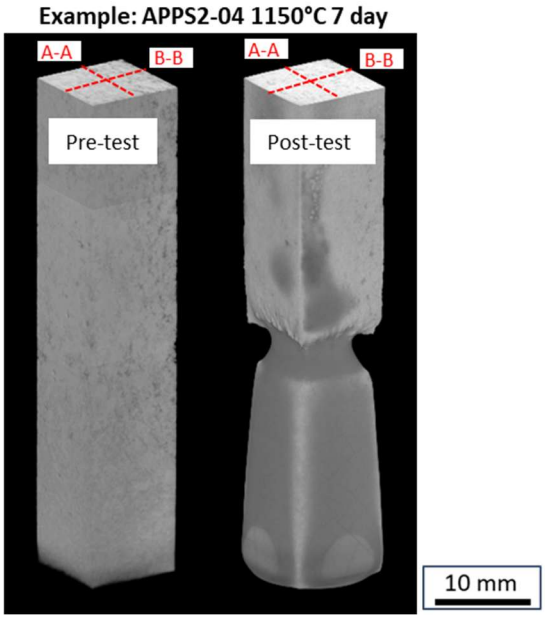


(a)

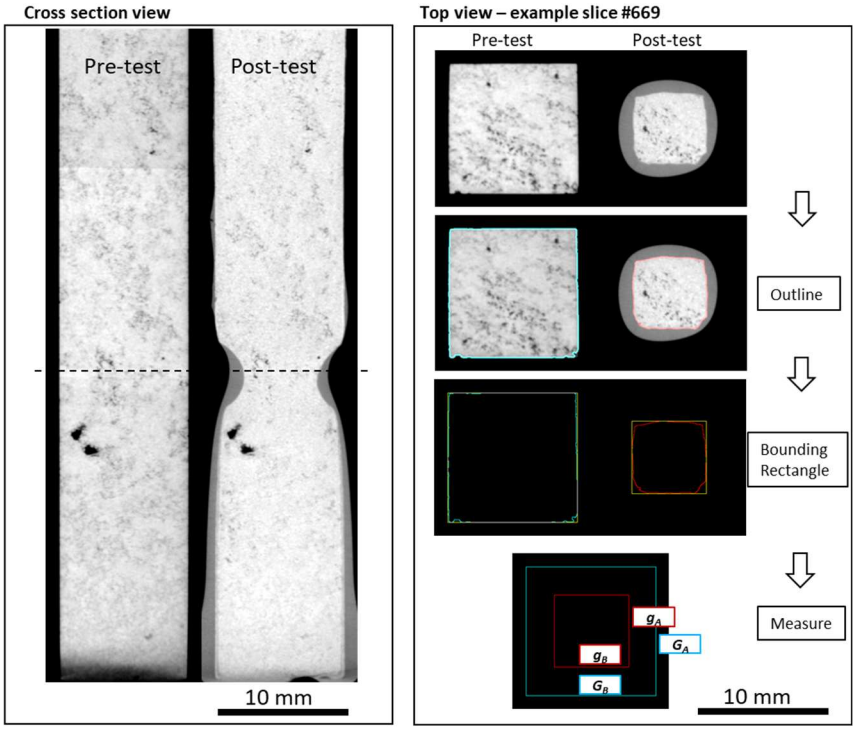


(b) (c)

Figure 2.8. Procedure of measuring refractory corrosion using micro-CT scanning images. The brighter material is the K-3 phase and the darker material is the glass remaining on the coupon surface after test. (a) 3D view of an example coupon APPS2-04 1150 °C 7 d, with the pre- and post-test scans aligned for analysis. (b) Cross section view showing the slices stacking from top to bottom; the dashed line shows the location of the example slice for dimension measurement. (c) An example top-view slice for measurement.

# 3.0 Results and Discussion

This section describes the results for the chemical composition, CCC, CF and $T_L$, sulfur solubility, density, viscosity, EC, PCT, TCLP, and K-3 refractory corrosion.

## 3.1 Glass Composition

In general, the glass colors of the 1-kg and 2-kg batches were similar. However, the colors of the APPS2-03 (Appendix A, Figure A.3) and APPS2-12 (Figure A.12) glasses were significantly different between the 1-kg and 2-kg batches. However, the glass compositions of both batches for APPS2-03 and APPS2-12 were similar with EPMA analysis. There is no explanation for this at this time.

The target and EPMA measured compositions of APPS2 glasses (1-kg and 2-kg batches) in wt% are provided in Appendix B. For 1-kg batches, the EPMA results showed that the sums of measured oxides for all glasses were between 94.8 and 102.0 wt% assuming the target $Li_2O$ wt%, indicating acceptable recovery of the glass components. For the 2-kg batches, the EPMA results showed that the sums of measured oxides for all glasses were between 90.4 and 105.3 wt%, including the target Li wt%.

A summary of the EPMA results is listed below:

- The RPD values of the main components, including $Al_2O_3$, $Na_2O$, and $SiO_2$, were generally less than 10% for both 1-kg and 2-kg batches.
- The RPD values of Cl were in the range of -15.8% to -39.4% for 1-kg batches and 19.4% to -34.4% for 2-kg batches. The RPD value of 19.4% was observed in the APPS2-13 2-kg sample with a low target Cl mass of 0.08 wt% and a measured mass of 0.10 wt%, which was near the EPMA detection limit, introducing more measurement error.
- The RPD values of F were in the range of -5.8% to -97.6% for 1-kg batches. The high RPD value of -97.6% was observed due to the low F target value of 0.1 wt%, which was near the detection limit.
- For 1-kg batches, 11 APPS2 glasses had 81% to 98% retention of $SO_3$, and the other five glasses had 67 to 77% retention. Among the glasses with lower $SO_3$ retention values, four glasses were melted three times with the third melt at 1200 °C, and one was melted two times at 1150 °C.
- For 2-kg batches, 10 APPS2 glasses had 80% to 96% retention of $SO_3$; five glasses had 63% to 76% retention. APPS2-05 with a low target $SO_3$ value of 0.053 wt% showed 123% retention due to higher error near the EPMA detection limit.

Relatively high fluctuation of RPD values for Cl and F was due to either their volatilities during the melting process or their concentrations being near detection limits. Eight glasses were melted three times (APPS2-01, -03, -07, -08, -09, -14-1, -15, and -16), with the third melt at 1200 °C for six of them (APPS2-01, -03, -07, -09, -14-1, and -16) due to the presence of undissolved particles and crystals, and this process could increase the volatilities of Cl and F. More than half of glasses (both 1-kg and 2-kg batches) showed higher MgO due to impurities in the raw materials used to batch the glasses. These inconsistencies in RPD are also likely due to the instrument uncertainties near the detection limits.

### 3.1.1 Secondary Phase Investigation in Quenched Glasses

The refined XRD patterns with crystalline phase wt% are provided in Appendix C. Eleven glasses were fully amorphous. Five glasses listed in Table 3.1 showed the presence of crystalline phases, and the normalized wt% values of crystalline phases are provided. The normalized wt% was calculated using Eq. (3.1), where *P* is the phase wt%, *C* is the standard crystallinity of 51.28%, and *S* is the added standard wt%:

$$\text{Normalized wt\% of a Phase} = \frac{P \times C}{100 - S} \tag{3.1}$$

APPS2-03, APPS2-08, and APPS2-12 contained spinel phases of $Al_{1.898}Fe_{1.102}O_4$, $Fe_3O_4$, and $ZnAlO_4$, respectively. The structures of these spinel phases are shown in Figure 3.1. With small amounts of spinel phases in the glasses, only two small peaks from diffraction of (h k l) planes (2 2 0) and (3 1 1) were present in the XRD patterns. Different elements in the spinel phases affect the unit cell parameters and shifts in peak positions, but it is still difficult to identify the chemistries of spinel phases solely based on XRD analysis. The +2 sites of spinel crystals can be occupied by either +2 or +3 cations, including Al, Cr, Ni, Fe, Mg, Mn, Zn, and others, whereas +3 sites are only occupied by +3 cations. Glass APPS2-10 showed the presence of $Cr_2O_3$, and APPS2-14-1 contained $ZrO_2$. Note that APPS2-10 contained the highest amount $Cr_2O_3$ in the target composition (1 wt%), whereas other 15 glasses had 0.1 to 0.6 wt% $Cr_2O_3$. APPS2-14-1 contained the second highest amount of $ZrO_2$ (9.1 wt%) for the target composition after APPS2-05 (9.3 wt%). The presence of $ZrO_2$ was not observed in the APPS2-05 glass. Overall, 15 out of 16 glasses were either fully amorphous or contained an amorphous fraction of > 99 wt%. Glass APPS2-08 had the highest crystalline wt% at 2.4% $Fe_3O_4$. It also had the highest iron fraction, with a target of 12.1 wt% $Fe_2O_3$.

Table 3.1. Crystalline phases and normalized wt% in quenched APPS2 glasses.

| Glass ID | Crystalline Phase | Normalized wt% |
|---|---|---|
| APPS2-01 | None | - |
| APPS2-02 | None | - |
| APPS2-03 | $Al_{1.898}Fe_{1.102}O_4$ | 0.28 |
| APPS2-04 | None | - |
| APPS2-05 | None | - |
| APPS2-06 | None | - |
| APPS2-07 | None | - |
| APPS2-08 | $Fe_3O_4$ | 2.40 |
| APPS2-09 | None | - |
| APPS2-10 | $Cr_2O_3$ | 0.52 |
| APPS2-11 | None | - |
| APPS2-12 | $ZnAlO_4$ | 0.85 |
| APPS2-13 | None | - |
| APPS2-14-1 | $ZrO_2$ | 0.93 |
| APPS2-15 | None | - |
| APPS2-16 | None | - |

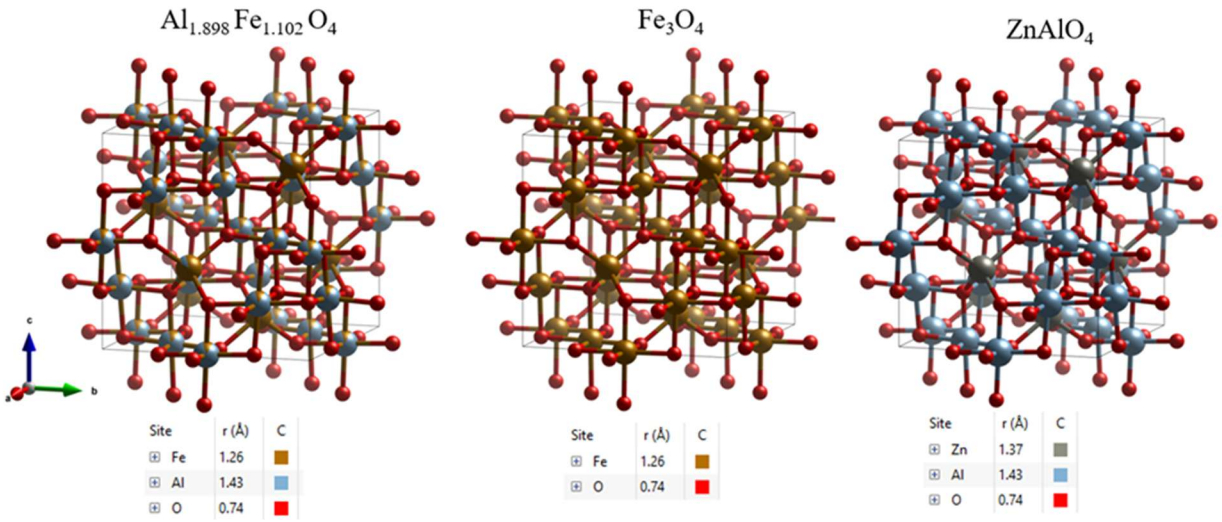


Figure 3.1. Structures of spinel phases in APPS2 glasses.

## 3.2 Crystal Identification in Canister Centerline Cooling Glasses

The slow cooling of the molten glass in the canister core might impact glass durability by changing the residual glass composition (Kim et al. 1995; Kroll et al. 2019). Not all crystals affect durability in the same way, so identifying the crystal content after CCC is an important step toward understanding crystallization impacts on glass durability. Moreover, property-prediction models were formulated using quenched data; therefore, differences of glass durability responses after CCC via PCT and TCLP should be evaluated.

This section presents and discusses the crystal content and phase identification from CCC glasses obtained using the methods discussed in Section 2.5. The effects of CCC on PCT and TCLP are reported in Sections 3.8 and 3.9, respectively.

A total of 7 out of 16 glasses were shown to be amorphous by XRD analysis after CCC. Of the remaining glasses, two had a crystal content ≤ 1 wt%, three had a crystal content ≤ 4 wt%, and the rest presented a crystal content > 4 wt%. XRD analysis identified a range of different crystal phases. The XRD crystal phases and amounts are summarized in Table 3.2.

Table 3.2. Crystal fraction in normalized wt% and identification of crystals by XRD in CCC glasses.

| Glass ID | wt% Crystallinity | Crystal Phase Identification |
|---|---|---|
| APPS2-01 | -- | None |
| APPS2-02 | 0.3 | $SiO_2$ |
| APPS2-03 | 4.9 | Spinel ($Al_{1.898}$ $Fe_{1.102}$ $O_4$) |
| APPS2-04 | -- | None |
| APPS2-05 | -- | None |
| APPS2-06 | 0.8 | Aluminum oxide ($Al_2O_3$) |
| APPS2-07 | -- | None |
| APPS2-08 | 3.9 | Magnetite ($Fe_3O_4$) |
| | 0.6 | Apatite ($Ca_{10}(PO_4)_6(Cl_{0.24}F_{1.9})$) |
| APPS2-09 | 2.7 | Spinel ($NiFe_2O_4$) |
| | 1.4 | Apatite ($Ca_{10}(PO_4)_6(Cl_{0.24}F_{1.9})$) |
| APPS2-10 | 8.1 | Nepheline ($Na_{6.8}(Al_{6.3}Si_{9.7}O_{32})$) |
| APPS2-11 | -- | None |
| APPS2-12 | 3.2 | Spinel ($ZnAlO_4$) |
| APPS2-13 | -- | None |
| APPS2-14-1 | 2.0 | Baddeleyite ($ZrO_2$) |
| | 1.1 | Spinel ($NiFe_2O_4$) |
| APPS2-15 | 1.5 | Sodium aluminium phosphate ($Na_{2.925}Al_{0.025}(PO_4)$) |
| APPS2-16 | -- | None |

-- = not measured

One glass (APPS2-10) formed > 8 wt% of nepheline. The most commonly detected crystal phase across all compositions after CCC was spinel (APPS2-03, -09, -12, and -14-1). Three chemical compositions of spinel were identified: $Al_{1.898}$ $Fe_{1.102}O_4$, $ZnAl_2O_4$, and $NiFe_2O_4$, of which $NiFe_2O_4$ was detected in glasses APPS2-09 and -14-1. Magnetite (a spinel) was found in glass APPS2-08, which had the highest $Fe_2O_3$ content of any composition in this matrix. Glasses APPS2-08, -09, and -15 contained some form of phosphate phase. These glasses contained the highest amount of phosphate among the compositions selected for APPS2.

Images of glasses after CCC and XRD scans when applicable are included in Appendix D.

## 3.3 Crystal Fraction and Liquidus Temperature

The long idling of the melter at low temperatures (~950 °C) might promote crystal formation, impacting glass processability by settling in the melter, clogging the pour spout (Vienna et al. 2001). One current constraint is < 2 vol% crystallinity at 950 °C ($C_{950}$). Therefore, the study of crystalline phases, quantities, and $T_L$ in isothermal heat-treatments is part of the regular investigation of HLW glasses. This section presents and discusses the CF, $T_L$, and $C_{950}$ results obtained using the methods discussed in Section 2.6.

The majority of the glasses have a $T_L$ below 900 °C, and only six have a $T_L$ above 950 °C. Table 3.3 summarizes the temperatures run, CF (wt%), phases identified, and $T_L$ and $C_{950}$ values. Note that $T_L$ is calculated based on the primary phase only.

Table 3.3. Crystal fraction in normalized wt%, identification of crystals, and $T_L$ for isothermally heat-treated glasses.

| Glass ID | Temp (°C) | CF (wt%) | Crystal Phase Identification | $T_L$ (°C) | $C_{950}$, vol% |
|---|---|---|---|---|---|
| APPS2-01 | 750 | 0 | None | <750 | 0 |
| | 900 | 0 | | | |
| APPS2-02 | 750 | 0 | None | < 750 | 0 |
| | 825 | 0 | | | |
| | 900 | 0 | | | |
| | 1050 | 0 | | | |
| APPS2-03 | 900 | 3.7 | Spinel ($Al_{1.898}$ $Fe_{1.102}$ $O_4$) | 1153 | 1.82 |
| | 1050 | 1.3 | Spinel ($Al_{1.898}$ $Fe_{1.102}$ $O_4$) | | |
| | 1125 | 0.6 | Spinel ($Al_{1.898}$ $Fe_{1.102}$ $O_4$) | | |
| APPS2-04 | 750 | 0 | None | < 750 | 0 |
| | 900 | 0 | | | |
| | 1050 | 0 | | | |
| APPS2-05 | 750 | 0 | None | <750 | 0 |
| | 900 | 0 | | | |
| APPS2-06 | 750 | 1.1, 0.3 | Nosean ($Na_8(Al_6Si_6O_{24})(SO_4)$), Apatite ($Ca_{10}(PO_4)_6(Cl_{0.24}F_{1.9})$) | 750<$T_L$<825 | 0 |
| | 825 | 0 | | | |
| | 900 | 0 | | | |
| | 1050 | 0 | | | |
| APPS2-07 | 750 | 0 | None | <750 | 0 |
| | 900 | 0 | | | |
| APPS2-08 | 750 | 3.7, 2.4, 2.5 | Magnetite ($Fe_3O_4$), Apatite ($Ca_{10}(PO_4)_6F_2$), Hematite ($Fe_2O_3$) | 1253 | 1.30 |
| | 850 | 3.7, 0.9 | Magnetite ($Fe_3O_4$), Apatite ($Ca_{10}(PO_4)_6F_2$) | | |
| | 900 | 2.7 | Magnetite ($Fe_3O_4$) | | |
| | 1050 | 1.9 | Magnetite ($Fe_3O_4$) | | |
| | 1125 | 1.9 | Magnetite ($Fe_3O_4$) | | |
| | 1200 | 3.6 | Magnetite ($Fe_3O_4$) | | |
| APPS2-09 | 750 | 2.3, 1.7 | Spinel ($NiFe_2O_4$), Monazite ($NdPO_4$) | 1210 | 0.72, 1.38 |
| | 900 | 1.6. 2.8 | Spinel ($NiFe_2O_4$), Monazite ($NdPO_4$) | | |
| | 950 | 1.4, 2.8 | Spinel ($NiFe_2O_4$), Monazite ($NdPO_4$) | | |
| | 1050 | 0.9 | Spinel ($NiFe_2O_4$) | | |
| | 1125 | 0.3 | Spinel ($NiFe_2O_4$) | | |
| APPS2-10 | 750 | 0.5 | Eskolaite ($Cr_2O_3$) | 1010 | 0.16 |
| | 850 | 0.5 | Eskolaite ($Cr_2O_3$) | | |
| | 900 | 0.4 | Eskolaite ($Cr_2O_3$) | | |
| | 1000 | 0.2 | Eskolaite ($Cr_2O_3$) | | |
| | 1050 | 0 | None | | |
| APPS2-11 | 750 | 0 | None | <750 | 0 |
| | 900 | 0 | | | |
| APPS2-12 | 900 | 2.7 | Spinel ($ZnAl_2O_4$) | 1242 | 1.33 |
| | 1050 | 1.4 | Spinel ($ZnAl_2O_4$) | | |
| | 1125 | 0.8 | Spinel ($ZnAl_2O_4$) | | |
| | 1200 | 0.5 | Spinel ($ZnAl_2O_4$) | | |
| APPS2-13 | 750 | 0 | None | <750 | 0 |
| | 900 | 0 | | | |
| APPS2-14-1 | 825 | 2.7, 1.0 | Baddeleyite ($ZrO_2$), Spinel ($NiFe_2O_4$) | 1682 | 1.10, 0.28 |
| | 900 | 2.5, 0.8 | Baddeleyite ($ZrO_2$), Spinel ($NiFe_2O_4$) | | |
| | 1050 | 2.2, 0.2 | Baddeleyite ($ZrO_2$), Spinel ($NiFe_2O_4$) | | |
| | 1200 | 1.6 | Baddeleyite ($ZrO_2$) | | |
| | 1400 | 1.0, 1.1 | Baddeleyite ($ZrO_2$), Spinel ($NiFe_2O_4$) | | |
| APPS2-15 | 750 | 1.9 | Sodium aluminum phosphate ($Na_{2.925}Al_{0.025}$ ($PO_4$)) | 900<$T_L$<950 | 0 |
| | 825 | 0 | None | | |

| Glass ID | Temp (°C) | CF (wt%) | Crystal Phase Identification | $T_L$ (°C) | $C_{950}$, vol% |
|---|---|---|---|---|---|
| APPS2-16 | 900 | 1.8 | Parakeldyshite ($Na_2ZrSi_2O_7$) | 750<$T_L$<825 | 0 |
| | 950 | 0 | | | |
| | 1000 | 0 | None | | |
| | 1050 | 0 | | | |
| | 750 | 0.9 | Disodium Zincotrisilicate ($Na_2ZnSi_3O_8$) | | 0 |
| | 825 | 0 | | | |
| | 900 | 0 | None | | |
| | 1050 | 0 | | | |

Nine glasses were found to have no crystal phases present by XRD at 825 °C, and therefore the $T_L$ could be easily bound by < 825 °C.

For APPS2-08, the $T_L$ is based on $Fe_3O_4$ using 825, 900, and 1050 °C. This is due to redox issues causing phase increase at higher temperatures, and removing 750 °C gives a slope for "worst case" $T_L$ of 1253 °C. Also, 750 °C contains $Fe_2O_3$ and $Fe_3O_4$, which obscures evaluation of the main phase $Fe_3O_4$.

APPS2-03, -09, and -12 all have some form of spinel present, resulting in a $T_L$ > 1150 °C.

For APPS2-10, the $T_L$ value of 1009.5 °C, determined using a non-linear fit (Figure 3.2, left), is more accurate. The low $R^2$ value of 0.805 from the linear fit (Figure 3.2, right) indicates the linear $T_L$ value (1044.1 °C) is unsuitable due to poor trendline fitting.

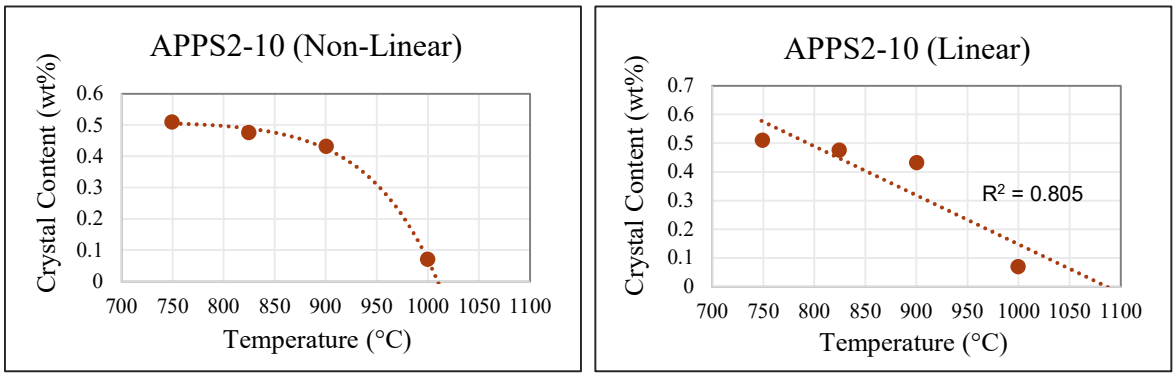


Figure 3.2. Non-linear and linear fits of crystal content in APPS2-10 glass.

For APPS2-14-1, a $T_L$ of 1681.5 °C was determined by a non-linear fit (Figure 3.3, left). This APPS2-14-1 composition has a reasonable $R^2$ value of 0.9927, indicating that the $T_L$ from a linear fit (1750.4 °C; Figure 3.3, right) is also reliable. However, the more closely fitting shape of the non-linear fit suggests that the non-linear value is more accurate. Also, spinel ($NiFe_2O_4$) is the secondary crystal formation present at all temperatures from 825 to 1400 °C (except for 1200 °C), but redox issues are suspected to cause issues with this phase. There was only 0.2 wt% $NiFe_2O_4$ in the 1050 °C sample, and 1200 °C had 0 wt% $NiFe_2O_4$; however, 1400 °C had 1.1 wt% $NiFe_2O_4$. Therefore, $ZrO_2$ was determined to be the better phase for determination of $T_L$. Regardless of the phase used, $T_L$ was greater than 1150 °C for this composition.

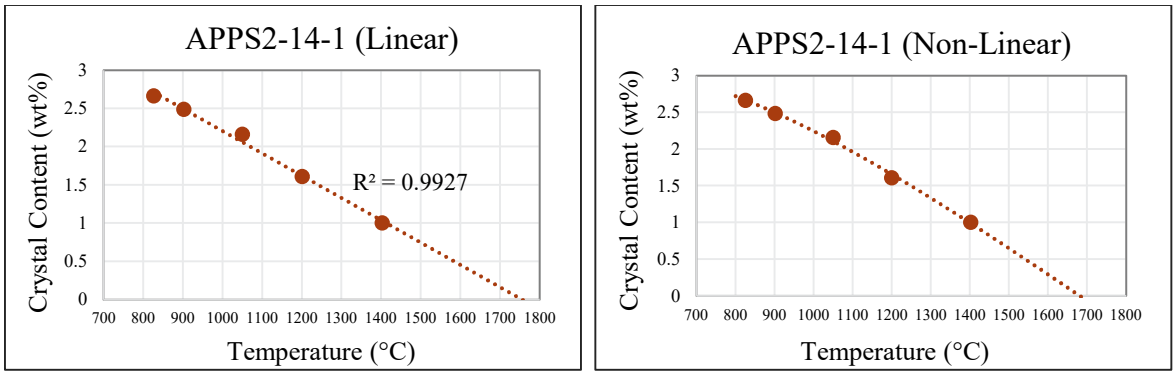


Figure 3.3. Non-linear and linear fits of crystal content in APPS2-14-1 glass.

APPS2-15 had an identified sodium aluminum phosphate phase ($Na_{2.92}Al_{0.025}(PO_4)$) at 750 °C, and no crystalline phases present at 825 °C. However, disodium zincotrisilicate ($Na_2ZnSi_3O_8$) appears at 900 °C. No crystalline phases were noted at 950 °C or above, leading to this composition being listed as 900 °C $<T_L<$950 °C.

Images of glasses after heat treatment and XRD scans when applicable are in Appendix E5.0Appendix E.

## 3.4 $SO_3$ Solubility

The $SO_3$ feed concentration is controlled to avoid salt formation that can cause excessive corrosion of melter materials at the melt-line. This section summarizes the sulfur-saturated melt (SSM) results from the APPS2 glasses and compares the predicted $SO_3$ solubilities from the 3TS model to the measured $SO_3$ solubilities.

### 3.4.1 SSM $SO_3$ Concentrations

The weight percent values of $SO_3$ in SSM and as-fabricated (quenched) samples from EPMA analysis are presented in Table 3.4. The SSM results (Figure 3.4) show that the $SO_3$ concentration of every APPS2 glass was higher in the SSM glass than the corresponding Q glass, as expected. The design of APPS2 glass compositions required that the predicted SSM $SO_3$ concentrations (Vienna et al. 2024) be 0.33 wt% below the target values to account for differences between solubility and melter tolerance.

Table 3.4. EPMA results on the $SO_3$ wt% in APPS2 glasses.

| Glass ID | SSM $SO_3$ (wt%) | Quenched $SO_3$ (wt%) |
|---|---|---|
| APPS2-01-SSM | 1.37 | 1.13 |
| APPS2-02-SSM | 1.20 | 0.28 |
| APPS2-03-SSM | 0.97 | 0.13 |
| APPS2-04-SSM | 1.38 | 1.19 |
| APPS2-05-SSM | 1.13 | 0.04 |
| APPS2-06-SSM | 1.85 | 1.45 |
| APPS2-07-SSM | 1.00 | 0.68 |
| APPS2-08-SSM | 0.98 | 0.28 |
| APPS2-09-SSM | 1.05 | 0.26 |
| APPS2-10-SSM | 0.65 | 0.23 |
| APPS2-11-SSM | 1.43 | 1.10 |
| APPS2-12-SSM | 1.03 | 0.13 |
| APPS2-13-SSM | 1.86 | 1.41 |
| APPS2-14-1-SSM | 0.69 | 0.09 |
| APPS2-15-SSM | 0.85 | 0.31 |
| APPS2-16-SSM | 1.14 | 0.11 |

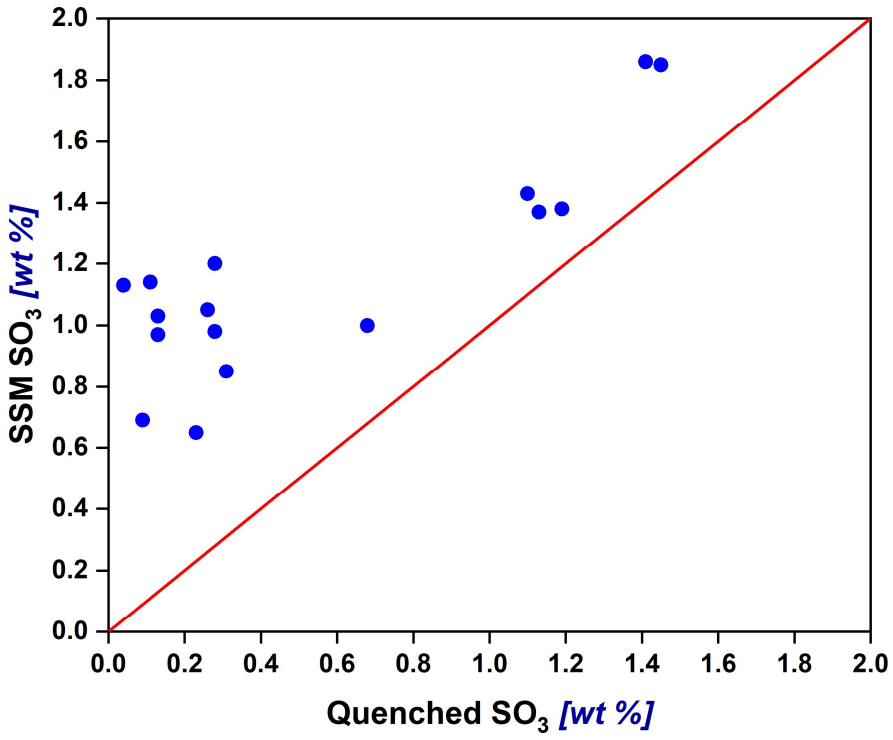


Figure 3.4. Measured $SO_3$ concentration in SSM and quenched glasses for the APPS2 matrix.

For 14 of the 16 APPS2 glasses, an excess sulfate phase was observed in all three melts, as seen in Figure 3.5 for APPS2-11 as an example. Two glasses, APPS2-08 and APPS2-09, showed no traces of salt phases on the surface (Figure 3.6). However, the salt phase was observed on the surfaces after the first and second melts for the APPS2-08 and APPS-09 glasses. Comparing the $SO_3$ values from EPMA

measurement and the 3TS model (EWG 2.5, Vienna et al. 2024), it is interesting to note that APPS2-08 and APPS-09 glasses have higher measured $SO_3$ values than predicted by the model, indicating that the maximum loading values are potentially higher than the model predicts as no salt phases were observed after the three melts. Among the 16 APPS2 glasses, APPS2-03, APPS-08, APPS-09, and APPS2-14-1 showed higher measured $SO_3$ values than the 3TS model predicted, whereas all other glasses showed lower-than-predicted $SO_3$ values.

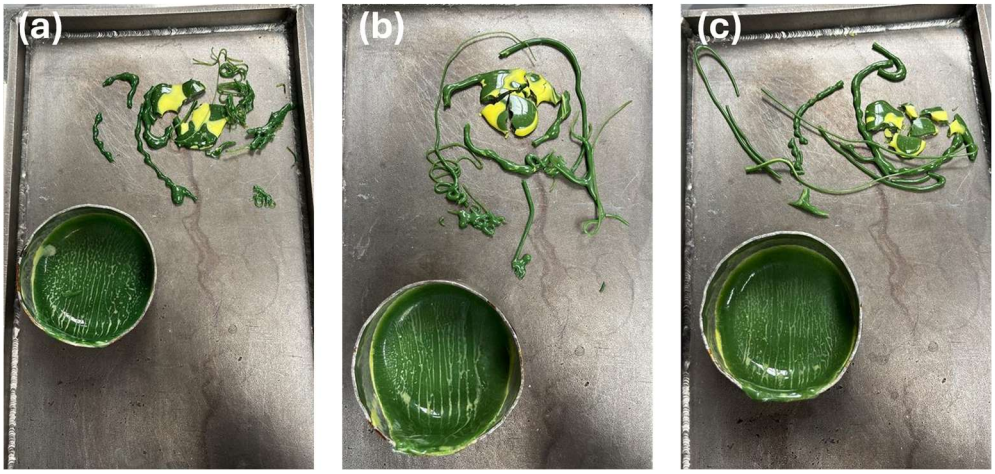


Figure 3.5. Photos of the (a) first, (b) second, and (c) third melts for APPS2-11.

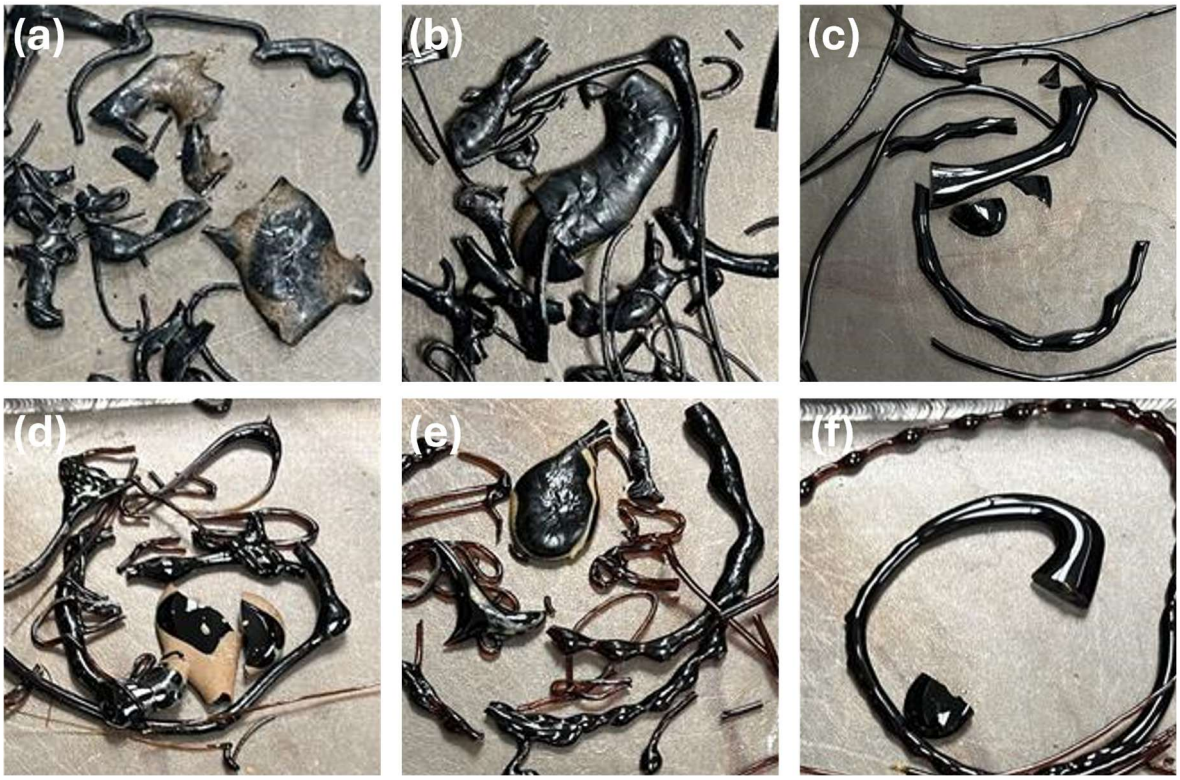


Figure 3.6. Photos of the (a) first, (b) second, (c) third melts of APPS2-08; photos of the (d) first, (e) second, and (f) third melts of APPS2-09.

### 3.4.2 Comparisons to Predicted $SO_3$ Saturation Concentrations

The $SO_3$ solubility values of APPS2 glasses from the 3TS prediction model (EWG 2.5, Vienna et al. 2024) and EPMA analysis were compared. Figure 3.7 is a plot of predicted $SO_3$ vs. measured $SO_3$ using 3TS, and Figure 3.8 is a plot of predicted $SO_3$ with an offset value of 0.33 wt% vs. measured $SO_3$. The plot with an offset value of 0.33 wt% was also included because Skidmore et al. (2019) showed that the 3TS measured values resulted in an average 0.33 wt% above the melter tolerance values of 13 glasses. The 90% prediction interval values were used as the error bars for the predicted values on y-axis, and 0.1548 wt% confidence value for 3TS measurements from a previous study (Gervasio et al. 2024) was used for the error bar for the measured values on the x-axis[1].

For the 3TS model (Figure 3.7), all the APPS2 glasses showed $SO_3$ predicted within the error bar range except the APPS2-10 glass. Overall, the predicted and measured $SO_3$ values were in good agreement, with 90% confidence.

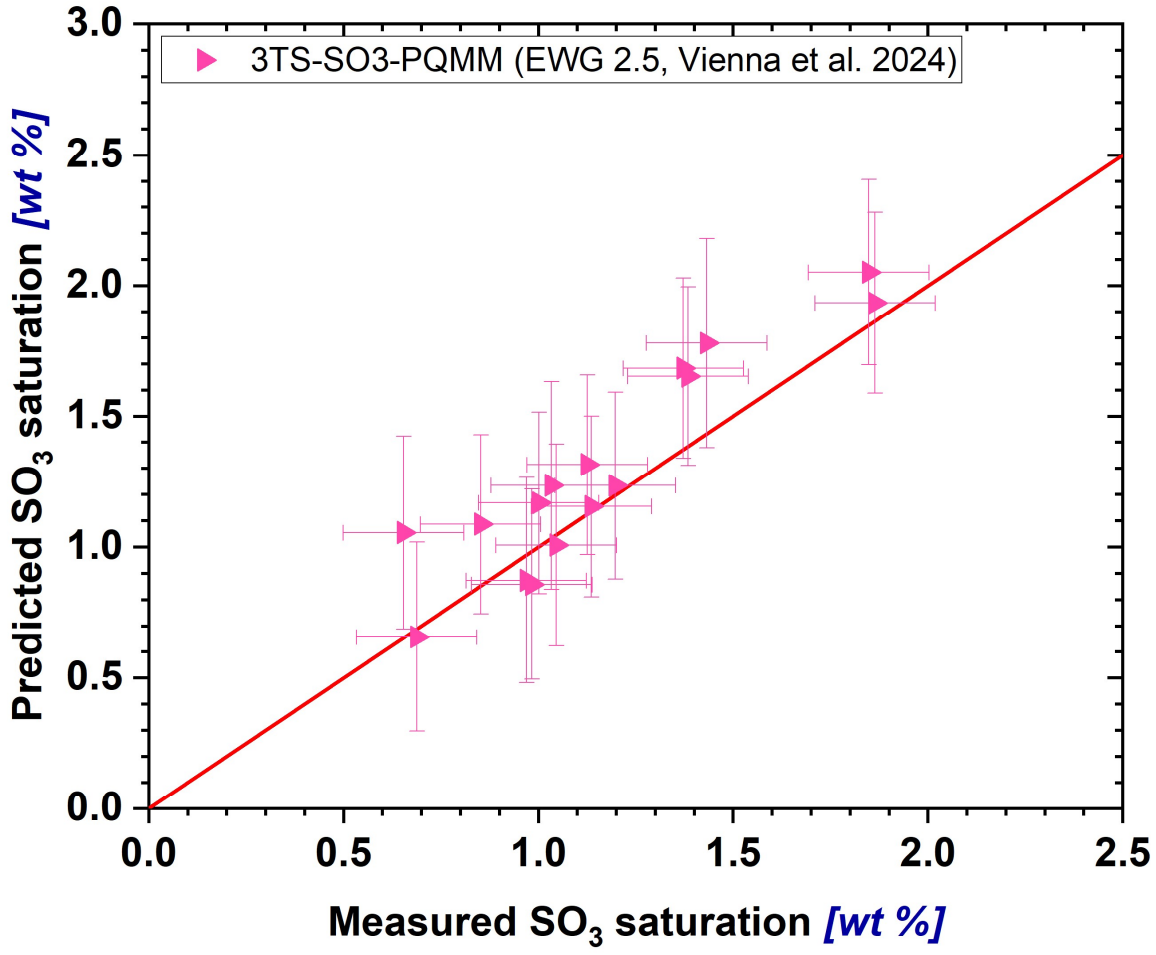


Figure 3.7. Predicted $SO_3$ vs. measured $SO_3$ of APPS2 glasses using 3TS model.

[1] The measurement uncertainty was based on replicate analyses using ICP-OES of 3TS SSM samples as no replicate measurements are available for EPMA analyses, although comparison of EPMA and ICP-OES shows excellent agreement.

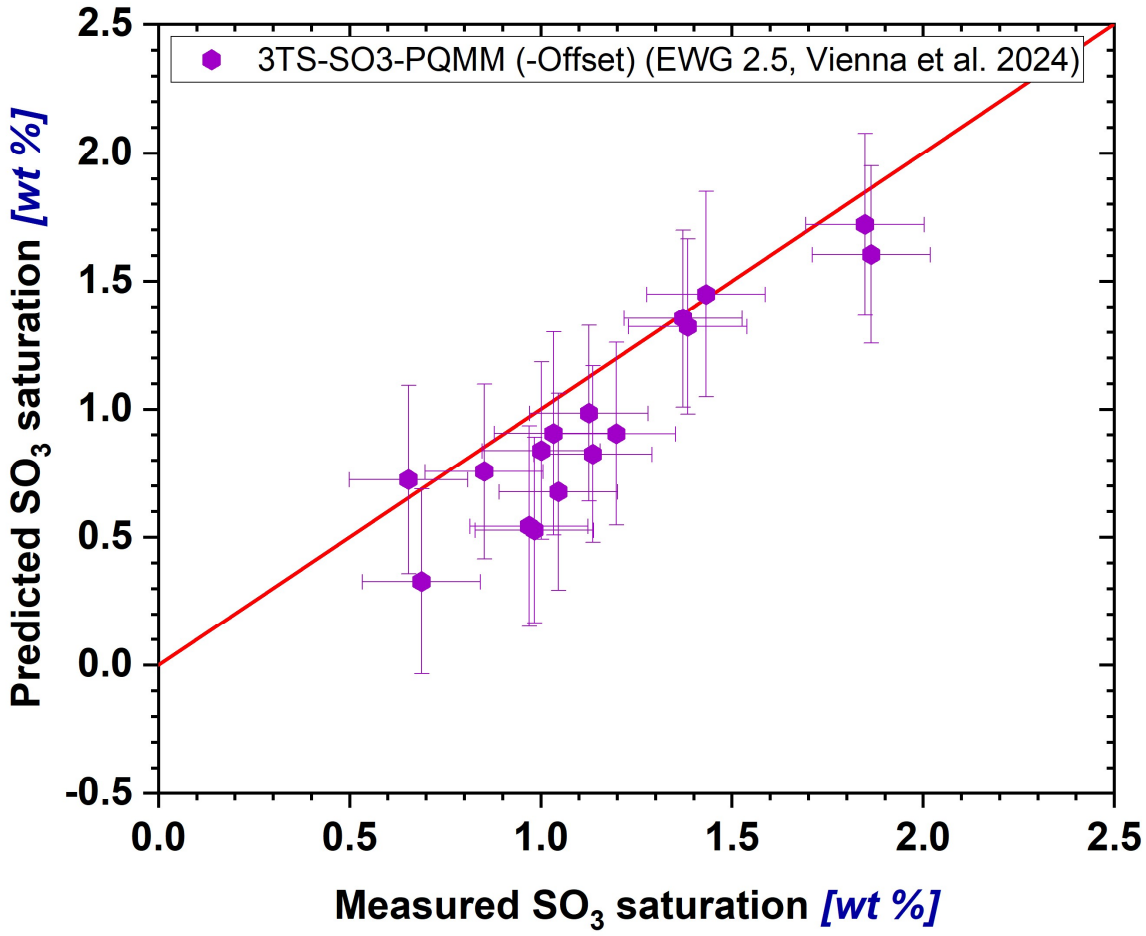


Figure 3.8. Predicted $SO_3$ with 0.33 wt% offset vs. measured $SO_3$ of APPS2 glasses using the 3TS model.

## 3.5 Density

Density measurements of the APPS2 glasses were obtained using the methods discussed in Section 2.8. The average of these density values is 2.59 g/cm$^3$, with a minimum of 2.44 g/cm$^3$ and a maximum of 2.71 g/cm$^3$ (Table 3.5).

Table 3.5. Measured densities of APPS2 glasses in g/cm$^3$.

| Glass ID | Measured Density (g/cm$^3$) | Glass ID | Measured Density (g/cm$^3$) |
|---|---|---|---|
| APPS2-01 | 2.63 | APPS2-09 | 2.51 |
| APPS2-02 | 2.50 | APPS2-10 | 2.46 |
| APPS2-03 | 2.49 | APPS2-11 | 2.65 |
| APPS2-04 | 2.65 | APPS2-12 | 2.44 |
| APPS2-05 | 2.71 | APPS2-13 | 2.64 |
| APPS2-06 | 2.53 | APPS2-14-1 | 2.65 |
| APPS2-07 | 2.68 | APPS2-15 | 2.67 |
| APPS2-08 | 2.67 | APPS2-16 | 2.66 |

The experimentally determined APPS2 glass densities were compared to predicted values based on models from Vienna et al. (2002) and the Hanford Tank Waste Operations Simulator (HTWOS) model (Vienna et al. 2009).

Figure 3.9 compares the values predicted by the models with the measured values. Predicted values from Vienna et al. (2002) are closer to measured values compared to values from the HTWOS model (Vienna et al. 2009). Based on the comparison, the Vienna et al. (2002) model should be used to predict the density of APPS2 glasses.

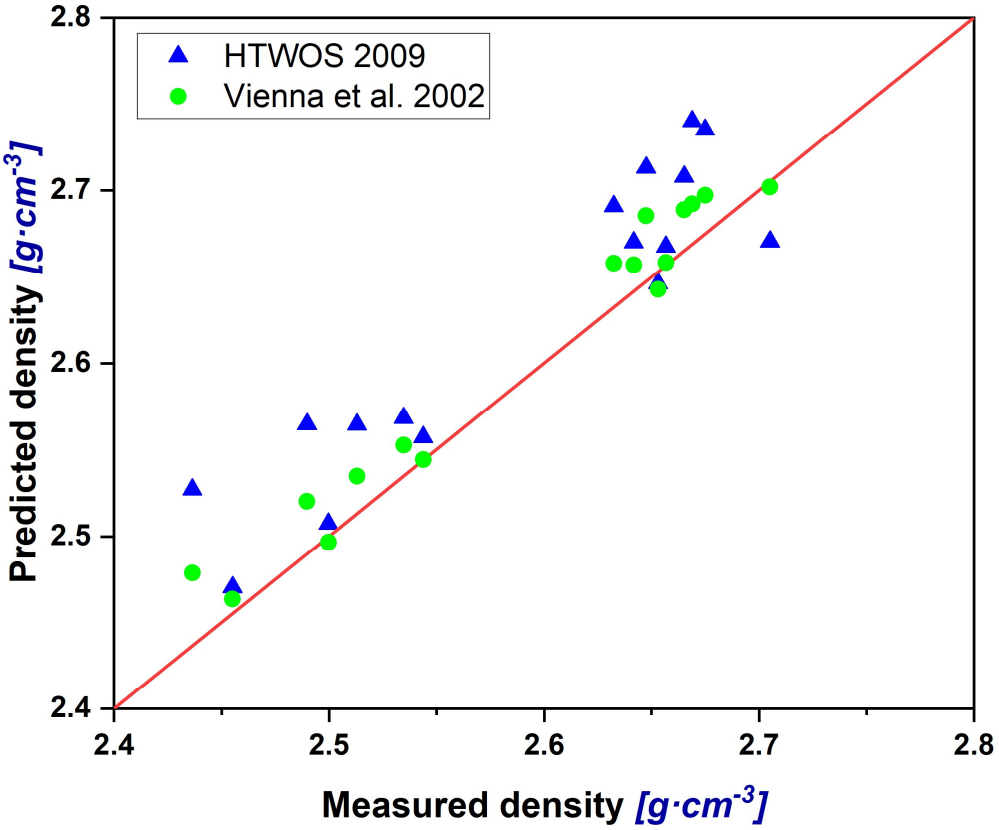


Figure 3.9. Measured and predicted densities for APPS2 glasses.

## 3.6 Viscosity

This section presents the viscosity results obtained using the methods discussed in Section 2.9. The results are summarized in Table 3.6 and individually reported in Appendix G. Note the reported temperatures are different than target temperatures listed in Section 2.9 because of a difference between the furnace control thermocouple and the viscosity measurement thermocouple.

Table 3.6. Measured ln η (Pa·s) values vs. target temperature (in the sequence of measurement).

| Target *T*, °C | 1155 | 1065 | 970 | 1155 | 1250 | 1155 |
|---|---|---|---|---|---|---|
| Glass ID | ln $\eta$ (Pa·s)[(a)] | ln $\eta$ (Pa·s)[(a)] | ln $\eta$ (Pa·s)[(a)] | ln $\eta$ (Pa·s)[(a)] | ln $\eta$ (Pa·s)[(a)] | ln $\eta$ (Pa·s)[(a)] |
| APPS2-01 | 1.588 | 2.407 | 3.436 | 1.586 | 0.939 | 1.620 |
| APPS2-02 | 1.380 | 2.053 | 2.958 | 1.336 | 0.790 | 1.378 |
| APPS2-03 | 1.958 | 2.813 | 3.839 | 1.970 | 1.251 | 1.977 |
| APPS2-04 | 1.540 | 2.324 | 3.310 | 1.490 | 0.812 | 1.477 |
| APPS2-05 | 1.263 | 2.134 | 3.296 | 1.214 | 0.509 | 1.250 |
| APPS2-06 | 1.142 | 1.849 | 2.771 | 1.131 | 0.536 | 1.146 |
| APPS2-07 | 1.766 | 2.574 | 3.581 | 1.773 | 1.136 | 1.788 |
| APPS2-08 | 2.268 | 3.647 | 5.195 | 2.411 | 1.316 | 2.194 |
| APPS2-09 | 1.980 | 3.030 | 4.537 | 1.968 | 1.187 | 1.927 |
| APPS2-10 | 1.643 | 2.349 | 3.314 | 1.602 | 0.994 | 1.617 |
| APPS2-11 | 1.321 | 2.148 | 3.221 | 1.337 | 0.646 | 1.431 |
| APPS2-12 | 1.977 | 2.864 | 3.907 | 2.045 | 1.305 | 2.035 |
| APPS2-13 | 1.358 | 2.100 | 3.042 | 1.348 | 0.701 | 1.368 |
| APPS2-14-1 | 1.621 | 2.628 | 3.658 | 1.580 | 0.740 | 1.598 |
| APPS2-15 | 1.432 | 2.318 | 3.473 | 1.450 | 0.719 | 1.484 |
| APPS2-16 | 1.557 | 2.247 | 3.174 | 1.496 | 0.904 | 1.512 |

(a) Average of three measurements.

The Arrhenius model was used to fit the viscosity-temperature data for each waste glass. The model form is the Arrhenius equation:

$$\ln(\eta) = A + \frac{B}{T_K} \tag{3.2}$$

where A and B are independent of temperature ($T_K$), which is in Kelvin (T(°C) + 273.15). For each glass, Table 3.7 provides the values for the A and B coefficients and summarizes the viscosity results at six target temperatures calculated using the Arrhenius equation [Eq. (3.2)].

Table 3.7. Fitted of Arrhenius coefficients and calculated η for specific temperatures.

| | Arrhenius Coefficients | | Temperature (°C) | | | | | |
|---|---|---|---|---|---|---|---|---|
| | A | B | 950 | 1050 | 1100 | 1150 | 1200 | 1250 |
| Glass ID | (ln Pa·s) | (ln Pa·s·K) | ln η [Pa·s] | | | | | |
| APPS2-01 | -10.5657 | 17431.8 | 3.688 | 2.610 | 2.130 | 1.684 | 1.269 | 0.880 |
| APPS2-02 | -9.2065 | 15156.2 | 3.186 | 2.249 | 1.832 | 1.444 | 1.083 | 0.745 |
| APPS2-03 | -10.6086 | 18006.3 | 4.114 | 3.002 | 2.506 | 2.045 | 1.616 | 1.214 |
| APPS2-04 | -10.6597 | 17413.0 | 3.578 | 2.502 | 2.023 | 1.577 | 1.162 | 0.774 |
| APPS2-05 | -12.3448 | 19471.6 | 3.576 | 2.373 | 1.837 | 1.339 | 0.874 | 0.440 |
| APPS2-06 | -9.7651 | 15610.1 | 2.999 | 2.034 | 1.604 | 1.205 | 0.832 | 0.485 |
| APPS2-07 | -10.1298 | 17046.6 | 3.809 | 2.755 | 2.286 | 1.850 | 1.443 | 1.063 |
| APPS2-08 | -16.8009 | 27337.1 | 5.552 | 3.862 | 3.110 | 2.410 | 1.758 | 1.149 |
| APPS2-09 | -14.3149 | 23322.2 | 4.755 | 3.313 | 2.671 | 2.075 | 1.518 | 0.998 |
| APPS2-10 | -9.3851 | 15695.0 | 3.448 | 2.478 | 2.046 | 1.644 | 1.270 | 0.920 |
| APPS2-11 | -11.0634 | 17741.7 | 3.443 | 2.347 | 1.858 | 1.404 | 0.981 | 0.586 |
| APPS2-12 | -10.6356 | 18098.1 | 4.163 | 3.044 | 2.546 | 2.083 | 1.651 | 1.248 |
| APPS2-13 | -9.9588 | 16182.1 | 3.273 | 2.273 | 1.827 | 1.413 | 1.027 | 0.666 |
| APPS2-14-1 | -12.6185 | 20306.6 | 3.985 | 2.730 | 2.172 | 1.652 | 1.167 | 0.715 |
| APPS2-15 | -11.8938 | 19082.5 | 3.709 | 2.530 | 2.005 | 1.516 | 1.061 | 0.636 |
| APPS2-16 | -9.4521 | 15690.6 | 3.377 | 2.408 | 1.976 | 1.574 | 1.200 | 0.850 |

The $\eta_{1150}$ values interpolated from measured data are compared to predicted values. A list of example models for predicting viscosity is provided in Table 3.8.

Table 3.8. Available glass property models with predicted viscosity.

| Model Description | Units for Predicted Values | References |
|---|---|---|
| $\eta_{1150}$ for HLW | Pa·s | Vienna et al. (2009) |
| $\eta_T$ for HLW | Pa·s | Piepel et al. (2008) |
| $\eta_{1150}$ for HLW | Pa·s | Vienna et al. (2016) |
| $\eta_T$ for HLW (Global Model) | P | Kot et al. (2019) |
| $\eta_T$ for LAW | P | Heredia-Langner et al. (2022) |
| $\eta_{1150}$ for LAW | P | Vienna et al. (2022) |

Figure 3.10 displays two plots with a one-to-one comparison of measured and predicted viscosity expressed either in ln(η, Pa·s) or ln(η, P) using the models in Table 3.8.

All models present some scatter around the 45° line, which is more accentuated at higher viscosity values except for the Heredia-Langner et al. (2022) model. Most of the models underestimate the property (points below the 45° line in Figure 3.10, both plots). The models that appear to best predict the current matrix viscosity are the HTWOS model (Vienna et al. 2009), with less scatter but still conservative, and the Heredia-Langner et al. (2022) model, with one overpredicted outlier at low viscosity.

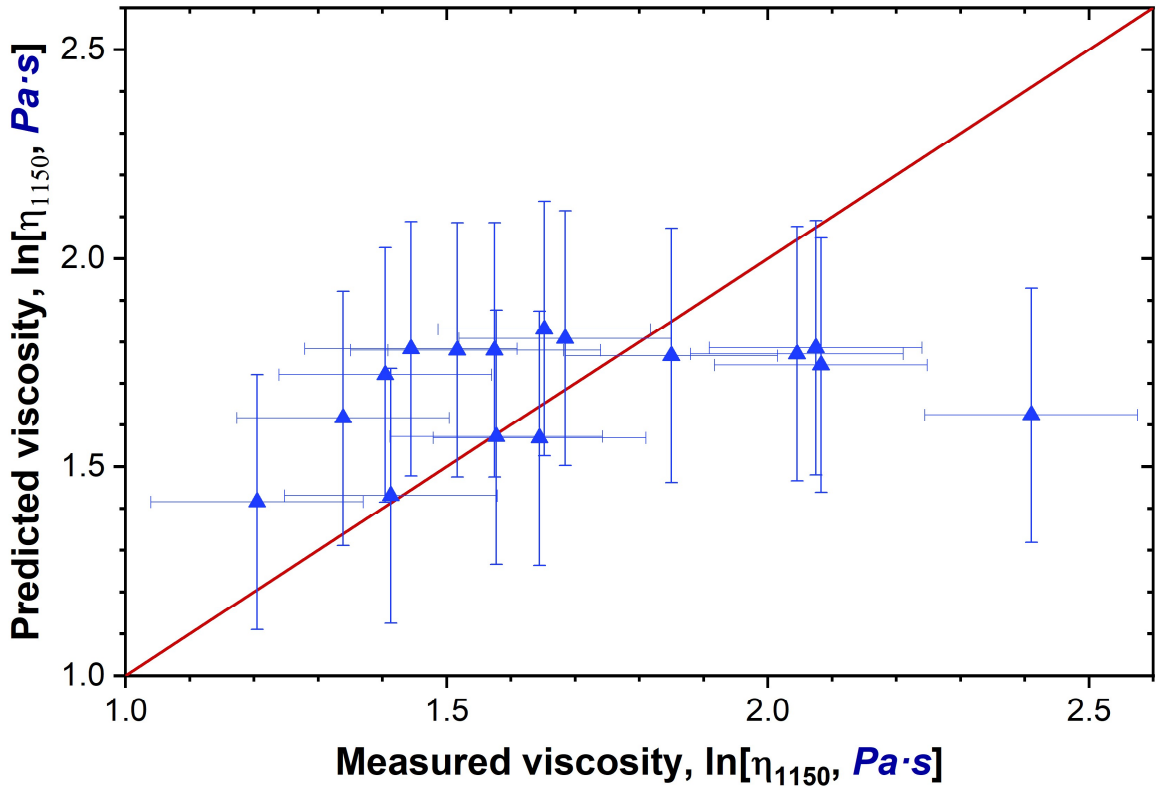


Figure 3.10. Measured vs. predicted ln($\eta_{1150}$) where model prediction for Pa·s is shown. Uncertainties for measured values are represented by $SD_{pooled}$ reported in Vienna et al. (2022).

## 3.7 Electrical Conductivity

This section presents the EC results obtained using the methods discussed in Section 2.10. The results are summarized in Table 3.9. Measured EC (S/m) values vs. temperatures are individually reported in Appendix H.

Table 3.9. Measured electrical conductivity (S/m) values vs. temperatures.

| Target *T*, °C | 950 | 1050 | 1150 | 1200 |
|---|---|---|---|---|
| Glass ID | | | | |
| APPS2-01 | 43.0 | 59.6 | 77.1 | 82.2 |
| APPS2-02 | 45.6 | 60.1 | 76.1 | 81.9 |
| APPS2-03 | 17.5 | 27.5 | 39.4 | 46.1 |
| APPS2-04 | 28.5 | 41.8 | 56.4 | 64.1 |
| APPS2-05 | 14.3 | 23.8 | 35.2 | 41.9 |
| APPS2-06 | 15.7 | 24.3 | 33.4 | 41.5 |
| APPS2-07 | 28.6 | 40.7 | 51.8 | 57.0 |
| APPS2-08 | 20.7 | 29.0 | 39.2 | NR |
| APPS2-09 | 10.8 | 17.3 | 21.6 | 24.5 |
| APPS2-10 | 20.8 | 33.0 | 41.0 | 44.0 |
| APPS2-11 | 14.5 | 23.9 | 35.0 | 43.3 |
| APPS2-12 | 15.9 | 24.0 | 32.9 | 37.2 |
| APPS2-13 | 29.2 | 43.2 | 57.7 | 64.4 |
| APPS2-14-1 | 21.0 | 31.6 | 42.2 | 48.1 |
| APPS2-15 | 30.4 | 44.3 | 59.0 | 66.4 |
| APPS2-16 | 28.0 | 39.5 | 51.9 | 57.9 |

The Arrhenius equation [Eq. (3.2)] was used to fit EC-temperature data for each waste glass. Arrhenius coefficients and calculated $\varepsilon_{1150}$ are reported in Table 3.10.

Table 3.10. Fitted coefficients of Arrhenius model for $\varepsilon_{1150}$.

| | Arrhenius Coefficients | | |
|---|---|---|---|
| Glass ID | A, ln[S/m] | B, ln[S/m]·K | $\varepsilon_{1150}$ (S/m) |
| APPS2-01 | 7.701 | -4804.1 | 75.6 |
| APPS2-02 | 7.334 | -4292.1 | 75.0 |
| APPS2-03 | 8.580 | -6984.7 | 39.3 |
| APPS2-04 | 8.143 | -5852.7 | 56.2 |
| APPS2-05 | 9.004 | -7746.4 | 35.2 |
| APPS2-06 | 8.340 | -3827.5 | 34.5 |
| APPS2-07 | 7.436 | -4971.9 | 51.5 |
| APPS2-08 | 7.580 | -5568.6 | 39.1 |
| APPS2-09 | 7.131 | -5758.3 | 21.9 |
| APPS2-10 | 7.481 | -5378.2 | 40.5 |
| APPS2-11 | 9.037 | -7774.8 | 35.6 |
| APPS2-12 | 7.797 | -6134.4 | 32.6 |
| APPS2-13 | 8.059 | -5710.3 | 57.2 |
| APPS2-14-1 | 7.936 | -5966.6 | 42.2 |
| APPS2-15 | 8.032 | -5633.7 | 58.7 |
| APPS2-16 | 7.635 | -5253.0 | 51.6 |

A comparison between measured and predicted values using the Vienna et al. (2024) model is shown in Figure 3.11.

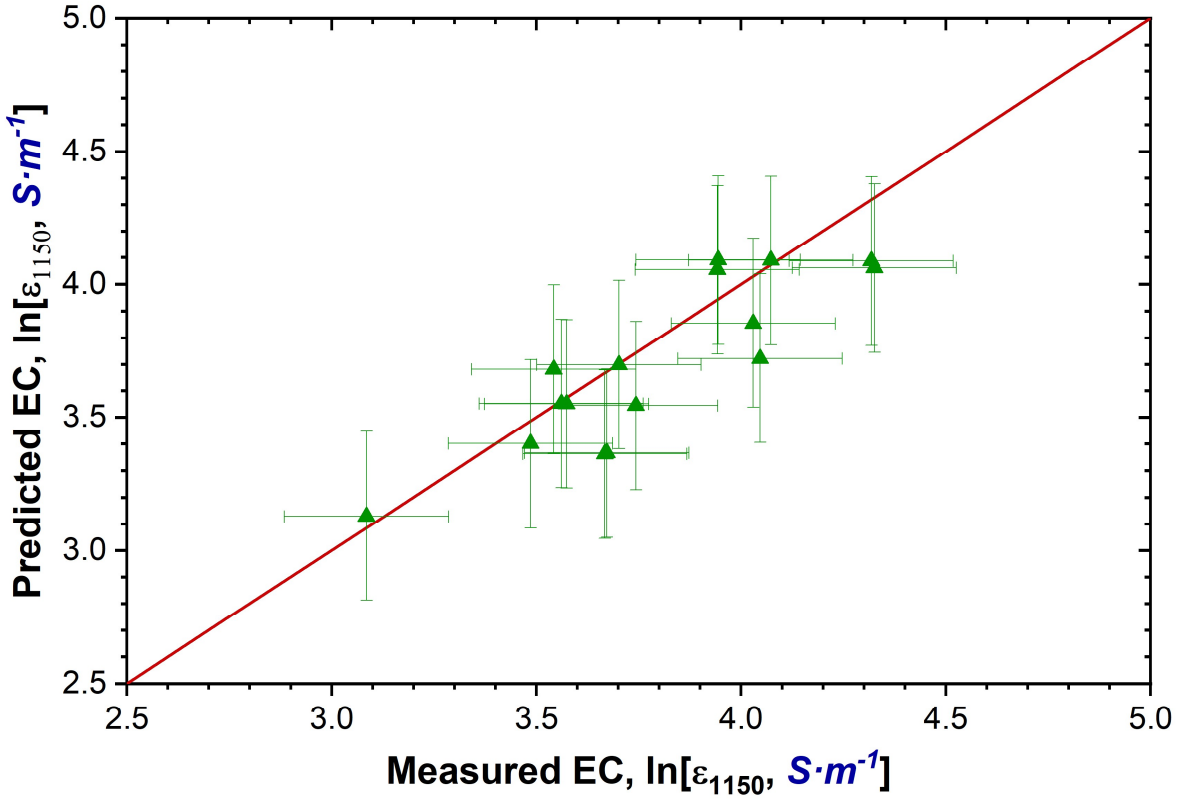


Figure 3.11. Measured vs. predicted $\ln(\varepsilon_{1150})$. Uncertainties for measured values are represented by $SD_{pooled}$ reported in Vienna et al. (2024).

Overall, there is good agreement between the predictions and measured values with data points sitting on both sides of the 45° line and most data points touching the line with the error bars. A few glasses are predicted to have lower conductivity than the measured value.

## 3.8 Product Consistency Test

This section presents the PCT results obtained using the methods discussed in Section 2.11. Data for the individual tests is provided in Appendix I.

Per the WTP contract (DOE 2000) and the Waste Acceptance Product Specification (DOE 1996), the $NC_B$, $NC_{Na}$, and $NC_{Li}$ values must be below the associated values of the DWPF Environmental Assessment (EA) glass, which are presented in Table 3.11. The average normalized concentrations ($NC_i$) for B, Na, Si, and Li for Q and CCC glass are reported in Table 3.12 and Table 3.13. No glasses exceed the contract limits for the Q glasses, and the only glass that exceeds the limits for CCC is APPS2-10. This is unsurprising as the CCC sample for this glass contains 8.1wt% nepheline (Table 3.2). Table 3.12 and Table 3.13 do not provide $NC_{Li}$ values for APPS2-02, APPS2-10, APPS2-15, and APPS2-16 because these glasses have the lowest concentrations of $Li_2O$ in the starting glass (< 0.05wt%). As the $NC_{Li}$ values are normalized to the amount of Li in the original glass, very small changes in the concentration used in the calculations will result in relatively large changes to $NC_{Li}$. For this reason, the reported $NC_B$ and $NC_{Na}$ values for these glasses are likely more accurate.

Table 3.11. WTP PCT normalized release limits to HLW glass (g/L).

| Constraint Description | Value | Source |
|---|---|---|
| PCT normalized B release | $NC_B$ <16.70 (g/L)<br>ln($NC_B$), g/L <2.82 | DOE 2000 |
| PCT normalized Li release | $NC_{Li}$ <9.57 (g/L)<br>ln($NC_{Li,}$), g/L <2.26 | DOE 2000 |
| PCT normalized Na release | $NC_{Na}$ <13.35 (g/L)<br>ln($NC_{Na}$), g/L <2.59 | DOE 2000 |

Table 3.12. Average normalized concentrations ($NC_i$) in g/L for the APPS2 quenched (Q) glasses. No values exceed the DWPF EA glass threshold listed in Table 3.11.

| Glass ID | $NC_B$ (g/L) | $NC_{Na}$ (g/L) | $NC_{Li}$ (g/L) | $NC_{Si}$ (g/L) |
|---|---|---|---|---|
| APPS2-01-Q | 6.62 ± 0.06 | 5.23 ± 0.03 | (a) | 1.28 ± 0.01 |
| APPS2-02-Q | 10.03 ± 0.07 | 6.83 ± 0.06 | (b) | 0.59 ± 0.01 |
| APPS2-03-Q | 4.25 ± 0.11 | 2.69 ±0.08 | 3.61 ± 0.11 | 0.25 ±0.00 |
| APPS2-04-Q | 1.51 ±0.03 | 1.92 ± 0.00 | (a) | 0.60 ±0.01 |
| APPS2-05-Q | 1.88 ± 0.04 | 1.67± 0.02 | 1.37 ± 0.04 | 0.38 ± 0.00 |
| APPS2-06-Q | 1.12 ± 0.02 | 1.08 ± 0.02 | 0.78 ± 0.02 | 0.25 ±0.00 |
| APPS2-07-Q | 1.01 ±0.01 | 1.74 ± 0.01 | (a) | 0.69 ± 0.00 |
| APPS2-08-Q | 1.70 ± 0.06 | 0.97 ± 0.03 | 1.42 ± 0.06 | 0.28 ±0.01 |
| APPS2-09-Q | 2.95 ± 0.10 | 1.82 ± 0.05 | 2.58 ± 0.08 | 0.24 ± 0.01 |
| APPS2-10-Q | 12.78 ± 0.12 | 6.87 ± 0.07 | (b) | 0.15 ± 0.00 |
| APPS2-11-Q | 2.10 ± 0.01 | 2.24 ± 0.01 | 1.82 ± 0.01 | 0.60 ± 0.03 |
| APPS2-12-Q | 9.94 ± 0.18 | 4.87 ± 0.08 | 7.44 ± 0.12 | 0.23 ± 0.00 |
| APPS2-13-Q | 0.63 ± 0.06 | 1.22 ± 0.03 | 0.89 ± 0.03 | 0.36 ± 0.01 |
| APPS2-14-1-Q | 4.84 ± 0.10 | 2.83 ± 0.03 | 3.38 ± 0.06 | 0.14 ± 0.00 |
| APPS2-15-Q | 6.07 ± 0.02 | 3.79 ± 0.00 | (b) | 0.32 ± 0.00 |
| APPS2-16-Q | 7.37 ± 0.04 | 5.32 ± 0.02 | (b) | 0.65 ± 0.01 |

(a) The glass does not contain Li.
(b) The $Li_2O$ wt% is less than 0.05, which is near the detection limit and can cause large uncertainties and thus the values are not reported.

Table 3.13. Average normalized concentrations ($NC_i$) in g/L for the APPS2 CCC glasses. Values in bold exceed the DWPF EA glass threshold listed in Table 3.11.

| Glass ID | $NC_B$ (g/L) | $NC_{Na}$ (g/L) | $NC_{Li}$ (g/L) | $NC_{Si}$ (g/L) |
|---|---|---|---|---|
| APPS2-01-CCC | 4.15 ± 0.03 | 3.42 ± 0.05 | (a) | 0.93 ± 0.06 |
| APPS2-02-CCC | 8.91 ± 0.07 | 6.10 ± 0.05 | (b) | 0.54 ± 0.01 |
| APPS2-03-CCC | 4.76 ± 0.04 | 2.84 ± 0.01 | 3.89 ± 0.03 | 0.26 ± 0.00 |
| APPS2-04-CCC | 0.87 ± 0.04 | 1.23 ± 0.02 | (a) | 0.42 ± 0.00 |
| APPS2-05-CCC | 1.78 ± 0.03 | 1.59 ± 0.02 | 1.57 ± 0.02 | 0.41 ± 0.00 |
| APPS2-06-CCC | 0.43 ± 0.01 | 0.57 ± 0.01 | 0.45 ± 0.01 | 0.20 ± 0.00 |
| APPS2-07-CCC | 0.81 ± 0.01 | 1.45 ± 0.00 | (a) | 0.63 ± 0.01 |
| APPS2-08-CCC | 5.24 ± 0.07 | 1.94 ± 0.03 | 2.81 ± 0.03 | 0.26 ± 0.01 |
| APPS2-09-CCC | 5.96 ± 0.04 | 2.94 ± 0.03 | 4.44 ± 0.05 | 0.25 ± 0.00 |
| APPS2-10-CCC | **46.37 ± 0.09** | **23.41 ± 0.11** | (b) | 0.16 ± 0.00 |
| APPS2-11-CCC | 1.68 ± 0.02 | 1.78 ± 0.01 | 1.69 ± 0.01 | 0.57 ± 0.00 |
| APPS2-12-CCC | 10.99 ± 0.06 | 5.07 ± 0.02 | 7.86 ± 0.02 | 0.23 ± 0.00 |
| APPS2-13-CCC | 0.40 ± 0.05 | 0.84 ± 0.01 | 0.73 ± 0.01 | 0.27 ± 0.00 |
| APPS2-14-1-CCC | 6.07 ± 0.02 | 3.41 ± 0.02 | 4.55 ± 0.05 | 0.16 ± 0.00 |
| APPS2-15-CCC | 4.43 ± 0.03 | 2.78 ± 0.01 | (b) | 0.28 ± 0.00 |
| APPS2-16-CCC | 6.63 ± 0.03 | 4.72 ± 0.01 | (b) | 0.60 ± 0.01 |

(a) The glass does not contain Li.
(b) The $Li_2O$ wt% is less than 0.05, which is near the detection limit and can cause large uncertainties and thus the values are not reported.

To determine if the difference between Q and CCC heat-treated glasses was within experimental error, the following hypothesis was tested (Rieck 2018):

$$p_Q - p_C = 0 \tag{3.3}$$

where $p_Q$ and $p_C$ are the true but unknown values of Q and the CCC ln($NC_B$) or ln($NC_{Na}$).

To test this hypothesis, we considered $\hat{p_C} - \hat{p_Q} \pm k \cdot SD(\hat{p_C} - \hat{p_Q})$ to see if:

$$0 \in \left(\hat{p_c} - \hat{p_Q} - k \cdot SD\left(\hat{p_C} - \hat{p_Q}\right), \hat{p_c} - \hat{p_Q} + k \cdot SD\left(\hat{p_C} - \hat{p_Q}\right)\right) \tag{3.4}$$

where $\hat{p_Q}$ and $\hat{p_c}$ are the measured values of the Q and the CCC ln($NC_B$) or ln($NC_{Na}$), k is a multiplying factor based on the assumed normal distribution of $\hat{p_C} - \hat{p_Q}$ and intended confidence level for the test (in the present study set at 95%), and $SD\left(\hat{p_C} - \hat{p_Q}\right)$ is the estimated standard deviation of $\hat{p_c} - \hat{p_Q}$. Assuming SD($\hat{p_C}$) = SD($\hat{p_Q}$) = SD, then:

$$\hat{p_c} - \hat{p_Q} \pm kSD\left(\hat{p_c} - \hat{p_Q}\right) = \hat{p_c} - \hat{p_Q} \pm k\sqrt{2}SD \tag{3.5}$$

That is, the measured property of CCC glass is considered the same as that of Q glass within the experimental error if the following condition is satisfied:

$$\hat{p_Q} \in \left(\hat{p_c} - k\sqrt{2}\ SD, \hat{p_c} + k\sqrt{2}\ SD\right) \tag{3.6}$$

The APPS2 glasses that did not satisfy the above condition for ln($NC_B$) were APPS2-06, APPS2-08, APPS2-09, and APPS2-10. Figure 3.12 provides $NL_B$, $NL_{Li}$, and $NL_{Na}$ [values were converted from NC using Eq. (3.6)] for all the glasses. The cases where the Q and CCC $NL_B$ and $NL_{Na}$ values for APPS2-06, APPS2-08, APPS-09 ($NL_B$ only), and APPS-10 do not meet the condition in Eq. (3.6) are explicitly highlighted in Figure 3.12. As discussed above, APPS2-10 contains 8.1 wt% nepheline in the CCC sample, so the large difference between the Q response and CCC response is expected. APPS2-06 had reduced PCT response after CCC, which is conservative. The other glasses ( -08 and -09) have relatively small fractions of apatite and spinel, whose presence is not necessarily associated with poorer durability; however, their impact on durability cannot be precluded. Another possibility is amorphous phase separation into two immiscible liquid phases, which could also result in poorer durability for the CCC sample.

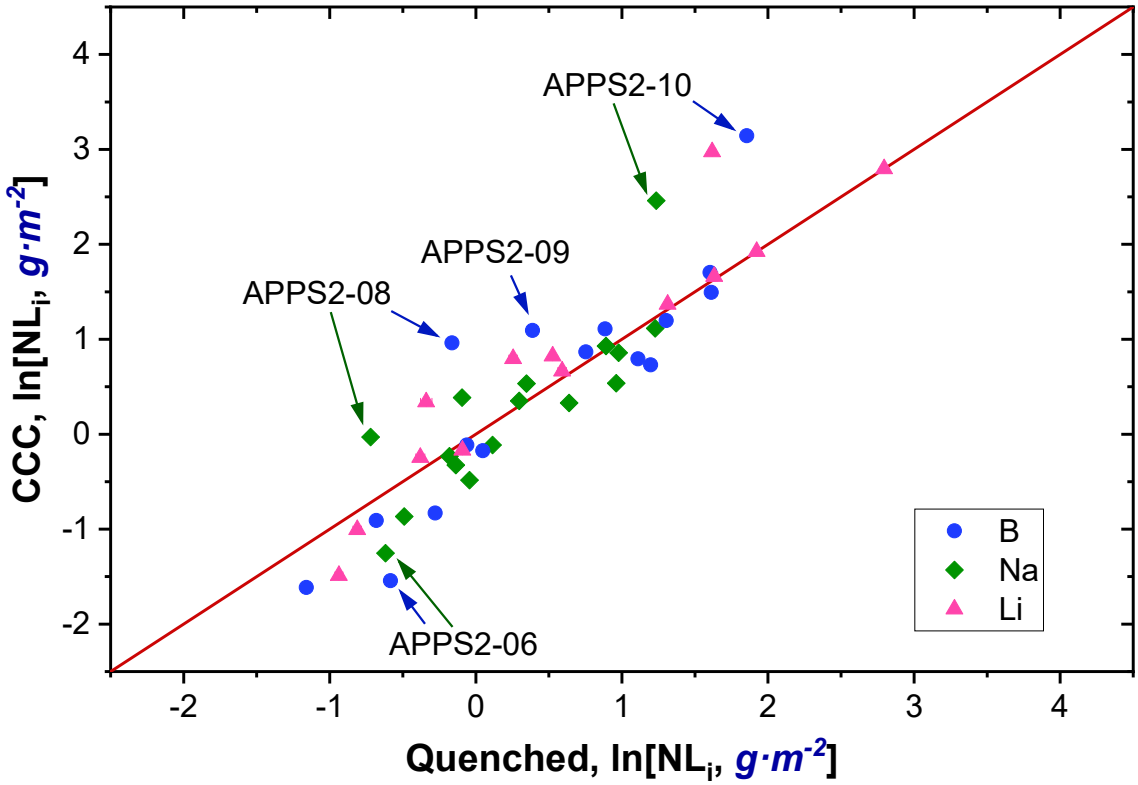


Figure 3.12. $NL_B$, $NL_{Li}$, and $NL_{Na}$ release in natural logarithm scale of Q vs. CCC DFHLW glasses. Glasses that do not satisfy Eq. (3.6) are identified on the plot.

Figure 3.13 shows the average of the measured average ln($NL_B$) and average ln($NL_{Na}$) values for Q glasses plotted against model predictions from Vienna et al. (2024) and Vienna and Crum (2018). All APPS2 glasses were designed to pass the PCT release limits provided in Table 3.11, and all of the Q samples passed the requirement. Neither model provided a good prediction; however, visually the Vienna and Crum (2018) model seems to predict slightly better than the Vienna et al. (2024) model.

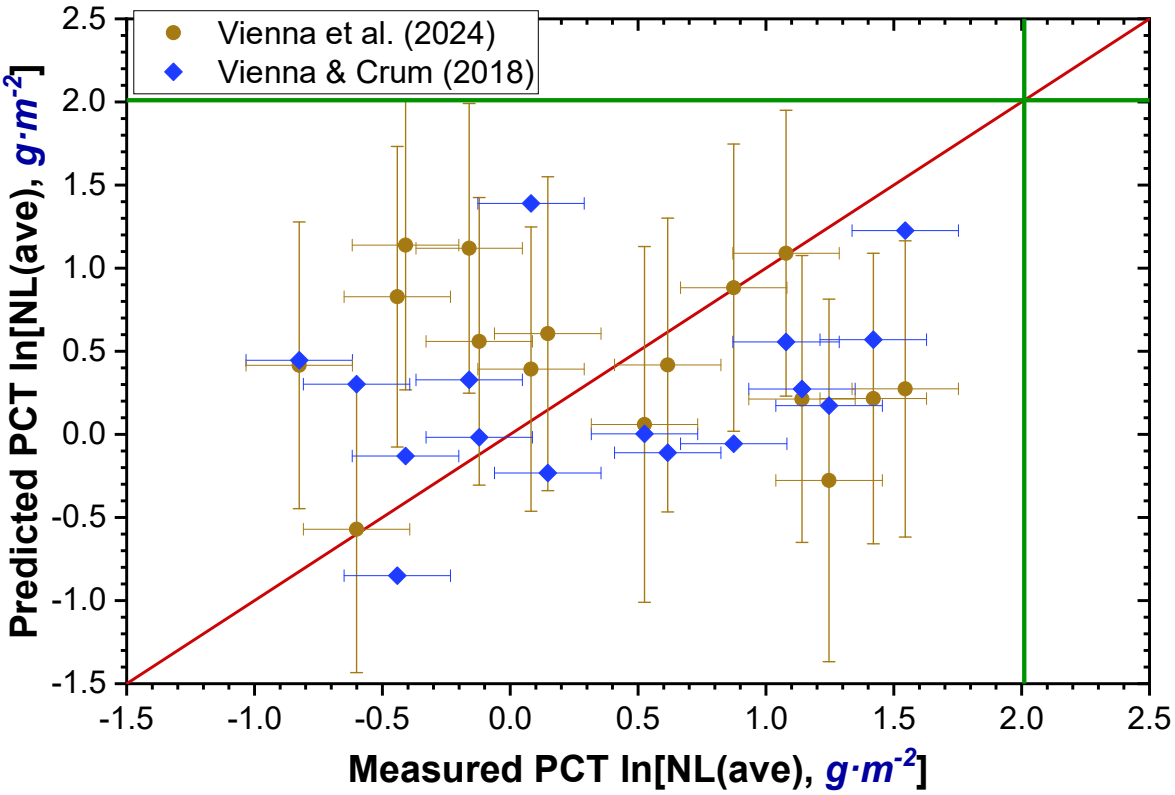


Figure 3.13. Natural log of predicted and measured NL values for the APPS2 glasses. Uncertainties for measured values are represented by $SD_{pooled}$ reported in Vienna et al. (2022). The release limit represented by the green line is the average of the $ln(NL_B)$ and $ln(NL_{Na})$ release limit provided in Table 3.11.

## 3.9 Toxicity Characteristic Leaching Procedure

### 3.9.1 Results and Comparisons to the Delisting Results

Figure 3.14 summarizes the measured TCLP leachate concentrations of B, Cr, Ni, Pb, V, and Zn for Q and CCC APPS2 glasses compared to the analytical detection limits and the constituent of concern delisting limits (Blumenkranz 2006). The detection limit value is provided for tests that had concentrations below detection limits. Full results are provided in Appendix I. Many glasses had concentrations below detection limits for most glasses, especially Ni and Pb. When TCLP leachate concentrations registered above detection limits, they mostly originated from CCC glasses (see Cr as an example). No glass surpassed the delisting limits for any of the constituents of concern (Cr, Ni, Pb, V, Zn).

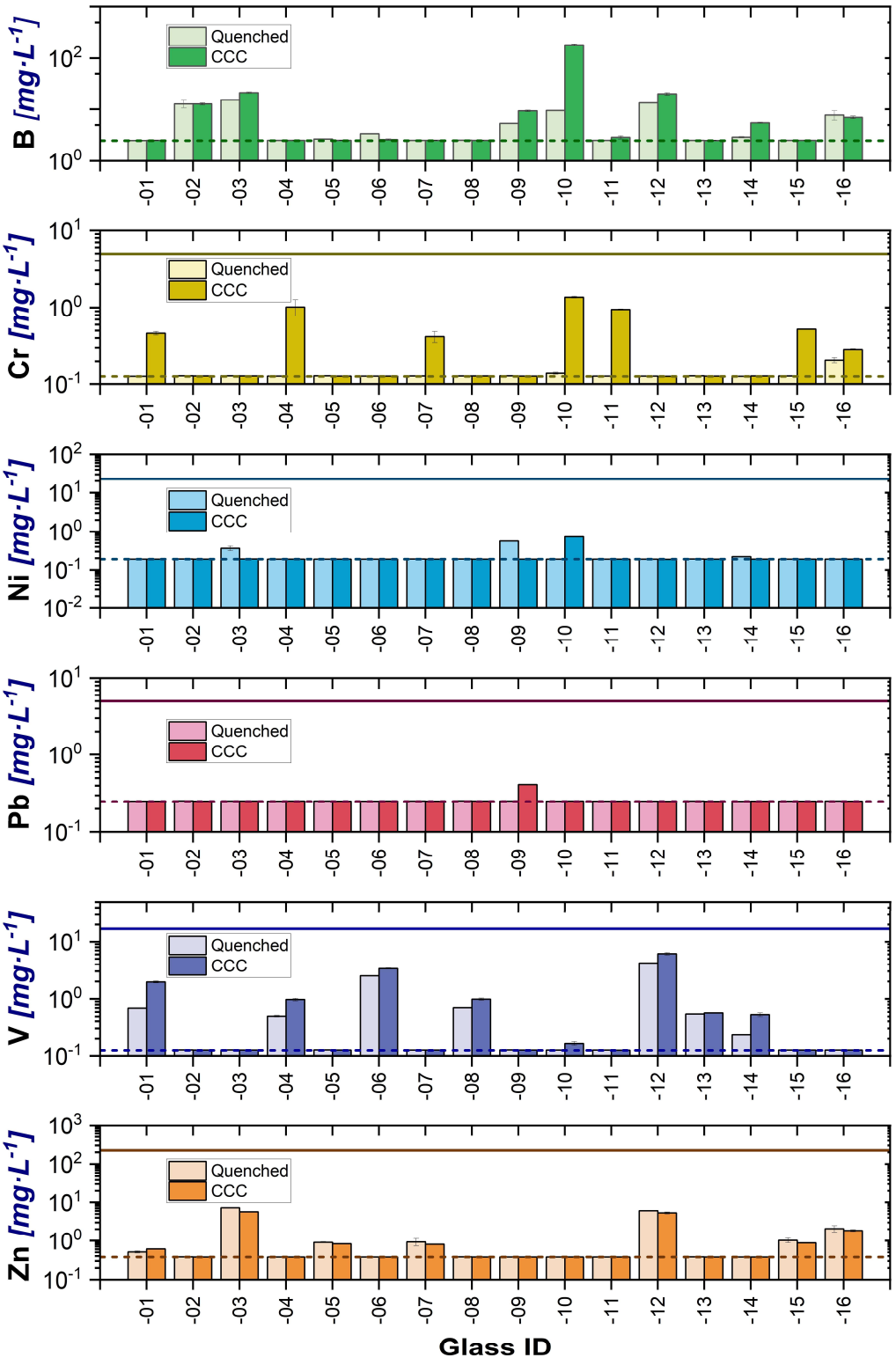


Figure 3.14. TCLP leachate concentrations for B, Cr, Ni, Pb, V, and Zn for Q and CCC APPS2 glasses. The solid colored line represents the delisting limits while the dashed lines specify the analytical detection limit.

Figure 3.15 plots the CCC and Q measured TCLP leachate concentrations together. In general, the concentrations of B, Cr, Ni, Pb, V, and Zn released from the CCC glasses are comparable to those released from the Q glasses, with some exceptions where some CCC glasses released higher concentrations than the corresponding Q glass. The large B and Cr responses are from APPS2-10-CCC, which contains 8.1% nepheline (Table 3.2), affecting overall durability. APPS2-10-CCC contained the highest amount of nepheline of the series.

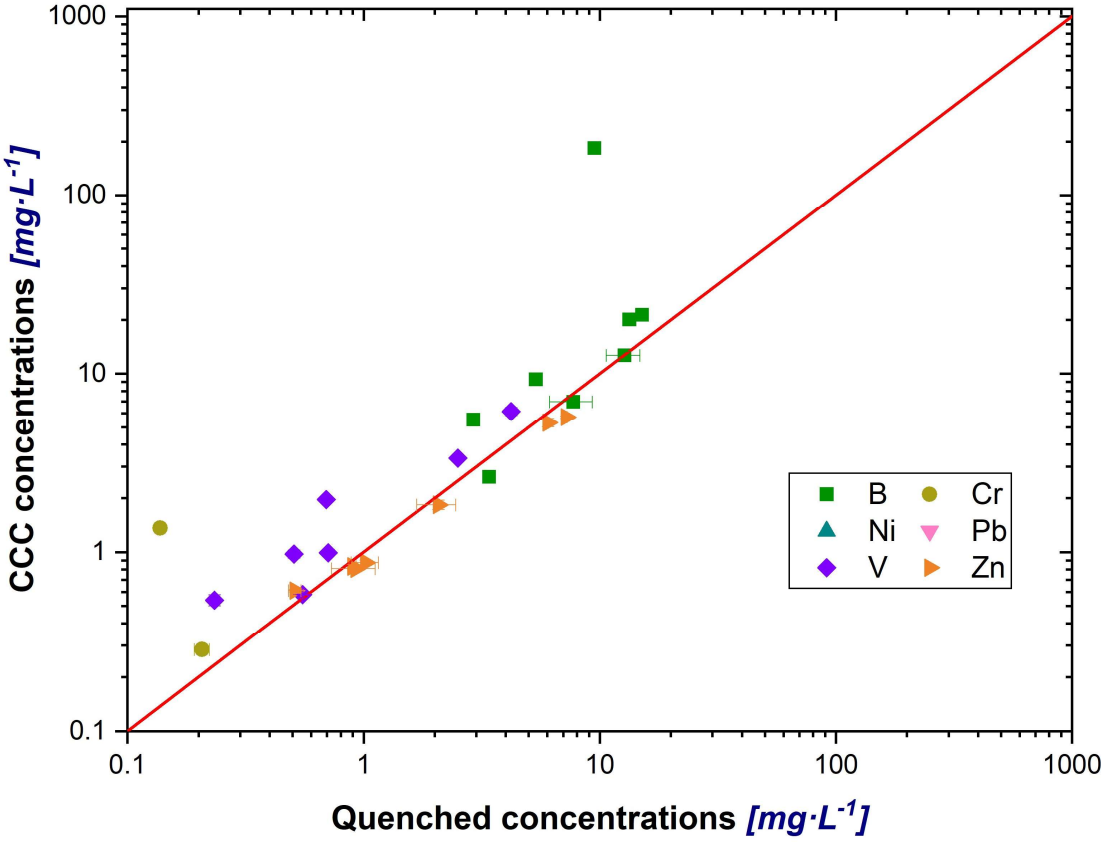


Figure 3.15. Measured TCLP leachate concentrations for B, Cr, Ni, Pb, V, and Zn for Q and CCC APPS2 glasses. All results that were below detections were excluded. The red line represents the 1-1 correlation between the Q and CCC values.

### 3.9.2 Comparisons to Predicted TCLP Leachate Concentrations

The NC(B) values from the Q glasses determined experimentally for the APPS2 matrix were compared to predicted NC(B) values generated from the TCLP models in Vienna et al. (2009) and Kim and Vienna (2002) and presented in Figure 3.16. Both models provide NC(B) values that are quite scattered across the 1-1 correlation line; however, in general, the predicted NC(B) values were higher.

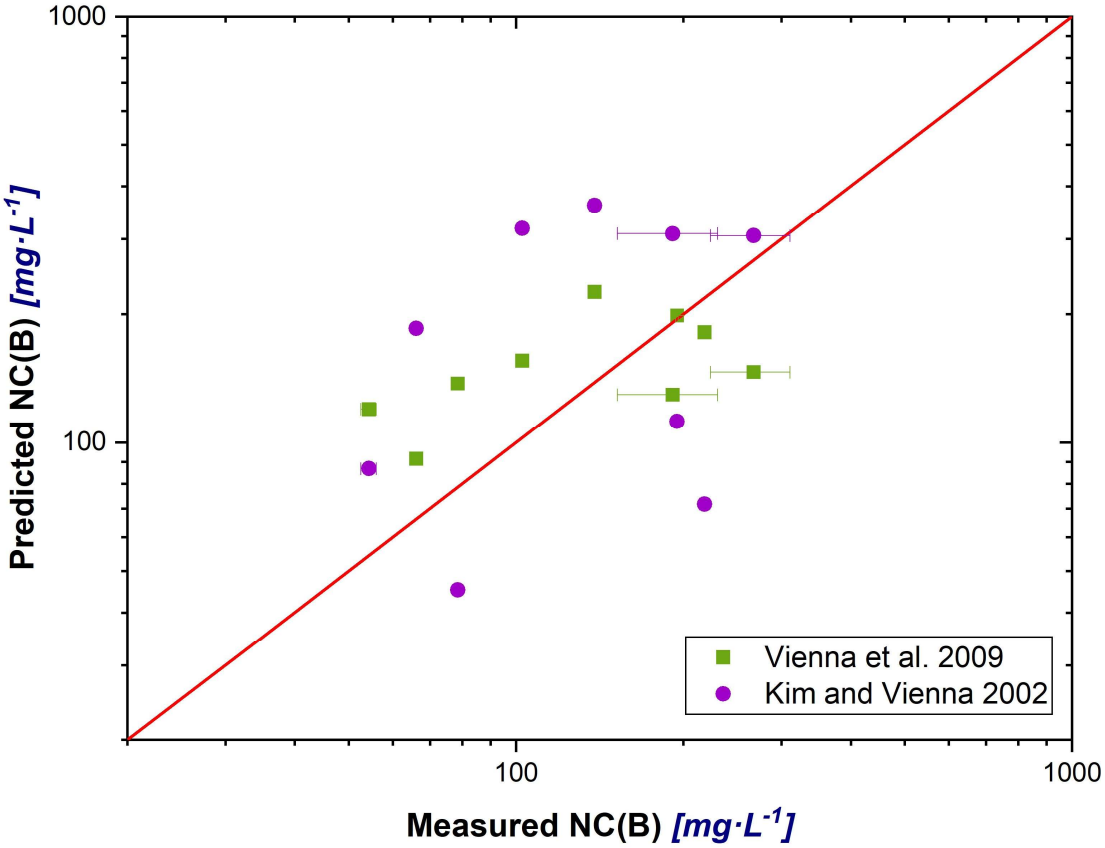


Figure 3.16. Measured Q and predicted NC(B) from the Vienna et al. (2009) and Kim and Vienna (2002) models. Results are only provided for measured NC(B) with results above the detection limits. The red line represents the 1-1 correlation between the measured and predicted values.

The predicted TCLP leachate concentration of element *i* ($c_{i,pred}$) using Eq. (3) from Kim and Vienna (2004) is:

$$c_{i,pred} = NC(B)_{pred} \cdot f_i \tag{3.7}$$

where $NC(B)_{pred}$ is the predicted *NC(B)* using the Kim and Vienna (2002) and Vienna et al. (2009) models and $f_i$ is the mass fraction of element *i* in the unaltered glass.

Figure 3.17 shows measured and predicted TCLP releases from (a) Kim and Vienna (2002) and (b) Vienna et al. (2009) for Cr, Ni, Pb, V, and Zn. All measured values below the detection limit were excluded. As a result, fewer results are available for some species such as Cr and Pb compared to other species such as V and Zn. The predicted values scatter around the 1-1 correlation line where the predicted values are higher than the measured Q values in most instances. Generally, both models have higher predicted values than measured values, providing conservative estimates. The Vienna et al. (2009) model provides predictions closer to experimental results, but a new TCLP model would be ideal to further reduce excessive conservativity.

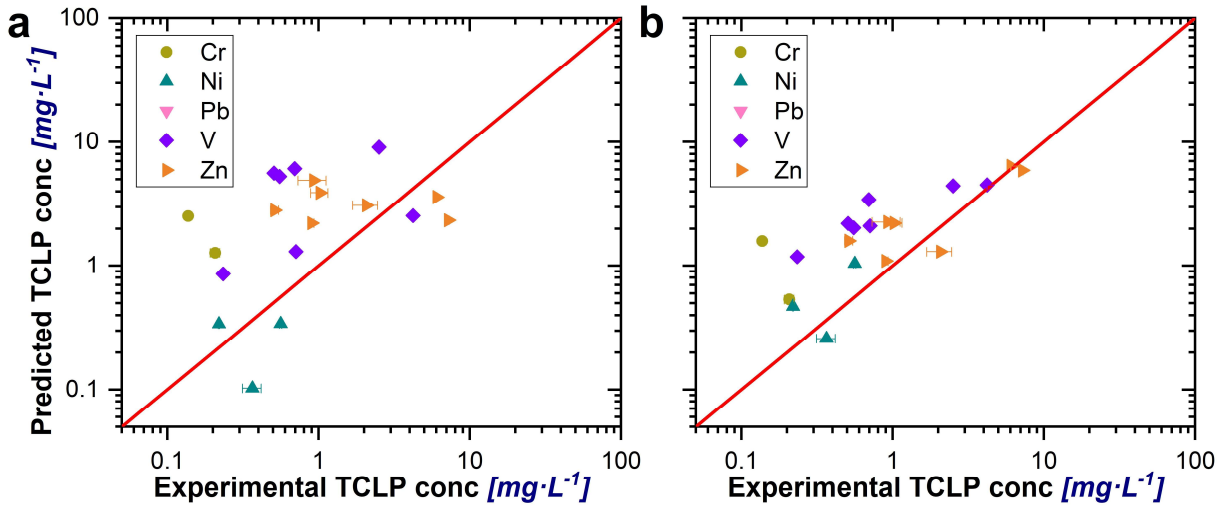


Figure 3.17. Measured Q and predicted TCLP releases from (a) Kim and Vienna (2002) and (b) Vienna et al. (2009) for Cr, Ni, Pb, V, and Zn. All measured values below detection limits were excluded. The red line represents the 1-1 correlation between the measured and predicted values.

## 3.10 Refractory Corrosion

Table 3.14 and Figure 3.18 summarize the measured neck depths of the APPS2 glasses. Each glass was tested in four different conditions: 1150 °C 3 days, 1150 °C 7 days, 1200 °C 3 days, and 1200 °C 7 days. Test coupon photos are shown in Appendix K and micro-CT scan images are shown in Appendix L. For each coupon, the neck depth was measured in two perpendicular directions as discussed in Section 2.13. The average values of the two measurements are reported with the standard deviation. Note that for some tests, the standard deviation from two measurements is zero, which does not represent the experiment uncertainty. During the micro-CT measurement, setting the threshold to outline the scanned materials can lead to a measurement uncertainty of ~1 to 3 voxels (0.04 to 0.12 mm). Therefore, a conservative estimated uncertainty is ~0.12 mm for the neck depth data. All conditions for APPS2-03 and -12 and some conditions for APPS2-08, -09, -10, and -14 produced test coupons with neck corrosion less than 0.12 mm, which should be considered as being within the experimental error.

Figure 3.19 shows the measured neck depth of the 1200 °C 7-day test samples plotted against model predictions from Vienna et al. (2024). Because the model was developed based on old data collected under different temperature and time, treatment of the experimental data is needed to evaluate the correlation. The model cannot predict the corrosion rate of highly corrosive glasses such as APPS2-01, -02, and -04.

Table 3.14. K-3 refractory corrosion neck depth, $d_{neck}$, mm.

| Glass/Test Condition | 1150 °C-3 Days | 1150 °C-7 Days | 1200 °C-3 Days | 1200 °C-7 Days |
|---|---|---|---|---|
| APPS2-01 | 0.95 ± 0.014 | 1.92 ± 0 | 1.49 ± 0.014 | 2.64 ± 0.057 |
| APPS2-02 | 2.12 ± 0.028 | 3.24 ± 0.057 | 2.39 ± 0.297 | 3.71 ± 0.184 |
| APPS2-03 | 0.08 ± 0 | 0.06 ± 0.057 | 0.08 ± 0.028 | 0.07 ± 0.014 |
| APPS2-04 | 1.11 ± 0.014 | 2.18 ± 0.057 | 2 ± 0.113 | 3.66 ± 0.141 |
| APPS2-05-1 | 0.41 ± 0.042 | 0.87 ± 0.014 | 0.81 ± 0.071 | 1.09 ± 0.042 |
| APPS2-06-1 | 0.46 ± 0.028 | 0.79 ± 0.014 | 0.62 ± 0 | 1.16 ± 0.057 |
| APPS2-07 | 0.29 ± 0.042 | 0.66 ± 0.028 | 0.48 ± 0 | 0.89 ± 0.014 |
| APPS2-08 | 0.07 ± 0.014 | 0.11 ± 0.014 | 0.17 ± 0.014 | 0.2 ± 0.028 |
| APPS2-09 | 0.09 ± 0.014 | 0.11 ± 0.042 | 0.08 ± 0 | 0.19 ± 0.014 |
| APPS2-10 | 0.08 ± 0 | 0.3 ± 0.057 | 0.17 ± 0.042 | 0.34 ± 0.085 |
| APPS2-11 | 0.35 ± 0.014 | 1 ± 0.057 | 0.68 ± 0.028 | 1.37 ± 0.014 |
| APPS2-12 | 0.05 ± 0.042 | 0.07 ± 0.014 | 0.04 ± 0 | 0.06 ± 0 |
| APPS2-13 | 0.47 ± 0.014 | 0.94 ± 0.028 | 0.61 ± 0.014 | 1.19 ± 0.014 |
| APPS2-14 | 0.1 ± 0 | 0.19 ± 0.042 | 0.18 ± 0.028 | 0.2 ± 0.057 |
| APPS2-15 | 0.58 ± 0.198 | 0.7 ± 0.226 | 0.44 ± 0.057 | 0.71 ± 0.042 |
| APPS2-16 | 1.06 ± 0 | 1.74 ± 0.057 | 1.3 ± 0.028 | 2.12 ± 0 |

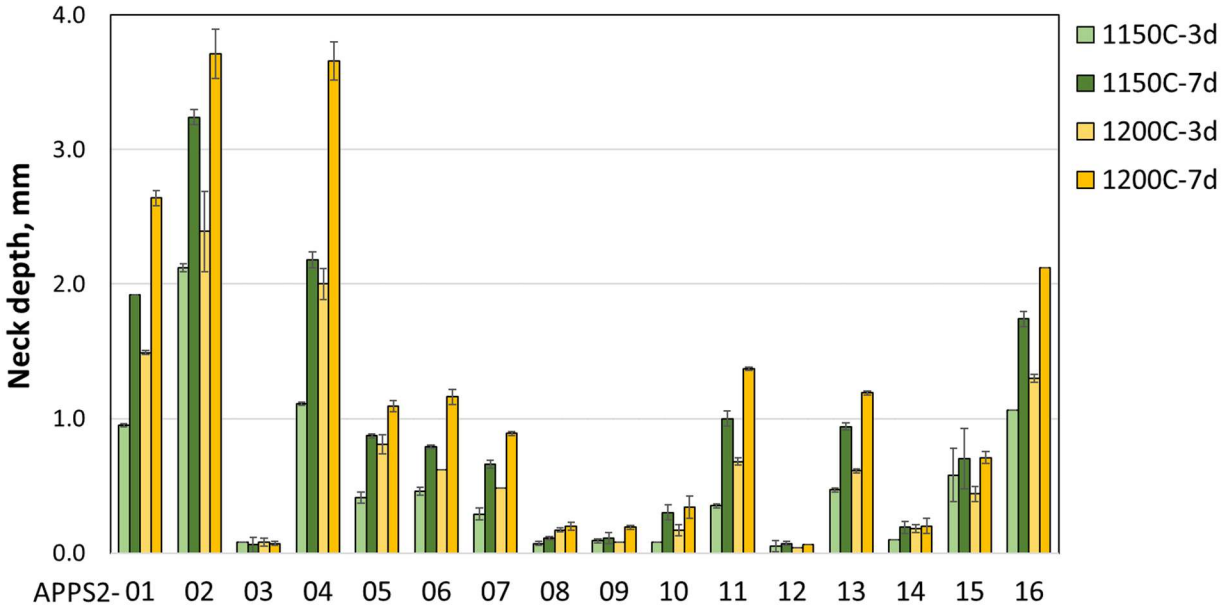


Figure 3.18. K-3 refractory corrosion neck depth.

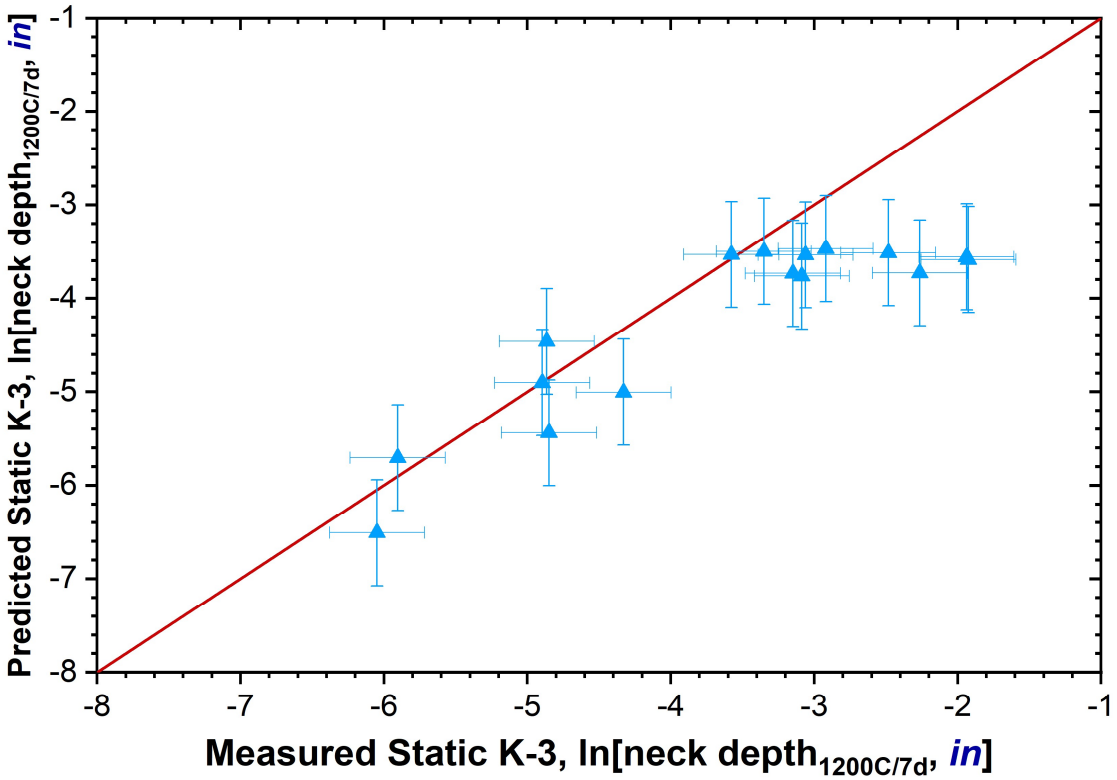


Figure 3.19. Measured and predicted (Vienna et al. 2024) K-3 refractory corrosion neck depth. Red line is the 1:1 line between the measured and predicted values. Uncertainties for measured values are represented by the pooled SD reported in Vienna et al. (2022).

## 3.11 Future Modeling and Formulation Recommendations

The purposes of this effort were to (1) generate data for improved DFHLW glass property modeling and formulation and (2) experimentally verify the use of the EWG2.5 models (Vienna et al. 2024) in APPS flowsheet models. A few models proved adequate for predicting DFHLW glass properties, while others require additional refits or offsets. Table 3.15 summarizes the status and recommendations for use of models for each of the modeled properties. It is recommended that new property models be developed for EWG3, as a lot of data is expected to be collected in pertinent compositional spaces where no data was previously available. To enable near-future calculations and formulations for designing DFHLW glasses and processing rate estimations, a formulation algorithm EWG2.6 (minor modifications on existing property models) will be developed before EWG3.

Model updates, where needed, are underway and the results will be reported separately in updated EWG formulation methods reports.

Table 3.15. Summary of EWG2.5 model performance and recommendation of future property model developments (EWG2.6 and EWG3).

| Property | EWG2.5 | EWG2.6 | EWG3 |
|---|---|---|---|
| CCC crystallinity | The p value was modified to 0.028 from the Lu et al. 2021 model to make the model more conservative. One (APPS2-10) out of the 16 APPS2 glasses formed 8 wt% nepheline after CCC, causing this sample to fail the PCT constraints. | Modify the p value to avoid glasses such as APPS-10 | New model |
| Isothermal crystallinity | Zirconia-containing phases $T_L$ model and spinel $T_{2\%}$ models from Vienna et al. 2016 successfully limited unacceptably high concentrations of these crystals at 950 °C, except APPS2-09 formed 2.1 vol% total crystals (0.7 vol% spinel and 1.4 vol% $NdPO_4$). | New model for 1 vol% ($T_{1\%}$) $\leq$ 950°C | New model for spinel |
| Phosphate | APPS2-08 and APPS2-09 formed phosphate crystals (< 2 wt%) after CCC. | New model for phosphate phase $T_L$ | New model |
| Sulfur solubility | Model slightly over-predicted the 3TS $SO_3$ solubility. | A more conservative melter offset or a slight modification on the EWG2.5 model by fitting model residuals | New model |
| Density | Densities of APPS2 glasses are well predicted by the Vienna et al. 2002 model and slightly over-predicted by the Vienna et al. 2009 model. | No change | No change |
| Viscosity | Viscosity was well predicted except APPS2-08 (under-predicted) which contained crystals and viscosities of APPS2 glasses are within constraints. | New model | New model |
| Electrical conductivity | ECs of APPS2 glasses are adequately predicted. | New model | New model |
| Product consistency test | PCT responses of the quenched glasses are not adequately predicted by the EWG2.5 model, while predictions are better using the Vienna and Crum 2018 model. All the APPS2 quenched glasses passed the constraints. Only APPS2-10 glass failed the limit after CCC due to nepheline formation. | Vienna and Crum 2018 model with prediction uncertainty. | New model |
| Toxicity | TCLP results for the APPS2 glasses are not adequately predicted by the Kim et al. 2002 model. Since all the 16 APPS2 glasses passed the constraints, the current model can be used for near-future DFHLW glass formulations. | Use Vienna et al. 2009 model | New model |
| K-3 refractory corrosion | K-3 neck corrosion by static testing was not well predicted by existing models, and improved models will be needed. Four of the 16 glasses failed the nominal 0.04-inch K-3 neck corrosion limit used during the formulation, assuming a 0.5949 ln[inch] offset applied to the 1200 °C 7-day test results. | New model | New model |

# 4.0 Conclusions

This report documents the results of the formulation, fabrication, and testing of a set of simulated DFHLW glasses (APPS2). Of 16 glasses tested, 13 satisfied all target property constraints. One glass, APPS2-10, formed nepheline on CCC heat-treatment and failed the PCT response limits. This glass also had high B and Cr release rates for the TCLP. APPS2-08 failed the viscosity constraint, likely due to crystals in the melt. APPS2-14 failed the $T_L$-Zr constraint. Of the 16 test glasses, 4 failed the nominal 0.04-in. K-3 neck corrosion limit assuming a 0.5949 ln[in] offset.

The measured property values were compared to predicted values from a set of current and new models (EWG2.5). A few models (e.g., EC, TCLP, density) proved adequate for designing DFHLW glasses in the near future, while others require additional refits or offsets. It is recommended that new property models be developed for EWG3, as a lot of the data (over 200 glasses) is expected to be collected in the compositional spaces where no data was previously available. To enable near-term calculations and formulations for designing DFHLW glasses and processing rate estimations, a formulation algorithm with minor modifications, EWG2.6, will be developed before EWG3.

# 5.0 Bibliography

10 CFR 830, *Nuclear Safety Management*. Code of Federal Regulations, as amended.

Alton J, J Plaisted, and P Hrma. 2002 "Kinetics of Growth of Spinel Crystals in a Borosilicate Glass." *Chemical Engineering Science* 57:2503-2509.

ASTM C621, *Standard Test Method for Isothermal Corrosion Resistance of Refractories to Molten Glass*. ASTM International, West Conshohocken, PA.

ASTM C1285, *Standard Test Methods for Determining Chemical Durability of Nuclear, Hazardous, and Mixed Waste Glasses and Multiphase Glass Ceramics: The Product Consistency Test (PCT).* ASTM International, West Conshohocken, PA.

ASTM C1720, *Standard Test Method for Determining Liquidus Temperature of Immobilized Waste Glasses and Simulated Waste Glasses*. ASTM International, West Conshohocken, PA.

Bernards JK, GA Hersi, KT Pak, AJ Schubick, LM Bergmann, AN Praga, and SN Tilanus. 2021. *High-Level Waste Analysis of Alternatives Model Results Report*. RPP-RPT-61957, Rev. 2, Washington River Protection Solutions, Richland, WA.

Bernards JK, GA Hersi, TM Hohl, RT Jasper, PD Mahoney, NK Pak, SD Reaksecker, AJ Schubick, EB West, LM Bergmann, et al. 2020. *River Protection Project System Plan*. ORP-11242, Rev. 9, U.S. Department of Energy, Office of River Protection, Richland, WA.

Blumenkranz DB. 2006. *Petition to Delist Immobilized High-Level Waste Generated at the Hanford Tank Waste Treatment and Immobilization Plant.* 24590-WTP-RPT- DB ENV-06-001, Rev. 0, River Protection Project, Hanford Tank Waste Treatment and Immobilization Plant, Richland, WA.

Britton MD and CK Anderson. 2024. *Direct-Feed High-Level Waste Feed Vectors Assessment*. RPP-RPT-64878, Rev. 0, Washington River Protection Solutions, Richland, WA.

DOE. 1996. *Waste Acceptance Product Specifications for Vitrified High-Level Waste Forms (WAPS)*. DOE/EM-0093, U.S. Department of Energy, Office of Environmental Management, Washington, D.C.

DOE. 2000. *Design, Construction, and Commissioning of the Hanford Tank Waste Treatment and Immobilization Plant*. Contract DE-AC27-01RV14136, as amended, U.S. Department of Energy, Office of River Protection, Richland, WA.

DOE. 2013. *Hanford Tank Waste Retrieval, Treatment, and Disposition Framework*. U.S. Department of Energy, Washington, D.C.

DOE Order 414.1D, *Quality Assurance*. U.S. Department of Energy, Washington, D.C.

Dunst KP. 2020. *Process Inputs Basis of Design (PIBOD) for HLW*. 24590-DB-PET-19-001, Rev. 1, River Protection Project, Waste Treatment Plant, Richland, WA.

EPA Method 1311, "Toxicity Characteristic Leaching Procedure (TCLP)." In *Test Methods for Evaluating Solid Waste, Physical/Chemical Methods*, EPA Publication SW–846.

Gebhardt MJ. 2011. *APPS System Design Description*. 24590-WTP-SWD-PET-08-002, Rev. 5, River Protection Project, Waste Treatment Plant, Richland, WA.

Gervasio V, X Lu, JT Reiser, M Peterson, NL Canfield, JB Lang, JC Rigby, J George, DA Cutforth, JM Westman, et al. 2024. *Direct Feed High-Level Waste APPS Model Glass Testing (DFHLW APPS) Matrix*. PNL-35503, Pacific Northwest Laboratory, Richland, WA.

Heredia-Langner A, V Gervasio, SK Cooley, CE Lonergan, DS Kim, AA Kruger, and JD Vienna. 2022. "Hanford low-activity waste glass composition-temperature-melt viscosity relationships." *International Journal of Applied Glass Science* 13(4):514-525.

Jantzen CM, NE Bibler, DC Beam, CL Crawford, and MA Pickett. 1993. *Characterization of the Defense Waste Processing Facility (DWPF) Environmental Assessment (EA) Glass Standard Reference Material (U)*. WSRC-TR-92-346, Rev. 1, Westinghouse Savannah River Company, Aiken, SC.

Jin T, D Kim, LP Darnell, BL Weese, NL Canfield, M Bliss, MJ Schweiger, JD Vienna, and AA Kruger. 2019. "A crucible salt saturation method for determining sulfur solubility in glass melt." *International Journal of Applied Glass Science* 10:92-102. https://doi.org/10.1111/ijag.12366

Kim DS and JD Vienna. 2002. *Model for TCLP Releases from Waste Glasses*. PNNL-14061, Pacific Northwest National Laboratory, Richland, WA.

Kim DS and JD Vienna 2004. "Glass composition-TCLP response model for waste glasses." In *Environmental Issues and Waste Management Technologies in the Ceramic & Nuclear Industries IX*: 297-305, American Ceramic Society.

Kim DS, D Peeler, and P Hrma. 1995. "Effect of Crystallization on the Chemical Durability of Simulated Nuclear Waste Glasses." In *Environmental Issues and Waste Management Technologies in the Ceramic and Nuclear Industries* 177-186.

Kot WK, K Gilbo, H Gan, and IL Pegg. 2019. *Enhancement of HLW Glass Property-Composition Models*. VSL-19R4480-1, Vitreous State Laboratory, The Catholic University of America, Washington, D.C.

Kroll JO, ZJ Nelson, CH Skidmore, DR Dixon, and JD Vienna. 2019. "Formulation of high-$Al_2O_3$ waste glasses from projected Hanford waste compositions." *Journal of Non-Crystalline Solids* 517:17-25.

Kruger, A. 2023. *Toxicity Characteristic Leaching Procedure (TCLP) Testing of Selected High-Level Waste (HLW) Simulant Glasses*. QAPP ID# CRESP-VU-ORP-2023-0001, U.S. Department of Energy, Office of River Protection, Richland, WA.

Lu X, I Sargin, and JD Vienna. 2021. "Predicting nepheline precipitation in waste glasses using ternary submixture model and machine learning." *Journal of American Ceramic Society* 104:5636-5647.

Lu, X, T Jin, JD Vienna, and CL Trivelpiece. 2023. *Waste Glass Property Database and Data Qualification Plan*. PNNL-34447, Pacific Northwest National Laboratory, Richland, WA.

Lu X, NA Lumetta, and JD Vienna. 2024a. *Design of a High Al Matrix to Expand DFHLW Glass Compositional Ranges*. PNNL-36304, Pacific Northwest National Laboratory, Richland, WA.

Lu X, ZD Weller, V Gervasio, and JD Vienna. 2024b. "Glass design using machine learning property models with prediction uncertainties: Nuclear waste glass formulation." *Journal of Non-Crystalline Solids*, Submitted.

Lu X, JD Vienna, and P Ferkl. 2024c. *Evaluation of DFHLW EWG Formulations and Processing Rates*. PNNL-36196, Pacific Northwest National Laboratory, Richland, WA.

Mellinger GB and JL Daniel. 1984. *Approved Reference and Testing Materials for Use in Nuclear Waste Management Research and Development Programs*. PNL-4955-2, Pacific Northwest Laboratory, Richland, WA. https://doi.org/10.2172/6224421

NQA-1-2012, *Quality Assurance Requirements for Nuclear Facility Application*. American Society of Mechanical Engineers, New York, NY.

Parsons. 2023. *Waste Treatment and Immobilization Plant High Level Waste Treatment Analysis of Alternatives*. DE-NA0002895, Parsons Corporation, Boston, MA.

Petkus LL. 2003. "Canister Centerline Cooling Data, Revision 1." To C.A. Musick, Oct. 29, 2003. CCN: 074851, River Protection Project, Waste Treatment Plant, Richland, WA.

Piepel GF, A Heredia-Langner, and SK Cooley. 2008. "Property–composition–temperature modeling of waste glass melt data subject to a randomization restriction." *Journal of the American Ceramic Society* 91(10):3222-3228.

Rieck BT. 2018. *ILAW Product Qualification Report – Waste Forming Testing*. 24590-LAWRPT-PENG-17-008-05, Rev 1, River Protection Project, Waste Treatment Plant. Richland, WA.

Russell RL, V Gervasio, SM Baird, DL Bellafotto, DA Cutforth, JL George, and JD Vienna. 2025. *Enhanced Hanford High-Aluminum Waste Glass Property Data Development*. EWG-RPT-045, Pacific Northwest National Laboratory, Richland, WA (in review).

Skidmore CH, JD Vienna, T Jin, DS Kim, BA Stanfill, KM Fox, and AA Kruger. 2019. "Sulfur solubility in low activity waste glass and its correlation to melter tolerance." *International Journal of Applied Glass Science*, 10(4): 558-568.

Smith GL. 1993. *Characterization of Analytical Reference Glass-1 (ARG-1)*. PNL-8992, Pacific Northwest Laboratory, Richland, WA.

Vienna JD, P Hrma, A Jiricka, DE Smith, TH Lorier, IA Reamer, and RL Schultz. 2001. *Hanford Immobilized LAW Product Acceptance Testing: Tanks Focus Area Results*. PNNL-13744, Pacific Northwest National Laboratory, Richland, WA.

Vienna JD, D Kim, and P Hrma. 2002. *Database and Interim Glass Property Models for Hanford HLW and LAW Glasses*. PNNL-14060, Pacific Northwest National Laboratory, Richland, WA.

Vienna JD, A Fluegel, DS Kim, and P Hrma. 2009. *Glass Property Data and Models for Estimating High-Level Waste Glass Volume*. PNNL-18501, Pacific Northwest National Laboratory, Richland, WA.

Vienna JD and DS Kim. 2014. *Preliminary IHLW Formulation Algorithm Description*. 24590-RPT-RT-05-001, Rev. 1, River Protection Project, Waste Treatment Plant, Richland, WA.

Vienna JD, GF Piepel, DS Kim, JV Crum, CE Lonergan, BA Stanfill, BJ Riley, SK Cooley, and T Jin. 2016. *Update of Hanford Glass Property Models and Constraints for Use in Estimating the Glass Mass to be Produced at Hanford by Implementing Current Enhanced Glass Formulation Efforts*. PNNL-25835, Pacific Northwest National Laboratory, Richland, WA.

Vienna JD and JV Crum. 2018. "Non-linear effects of alumina concentration on Product Consistency Test response of waste glasses." *Journal of Nuclear Materials* 511:396-405.

Vienna JD, A Heredia-Langner, SK Cooley, AE Holmes, DS Kim, and NA Lumetta. 2022. *Glass Property-Composition Models for Support of Hanford WTP LAW Facility Operation*. PNNL-30932, Rev. 2, Pacific Northwest National Laboratory, Richland, WA.

Vienna JD, X Lu, P Ferkl, J Marcial, MS Fountain, M Trenidad, R Hanson, MD Britton, L Cree, and W Abdul. 2023. "High-Level Waste Glass Processing over Broad Range of Alternative Feed Compositions." In *Proceedings of the 2023 Waste Management Symposia*, Phoenix, AZ.

Vienna JD, Lu X, Ferkl P, Gunnell LL, Heredia-Langner A, Lumetta NA, Jin T, et al. 2024. *Glass Property-Composition Models Update for use in Direct Feed High-Level Waste Flowsheet Development*. PNNL-35884, Pacific Northwest National Laboratory, Richland, WA.

Voss S. 2024. *DFHLW Configuration Optimized WAC Formal Engineering Study.* 24590-ES-TD-24-001, Bechtel National Inc., Richland, WA.

# Appendix A – Morphology/Color of Quenched Glasses

The photographs in this appendix show each glass after melting in a Deltech furnace in a Pt/Rh crucible or a tilt-pour furnace at the melt temperatures and times specified in Section 2.2 of the main report.

Figure A.1. Photographs of (left) APPS2-01 (1-kg batch) after the third melt using a Deltech furnace; (right) APPS2-01 (2-kg batch) after the first melt using a tilt-pour furnace.

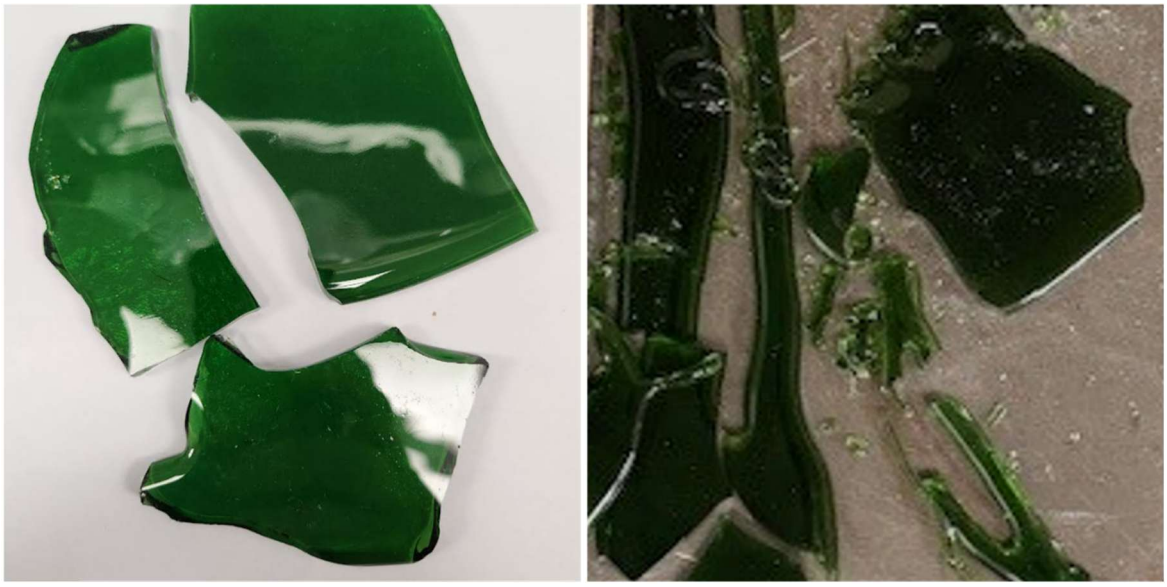

Figure A.2. Photographs of (left) APPS2-02 (1-kg batch) after the second melt using a Deltech furnace; (right) APPS2-02 (2-kg batch) after the second melt using a tilt-pour furnace.

Figure A.3. Photographs of (left) APPS2-03 (1-kg batch) after the third melt using a Deltech furnace; (right) APPS2-03 (2-kg batch) after the first melt using a tilt-pour furnace.

Figure A.4. Photographs of (left) APPS2-04 (1-kg batch) after the second melt using a Deltech furnace; (right) APPS2-04 (2-kg batch) after the first melt using a tilt-pour furnace.

Figure A.5. Photographs of (left) APPS2-05 (1-kg batch) after the second melt using a Deltech furnace; (right) APPS2-05-1 (2-kg batch) after the second melt using a Deltech furnace.

Figure A.6. Photographs of (left) APPS2-06 (1-kg batch) after the second melt using a Deltech furnace; (right) APPS2-06-1 (2-kg batch) after the first melt using a tilt-pour furnace.

Figure A.7. Photographs of (left) APPS2-07 (1-kg batch) after the third melt using a Deltech furnace; (right) APPS2-07 (2-kg batch) after the first melt using a tilt-pour furnace.

Figure A.8. Photographs of (left) APPS2-08 (1-kg batch) after the second melt using a Deltech furnace; (right) APPS2-08 (2-kg batch) after the first melt using a tilt-pour furnace.

Figure A.9. Photographs of (left) APPS2-09 (1-kg batch) after the third melt using a Deltech furnace; (right) APPS2-09 (2-kg batch) after the first melt using a tilt-pour furnace.

Figure A.10. Photographs of (left) APPS2-10 (1-kg batch) after the second melt using a Deltech furnace; (right) APPS2-10 (2-kg batch) after the first melt using a tilt-pour furnace.

Figure A.11. Photographs of (left) APPS2-11 (1-kg batch) after the second melt using a Deltech furnace; (right) APPS2-11 (2-kg batch) after the first melt using a tilt-pour furnace.

Figure A.12. Photographs of (left) APPS2-12 (1-kg batch) after the second melt using a Deltech furnace; (right) APPS2-12 (2-kg batch) after the first melt using a tilt-pour furnace.

Figure A.13. Photographs of (left) APPS2-13 (1-kg batch) after the second melt using a Deltech furnace; (right) APPS2-13 (2-kg batch) after the first melt using a tilt-pour furnace.

Figure A.14. Photographs of (left) APPS2-14-1 (1-kg batch) after the third melt using a Deltech furnace; (right) APPS2-14-1 (2-kg batch) after the first melt using a tilt-pour furnace.

Figure A.15. Photographs of (left) APPS2-15 (1-kg batch) after the second melt using a Deltech furnace; (right) APPS2-15 (2-kg batch) after the first melt using a tilt-pour furnace.

Figure A.16. Photographs of (left) APPS2-16 (1-kg batch) after the third melt using a Deltech furnace; (right) APPS2-16 (2-kg batch) after the second melt using a tilt-pour furnace.

# Appendix B – Comparison Measured and Target Chemical Compositions

The tables in this appendix compare the targeted glass compositions with the analyzed glass compositions and their percent differences.

Table B.1. Targeted vs. measured composition (mass fraction) for the APPS2-01 glass.

| | APPS2-01 | APPS2-01-Q (1kg) | | | APPS2-01-Q (2kg) | | |
|---|---|---|---|---|---|---|---|
| Oxide | Target (wt%) | Measured (wt%) | σ (wt%) | RPD* (%) | Measured | σ (wt%) | RPD (%) |
| $Ag_2O$ | 0.00 | 0.01 | 0.01 | NM | 0.02 | 0.02 | NM |
| $Al_2O_3$ | 5.78 | 5.67 | 0.10 | -1.9 | 5.36 | 0.08 | -7.2 |
| $B_2O_3$ | 5.83 | 5.75 | 1.70 | -1.4 | 6.15 | 1.01 | 5.4 |
| $Bi_2O_3$ | 0.00 | 0.02 | 0.03 | 684.4 | 0.00 | 0.01 | -5.5 |
| CaO | 2.83 | 2.94 | 0.07 | 3.8 | 2.79 | 0.06 | -1.4 |
| Cl | 0.20 | 0.15 | 0.01 | -22.9 | 0.17 | 0.01 | -13.3 |
| $Cr_2O_3$ | 0.61 | 0.56 | 0.05 | -7.5 | 0.55 | 0.04 | -9.2 |
| F | 1.62 | 1.19 | 0.16 | -26.5 | 1.65 | 0.24 | 2.0 |
| $Fe_2O_3$ | 1.67 | 1.66 | 0.06 | -0.5 | 1.61 | 0.04 | -3.6 |
| $K_2O$ | 0.07 | 0.10 | 0.01 | 31.4 | 0.10 | 0.01 | 30.6 |
| $Li_2O$ | 0.00 | NM | NM | NM | NM | NM | NM |
| MgO | 0.01 | 0.01 | 0.01 | 19.0 | 0.02 | 0.02 | 120.2 |
| MnO | 0.17 | 0.17 | 0.03 | 1.1 | 0.15 | 0.04 | -9.3 |
| $Na_2O$ | 22.37 | 21.40 | 0.19 | -4.3 | 25.50 | 0.29 | 14.0 |
| $Nd_2O_3$ | 1.17 | 1.18 | 0.10 | 0.9 | 1.15 | 0.11 | -1.9 |
| NiO | 0.52 | 0.55 | 0.02 | 5.1 | 0.51 | 0.03 | -2.7 |
| $P_2O_5$ | 1.83 | 1.79 | 0.05 | -1.9 | 1.77 | 0.08 | -3.3 |
| PbO | 0.09 | 0.05 | 0.07 | -48.9 | 0.11 | 0.08 | 22.3 |
| $RuO_2$ | 0.00 | 0.00 | 0.00 | NM | 0.00 | 0.01 | NM |
| $SO_3$ | 1.21 | 1.13 | 0.06 | -6.2 | 1.03 | 0.05 | -14.4 |
| $SiO_2$ | 45.35 | 46.30 | 0.28 | 2.1 | 44.71 | 0.57 | -1.4 |
| $V_2O_5$ | 5.14 | 5.13 | 0.09 | -0.3 | 4.79 | 0.11 | -6.9 |
| ZnO | 1.66 | 1.75 | 0.14 | 5.5 | 1.72 | 0.10 | 3.4 |
| $ZrO_2$ | 1.87 | 1.68 | 0.11 | -10.0 | 1.71 | 0.13 | -8.4 |
| SUM | 100 | 99.20 | NM | NM | 101.57 | NM | NM |

* RPD – Relative Percentage Difference
** NM – not measured

Table B.2. Targeted vs. measured composition (mass fraction) for the APPS2-02 glass.

| | APPS2-02 | APPS2-02-Q (1kg) | | | APPS2-02-Q (2kg) | | |
|---|---|---|---|---|---|---|---|
| Oxide | Target (wt%) | Measured (wt%) | σ (wt%) | RPD* (%) | Measured | σ (wt%) | RPD (%) |
| $Ag_2O$ | 0.005 | 0.01 | 0.02 | 167.7 | 0.02 | 0.03 | NM |
| $Al_2O_3$ | 12.748 | 12.19 | 0.13 | -4.4 | 11.93 | 0.15 | -7.2 |
| $B_2O_3$ | 15.33 | 13.56 | 1.38 | -11.6 | 14.75 | 0.87 | 5.4 |
| $Bi_2O_3$ | 0.014 | 0.01 | 0.03 | -40.4 | 0.03 | 0.03 | -5.5 |
| CaO | 0.213 | 0.23 | 0.02 | 8.4 | 0.25 | 0.02 | -1.4 |
| Cl | 0.219 | 0.18 | 0.01 | -18.4 | 0.17 | 0.01 | -13.3 |
| $Cr_2O_3$ | 0.167 | 0.18 | 0.03 | 5.8 | 0.15 | 0.03 | -9.2 |
| F | 0.1 | 0.00 | 0.00 | -97.6 | 0.11 | 0.09 | 2.0 |
| $Fe_2O_3$ | 0.13 | 0.14 | 0.04 | 9.2 | 0.13 | 0.03 | -3.6 |
| $K_2O$ | 0.963 | 0.97 | 0.01 | 0.6 | 0.97 | 0.03 | 30.6 |
| $Li_2O$ | 0.012 | NM | NM | NM | NM | NM | NM |
| MgO | 0.095 | 0.09 | 0.01 | -9.7 | 0.10 | 0.01 | 120.2 |
| MnO | 0.007 | 0.01 | 0.02 | 100.6 | 0.01 | 0.01 | -9.3 |
| $Na_2O$ | 25.08 | 24.64 | 0.31 | -1.8 | 24.05 | 0.18 | 14.0 |
| $Nd_2O_3$ | 0.217 | 0.20 | 0.04 | -6.5 | 0.21 | 0.07 | -1.9 |
| NiO | 0.017 | 0.02 | 0.03 | 15.8 | 0.03 | 0.02 | -2.7 |
| $P_2O_5$ | 0.357 | 0.36 | 0.05 | 1.7 | 0.34 | 0.02 | -3.3 |
| PbO | 0.058 | 0.06 | 0.09 | 9.6 | 0.02 | 0.03 | 22.3 |
| $RuO_2$ | 0 | 0.01 | 0.01 | NM | 0.00 | 0.01 | NM |
| $SO_3$ | 0.369 | 0.28 | 0.05 | -23.1 | 0.23 | 0.04 | -14.4 |
| $SiO_2$ | 43.83 | 44.95 | 0.25 | 2.6 | 44.93 | 0.47 | -1.4 |
| $V_2O_5$ | 0.049 | 0.02 | 0.05 | -63.6 | 0.03 | 0.03 | -6.9 |
| ZnO | 0.008 | 0.03 | 0.03 | 212.9 | 0.03 | 0.02 | 3.4 |
| $ZrO_2$ | 0.012 | 0.05 | 0.03 | 324.2 | 0.03 | 0.06 | -8.4 |
| SUM | 100 | 98.20 | NM | NM | 98.51 | NM | NM |

* RPD – Relative Percentage Difference
** NM – not measured

Table B.3. Targeted vs. measured composition (mass fraction) for the APPS2-03 glass.

| | APPS2-03 | APPS2-03-Q (1kg) | | | APPS2-03-Q (2kg) | | |
|---|---|---|---|---|---|---|---|
| Oxide | Target (wt%) | Measured (wt%) | σ (wt%) | RPD* (%) | Measured | σ (wt%) | RPD (%) |
| $Ag_2O$ | 0 | 0.01 | 0.01 | NM | 0.01 | 0.01 | NM |
| $Al_2O_3$ | 25.694 | 24.49 | 0.18 | -4.7 | 23.81 | 0.28 | -7.3 |
| $B_2O_3$ | 22.289 | 19.34 | 1.23 | -13.2 | 19.83 | 0.94 | -11.0 |
| $Bi_2O_3$ | 0.029 | 0.03 | 0.01 | 17.4 | 0.03 | 0.03 | 15.1 |
| CaO | 0.416 | 0.43 | 0.03 | 3.5 | 0.43 | 0.03 | 3.3 |
| Cl | 0.088 | 0.07 | 0.01 | -26.1 | 0.08 | 0.02 | -12.2 |
| $Cr_2O_3$ | 0.085 | 0.05 | 0.02 | -36.8 | 0.07 | 0.04 | -18.1 |
| F | 0.223 | 0.19 | 0.07 | -15.4 | 0.26 | 0.08 | 14.4 |
| $Fe_2O_3$ | 1.266 | 1.24 | 0.06 | -2.2 | 1.24 | 0.06 | -2.1 |
| $K_2O$ | 0.066 | 0.08 | 0.01 | 27.3 | 0.08 | 0.01 | 27.1 |
| $Li_2O$ | 1.815 | NM | NM | NM | NM | NM | NM |
| MgO | 0.002 | 0.01 | 0.01 | 470.9 | 0.00 | 0.00 | 20.8 |
| MnO | 0.529 | 0.56 | 0.04 | 5.4 | 0.57 | 0.02 | 7.5 |
| $Na_2O$ | 13.735 | 13.72 | 0.14 | -0.1 | 13.63 | 0.20 | -0.8 |
| $Nd_2O_3$ | 1.819 | 1.72 | 0.11 | -5.4 | 1.86 | 0.07 | 2.2 |
| NiO | 0.182 | 0.19 | 0.03 | 2.2 | 0.18 | 0.02 | -2.5 |
| $P_2O_5$ | 0.27 | 0.24 | 0.04 | -9.6 | 0.30 | 0.04 | 9.3 |
| PbO | 0.07 | 0.12 | 0.07 | 73.6 | 0.07 | 0.08 | 2.5 |
| $RuO_2$ | 0 | 0.01 | 0.01 | NM | 0.01 | 0.01 | NM |
| $SO_3$ | 0.149 | 0.13 | 0.04 | -12.1 | 0.13 | 0.04 | -14.0 |
| $SiO_2$ | 27.165 | 27.72 | 0.24 | 2.0 | 27.62 | 0.49 | 1.7 |
| $V_2O_5$ | 0 | 0.01 | 0.01 | NA | 0.02 | 0.05 | NA |
| ZnO | 4.053 | 4.11 | 0.17 | 1.4 | 4.31 | 0.19 | 6.3 |
| $ZrO_2$ | 0.055 | 0.07 | 0.04 | 34.6 | 0.06 | 0.06 | 13.6 |
| SUM | 100 | 94.53 | NM | NM | 94.58 | NM | NM |

* RPD – Relative Percentage Difference
** NM – not measured

Table B.4. Targeted vs. measured composition (mass fraction) for the APPS2-04 glass.

| | APPS2-04 | APPS2-04-Q (1kg) | | | APPS2-04-Q (2kg) | | |
|---|---|---|---|---|---|---|---|
| Oxide | Target (wt%) | Measured (wt%) | σ (wt%) | RPD* (%) | Measured | σ (wt%) | RPD (%) |
| $Ag_2O$ | 0.009 | 0.01 | 0.02 | 9.9 | 0.03 | 0.02 | 194.0 |
| $Al_2O_3$ | 5.428 | 5.27 | 0.10 | -2.9 | 4.97 | 0.04 | -8.4 |
| $B_2O_3$ | 4.975 | 5.38 | 1.35 | 8.1 | 6.02 | 0.98 | 21.1 |
| $Bi_2O_3$ | 0.007 | 0.01 | 0.01 | 40.6 | 0.00 | 0.02 | -37.4 |
| CaO | 6.249 | 6.48 | 0.08 | 3.7 | 6.14 | 0.09 | -1.7 |
| Cl | 0.222 | 0.17 | 0.01 | -23.0 | 0.19 | 0.01 | -15.7 |
| $Cr_2O_3$ | 0.602 | 0.60 | 0.04 | -0.1 | 0.60 | 0.04 | -0.2 |
| F | 1.293 | 1.17 | 0.22 | -9.3 | 0.87 | 0.10 | -32.8 |
| $Fe_2O_3$ | 7.156 | 7.07 | 0.09 | -1.2 | 6.79 | 0.16 | -5.2 |
| $K_2O$ | 0.06 | 0.08 | 0.01 | 29.3 | 0.08 | 0.01 | 39.2 |
| $Li_2O$ | 0 | NM | NM | NM | NM | NM | NM |
| MgO | 0.068 | 0.03 | 0.03 | -52.6 | 0.06 | 0.02 | -17.8 |
| MnO | 0.661 | 0.74 | 0.05 | 12.6 | 0.71 | 0.05 | 6.9 |
| $Na_2O$ | 20.22 | 18.98 | 0.28 | -6.1 | 22.36 | 0.15 | 10.6 |
| $Nd_2O_3$ | 0.328 | 0.36 | 0.06 | 9.4 | 0.34 | 0.05 | 3.3 |
| NiO | 0.263 | 0.28 | 0.03 | 7.2 | 0.27 | 0.03 | 3.6 |
| $P_2O_5$ | 0.549 | 0.59 | 0.05 | 8.3 | 0.53 | 0.04 | -2.7 |
| PbO | 0.272 | 0.25 | 0.17 | -9.7 | 0.21 | 0.15 | -22.8 |
| $RuO_2$ | 0.037 | 0.01 | 0.02 | -68.9 | 0.01 | 0.01 | -79.1 |
| $SO_3$ | 1.206 | 1.19 | 0.06 | -1.2 | 1.10 | 0.07 | -8.5 |
| $SiO_2$ | 45.197 | 45.69 | 0.46 | 1.1 | 45.48 | 0.25 | 0.6 |
| $V_2O_5$ | 5.101 | 5.01 | 0.07 | -1.7 | 4.71 | 0.10 | -7.6 |
| ZnO | 0.013 | 0.04 | 0.06 | 240.7 | 0.05 | 0.04 | 288.9 |
| $ZrO_2$ | 0.084 | 0.06 | 0.07 | -29.7 | 0.09 | 0.05 | 7.8 |
| SUM | 100 | 99.48 | NM | NM | 101.61 | NM | NM |

* RPD – Relative Percentage Difference
** NM – not measured

Table B.5. Targeted vs. measured composition (mass fraction) for the APPS2-05 glass.

| | APPS2-05 | APPS2-05-Q (1kg) | | | APPS2-05-1-Q (2kg) | | |
|---|---|---|---|---|---|---|---|
| Oxide | Target (wt%) | Measured (wt%) | σ (wt%) | RPD* (%) | Measured | σ (wt%) | RPD (%) |
| $Ag_2O$ | 0.031 | 0.03 | 0.02 | 12.2 | 0.04 | 0.03 | 15.9 |
| $Al_2O_3$ | 4.336 | 4.17 | 0.06 | -3.8 | 4.18 | 0.07 | -3.6 |
| $B_2O_3$ | 13.015 | 13.52 | 1.04 | 3.9 | 14.41 | 1.20 | 10.7 |
| $Bi_2O_3$ | 0.015 | 0.02 | 0.02 | 60.9 | 0.01 | 0.02 | -14.3 |
| CaO | 5.722 | 5.89 | 0.09 | 2.9 | 5.75 | 0.10 | 0.6 |
| Cl | 0.036 | 0.03 | 0.01 | -15.8 | 0.03 | 0.01 | -4.0 |
| $Cr_2O_3$ | 0.177 | 0.17 | 0.04 | -3.5 | 0.16 | 0.05 | -12.0 |
| F | 1.317 | 0.80 | 0.12 | -39.1 | 0.67 | 0.13 | -49.1 |
| $Fe_2O_3$ | 0.39 | 0.39 | 0.05 | -0.1 | 0.38 | 0.06 | -2.7 |
| $K_2O$ | 0.296 | 0.31 | 0.01 | 3.1 | 0.30 | 0.01 | 2.2 |
| $Li_2O$ | 1.02 | NM | NM | NM | NM | NM | NM |
| MgO | 0.087 | 0.06 | 0.02 | -29.3 | 0.10 | 0.02 | 9.2 |
| MnO | 0.2 | 0.21 | 0.03 | 6.9 | 0.23 | 0.04 | 15.2 |
| $Na_2O$ | 17.292 | 16.50 | 0.20 | -4.6 | 18.80 | 0.29 | 8.7 |
| $Nd_2O_3$ | 0.964 | 0.93 | 0.09 | -3.2 | 0.94 | 0.07 | -2.4 |
| NiO | 0.013 | 0.02 | 0.02 | 36.1 | 0.01 | 0.02 | 0.3 |
| $P_2O_5$ | 0.076 | 0.07 | 0.04 | -7.8 | 0.07 | 0.03 | -3.9 |
| PbO | 0.011 | 0.02 | 0.04 | 106.9 | 0.02 | 0.11 | 73.2 |
| $RuO_2$ | 0 | 0.02 | 0.02 | NM | 0.01 | 0.01 | NM |
| $SO_3$ | 0.053 | 0.04 | 0.04 | -17.5 | 0.07 | 0.07 | 23.7 |
| $SiO_2$ | 44.143 | 44.59 | 0.43 | 1.0 | 42.91 | 0.45 | -2.8 |
| $V_2O_5$ | 0.002 | 0.01 | 0.02 | 363.6 | 0.00 | 0.09 | -76.7 |
| ZnO | 1.487 | 1.54 | 0.15 | 3.6 | 1.52 | 0.06 | 2.5 |
| $ZrO_2$ | 9.317 | 8.41 | 0.27 | -9.7 | 8.24 | 0.07 | -11.5 |
| SUM | 100 | 97.78 | NM | NM | 98.85 | NM | NM |

* RPD – Relative Percentage Difference
** NM – not measured

Table B.6. Targeted vs. measured composition (mass fraction) for the APPS2-06 glass.

| | APPS2-06 | APPS2-06-Q (1kg) | | | APPS2-06-1-Q (2kg) | | |
|---|---|---|---|---|---|---|---|
| Oxide | Target (wt%) | Measured (wt%) | σ (wt%) | RPD* (%) | Measured | σ (wt%) | RPD (%) |
| $Ag_2O$ | 0.002 | 0.02 | 0.02 | 810.8 | 0.01 | 0.02 | 250.0 |
| $Al_2O_3$ | 11.473 | 10.97 | 0.10 | -4.4 | 11.13 | 3.61 | -3.0 |
| $B_2O_3$ | 10.66 | 9.83 | 1.79 | -7.8 | 6.38 | 7.05 | -40.1 |
| $Bi_2O_3$ | 0.002 | 0.02 | 0.02 | 732.6 | 0.02 | 0.03 | 750.0 |
| CaO | 7.461 | 7.66 | 0.07 | 2.6 | 7.63 | 2.57 | 2.2 |
| Cl | 0.146 | 0.12 | 0.01 | -20.3 | 0.11 | 0.08 | -21.9 |
| $Cr_2O_3$ | 0.079 | 0.09 | 0.03 | 8.1 | 0.09 | 0.04 | 11.4 |
| F | 2.167 | 1.73 | 0.22 | -20.2 | 1.91 | 0.47 | -12.0 |
| $Fe_2O_3$ | 0.086 | 0.11 | 0.05 | 26.4 | 0.12 | 0.04 | 37.2 |
| $K_2O$ | 0.202 | 0.22 | 0.01 | 9.9 | 0.29 | 0.08 | 41.1 |
| $Li_2O$ | 1.419 | NM | NM | NM | NM | NM | NM |
| MgO | 0.027 | 0.00 | 0.00 | -98.5 | 0.01 | 0.02 | -77.8 |
| MnO | 0.017 | 0.01 | 0.01 | -15.8 | 0.03 | 0.03 | 64.7 |
| $Na_2O$ | 17.235 | 16.50 | 0.19 | -4.2 | 17.02 | 5.72 | -1.3 |
| $Nd_2O_3$ | 0.036 | 0.04 | 0.04 | 13.9 | 0.03 | 0.04 | -27.8 |
| NiO | 0.003 | 0.01 | 0.01 | 174.1 | 0.01 | 0.01 | 366.7 |
| $P_2O_5$ | 0.485 | 0.49 | 0.05 | 0.1 | 0.48 | 0.16 | -1.9 |
| PbO | 0.01 | 0.04 | 0.05 | 266.8 | 0.04 | 0.03 | 330.0 |
| $RuO_2$ | 0 | 0.00 | 0.01 | NM | 0.02 | 0.00 | NM |
| $SO_3$ | 1.581 | 1.45 | 0.04 | -8.0 | 1.49 | 0.51 | -5.8 |
| $SiO_2$ | 41.813 | 41.54 | 0.56 | -0.7 | 42.25 | 14.16 | 1.0 |
| $V_2O_5$ | 5.084 | 4.98 | 0.12 | -2.1 | 4.94 | 1.69 | -2.8 |
| ZnO | 0.005 | 0.04 | 0.03 | 773.8 | 0.01 | 0.04 | 160.0 |
| $ZrO_2$ | 0.007 | 0.05 | 0.04 | 561.7 | 0.03 | 0.04 | 371.4 |
| SUM | 100 | 95.90 | NM | NM | 94.03 | NM | NM |

* RPD – Relative Percentage Difference
** NM – not measured

Table B.7. Targeted vs. measured composition (mass fraction) for the APPS2-07 glass.

| | APPS2-07 | APPS2-07-Q (1kg) | | | APPS2-07-Q (2kg) | | |
|---|---|---|---|---|---|---|---|
| Oxide | Target (wt%) | Measured (wt%) | σ (wt%) | RPD* (%) | Measured | σ (wt%) | RPD (%) |
| $Ag_2O$ | 0 | 0.01 | 0.02 | NM | 0.02 | 0.02 | NM |
| $Al_2O_3$ | 6.171 | 5.97 | 0.07 | -3.2 | 5.99 | 0.07 | -3.0 |
| $B_2O_3$ | 5.591 | 6.03 | 1.06 | 7.9 | 4.74 | 8.44 | -15.2 |
| $Bi_2O_3$ | 0.535 | 0.50 | 0.04 | -7.2 | 0.49 | 0.03 | -9.0 |
| CaO | 2.498 | 2.58 | 0.05 | 3.3 | 2.72 | 0.32 | 8.8 |
| Cl | 0.277 | 0.20 | 0.01 | -26.8 | 0.24 | 0.01 | -11.9 |
| $Cr_2O_3$ | 0.602 | 0.62 | 0.03 | 2.2 | 0.64 | 0.10 | 6.0 |
| F | 0.402 | 0.27 | 0.11 | -32.3 | 0.42 | 0.11 | 4.9 |
| $Fe_2O_3$ | 6.982 | 6.99 | 0.17 | 0.2 | 6.90 | 0.17 | -1.2 |
| $K_2O$ | 0.026 | 0.05 | 0.01 | 98.7 | 0.05 | 0.02 | 99.6 |
| $Li_2O$ | 0 | NM | NM | NM | NM | NM | NM |
| MgO | 0.008 | 0.01 | 0.01 | 22.2 | 0.02 | 0.04 | 201.2 |
| MnO | 0.312 | 0.36 | 0.05 | 16.0 | 0.36 | 0.03 | 16.0 |
| $Na_2O$ | 23.193 | 23.27 | 0.33 | 0.3 | 23.21 | 0.39 | 0.1 |
| $Nd_2O_3$ | 0.305 | 0.31 | 0.06 | 3.3 | 0.30 | 0.05 | -0.4 |
| NiO | 0.186 | 0.20 | 0.03 | 5.6 | 0.19 | 0.03 | 3.9 |
| $P_2O_5$ | 2.408 | 2.34 | 0.08 | -2.8 | 2.37 | 0.11 | -1.5 |
| PbO | 0.516 | 0.54 | 0.01 | 4.8 | 0.46 | 0.10 | -11.3 |
| $RuO_2$ | 0 | 0.00 | 0.12 | NM | 0.00 | 0.00 | NM |
| $SO_3$ | 0.714 | 0.68 | 0.05 | -5.0 | 0.69 | 0.07 | -3.3 |
| $SiO_2$ | 45.679 | 47.26 | 0.38 | 3.5 | 45.86 | 0.94 | 0.4 |
| $V_2O_5$ | 0 | 0.01 | 0.02 | NA | 0.01 | 0.02 | NA |
| ZnO | 3.574 | 3.78 | 0.16 | 5.9 | 3.72 | 0.22 | 4.0 |
| $ZrO_2$ | 0.021 | 0.02 | 0.03 | 1.1 | 0.05 | 0.04 | 125.3 |
| SUM | 100 | 102.02 | NM | NM | 99.45 | NM | NM |

* RPD – Relative Percentage Difference
** NM – not measured

Table B.8. Targeted vs. measured composition (mass fraction) for the APPS2-08 glass.

| | APPS2-08 | APPS2-08-Q (1kg) | | | APPS2-08-Q (2kg) | | |
|---|---|---|---|---|---|---|---|
| Oxide | Target (wt%) | Measured (wt%) | σ (wt%) | RPD* (%) | Measured | σ (wt%) | RPD (%) |
| $Ag_2O$ | 0 | 0.01 | 0.01 | NM | 0.00 | 0.01 | NM |
| $Al_2O_3$ | 14.695 | 14.03 | 0.31 | -4.6 | 13.65 | 1.00 | -7.1 |
| $B_2O_3$ | 13.935 | 13.56 | 0.77 | -2.7 | 8.39 | 10.36 | -39.8 |
| $Bi_2O_3$ | 1.548 | 1.41 | 0.08 | -9.2 | 1.38 | 0.16 | -10.8 |
| CaO | 1.001 | 1.03 | 0.04 | 3.2 | 1.16 | 0.30 | 15.5 |
| Cl | 0.116 | 0.07 | 0.01 | -39.4 | 0.08 | 0.01 | -34.4 |
| $Cr_2O_3$ | 0.163 | 0.11 | 0.17 | -31.8 | 0.12 | 0.05 | -26.7 |
| F | 0.415 | 0.12 | 0.10 | -70.8 | 0.36 | 0.13 | -14.4 |
| $Fe_2O_3$ | 12.059 | 11.50 | 1.42 | -4.7 | 11.38 | 1.08 | -5.7 |
| $K_2O$ | 0.068 | 0.09 | 0.01 | 28.5 | 0.08 | 0.01 | 15.3 |
| $Li_2O$ | 0.713 | NM | NM | NM | NM | NM | NM |
| MgO | 0.003 | 0.01 | 0.01 | 218.1 | 0.03 | 0.05 | 785.9 |
| MnO | 0.714 | 0.78 | 0.06 | 8.9 | 0.77 | 0.06 | 8.2 |
| $Na_2O$ | 13.19 | 13.34 | 0.22 | 1.2 | 13.04 | 0.83 | -1.2 |
| $Nd_2O_3$ | 0.797 | 0.82 | 0.12 | 2.6 | 0.77 | 0.14 | -3.2 |
| NiO | 0.726 | 0.60 | 0.54 | -17.0 | 0.66 | 0.10 | -9.8 |
| $P_2O_5$ | 2.105 | 2.07 | 0.12 | -1.8 | 2.12 | 0.19 | 0.7 |
| PbO | 0.828 | 0.73 | 0.01 | -11.4 | 0.75 | 0.13 | -9.8 |
| $RuO_2$ | 0 | 0.00 | 0.09 | NM | 0.00 | 0.00 | NM |
| $SO_3$ | 0.35 | 0.28 | 0.04 | -20.0 | 0.40 | 0.31 | 13.5 |
| $SiO_2$ | 30.826 | 31.70 | 0.90 | 2.8 | 30.66 | 3.03 | -0.5 |
| $V_2O_5$ | 4.948 | 4.97 | 0.21 | 0.4 | 4.79 | 0.43 | -3.1 |
| ZnO | 0.475 | 0.53 | 0.12 | 11.2 | 0.50 | 0.11 | 5.9 |
| $ZrO_2$ | 0.325 | 0.34 | 0.07 | 4.2 | 0.30 | 0.08 | -6.2 |
| SUM | 100 | 98.09 | NM | NM | 91.38 | NM | NM |

* RPD – Relative Percentage Difference
** NM – not measured

Table B.9. Targeted vs. measured composition (mass fraction) for the APPS2-09 glass.

| | APPS2-09 | APPS2-09-Q (1kg) | | | APPS2-09-Q (2kg) | | |
|---|---|---|---|---|---|---|---|
| Oxide | Target (wt%) | Measured (wt%) | σ (wt%) | RPD* (%) | Measured | σ (wt%) | RPD (%) |
| $Ag_2O$ | 0 | 0.00 | 0.01 | NM | 0.01 | 0.01 | NM |
| $Al_2O_3$ | 22.569 | 21.09 | 0.55 | -6.6 | 20.98 | 0.25 | -7.0 |
| $B_2O_3$ | 21.983 | 19.02 | 9.89 | -13.5 | 15.93 | 1.03 | -27.5 |
| $Bi_2O_3$ | 0.032 | 0.03 | 0.02 | -12.8 | 0.02 | 0.02 | -26.9 |
| CaO | 2.068 | 2.10 | 0.08 | 1.6 | 2.14 | 0.05 | 3.4 |
| Cl | 0.114 | 0.07 | 0.02 | -39.2 | 0.10 | 0.01 | -14.7 |
| $Cr_2O_3$ | 0.066 | 0.05 | 0.02 | -29.5 | 0.04 | 0.03 | -37.1 |
| F | 0.204 | 0.07 | 0.12 | -64.5 | 0.27 | 0.08 | 32.7 |
| $Fe_2O_3$ | 4.163 | 4.03 | 0.19 | -3.3 | 3.98 | 0.07 | -4.4 |
| $K_2O$ | 0.038 | 0.06 | 0.01 | 59.8 | 0.05 | 0.01 | 31.7 |
| $Li_2O$ | 1.653 | NM | NM | NM | NM | NM | NM |
| MgO | 0.003 | 0.01 | 0.02 | 354.7 | 0.02 | 0.02 | 512.3 |
| MnO | 0.058 | 0.07 | 0.03 | 15.9 | 0.06 | 0.04 | 10.1 |
| $Na_2O$ | 11.931 | 11.80 | 0.43 | -1.1 | 11.56 | 0.12 | -3.1 |
| $Nd_2O_3$ | 2.88 | 2.77 | 0.10 | -3.8 | 2.77 | 0.07 | -3.8 |
| NiO | 0.96 | 0.98 | 0.06 | 2.2 | 0.91 | 0.04 | -5.5 |
| $P_2O_5$ | 1.554 | 1.49 | 0.10 | -3.8 | 1.52 | 0.05 | -2.1 |
| PbO | 0.378 | 0.39 | 0.18 | 3.5 | 0.32 | 0.01 | -16.6 |
| $RuO_2$ | 0 | 0.01 | 0.01 | NM | 0.01 | 0.11 | NM |
| $SO_3$ | 0.378 | 0.26 | 0.08 | -32.3 | 0.35 | 0.05 | -7.1 |
| $SiO_2$ | 28.649 | 28.51 | 1.45 | -0.5 | 28.45 | 0.57 | -0.7 |
| $V_2O_5$ | 0 | 0.01 | 0.01 | NA | 0.01 | 0.02 | NA |
| ZnO | 0.193 | 0.23 | 0.04 | 16.8 | 0.19 | 0.07 | -3.5 |
| $ZrO_2$ | 0.126 | 0.08 | 0.07 | -37.8 | 0.08 | 0.07 | -34.9 |
| SUM | 100 | 93.13 | NM | NM | 89.75 | NM | NM |

* RPD – Relative Percentage Difference
** NM – not measured

Table B.10. Targeted vs. measured composition (mass fraction) for the APPS2-10 glass.

| | APPS2-10 | APPS2-10-Q (1kg) | | | APPS2-10-Q (2kg) | | |
|---|---|---|---|---|---|---|---|
| Oxide | Target (wt%) | Measured (wt%) | σ (wt%) | RPD* (%) | Measured | σ (wt%) | RPD (%) |
| $Ag_2O$ | 0.011 | 0.02 | 0.02 | 64.8 | 0.02 | 0.02 | 109.9 |
| $Al_2O_3$ | 18.567 | 17.67 | 0.19 | -4.8 | 17.85 | 0.24 | -3.9 |
| $B_2O_3$ | 22.063 | 18.59 | 0.89 | -15.7 | 21.45 | 10.50 | -2.8 |
| $Bi_2O_3$ | 0.008 | 0.02 | 0.04 | 194.7 | 0.02 | 0.02 | 166.0 |
| CaO | 0.254 | 0.28 | 0.02 | 9.0 | 0.29 | 0.02 | 15.6 |
| Cl | 0.193 | 0.15 | 0.01 | -24.7 | 0.17 | 0.01 | -12.0 |
| $Cr_2O_3$ | 1.025 | 0.89 | 0.21 | -13.2 | 0.83 | 0.73 | -18.9 |
| F | 0.204 | 0.09 | 0.08 | -55.6 | 0.07 | 0.08 | -67.4 |
| $Fe_2O_3$ | 0.175 | 0.17 | 0.04 | -4.7 | 0.21 | 0.05 | 17.3 |
| $K_2O$ | 1.563 | 1.56 | 0.02 | -0.4 | 1.60 | 0.02 | 2.2 |
| $Li_2O$ | 0.023 | NM | NM | NM | NM | NM | NM |
| MgO | 0.046 | 0.03 | 0.02 | -25.5 | 0.05 | 0.02 | 15.5 |
| MnO | 0.015 | 0.02 | 0.02 | 19.0 | 0.02 | 0.02 | 32.5 |
| $Na_2O$ | 20.668 | 20.27 | 0.19 | -1.9 | 20.53 | 0.39 | -0.7 |
| $Nd_2O_3$ | 0.115 | 0.11 | 0.06 | -4.2 | 0.14 | 0.05 | 22.3 |
| NiO | 0.052 | 0.05 | 0.02 | 1.0 | 0.05 | 0.02 | -11.0 |
| $P_2O_5$ | 0.448 | 0.43 | 0.07 | -3.0 | 0.43 | 0.03 | -4.6 |
| PbO | 0.027 | 0.03 | 0.00 | 3.4 | 0.04 | 0.05 | 35.9 |
| $RuO_2$ | 0 | 0.00 | 0.04 | NM | 0.00 | 0.01 | NM |
| $SO_3$ | 0.267 | 0.23 | 0.04 | -14.2 | 0.19 | 0.05 | -27.7 |
| $SiO_2$ | 34.22 | 34.94 | 0.45 | 2.1 | 33.85 | 0.50 | -1.1 |
| $V_2O_5$ | 0.023 | 0.01 | 0.02 | -51.9 | 0.01 | 0.01 | -61.6 |
| ZnO | 0.017 | 0.04 | 0.03 | 110.0 | 0.03 | 0.03 | 59.1 |
| $ZrO_2$ | 0.016 | 0.04 | 0.05 | 138.1 | 0.02 | 0.03 | 17.4 |
| SUM | 100 | 95.63 | NM | NM | 97.86 | NM | NM |

* RPD – Relative Percentage Difference
** NM – not measured

Table B.11. Targeted vs. measured composition (mass fraction) for the APPS2-11 glass.

| | APPS2-11 | APPS2-11-Q (1kg) | | | APPS2-11-Q (2kg) | | |
|---|---|---|---|---|---|---|---|
| Oxide | Target (wt%) | Measured (wt%) | σ (wt%) | RPD* (%) | Measured | σ (wt%) | RPD (%) |
| $Ag_2O$ | 0.019 | 0.02 | 0.02 | 7.5 | 0.02 | 0.02 | 27.2 |
| $Al_2O_3$ | 3.867 | 3.77 | 0.05 | -2.6 | 3.81 | 0.04 | -1.6 |
| $B_2O_3$ | 8.145 | 8.89 | 1.36 | 9.1 | 12.21 | 8.94 | 49.9 |
| $Bi_2O_3$ | 0.016 | 0.01 | 0.02 | -8.7 | 0.03 | 0.04 | 67.8 |
| CaO | 8.662 | 8.92 | 0.08 | 3.0 | 9.14 | 0.11 | 5.6 |
| Cl | 0.105 | 0.08 | 0.01 | -25.1 | 0.09 | 0.01 | -15.8 |
| $Cr_2O_3$ | 0.585 | 0.60 | 0.04 | 2.3 | 0.58 | 0.03 | -1.4 |
| F | 4.513 | 4.25 | 0.28 | -5.8 | 4.15 | 0.41 | -8.1 |
| $Fe_2O_3$ | 0.183 | 0.22 | 0.03 | 18.0 | 0.20 | 0.03 | 8.7 |
| $K_2O$ | 0.508 | 0.54 | 0.01 | 6.0 | 0.54 | 0.02 | 6.0 |
| $Li_2O$ | 1.563 | NM | NM | NM | NM | NM | NM |
| MgO | 0.075 | 0.06 | 0.02 | -20.5 | 0.08 | 0.02 | 6.1 |
| MnO | 0.022 | 0.03 | 0.02 | 29.8 | 0.02 | 0.02 | 8.9 |
| $Na_2O$ | 16.144 | 16.16 | 0.19 | 0.1 | 16.18 | 0.36 | 0.2 |
| $Nd_2O_3$ | 0.303 | 0.28 | 0.08 | -8.0 | 0.32 | 0.07 | 6.5 |
| NiO | 0.005 | 0.01 | 0.01 | 98.6 | 0.02 | 0.02 | 220.7 |
| $P_2O_5$ | 0.381 | 0.39 | 0.05 | 1.8 | 0.35 | 0.07 | -9.0 |
| PbO | 0.003 | 0.06 | 0.01 | 2033.2 | 0.02 | 0.03 | 728.6 |
| $RuO_2$ | 0 | 0.00 | 0.07 | NM | 0.01 | 0.01 | NM |
| $SO_3$ | 1.201 | 1.10 | 0.07 | -8.6 | 1.12 | 0.07 | -6.9 |
| $SiO_2$ | 48.034 | 49.53 | 0.89 | 3.1 | 49.67 | 0.84 | 3.4 |
| $V_2O_5$ | 0.002 | 0.01 | 0.03 | 587.4 | 0.01 | 0.02 | 325.8 |
| ZnO | 0.019 | 0.03 | 0.03 | 50.9 | 0.02 | 0.03 | 24.0 |
| $ZrO_2$ | 5.645 | 5.21 | 0.16 | -7.7 | 5.20 | 0.18 | -7.9 |
| SUM | 100 | 100.17 | NM | NM | 103.78 | NM | NM |

* RPD – Relative Percentage Difference
** NM – not measured

Table B.12. Targeted vs. measured composition (mass fraction) for the APPS2-12 glass.

| | APPS2-12 | APPS2-12-Q (1kg) | | | APPS2-12-Q (2kg) | | |
|---|---|---|---|---|---|---|---|
| Oxide | Target (wt%) | Measured (wt%) | σ (wt%) | RPD* (%) | Measured | σ (wt%) | RPD (%) |
| $Ag_2O$ | 0.004 | 0.01 | 0.01 | 209.9 | 0.01 | 0.02 | 240.1 |
| $Al_2O_3$ | 25.758 | 24.21 | 0.25 | -6.0 | 21.84 | 7.68 | -15.2 |
| $B_2O_3$ | 22.029 | 18.85 | 0.98 | -14.4 | 21.23 | 14.30 | -3.6 |
| $Bi_2O_3$ | 0.004 | 0.02 | 0.02 | 341.3 | 0.02 | 0.02 | 302.2 |
| CaO | 0.064 | 0.08 | 0.02 | 23.4 | 0.09 | 0.03 | 37.3 |
| Cl | 0.173 | 0.12 | 0.02 | -29.4 | 0.16 | 0.08 | -5.6 |
| $Cr_2O_3$ | 0.161 | 0.14 | 0.03 | -14.7 | 0.13 | 0.18 | -20.6 |
| F | 0.147 | 0.01 | 0.03 | -90.6 | 0.15 | 0.26 | -0.8 |
| $Fe_2O_3$ | 0.024 | 0.05 | 0.03 | 94.8 | 0.04 | 0.03 | 47.3 |
| $K_2O$ | 0.334 | 0.34 | 0.01 | 0.5 | 0.33 | 0.12 | -1.1 |
| $Li_2O$ | 1.74 | NM | NM | NM | NM | NM | NM |
| MgO | 0.027 | 0.03 | 0.02 | 10.0 | 0.02 | 0.01 | -19.4 |
| MnO | 0.002 | 0.01 | 0.01 | 396.8 | 0.01 | 0.01 | 169.3 |
| $Na_2O$ | 13.811 | 13.72 | 0.17 | -0.6 | 12.52 | 4.40 | -9.4 |
| $Nd_2O_3$ | 0.025 | 0.04 | 0.04 | 57.8 | 0.03 | 0.04 | 38.5 |
| NiO | 0.004 | 0.01 | 0.02 | 156.4 | 0.00 | 0.01 | 16.6 |
| $P_2O_5$ | 0.118 | 0.11 | 0.04 | -3.2 | 0.11 | 0.05 | -3.1 |
| PbO | 0.016 | 0.02 | 0.02 | 48.5 | 0.04 | 0.05 | 144.4 |
| $RuO_2$ | 0 | 0.01 | 0.05 | NM | 0.01 | 0.01 | NM |
| $SO_3$ | 0.142 | 0.13 | 0.03 | -10.4 | 0.12 | 0.05 | -17.1 |
| $SiO_2$ | 27.35 | 27.67 | 0.35 | 1.2 | 24.46 | 8.60 | -10.6 |
| $V_2O_5$ | 4.06 | 4.04 | 0.09 | -0.5 | 3.59 | 1.26 | -11.6 |
| ZnO | 4.005 | 4.01 | 0.26 | 0.2 | 3.76 | 1.35 | -6.2 |
| $ZrO_2$ | 0.002 | 0.02 | 0.03 | 1000.8 | 0.03 | 0.03 | 1296.5 |
| SUM | 100 | 93.66 | NM | NM | 88.68 | NM | NM |

* RPD – Relative Percentage Difference
** NM – not measured

Table B.13. Targeted vs. measured composition (mass fraction) for the APPS2-13 glass.

| | APPS2-13 | APPS2-13-Q (1kg) | | | APPS2-13-Q (2kg) | | |
|---|---|---|---|---|---|---|---|
| Oxide | Target (wt%) | Measured (wt%) | σ (wt%) | RPD* (%) | Measured | σ (wt%) | RPD (%) |
| $Ag_2O$ | 0 | 0.01 | 0.01 | NM | 0.01 | 0.02 | NM |
| $Al_2O_3$ | 5.06 | 4.80 | 0.10 | -5.1 | 4.57 | 1.06 | -9.6 |
| $B_2O_3$ | 4.722 | 5.26 | 1.16 | 11.3 | 4.18 | 4.90 | -11.4 |
| $Bi_2O_3$ | 0.001 | 0.00 | 0.01 | 338.8 | 0.01 | 0.02 | 1155.8 |
| CaO | 8.371 | 8.50 | 0.10 | 1.5 | 8.37 | 1.34 | 0.0 |
| Cl | 0.08 | 0.05 | 0.01 | -36.0 | 0.10 | 0.08 | 19.4 |
| $Cr_2O_3$ | 0.445 | 0.43 | 0.06 | -3.1 | 0.40 | 0.07 | -9.4 |
| F | 1.992 | 1.70 | 0.16 | -14.8 | 1.78 | 0.37 | -10.5 |
| $Fe_2O_3$ | 5.239 | 5.12 | 0.12 | -2.3 | 4.90 | 0.85 | -6.5 |
| $K_2O$ | 0.128 | 0.15 | 0.01 | 13.8 | 0.15 | 0.01 | 15.2 |
| $Li_2O$ | 1.768 | NM | NM | NM | NM | NM | NM |
| MgO | 0.018 | 0.00 | 0.01 | -76.3 | 0.02 | 0.02 | -3.5 |
| MnO | 0.382 | 0.40 | 0.03 | 5.0 | 0.41 | 0.08 | 7.3 |
| $Na_2O$ | 16.29 | 15.86 | 0.22 | -2.6 | 14.91 | 3.59 | -8.4 |
| $Nd_2O_3$ | 0.06 | 0.05 | 0.05 | -18.0 | 0.03 | 0.03 | -47.7 |
| NiO | 0.223 | 0.24 | 0.03 | 8.4 | 0.21 | 0.04 | -3.9 |
| $P_2O_5$ | 0.408 | 0.38 | 0.06 | -5.7 | 0.39 | 0.08 | -5.6 |
| PbO | 0.101 | 0.07 | 0.02 | -26.1 | 0.10 | 0.08 | -0.7 |
| $RuO_2$ | 0 | 0.01 | 0.09 | NM | 0.00 | 0.00 | NM |
| $SO_3$ | 1.473 | 1.41 | 0.04 | -4.2 | 1.41 | 0.10 | -3.9 |
| $SiO_2$ | 47.972 | 48.19 | 1.03 | 0.4 | 46.27 | 8.20 | -3.6 |
| $V_2O_5$ | 5.098 | 5.06 | 0.11 | -0.7 | 4.76 | 0.83 | -6.6 |
| ZnO | 0 | 0.02 | 0.03 | NA | 0.03 | 0.04 | NA |
| $ZrO_2$ | 0.169 | 0.13 | 0.08 | -24.3 | 0.15 | 0.08 | -13.3 |
| SUM | 100 | 97.86 | NM | NM | 93.17 | NM | NM |

* RPD – Relative Percentage Difference
** NM – not measured

Table B.14. Targeted vs. measured composition (mass fraction) for the APPS2-14-1 glass.

| | APPS2-14-1 | APPS2-14-1-Q (1kg) | | | APPS2-14-Q (2kg) | | |
|---|---|---|---|---|---|---|---|
| Oxide | Target (wt%) | Measured (wt%) | σ (wt%) | RPD* (%) | Measured | σ (wt%) | RPD (%) |
| $Ag_2O$ | 0 | 0.01 | 0.02 | NM | 0.01 | 0.02 | NM |
| $Al_2O_3$ | 14.012 | 13.45 | 0.11 | -4.0 | 13.18 | 0.38 | -5.9 |
| $B_2O_3$ | 17.265 | 15.08 | 0.80 | -12.6 | 13.56 | 6.75 | -21.5 |
| $Bi_2O_3$ | 0.001 | 0.01 | 0.02 | 600.0 | 0.00 | 0.01 | 386.0 |
| CaO | 0.733 | 0.79 | 0.04 | 7.1 | 0.80 | 0.06 | 9.1 |
| Cl | 0.097 | 0.07 | 0.01 | -27.8 | 0.07 | 0.01 | -25.5 |
| $Cr_2O_3$ | 0.52 | 0.45 | 0.07 | -13.3 | 0.51 | 0.16 | -2.5 |
| F | 1.222 | 1.03 | 0.19 | -15.5 | 0.89 | 0.17 | -27.0 |
| $Fe_2O_3$ | 3.817 | 3.85 | 0.08 | 1.0 | 3.74 | 0.10 | -1.9 |
| $K_2O$ | 0.101 | 0.11 | 0.01 | 11.9 | 0.12 | 0.01 | 16.7 |
| $Li_2O$ | 0.092 | NM | NM | NM | NM | NM | NM |
| MgO | 0.002 | 0.01 | 0.01 | 300.0 | 0.01 | 0.01 | 306.7 |
| MnO | 0.774 | 0.90 | 0.05 | 16.0 | 0.83 | 0.03 | 7.6 |
| $Na_2O$ | 17.664 | 17.74 | 0.27 | 0.4 | 19.43 | 0.49 | 10.0 |
| $Nd_2O_3$ | 2.116 | 2.23 | 0.10 | 5.2 | 2.16 | 0.08 | 1.9 |
| NiO | 0.498 | 0.52 | 0.03 | 5.0 | 0.48 | 0.03 | -4.6 |
| $P_2O_5$ | 0.21 | 0.22 | 0.03 | 4.3 | 0.20 | 0.05 | -5.1 |
| PbO | 0.1 | 0.08 | 0.01 | -25.0 | 0.11 | 0.10 | 6.4 |
| $RuO_2$ | 0 | 0.01 | 0.08 | NM | 0.01 | 0.02 | NM |
| $SO_3$ | 0.117 | 0.08 | 0.04 | -30.8 | 0.09 | 0.03 | -26.1 |
| $SiO_2$ | 29.813 | 31.27 | 0.42 | 4.9 | 29.83 | 1.18 | 0.1 |
| $V_2O_5$ | 1.762 | 1.76 | 0.06 | -0.2 | 1.70 | 0.08 | -3.5 |
| ZnO | 0 | 0.05 | 0.04 | NA | 0.01 | 0.02 | NA |
| $ZrO_2$ | 9.084 | 7.26 | 0.19 | -20.1 | 8.22 | 2.12 | -9.5 |
| SUM | 100 | 96.95 | NM | NM | 95.95 | NM | NM |

* RPD – Relative Percentage Difference
** NM – not measured

Table B.15. Targeted vs. measured composition (mass fraction) for the APPS2-15 glass.

| | APPS2-15 | APPS2-15-Q (1kg) | | | APPS2-15-Q (2kg) | | |
|---|---|---|---|---|---|---|---|
| Oxide | Target (wt%) | Measured (wt%) | σ (wt%) | RPD* (%) | Measured | σ (wt%) | RPD (%) |
| $Ag_2O$ | 0.034 | 0.04 | 0.02 | 22.0 | 0.04 | 0.02 | 11.1 |
| $Al_2O_3$ | 9.123 | 8.76 | 0.11 | -4.0 | 8.68 | 0.10 | -4.9 |
| $B_2O_3$ | 12.172 | 11.91 | 1.15 | -2.1 | 6.22 | 4.84 | -48.9 |
| $Bi_2O_3$ | 0.024 | 0.01 | 0.01 | -57.3 | 0.02 | 0.02 | -13.4 |
| CaO | 0.118 | 0.14 | 0.01 | 17.9 | 0.16 | 0.02 | 31.5 |
| Cl | 0.279 | 0.22 | 0.01 | -22.3 | 0.24 | 0.01 | -13.0 |
| $Cr_2O_3$ | 0.603 | 0.59 | 0.10 | -2.0 | 0.57 | 0.10 | -4.8 |
| F | 0.498 | 0.19 | 0.12 | -61.6 | 0.20 | 0.06 | -60.6 |
| $Fe_2O_3$ | 0.261 | 0.25 | 0.06 | -2.3 | 0.25 | 0.04 | -2.5 |
| $K_2O$ | 0.895 | 0.91 | 0.01 | 1.6 | 0.92 | 0.02 | 3.3 |
| $Li_2O$ | 0.005 | NM | NM | NM | NM | NM | NM |
| MgO | 0.106 | 0.09 | 0.02 | -11.3 | 0.10 | 0.02 | -10.1 |
| MnO | 0.071 | 0.09 | 0.03 | 20.6 | 0.10 | 0.02 | 38.0 |
| $Na_2O$ | 24.504 | 24.47 | 0.28 | -0.1 | 24.24 | 0.19 | -1.1 |
| $Nd_2O_3$ | 0.555 | 0.58 | 0.06 | 4.6 | 0.60 | 0.07 | 7.3 |
| NiO | 0.013 | 0.03 | 0.02 | 101.9 | 0.02 | 0.02 | 45.9 |
| $P_2O_5$ | 1.959 | 1.95 | 0.09 | -0.4 | 2.00 | 0.09 | 2.2 |
| PbO | 0.048 | 0.04 | 0.00 | -15.2 | 0.06 | 0.05 | 22.6 |
| $RuO_2$ | 0 | 0.00 | 0.04 | NM | 0.01 | 0.01 | NM |
| $SO_3$ | 0.421 | 0.31 | 0.03 | -26.1 | 0.32 | 0.04 | -23.7 |
| $SiO_2$ | 37.818 | 38.44 | 0.44 | 1.6 | 39.27 | 0.54 | 3.8 |
| $V_2O_5$ | 0.005 | 0.02 | 0.03 | 327.8 | 0.00 | 0.01 | -42.9 |
| ZnO | 1.818 | 2.01 | 0.16 | 10.7 | 1.99 | 0.07 | 9.3 |
| $ZrO_2$ | 8.67 | 8.11 | 0.22 | -6.4 | 8.33 | 0.19 | -3.9 |
| SUM | 100 | 99.16 | NM | NM | 94.33 | NM | NM |

* RPD – Relative Percentage Difference
** NM – not measured

Table B.16. Targeted vs. measured composition (mass fraction) for the APPS2-16 glass.

| | APPS2-16 | APPS2-16-Q (1kg) | | | APPS2-16-Q (2kg) | | |
|---|---|---|---|---|---|---|---|
| Oxide | Target (wt%) | Measured (wt%) | σ (wt%) | RPD* (%) | Measured | σ (wt%) | RPD (%) |
| $Ag_2O$ | 0.014 | 0.03 | 0.02 | 105.4 | 0.02 | 0.02 | 42.5 |
| $Al_2O_3$ | 11.671 | 11.07 | 0.08 | -5.1 | 10.99 | 0.08 | -5.8 |
| $B_2O_3$ | 13.012 | 13.02 | 1.19 | 0.1 | 8.42 | 8.40 | -35.3 |
| $Bi_2O_3$ | 0.007 | 0.02 | 0.02 | 134.7 | 0.01 | 0.02 | 81.7 |
| CaO | 0.278 | 0.30 | 0.02 | 7.3 | 0.32 | 0.01 | 16.3 |
| Cl | 0.152 | 0.12 | 0.01 | -20.2 | 0.13 | 0.01 | -12.6 |
| $Cr_2O_3$ | 0.603 | 0.58 | 0.04 | -3.1 | 0.59 | 0.04 | -2.0 |
| F | 0.173 | 0.01 | 0.03 | -92.8 | 0.08 | 0.08 | -52.9 |
| $Fe_2O_3$ | 1.116 | 1.16 | 0.04 | 3.9 | 1.11 | 0.07 | -0.8 |
| $K_2O$ | 2.525 | 2.54 | 0.03 | 0.6 | 2.59 | 0.04 | 2.8 |
| $Li_2O$ | 0.016 | NM | NM | NM | NM | NM | NM |
| MgO | 0.087 | 0.08 | 0.02 | -4.0 | 0.09 | 0.02 | 8.3 |
| MnO | 0.269 | 0.31 | 0.03 | 13.6 | 0.31 | 0.04 | 15.5 |
| $Na_2O$ | 24.027 | 23.77 | 0.25 | -1.1 | 23.69 | 0.41 | -1.4 |
| $Nd_2O_3$ | 0.445 | 0.45 | 0.09 | 2.0 | 0.44 | 0.09 | -0.7 |
| NiO | 0.046 | 0.05 | 0.02 | 18.5 | 0.05 | 0.02 | -0.7 |
| $P_2O_5$ | 0.134 | 0.14 | 0.03 | 6.1 | 0.14 | 0.04 | 2.8 |
| PbO | 0.165 | 0.11 | 0.03 | -30.4 | 0.19 | 0.08 | 12.9 |
| $RuO_2$ | 0.004 | 0.01 | 0.10 | 198.8 | 0.00 | 0.00 | -100.0 |
| $SO_3$ | 0.153 | 0.11 | 0.03 | -25.6 | 0.11 | 0.03 | -30.4 |
| $SiO_2$ | 43.784 | 44.67 | 0.52 | 2.0 | 44.57 | 0.48 | 1.8 |
| $V_2O_5$ | 0.005 | 0.00 | 0.01 | -9.2 | 0.00 | 0.00 | -48.2 |
| ZnO | 1.248 | 1.36 | 0.13 | 9.0 | 1.37 | 0.15 | 9.8 |
| $ZrO_2$ | 0.066 | 0.09 | 0.08 | 37.5 | 0.06 | 0.06 | -7.6 |
| SUM | 100 | 100.03 | NM | NM | 95.28 | NM | NM |

* RPD – Relative Percentage Difference
** NM – not measured

# Appendix C – XRD Patterns of Quenched Samples with Crystalline Phases Present

The refined X-ray diffraction (XRD) data with wt% of crystalline phases are shown in this appendix. $CeO_2$ was added as a standard to quantify the crystalline phases. Red is calculated and blue is experimental data. The gray line shows the difference between the experimental and calculated values. The normalized wt% of crystalline phase are provided in Table 3.1.

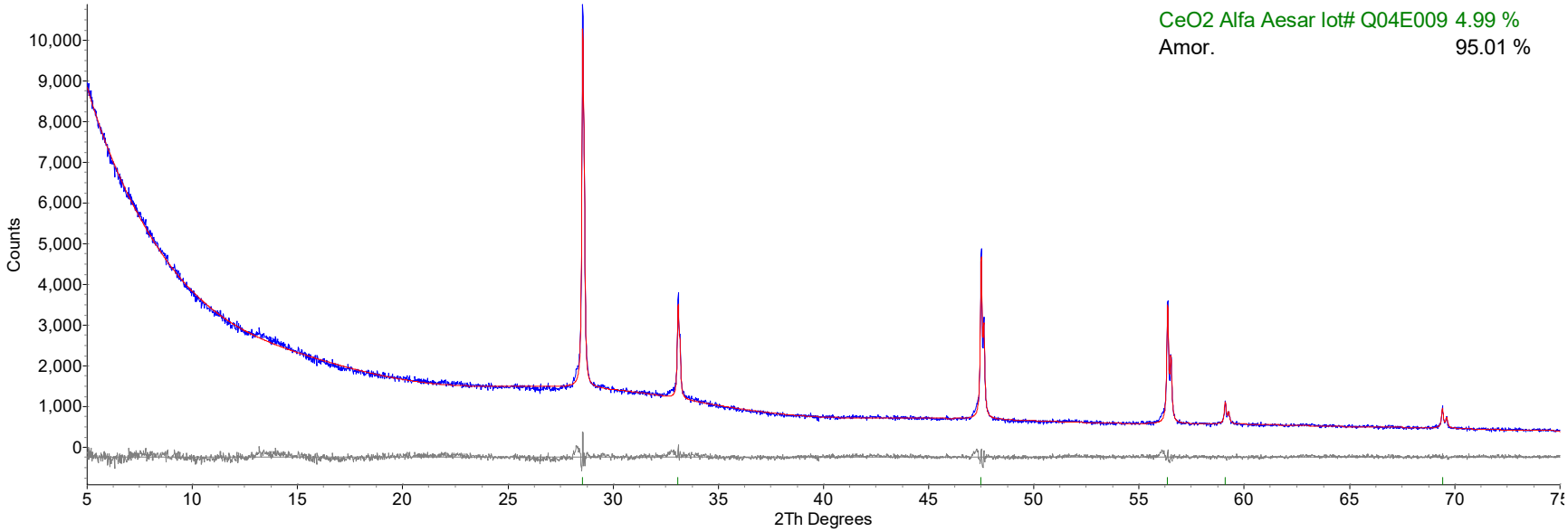


Figure C.1. X-ray diffraction pattern of APPS2-01.

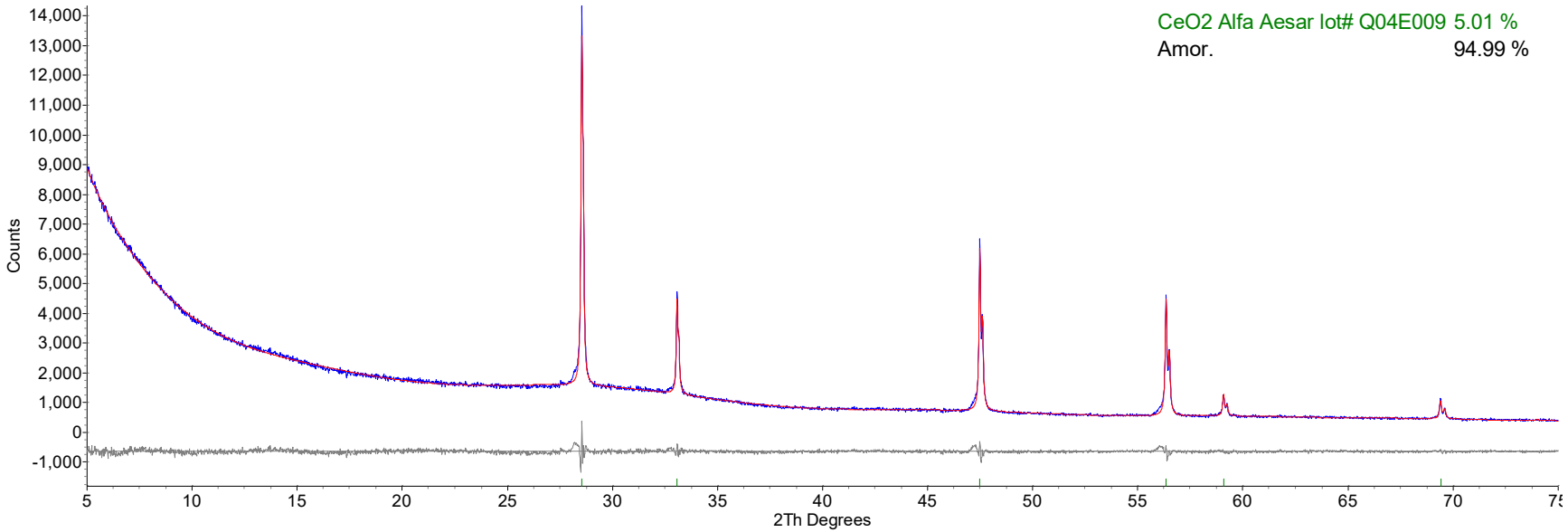


Figure C.2. X-ray diffraction pattern of APPS2-02.

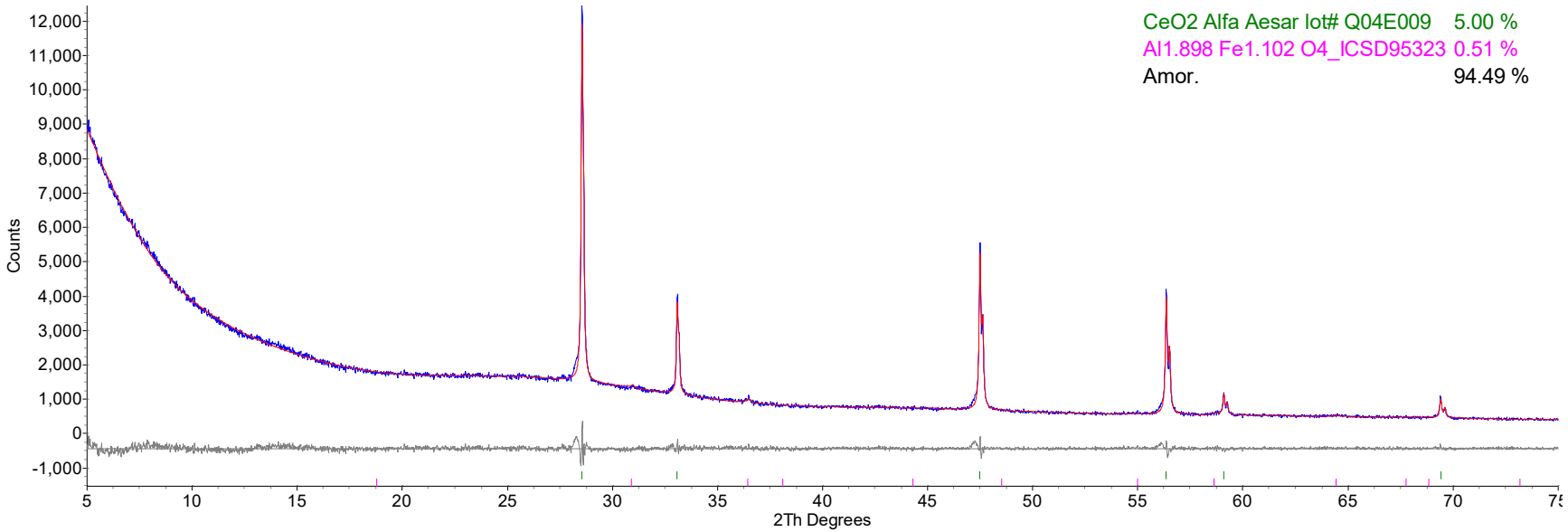


Figure C.3. X-ray diffraction pattern of APPS2-03.

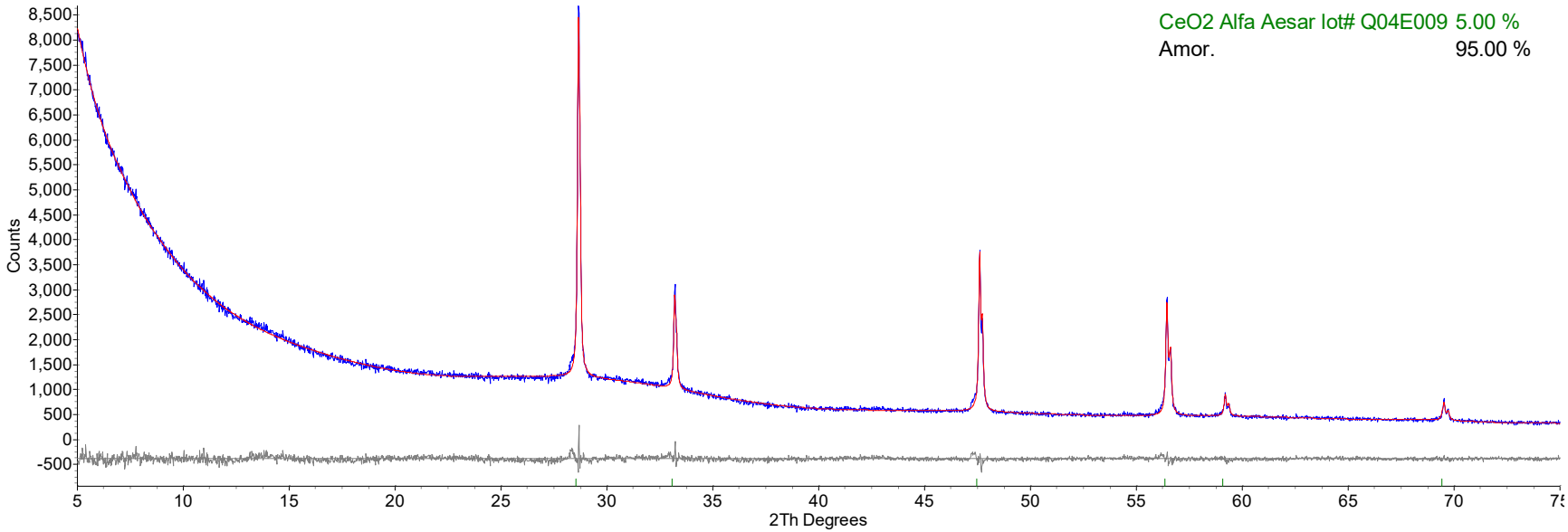


Figure C.4. X-ray diffraction pattern of APPS2-04.

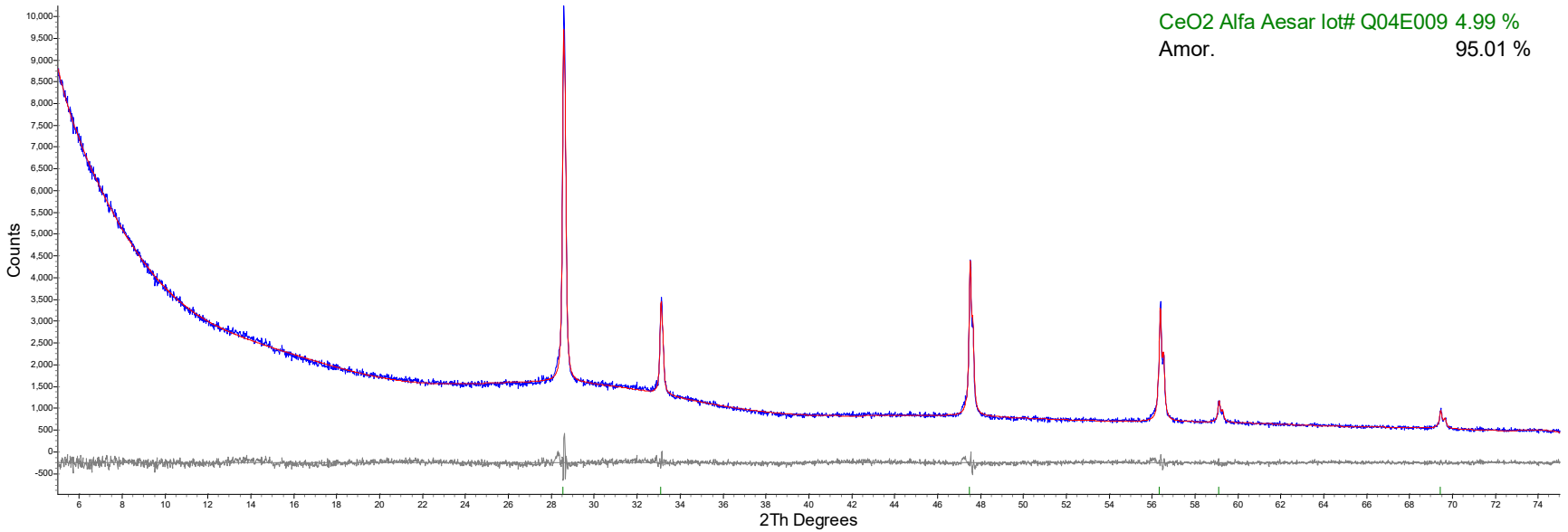


Figure C.5. X-ray diffraction pattern of APPS2-05.

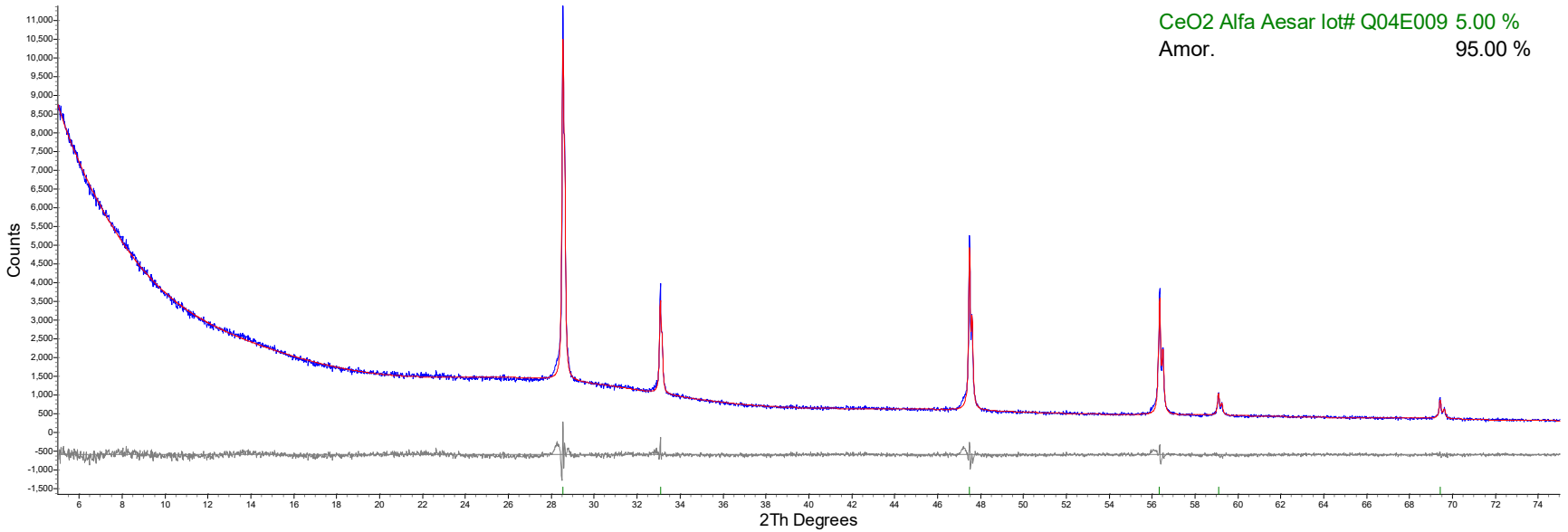


Figure C.6. X-ray diffraction pattern of APPS2-06.

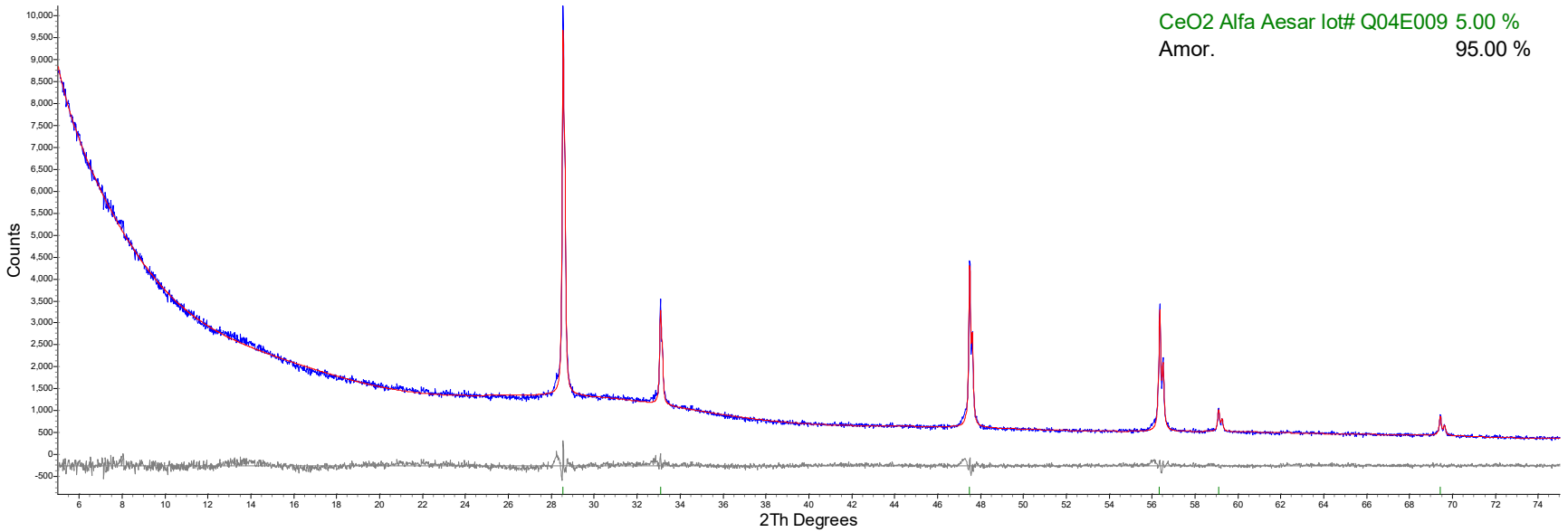


Figure C.7. X-ray diffraction pattern of APPS2-07.

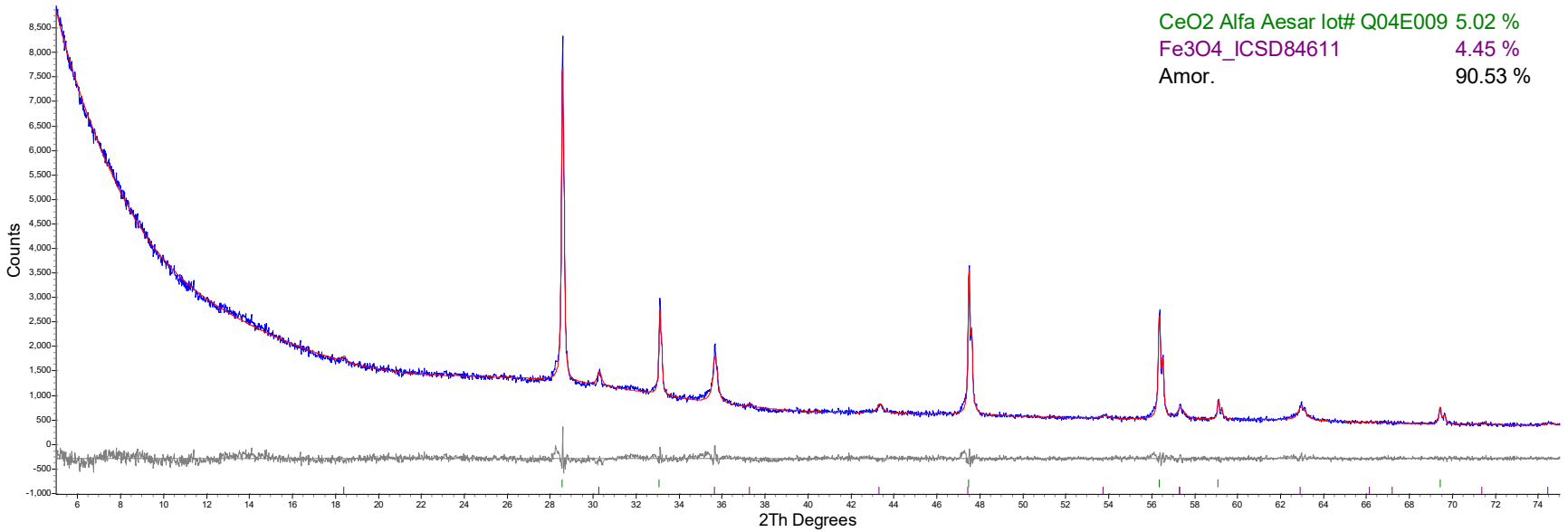


Figure C.8. X-ray diffraction pattern of APPS2-08.

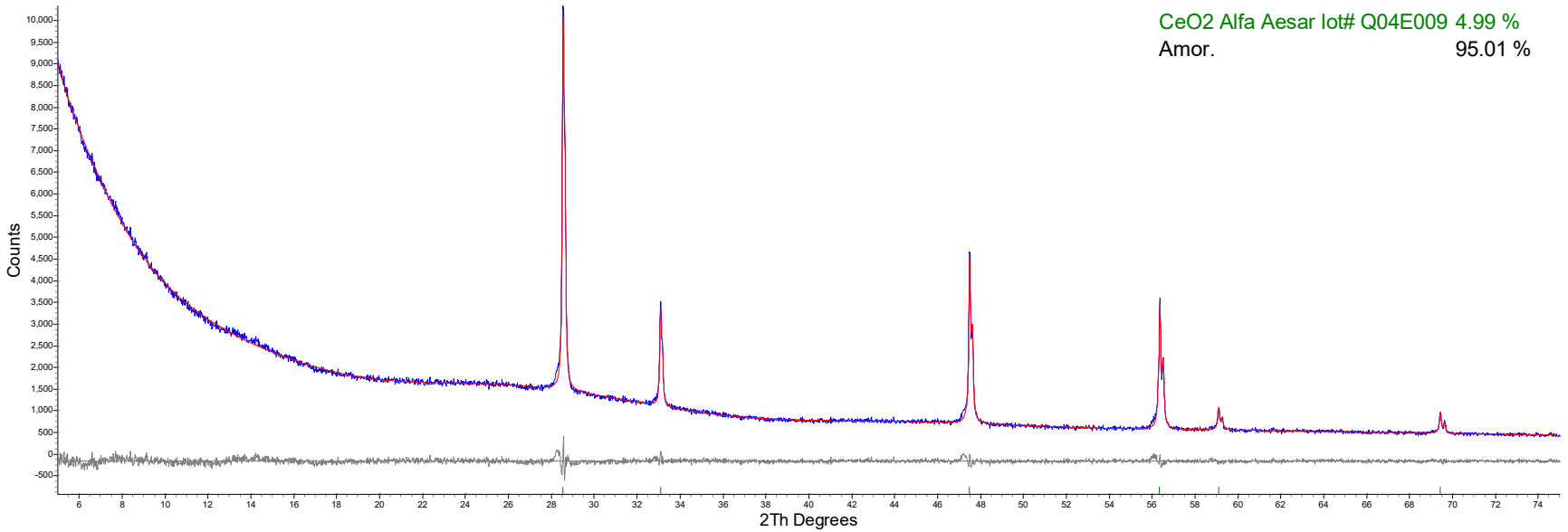


Figure C.9. X-ray diffraction pattern of APPS2-09.

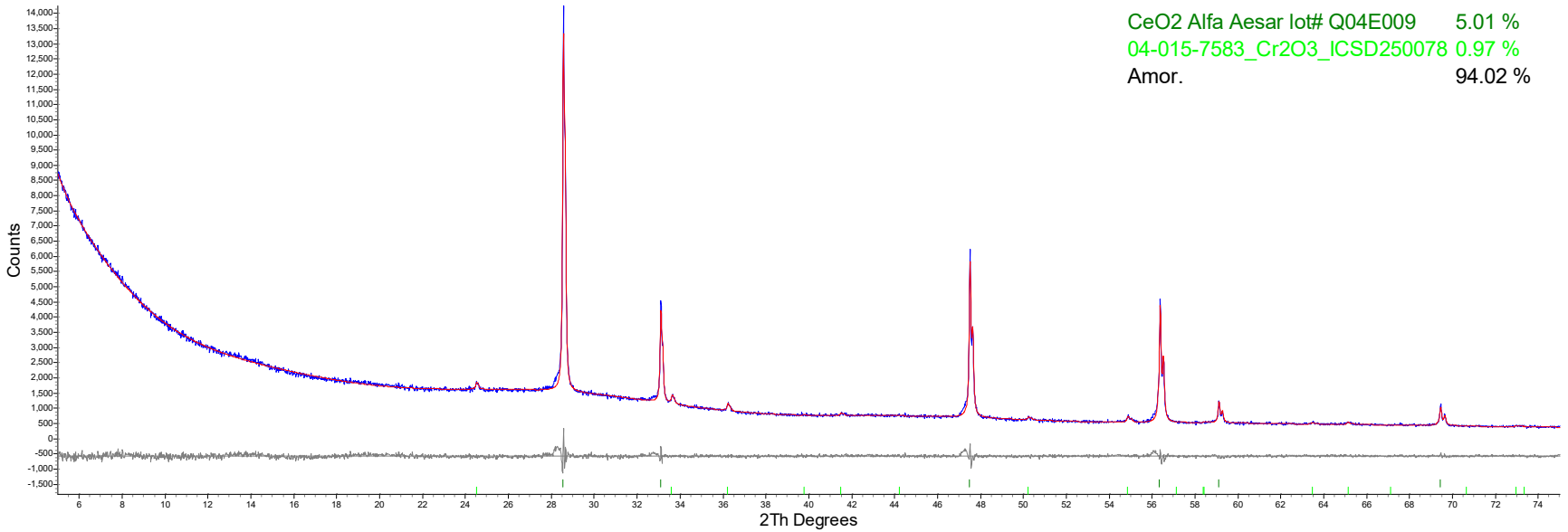


Figure C.10. X-ray diffraction pattern of APPS2-10.

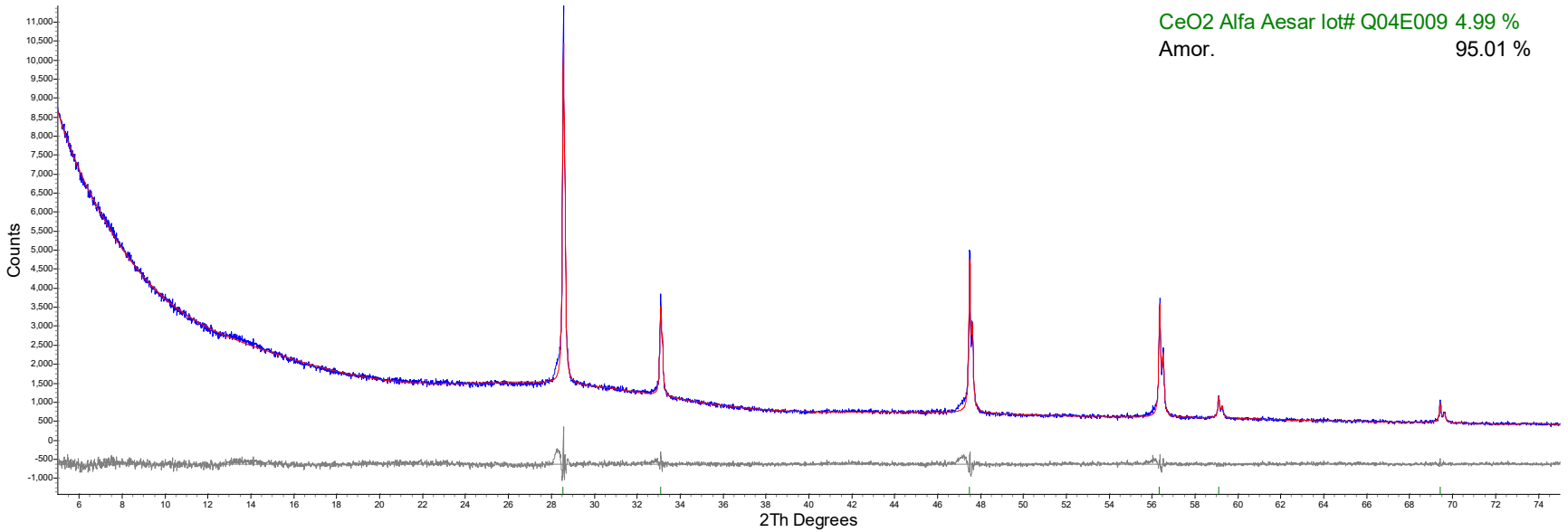


Figure C.11. X-ray diffraction pattern of APPS2-11.

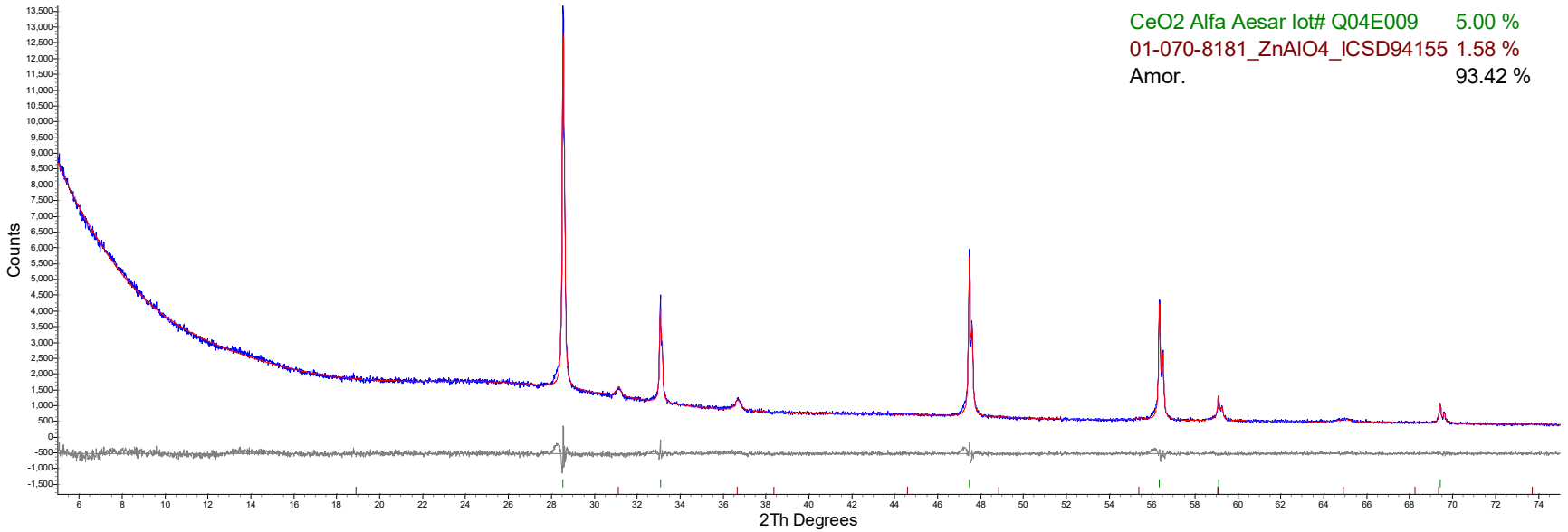


Figure C.12. X-ray diffraction pattern of APPS2-12.

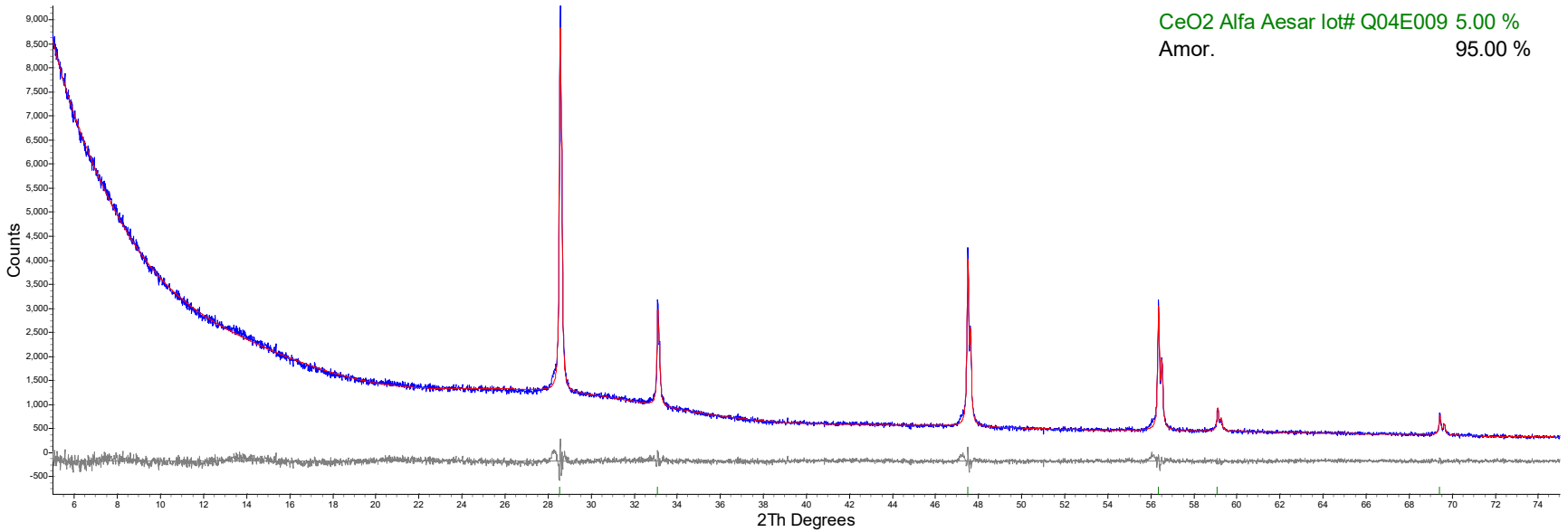


Figure C.13. X-ray diffraction pattern of APPS2-13.

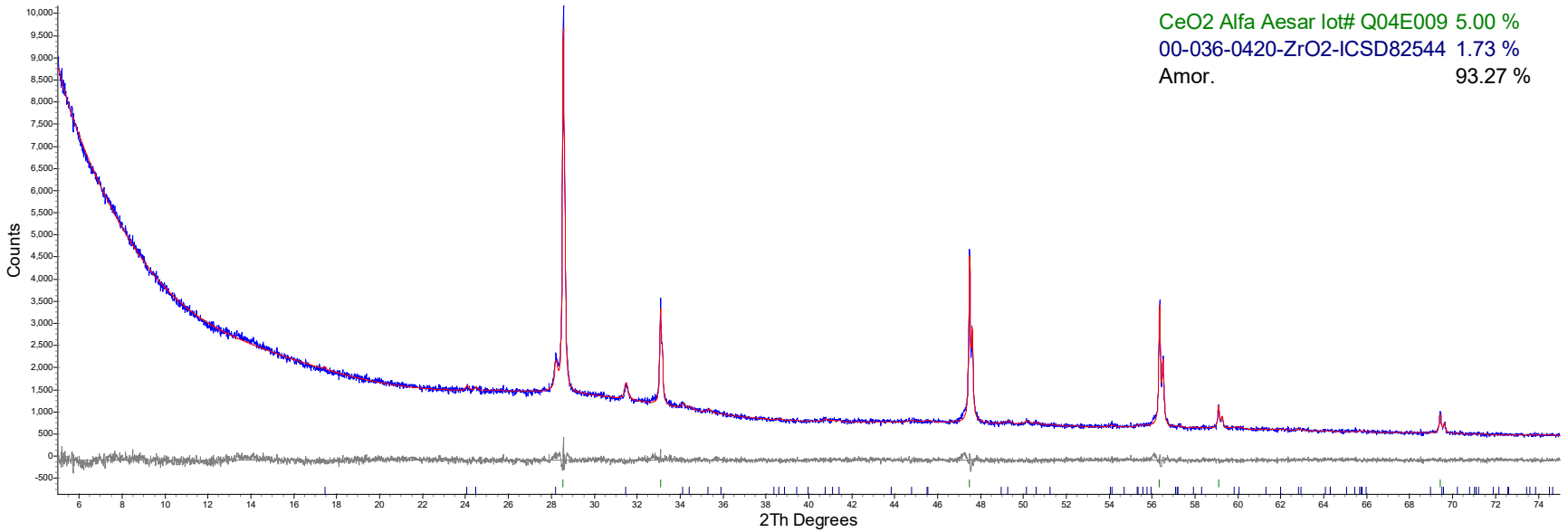


Figure C.14. X-ray diffraction pattern of APPS2-14-1.

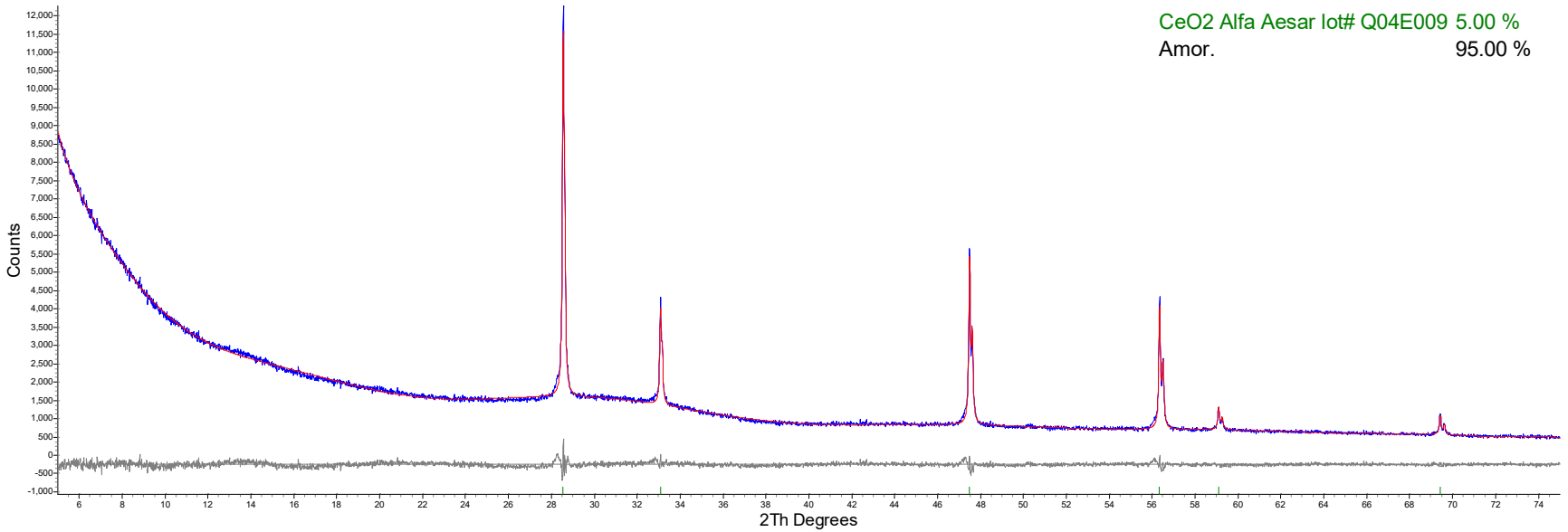


Figure C.15. X-ray diffraction pattern of APPS2-15.

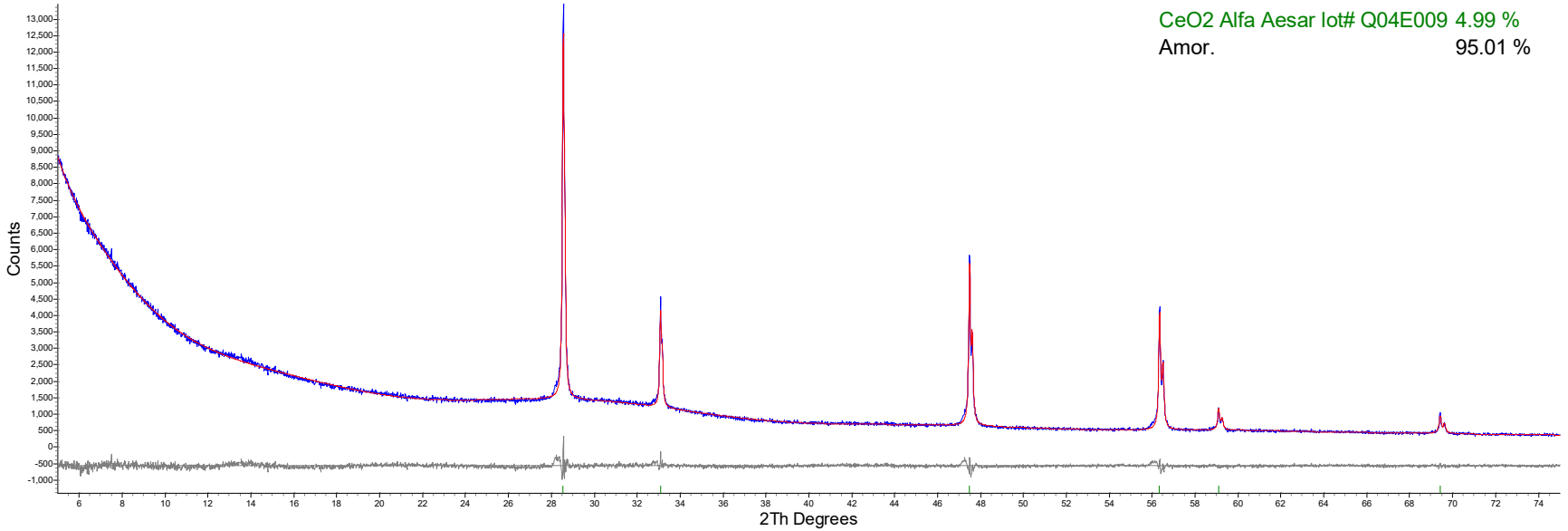


Figure C.16. X-ray diffraction pattern of APPS2-16.

# Appendix D – Morphology/Color of Each Glass after Canister Centerline Cooling

The photographs in this appendix show each glass after canister centerline cooling (CCC) as described in Section 2.5 of the main report. When applicable, X-ray diffraction (XRD) scans are reported.

Figure D.1. Glass APPS2-01 morphology after CCC.

Figure D.2. Glass APPS2-02 morphology after CCC

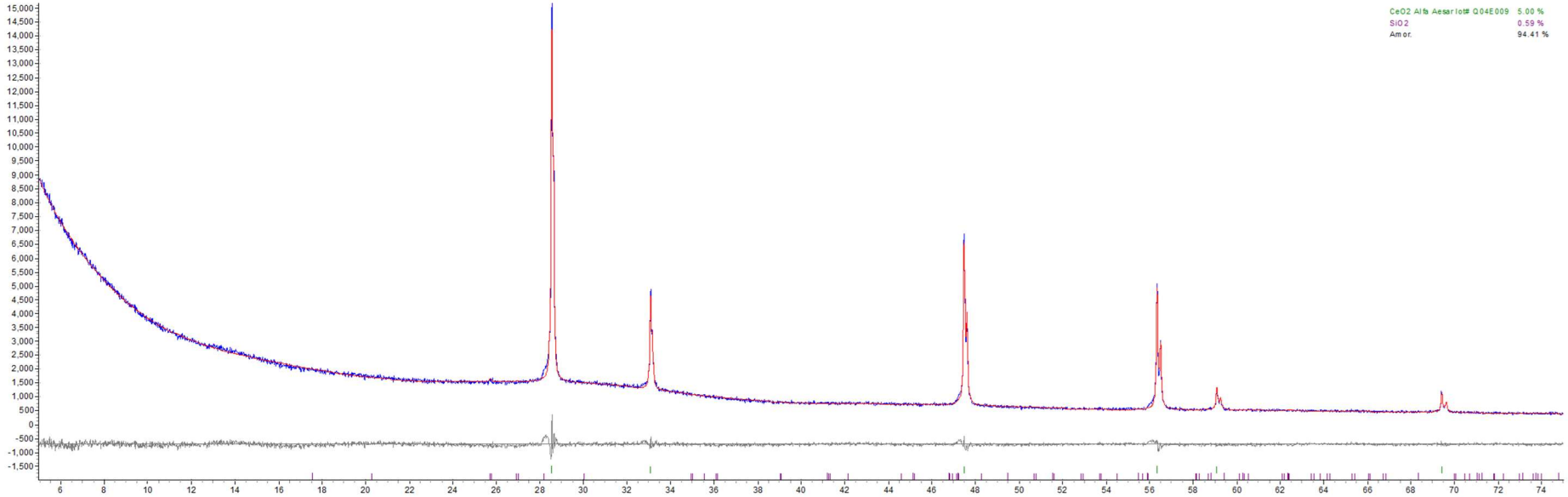


| Phase Name | Wt% Measured | Wt% Corrected | Wt% in Original Sample |
|---|---|---|---|
| $CeO_2$ | 5.00 | 2.56 | |
| $SiO_2$ | 0.59 | 0.30 | 0.32 |

Figure D.3. XRD scan of glass APPS2-02 after CCC.

Figure D.4. Glass APPS2-03 morphology after CCC.

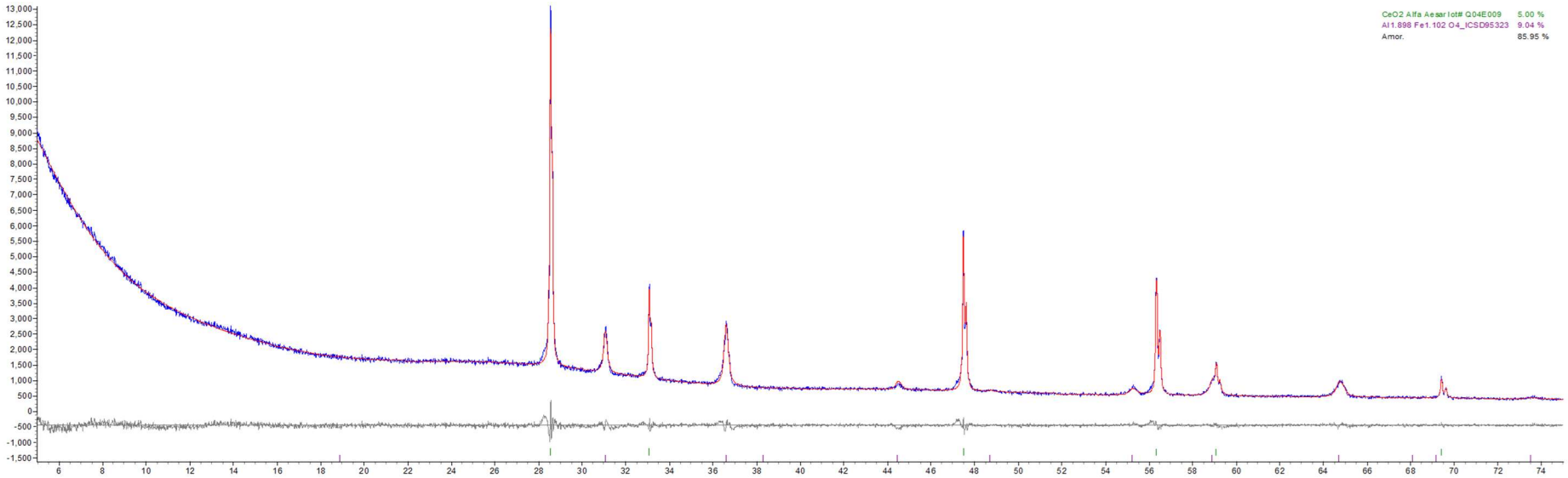


| Phase Name | Wt% Measured | Wt% Corrected | Wt% in Original Sample |
|---|---|---|---|
| $CeO_2$ | 5.00 | 2.57 | |
| $Al_{1.898}Fe_{1.102}O_4$ | 9.04 | 4.64 | 4.88 |

Figure D.5. XRD scan of glass APPS2-03 after CCC.

Figure D.6. Glass APPS2-04 morphology after CCC.

Figure D.7. Glass APPS2-05 morphology after CCC.

Figure D.8. Glass APPS2-06 morphology after CCC.

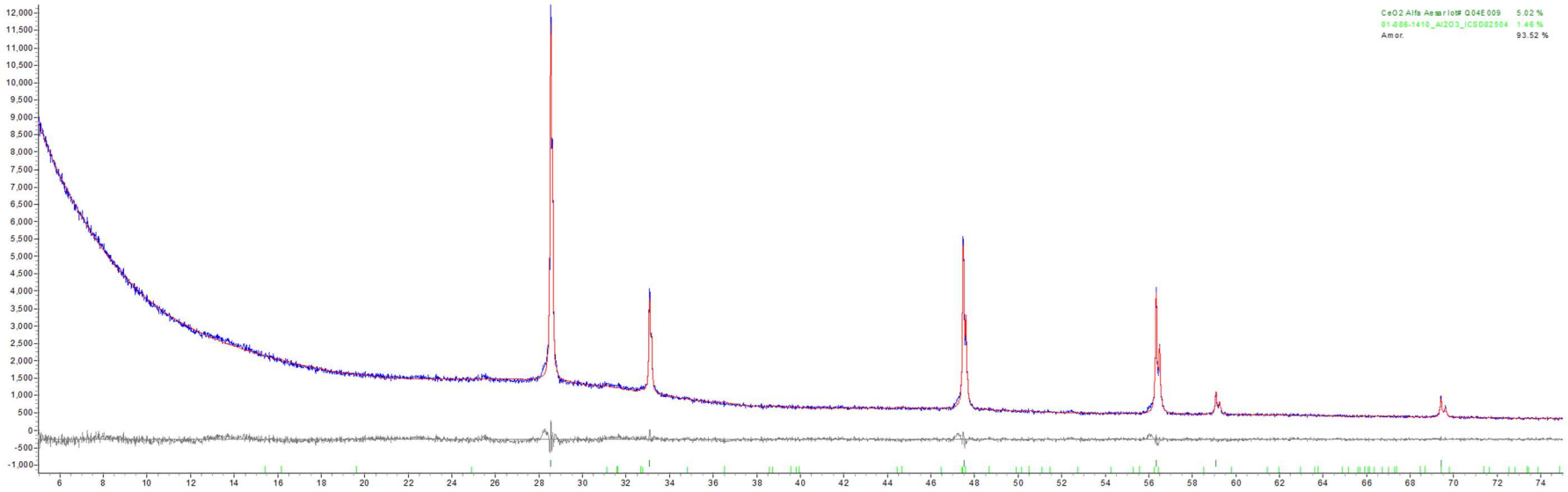


| Phase Name | Wt% Measured | Wt% Corrected | Wt% in Original Sample |
|---|---|---|---|
| $CeO_2$ | 5.02 | 2.57 | |
| $Al_2O_3$ | 1.46 | 0.75 | 0.79 |

Figure D.9. XRD scan of glass APPS2-06 after CCC.

Figure D.10. Glass APPS2-07 morphology after CCC.

Figure D.11. Glass APPS2-08 morphology after CCC.

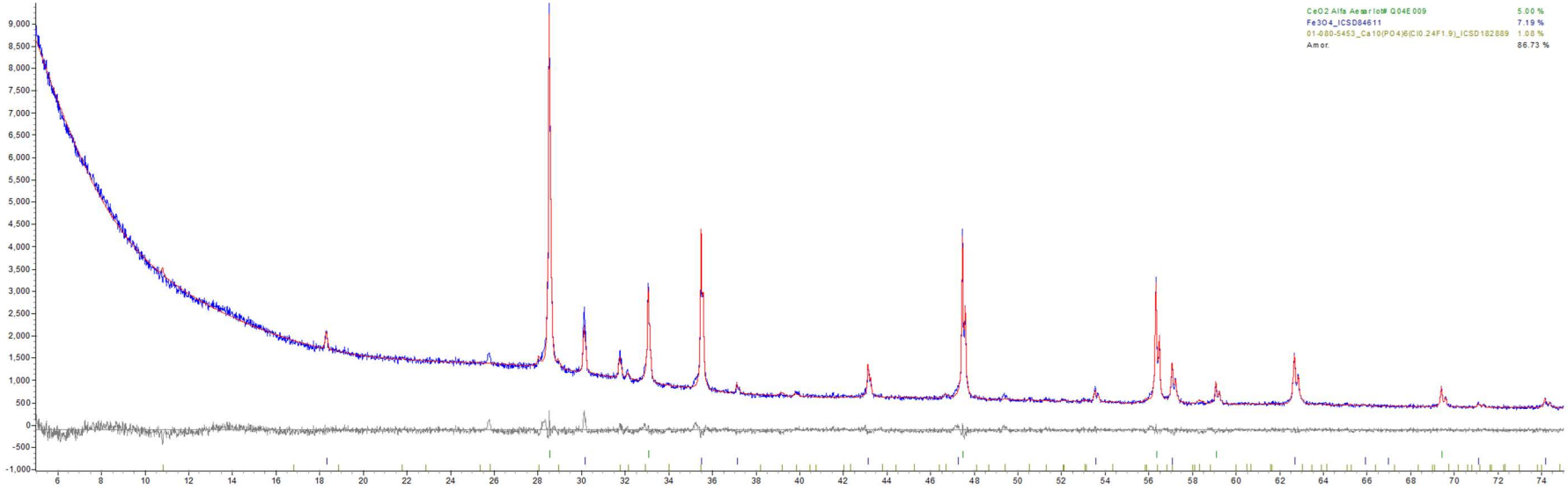


| Phase Name | Wt% Measured | Wt% Corrected | Wt% in Original Sample |
|---|---|---|---|
| $CeO_2$ | 5.02 | 2.58 | |
| $Fe_3O_4$ | 7.21 | 3.70 | 3.89 |
| $Ca_{10}(PO_4)_6(Cl_{0.24}F_{1.9})$ | 1.06 | 0.54 | 0.57 |

Figure D.12. XRD scan of glass APPS2-08 after CCC.

Figure D.13. Glass APPS2-09 morphology after CCC.

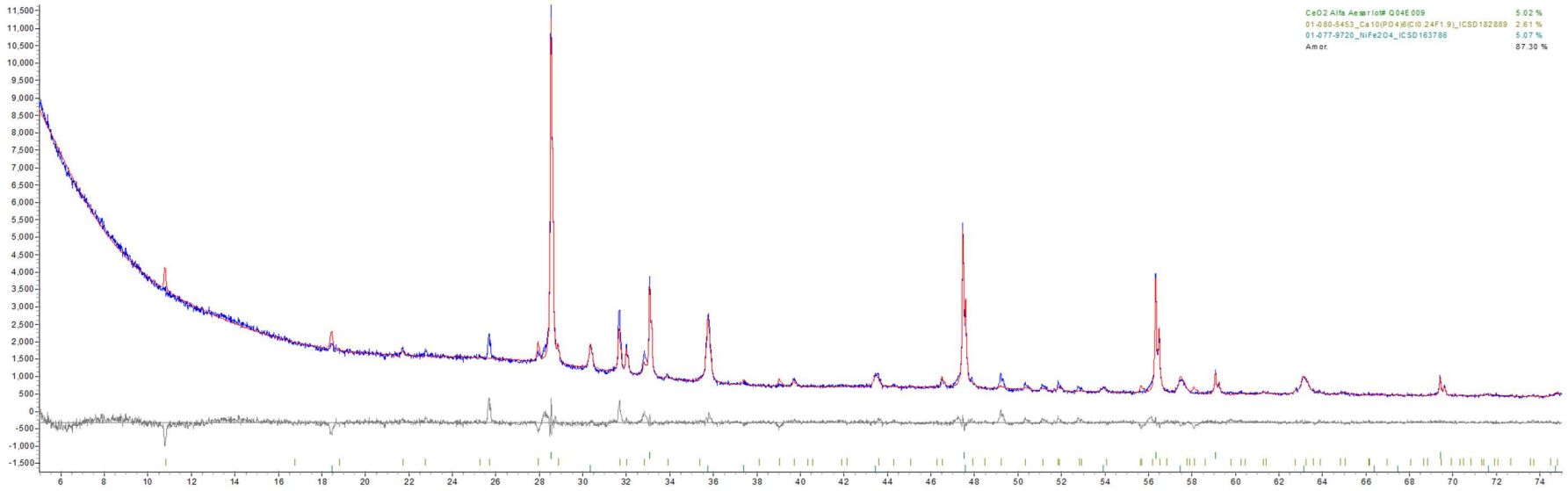


| Phase Name | Wt% Measured | Wt% Corrected | Wt% in Original Sample |
|---|---|---|---|
| $CeO_2$ | 5.02 | 2.57 | |
| $NiFe_2O_4$ | 5.07 | 2.60 | 2.74 |
| $Ca_{10}(PO_4)_6(Cl_{0.24}F_{1.9})$ | 2.61 | 1.34 | 1.41 |

Figure D.14. XRD scan of glass APPS2-09 after CCC.

Figure D.15. Glass APPS2-10 morphology after CCC.

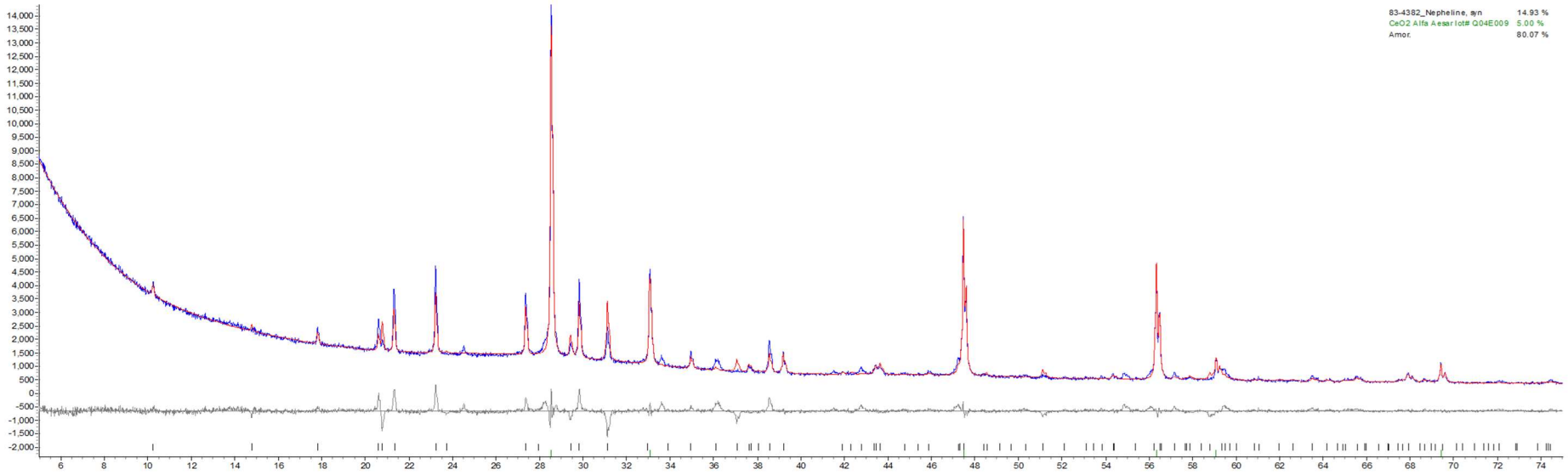


| Phase Name | Wt% Measured | Wt% Corrected | Wt% in Original Sample |
|---|---|---|---|
| $CeO_2$ | 5.00 | 2.57 | |
| Nepheline | 14.9 | 7.66 | 8.06 |

Figure D.16. XRD scan of glass APPS2-10 after CCC.

Figure D.17. Glass APPS2-11 morphology after CCC.

Figure D.18. Glass APPS2-12 morphology after CCC.

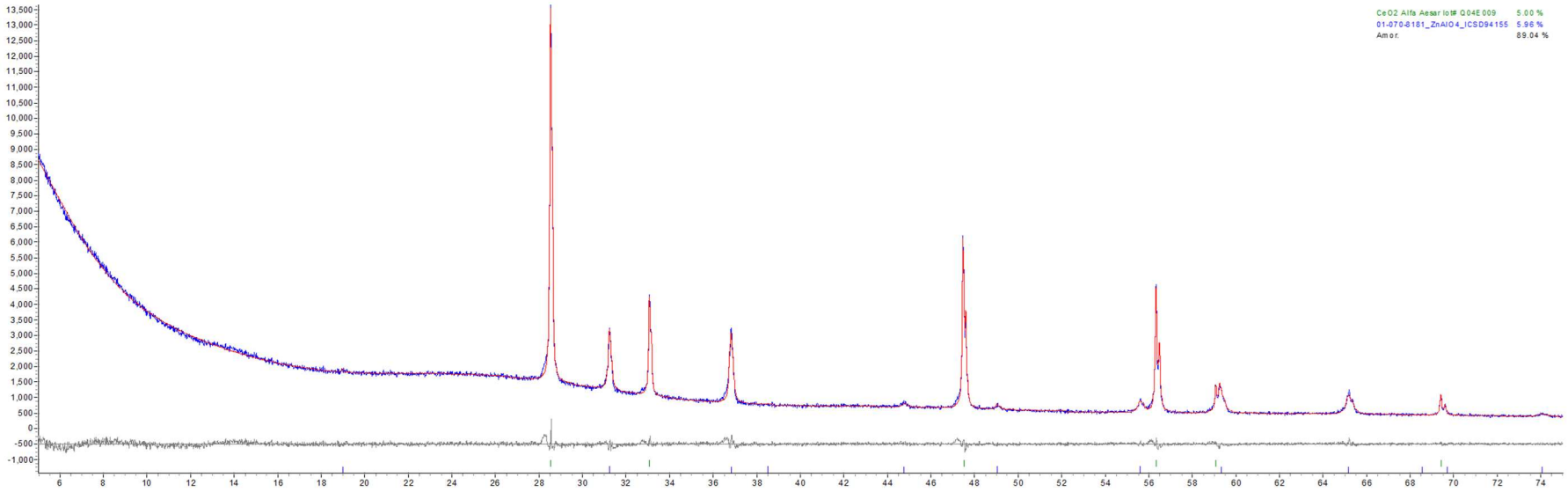


| Phase Name | Wt% Measured | Wt% Corrected | Wt% in Original Sample |
|---|---|---|---|
| $CeO_2$ | 5.00 | 2.56 | |
| $ZnAlO_4$ | 5.96 | 3.06 | 3.22 |

Figure D.19. XRD scan of glass APPS-12 after CCC.

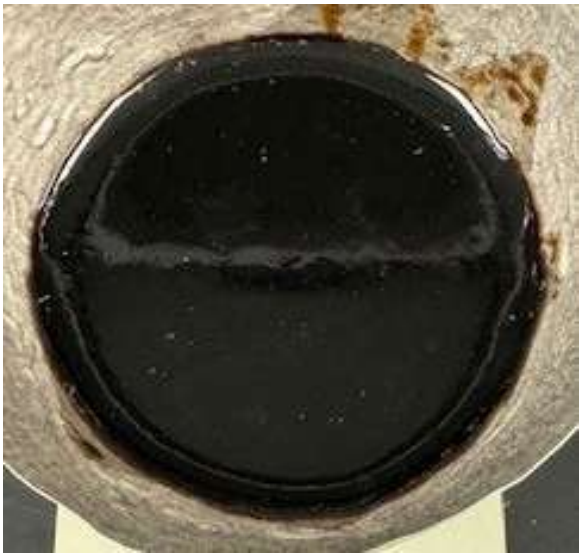

Figure D.20. Glass APPS2-13 morphology after CCC.

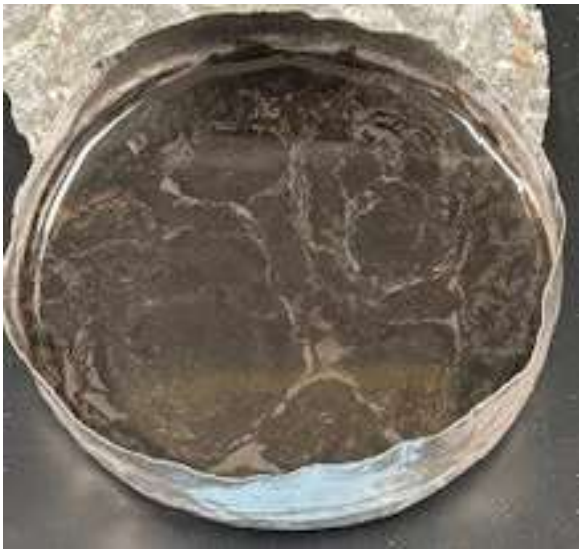

Figure D.21. Glass APPS2-14-1 morphology after CCC.

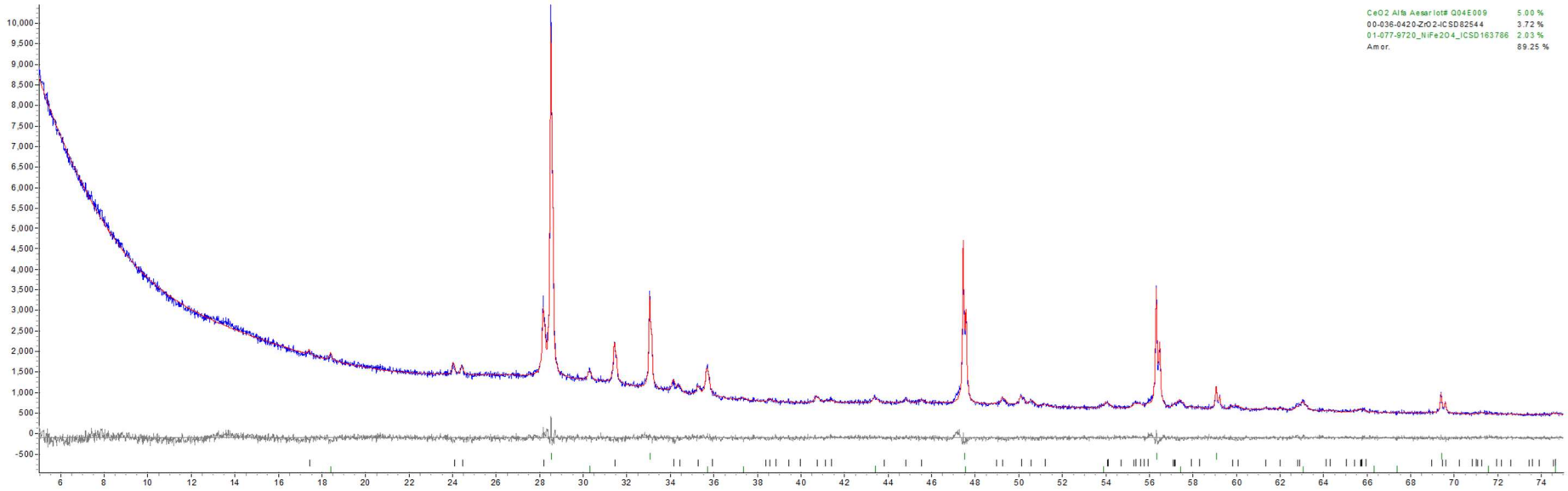


| Phase Name | Wt% Measured | Wt% Corrected | Wt% in Original Sample |
|---|---|---|---|
| $CeO_2$ | 5.00 | 2.56 | |
| $ZrO_2$ | 3.72 | 1.91 | 2.01 |
| $NiFe_2O_4$ | 2.03 | 1.04 | 1.09 |

Figure D.22. XRD scan of glass APPS2-14-1 after CCC.

Figure D.23. Glass APPS2-15 morphology after CCC.

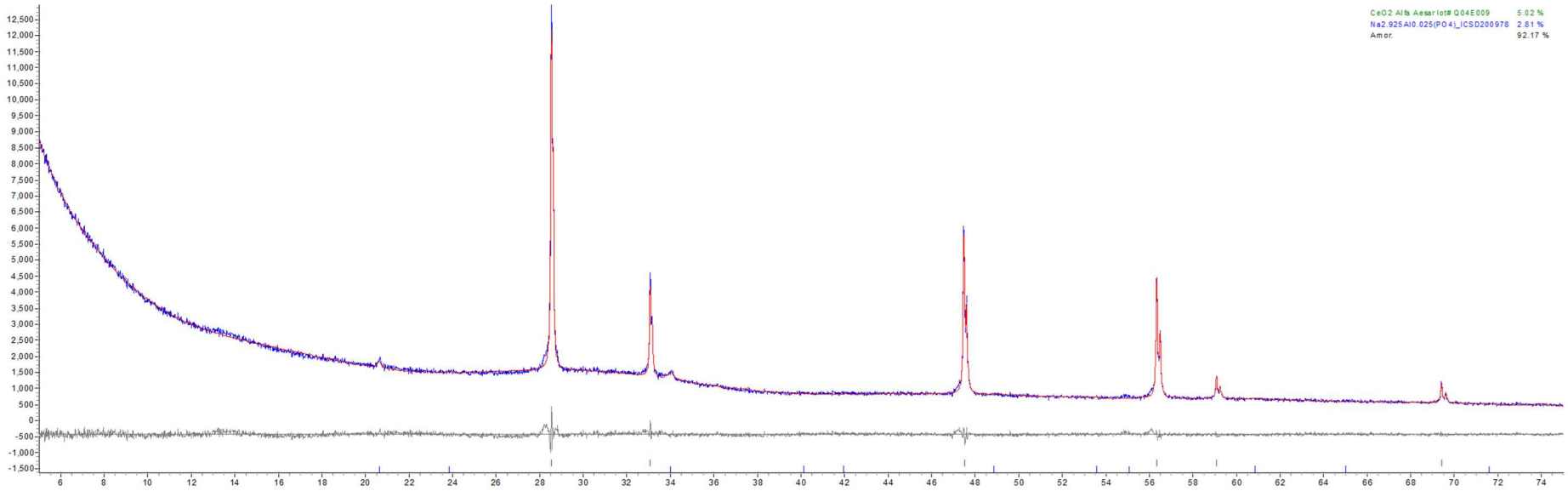


| Phase Name | Wt% Measured | Wt% Corrected | Wt% in Original Sample |
|---|---|---|---|
| $CeO_2$ | 5.00 | 2.56 | |
| $Na_{2.925}Al_{0.025}(PO_4)$ | 2.81 | 1.44 | 1.52 |

Figure D.2424. XRD scan of glass APPS2-15 after CCC.

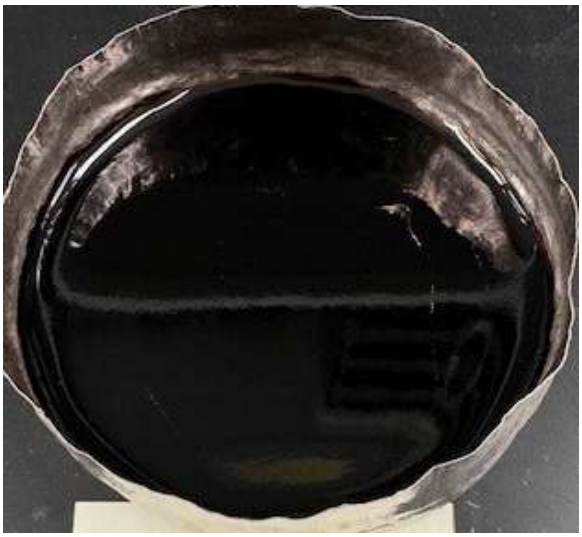

Figure D.25. Glass APPS2-16 morphology after CCC.

# Appendix E – Morphology/Color of Isothermally Heat-Treated Glasses

This appendix contains photographs of the APPS2 glasses after they were heat-treated at 900 °C for 24 h, which should conservatively represent the potential presence of crystal fractions below 950 °C. X-ray diffraction (XRD) analysis is included as well. Percentage of crystal content in the reported XRD images is reported before adjustment was made by spiking with 5 wt% high-purity cerium oxide.

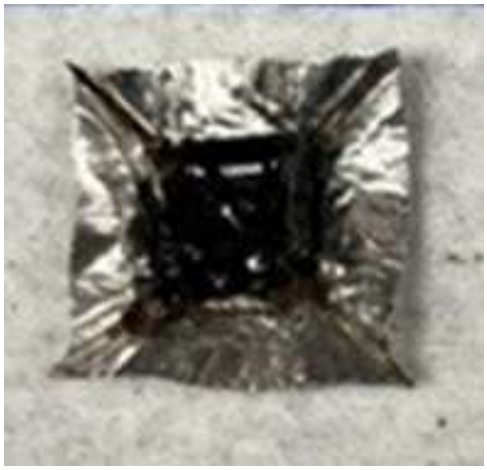

Figure E.1. Glass APPS2-01 after isothermal heat treatment at 900 °C for 24 h.

Figure E.2. Glass APPS2-02 after isothermal heat treatment at 900 °C for 24 h.

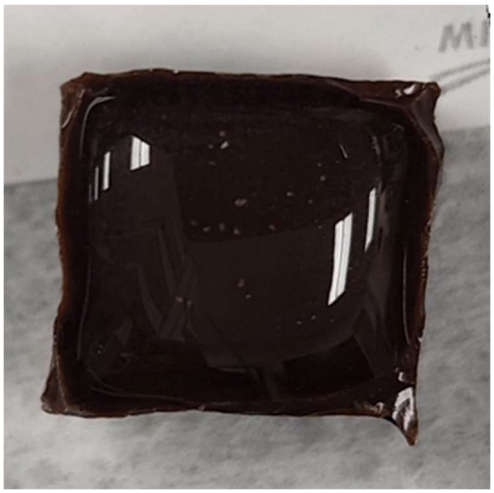

Figure E.3. Glass APPS2-03 after isothermal heat treatment at 900 °C for 24 h.

Figure E.4. Glass APPS2-04 after isothermal heat treatment at 900 °C for 24 h.

Figure E.5. Glass APPS2-05 after isothermal heat treatment at 900 °C for 24 h.

Figure E.6. Glass APPS2-06 after isothermal heat treatment at 900 °C for 24 h.

Figure E.7. Glass APPS2-07 after isothermal heat treatment at 900 °C for 24 h.

Figure E.8. Glass APPS2-08 after isothermal heat treatment at 900 °C for 24 h.

Figure E.9. Glass APPS2-09 after isothermal heat treatment at 950 °C for 24 h.

Figure E.10. Glass APPS2-10 after isothermal heat treatment at 900 °C for 24 h.

Figure E.11. Glass APPS2-11 after isothermal heat treatment at 900 °C for 24 h.

Figure E.12. Glass APPS2-12 after isothermal heat treatment at 900 °C for 24 h.

Figure E.13. Glass APPS2-13 after isothermal heat treatment at 900 °C for 24 h.

Figure E.14. Glass APPS2-14-1 after isothermal heat treatment at 900 °C for 24 h.

Figure E.15. Glass APPS2-15 after isothermal heat treatment at 950 °C for 24 h.

Figure E.16. Glass APPS2-16 after isothermal heat treatment at 900 °C for 24 h.

# Appendix F – XRD and Liquidus Temperature Plots for CF Glasses

When the $T_L$ was estimated to be > 850 °C, the glass measured temperatures (°C), crystal content (wt%) and relative plot of the main crystalline phase for that glass is reported.

| Temperature (°C) | Spinel ($Al_{1.898}$ $Fe_{1.102}$ $O_4$) |
|---|---|
| 900 | 3.69 |
| 1051.2 | 1.27 |
| 1125.1 | 0.55 |

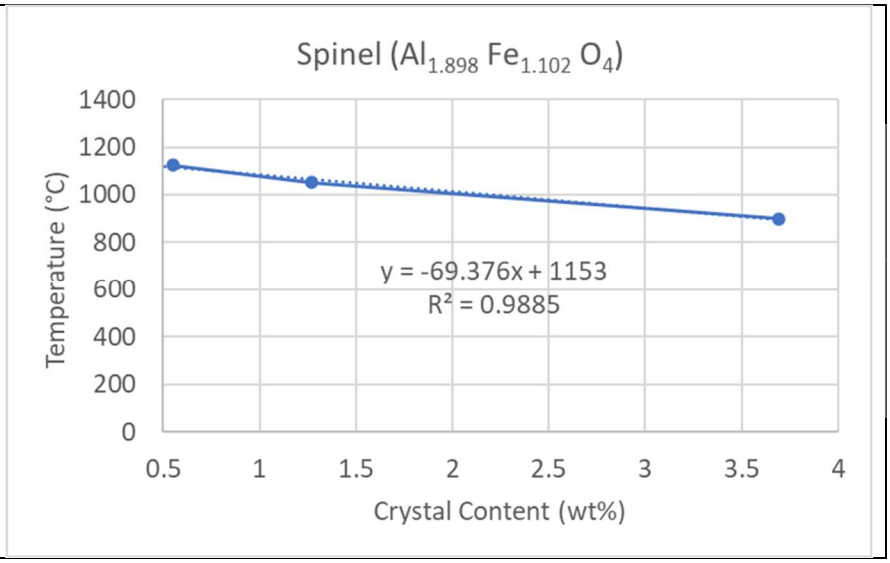


Figure F.1. APPS2-03 glass $T_L$ calculated by extrapolating CF as a function of temperature to zero crystals for the main crystalline phase.

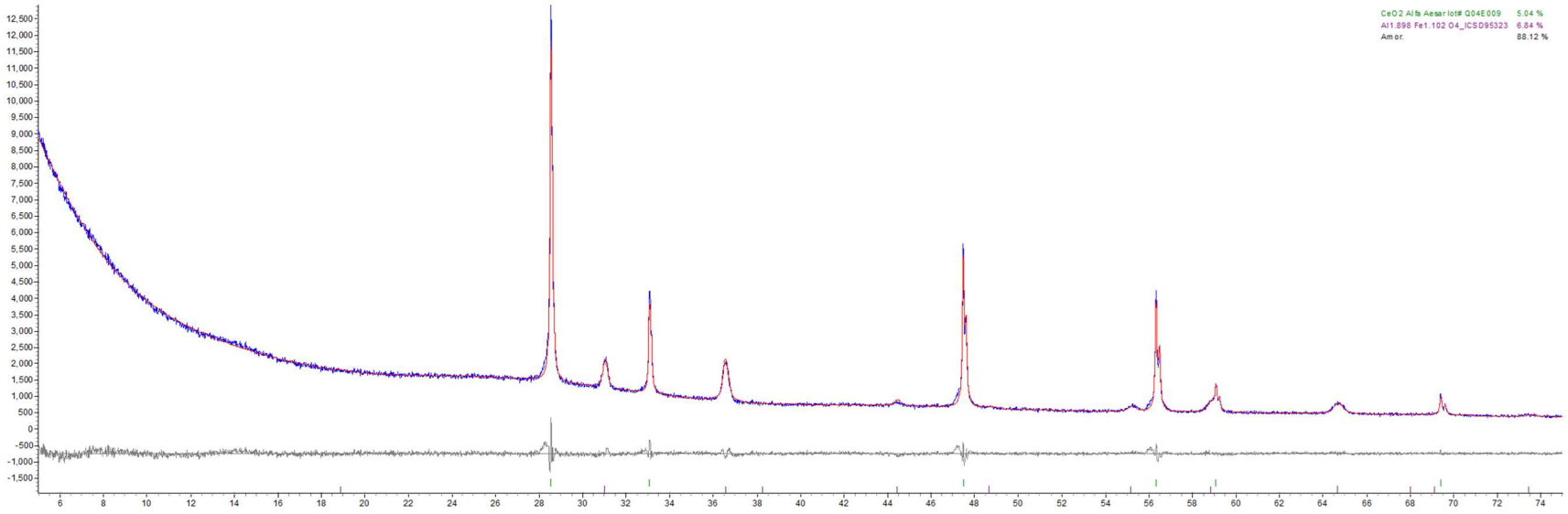


| Phase Name | Wt% Measured | Wt% Corrected | Wt% in Original Sample |
|---|---|---|---|
| $CeO_2$ | 5.04 | 2.58 | |
| $Al_{1.898}Fe_{1.102}O_4$ | 6.84 | 3.51 | 3.69 |

Figure F.2. Glass APPS2-03 heat treated at 900 °C XRD scan.

| Temperature (°C) | Spinel ($NiFe_2O_4$) |
|---|---|
| 749.2 | 2.27 |
| 900 | 1.60 |
| 950 | 1.44 |
| 1051.2 | 0.90 |
| 1125.1 | 0.32 |

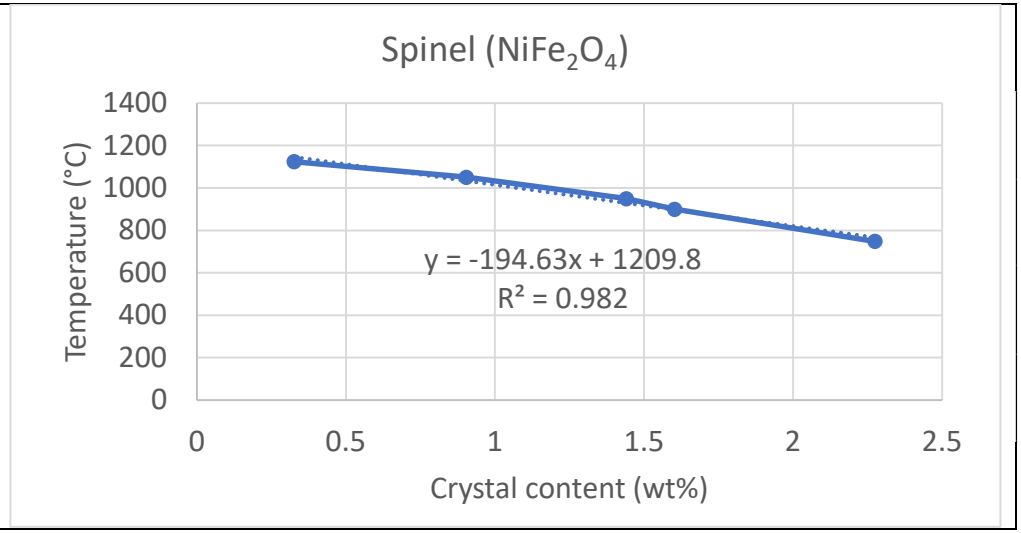


Figure F.3. APPS2-09 glass $T_L$ calculated by extrapolating CF as a function of temperature to zero crystals for the main crystalline phase.

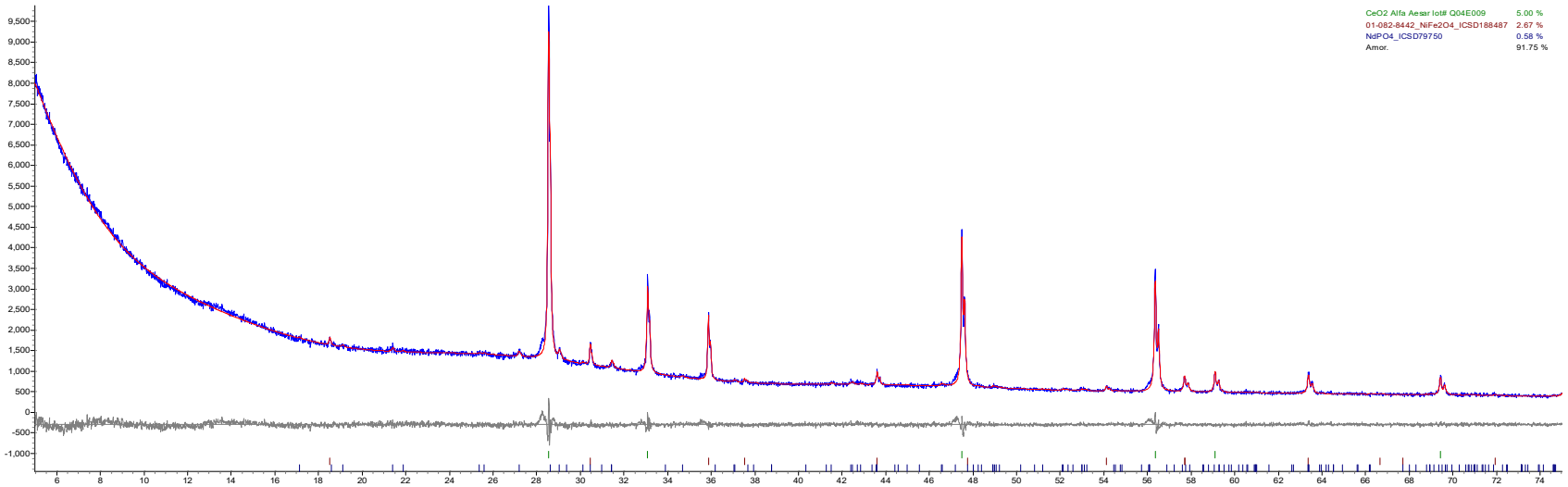


| Phase Name | Wt% Measured | Wt% Corrected | Wt% in Original Sample |
|---|---|---|---|
| $CeO_2$ | 5.01 | 2.57 | |
| $NiFe_2O_4$ | 2.67 | 1.37 | 1.44 |
| $NdPO_4$ | 0.58 | 2.64 | 2.78 |

Figure F.4. Glass APPS2-09 heat treated at 950 °C XRD scan.

| Temperature (°C) | Eskolaite ($Cr_2O_3$) |
|---|---|
| 749.2 | 0.51 |
| 824.3 | 0.48 |
| 900.2 | 0.43 |
| 999.4 | 0.071 |

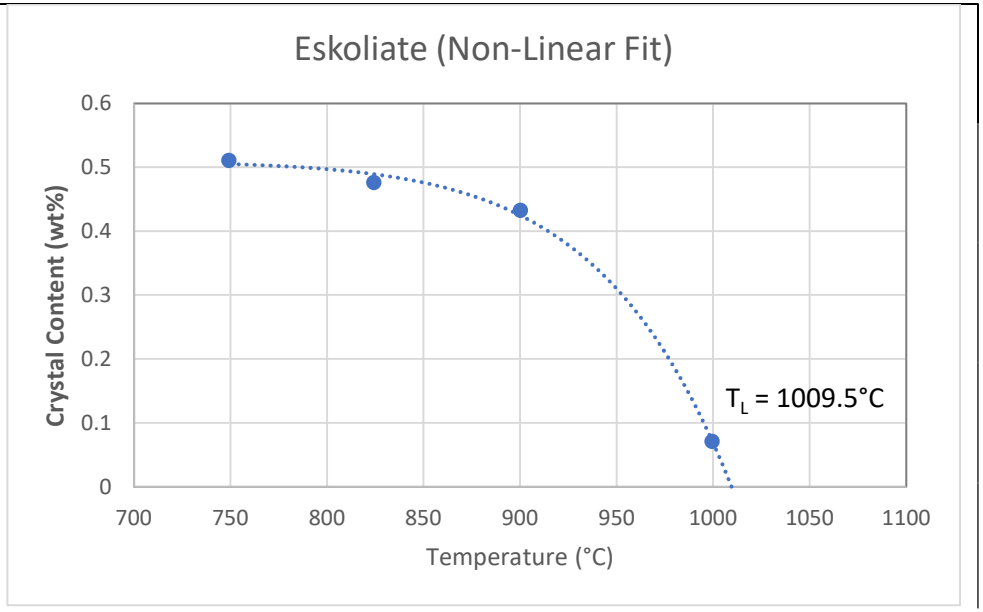


Figure F.5. APPS2-10 glass $T_{L\ calculated}$ by extrapolating CF as a function of temperature to zero crystals for the main crystalline phase.

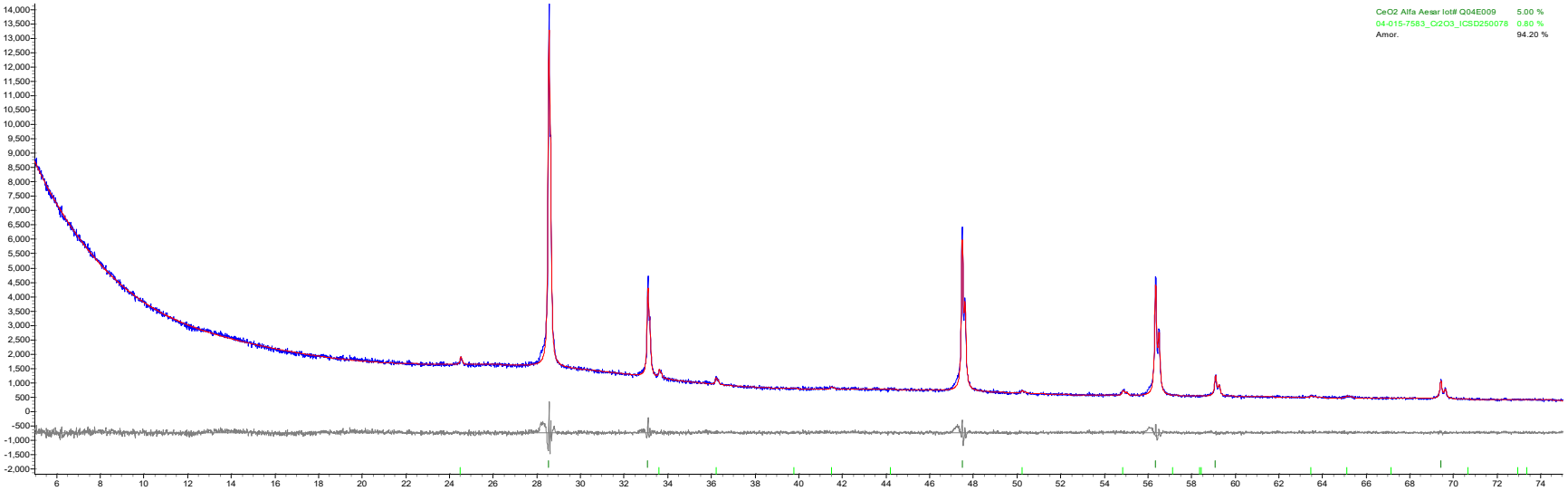


| Phase Name | Wt% Measured | Wt% Corrected | Wt% in Original Sample |
|---|---|---|---|
| $CeO_2$ | 5.00 | 2.56 | |
| $Cr_2O_3$ | 0.84 | 0.41 | 0.43 |

Figure F.6. Glass APPS2-10 heat treated at 900 °C XRD scan.

| Temperature (°C) | Gahnite ($ZnAl_2O_4$) |
|---|---|
| 900.1 | 2.73 |
| 1049.7 | 1.38 |
| 1125.1 | 0.84 |
| 1200.4 | 0.46 |

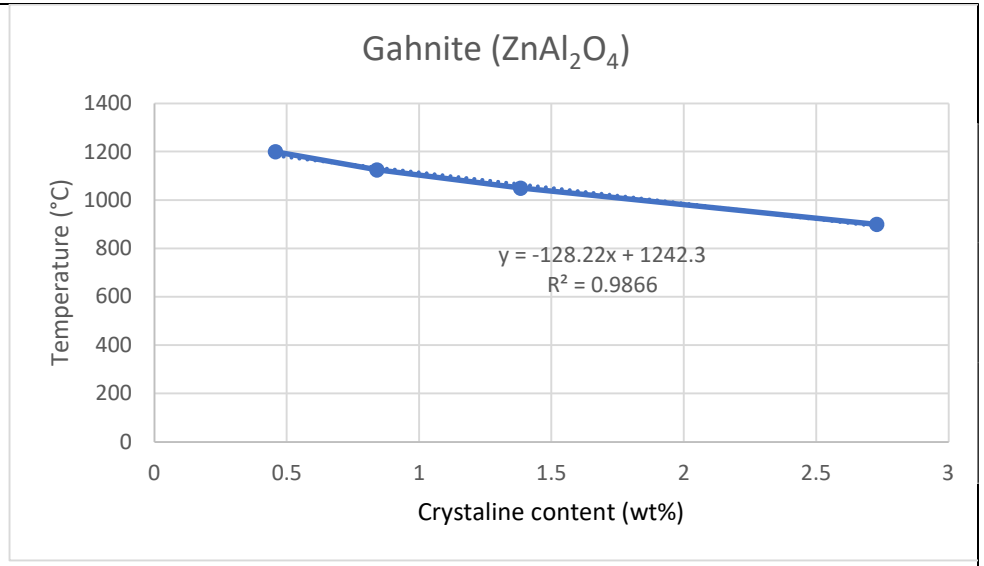


Figure F.7. APPS2-12 glass $T_L$ calculated by extrapolating CF as a function of temperature to zero crystals for the main crystalline phase.

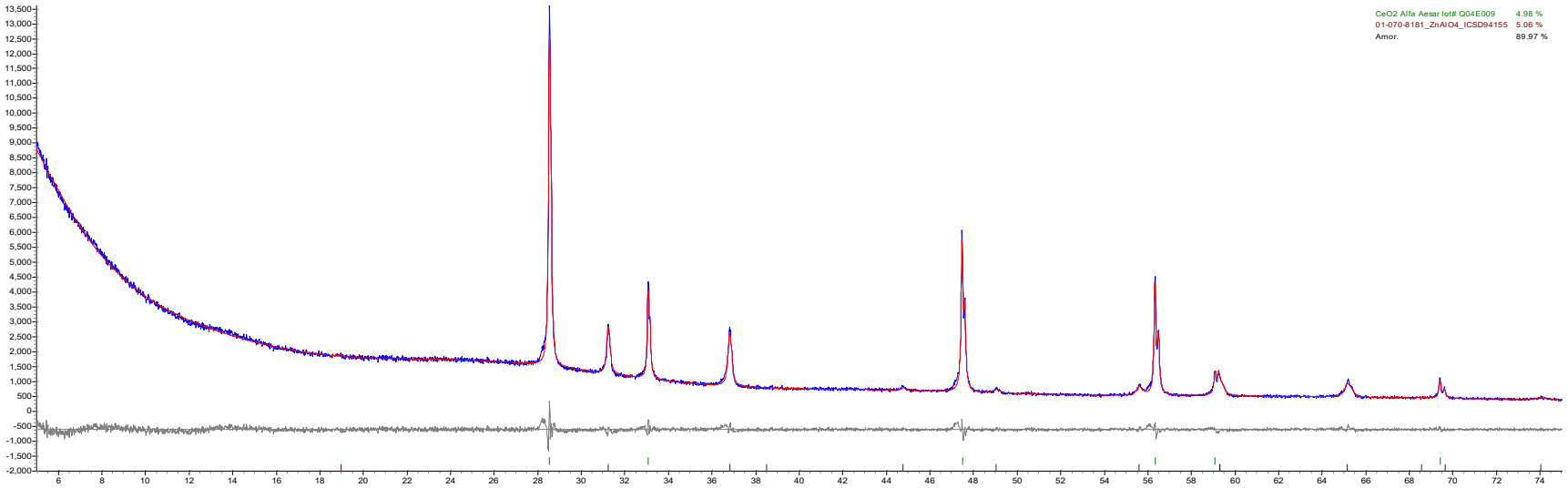


| Phase Name | Wt% Measured | Wt% Corrected | Wt% in Original Sample |
|---|---|---|---|
| $CeO_2$ | 4.98 | 2.55 | |
| $ZnAlO_4$ | 5.06 | 2.59 | 2.73 |

Figure F.8. Glass APPS2-12 heat treated at 900 °C XRD scan.

| Temperature (°C) | Baddeleyite (ZrO2) |
|---|---|
| 825.9 | 2.66 |
| 901.9 | 2.48 |
| 1050.6 | 2.16 |
| 1200.4 | 1.61 |
| 1402.1 | 1.00 |

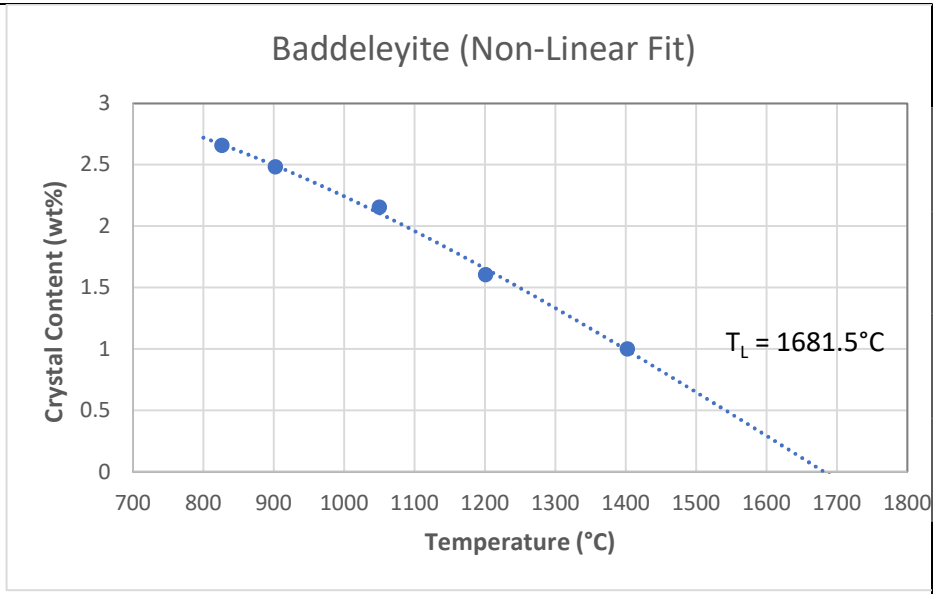


Figure F.9. APPS2-14-1 glass $T_L$ calculated by extrapolating CF as a function of temperature to zero crystals for the main crystalline phase.

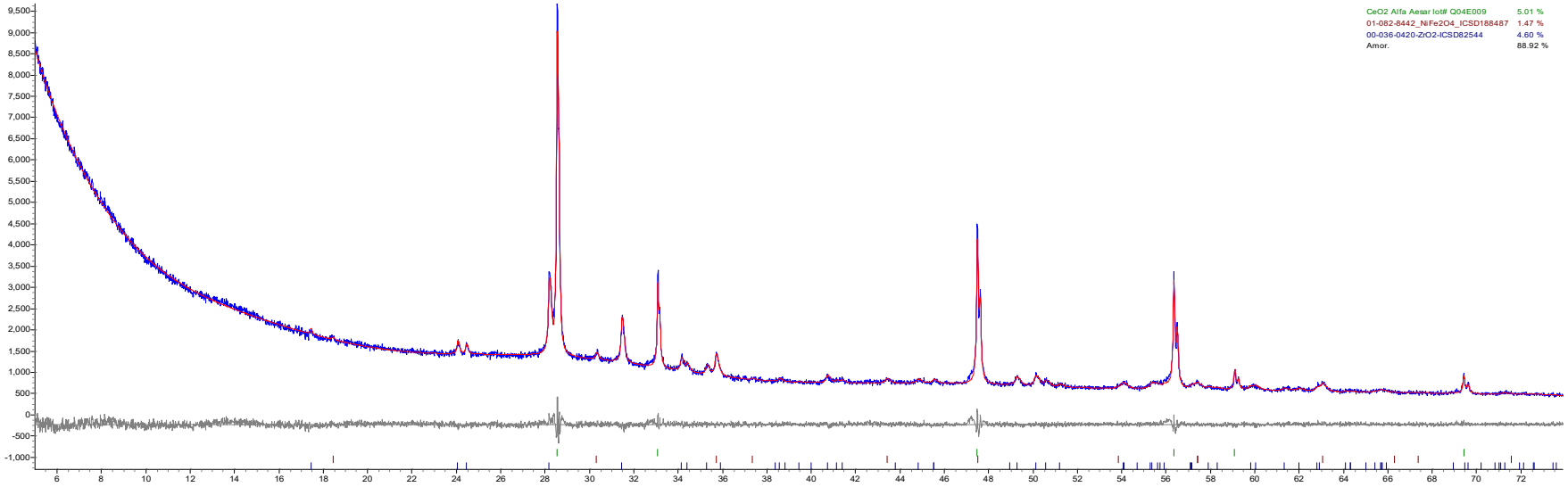


| Phase Name | Wt% Measured | Wt% Corrected | Wt% in Original Sample |
|---|---|---|---|
| $CeO_2$ | 5.01 | 2.57 | |
| $ZrO_2$ | 4.60 | 2.36 | 2.48 |
| $NiFe_2O_4$ | 1.47 | 0.75 | 0.79 |

Figure F.10. Glass APPS2-14-1 heat treated at 900 °C XRD scan.

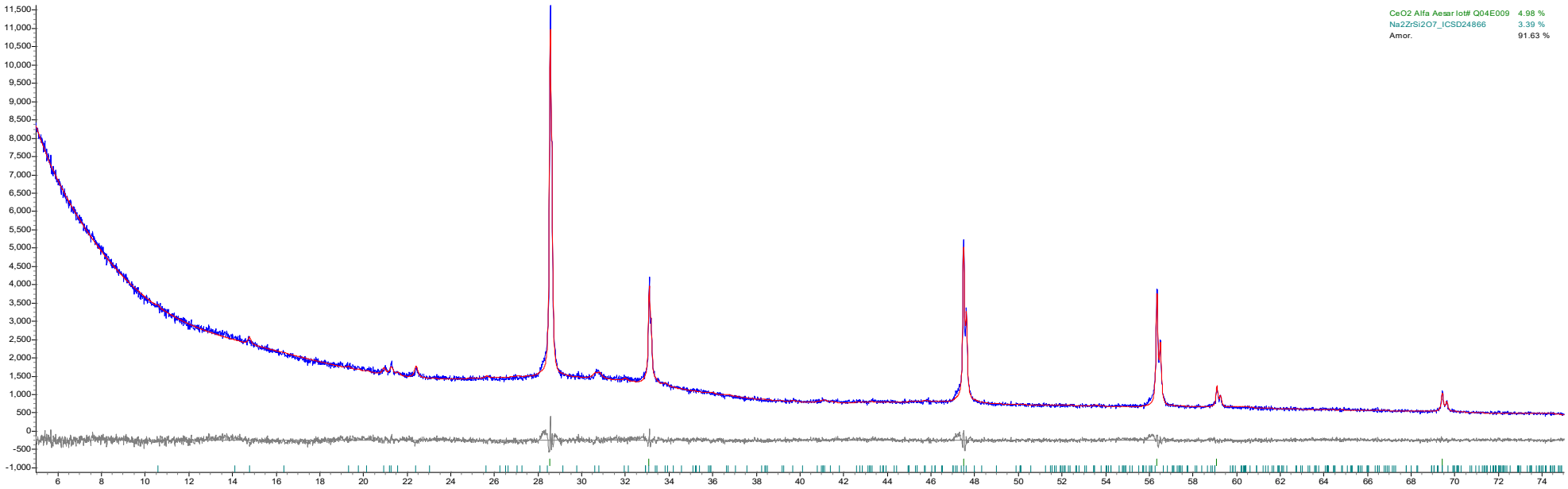


| Phase Name | Wt% Measured | Wt% Corrected | Wt% in Original Sample |
|---|---|---|---|
| $CeO_2$ | 4.98 | 2.56 | |
| $Na_2Zr(Si_2O_7)_4$ | 3.39 | 1.74 | 1.83 |

Figure F.11. Glass APPS2-15 heat treated at 900 °C XRD scan

.

# Appendix G – Viscosity Data

This appendix presents the temperatures at which viscosity was measured, and the measured viscosity data, also found in Table 3.6, for each of the glasses in this matrix. The plots shown in this appendix are fitted to the Arrhenius equation:

$$\ln(\eta) = A + \frac{B}{T_K} \quad \text{G.1}$$

where A and B are independent of temperature and temperature ($T_K$) is in K (T(°C) + 273.15).

Table G.1. Temperatures (°C) at which the viscosities have been measured in order of measurement.

| Glass ID | Temperature (°C) | | | | | |
|---|---|---|---|---|---|---|
| APPS2-01 | 1157.4 | 1067.1 | 975.2 | 1158.6 | 1248.7 | 1158.3 |
| APPS2-02 | 1159.4 | 1068.6 | 976.2 | 1159.4 | 1248.8 | 1159.0 |
| APPS2-03 | 1157.4 | 1066.9 | 974.7 | 1158.0 | 1248.0 | 1158.3 |
| APPS2-04 | 1158.4 | 1066.7 | 974.9 | 1157.1 | 1247.8 | 1158.0 |
| APPS2-05 | 1158.4 | 1067.3 | 975.5 | 1158.9 | 1248.2 | 1157.7 |
| APPS2-06 | 1157.2 | 1066.6 | 975.3 | 1157.7 | 1247.2 | 1157.3 |
| APPS2-07 | 1156.3 | 1065.8 | 973.4 | 1156.9 | 1247.1 | 1156.5 |
| APPS2-08 | 1155.3 | 1064.6 | 972.1 | 1154.4 | 1245.2 | 1154.8 |
| APPS2-09 | 1156.0 | 1064.0 | 971.0 | 1155.0 | 1246.0 | 1156.0 |
| APPS2-10 | 1146.0 | 1060.0 | 968.0 | 1151.0 | 1250.0 | 1151.0 |
| APPS2-11 | 1157.3 | 1064.7 | 972.1 | 1155.8 | 1246.3 | 1149.3 |
| APPS2-12 | 1155.2 | 1065.3 | 973.6 | 1156.4 | 1247.0 | 1155.8 |
| APPS2-13 | 1156.4 | 1065.5 | 973.8 | 1156.4 | 1247.5 | 1157.0 |
| APPS2-14-1 | 1156.0 | 1064.0 | 972.0 | 1154.0 | 1245.0 | 1155.0 |
| APPS2-15 | 1157.0 | 1065.0 | 972.0 | 1154.0 | 1245.0 | 1155.0 |
| APPS2-16 | 1155.1 | 1064.3 | 972.4 | 1155.9 | 1246.5 | 1156.4 |

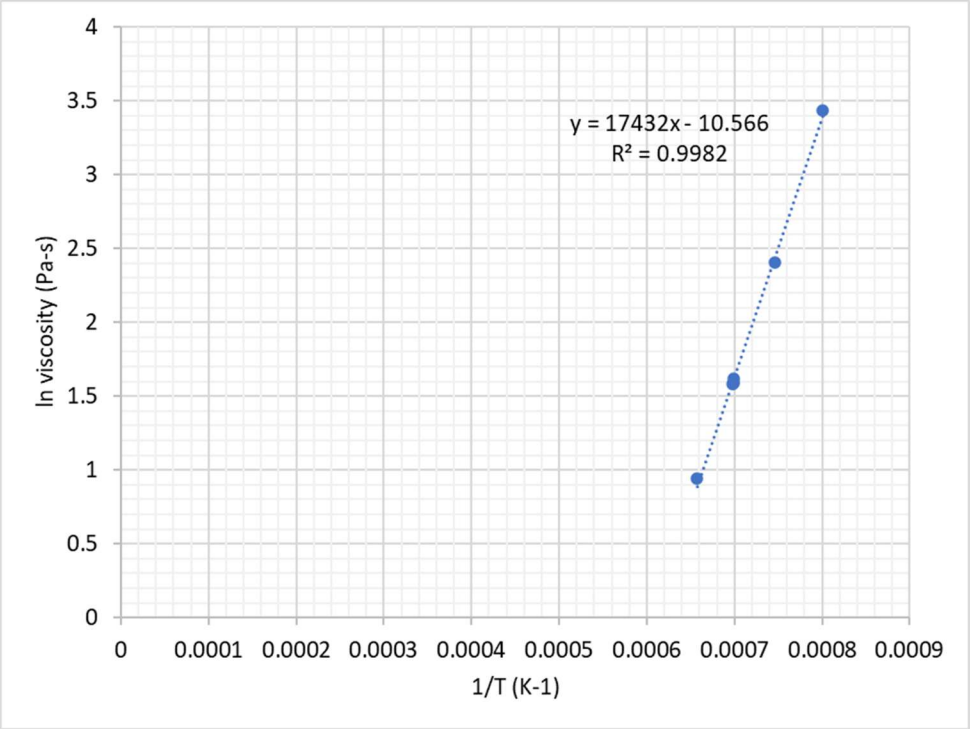


Figure G.1. Viscosity-temperature data and Arrhenius equation fit for APPS2-01.

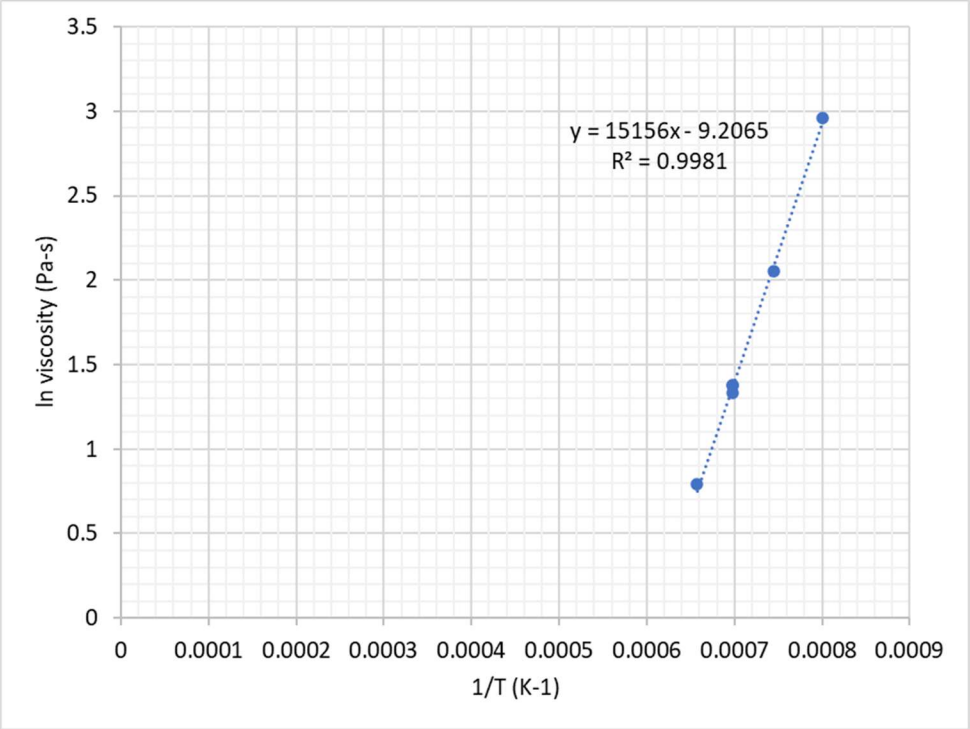


Figure G.2. Viscosity-temperature data and Arrhenius equation fit for APPS2-02.

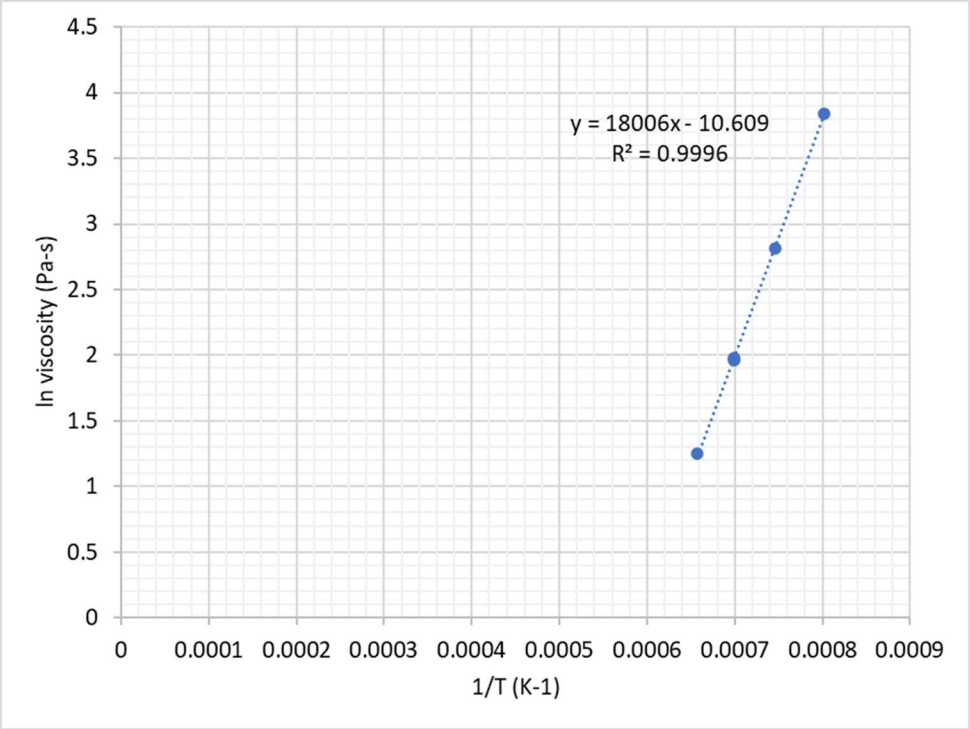


Figure G.3. Viscosity-temperature data and Arrhenius equation fit for APPS2-03.

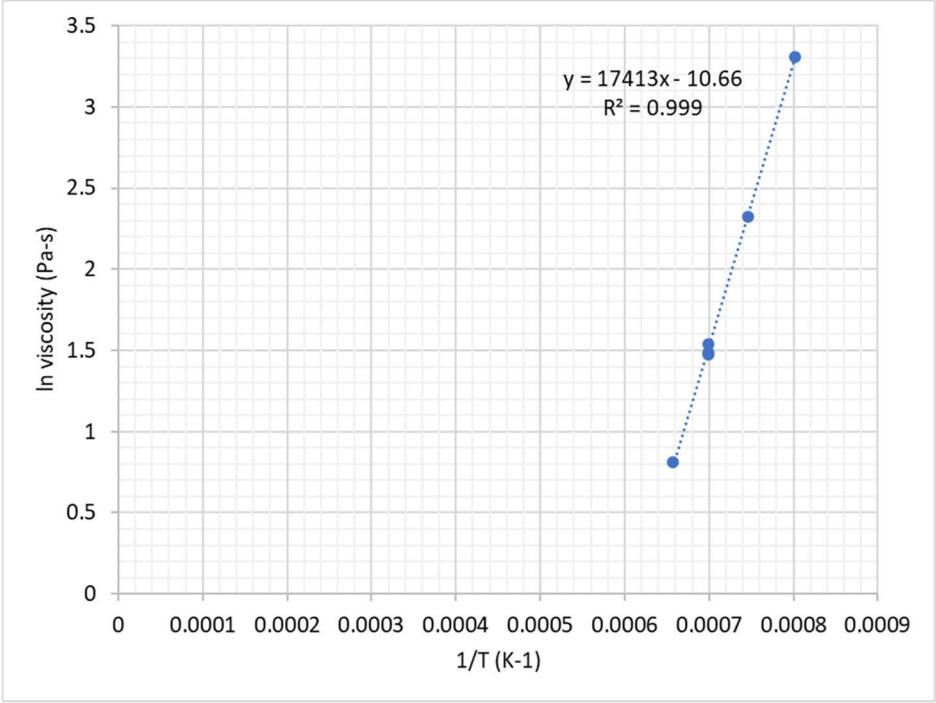


Figure G.4. Viscosity-temperature data and Arrhenius equation fit for APPS2-04.

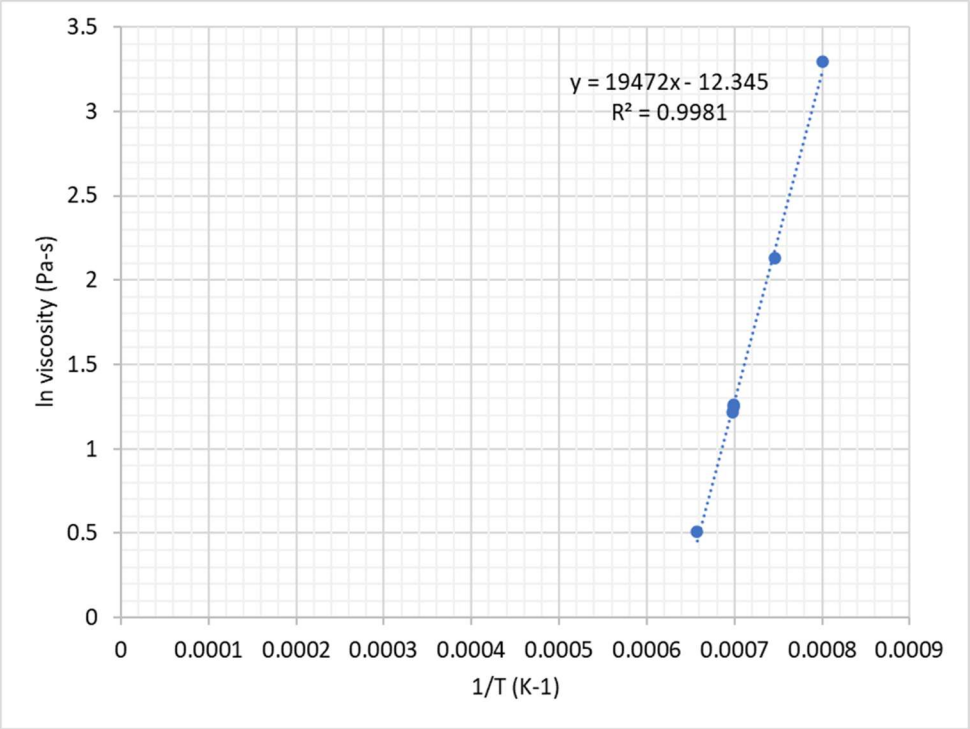


Figure G.5. Viscosity-temperature data and Arrhenius equation fit for APPS2-05.

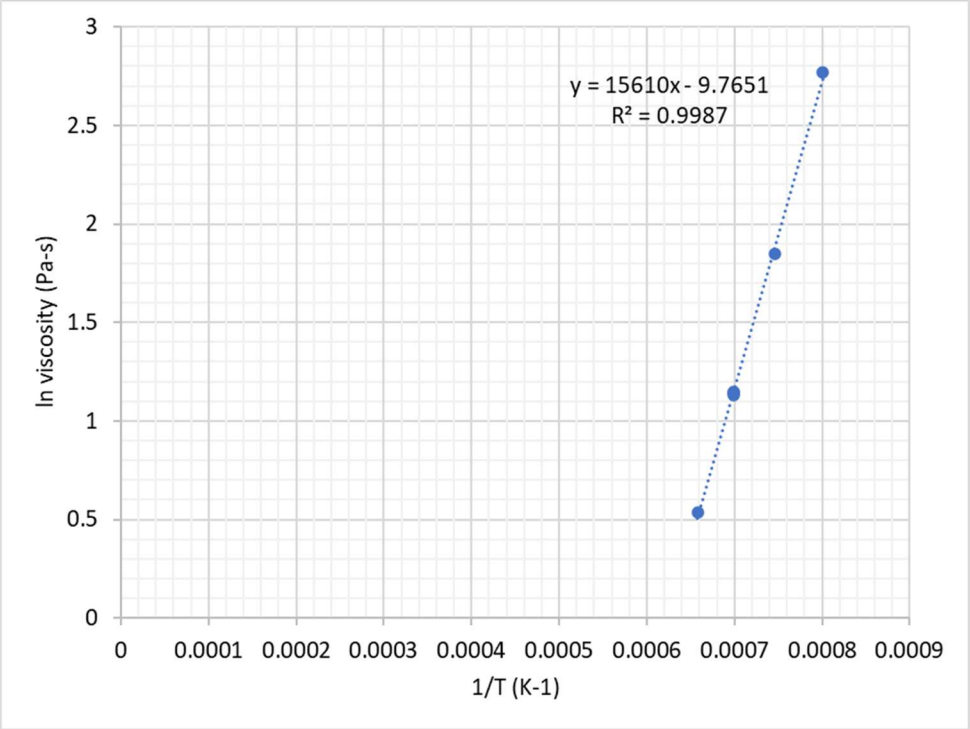


Figure G.6. Viscosity-temperature data and Arrhenius equation fit for APPS2-06.

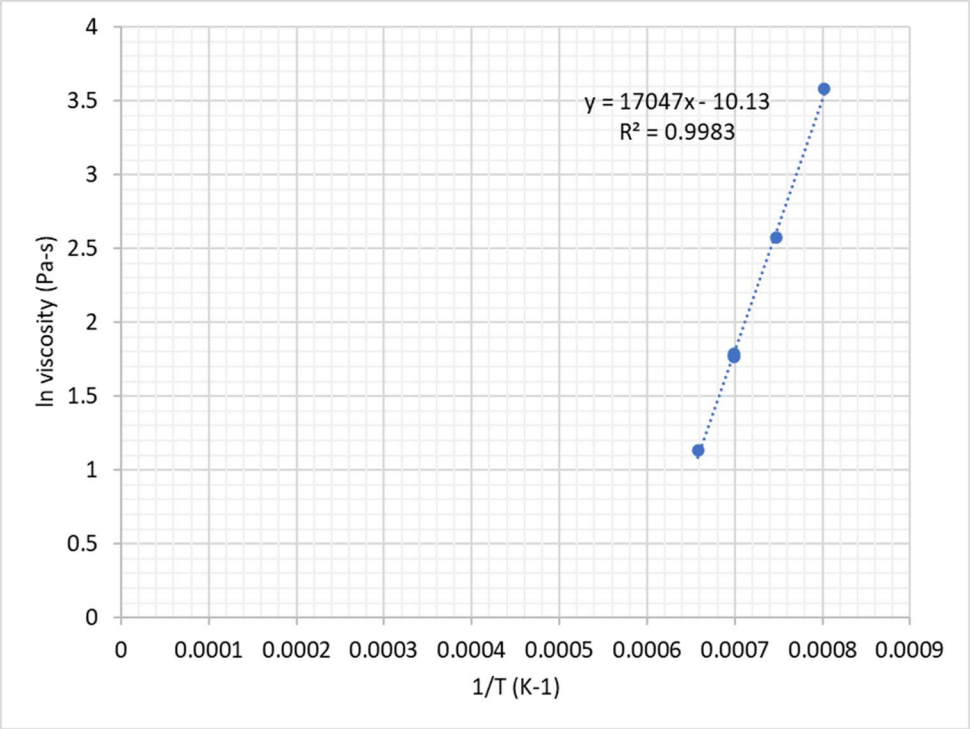


Figure G.7. Viscosity-temperature data and Arrhenius equation fit for APPS2-07.

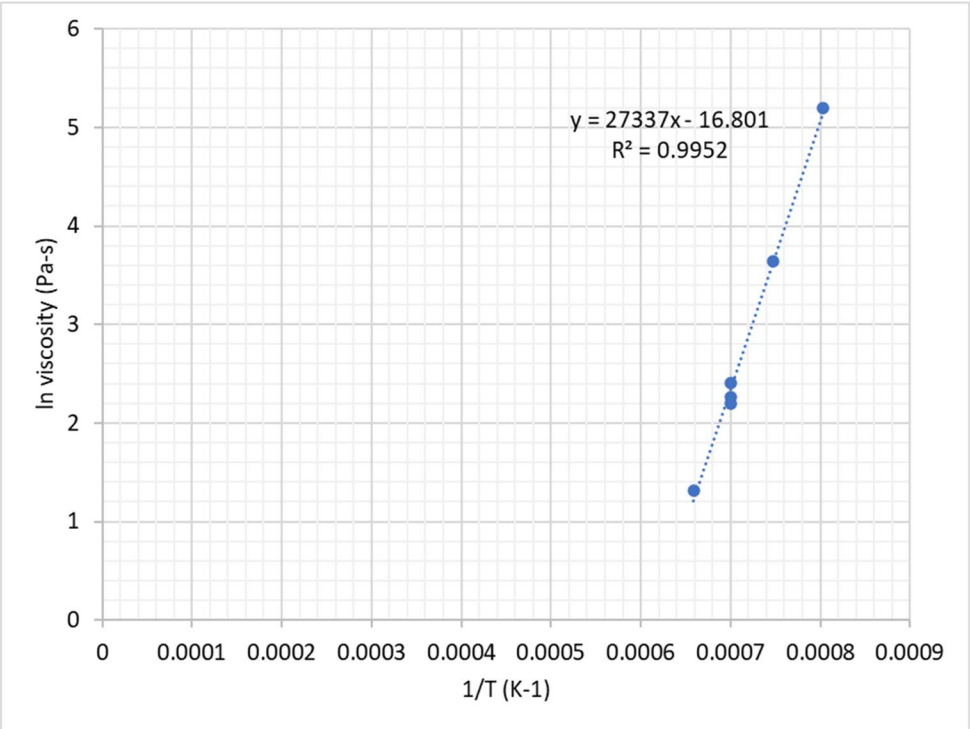


Figure G.8. Viscosity-temperature data and Arrhenius equation fit for APPS2-08.

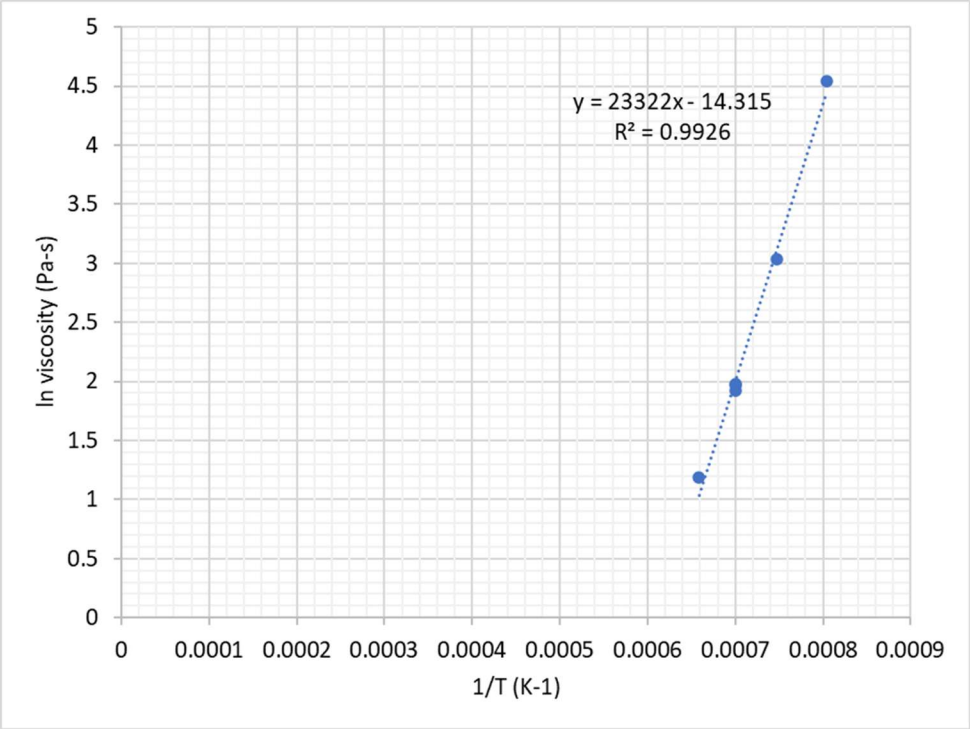


Figure G.9. Viscosity-temperature data and Arrhenius equation fit for APPS2-09.

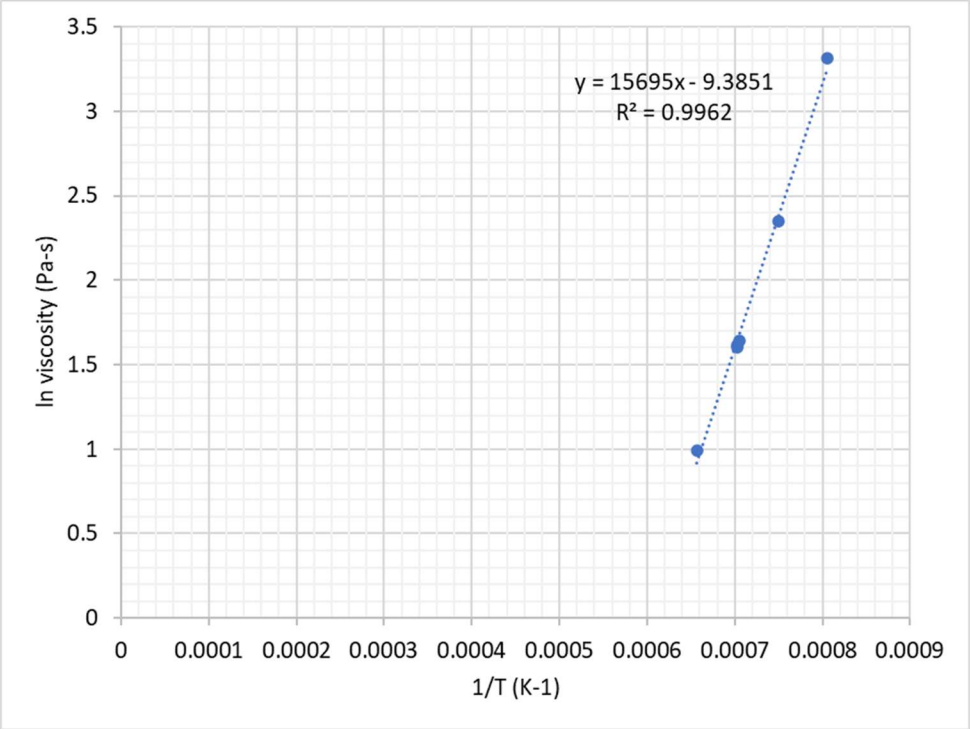


Figure G.10. Viscosity-temperature data and Arrhenius equation fit for APPS2-10.

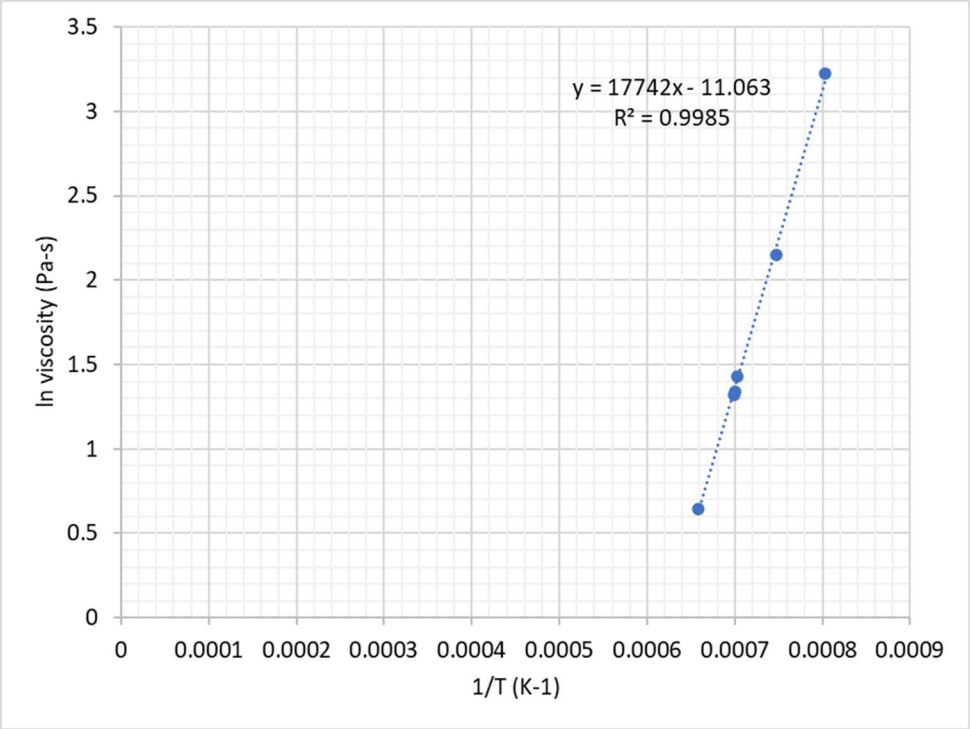


Figure G.11. Viscosity-temperature data and Arrhenius equation fit for APPS2-11.

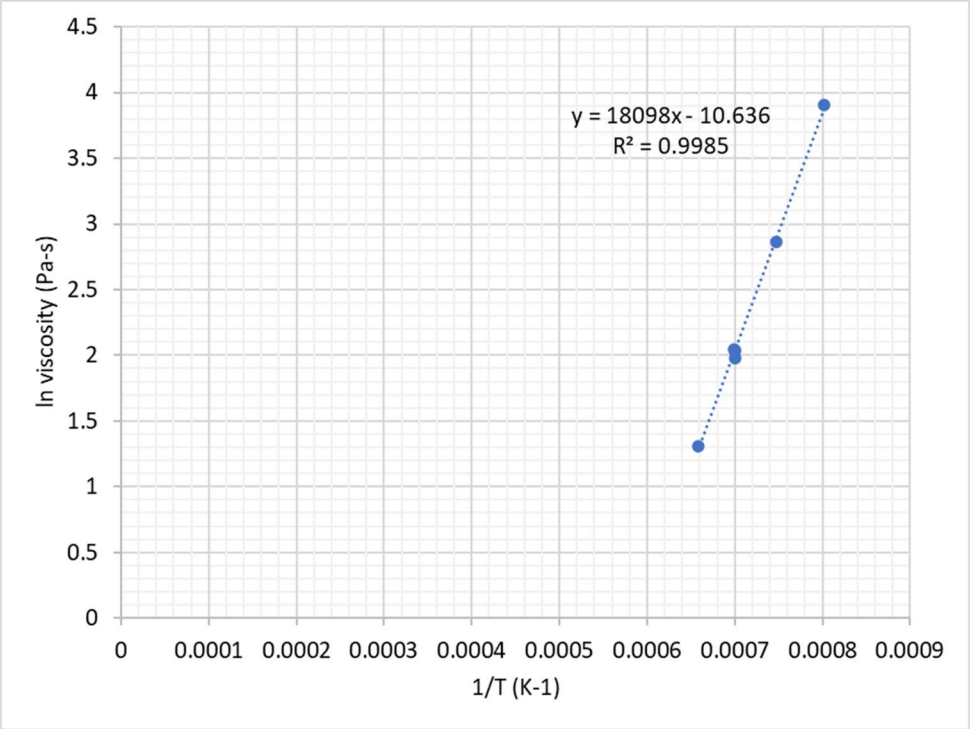


Figure G.12. Viscosity-temperature data and Arrhenius equation fit for APPS2-12.

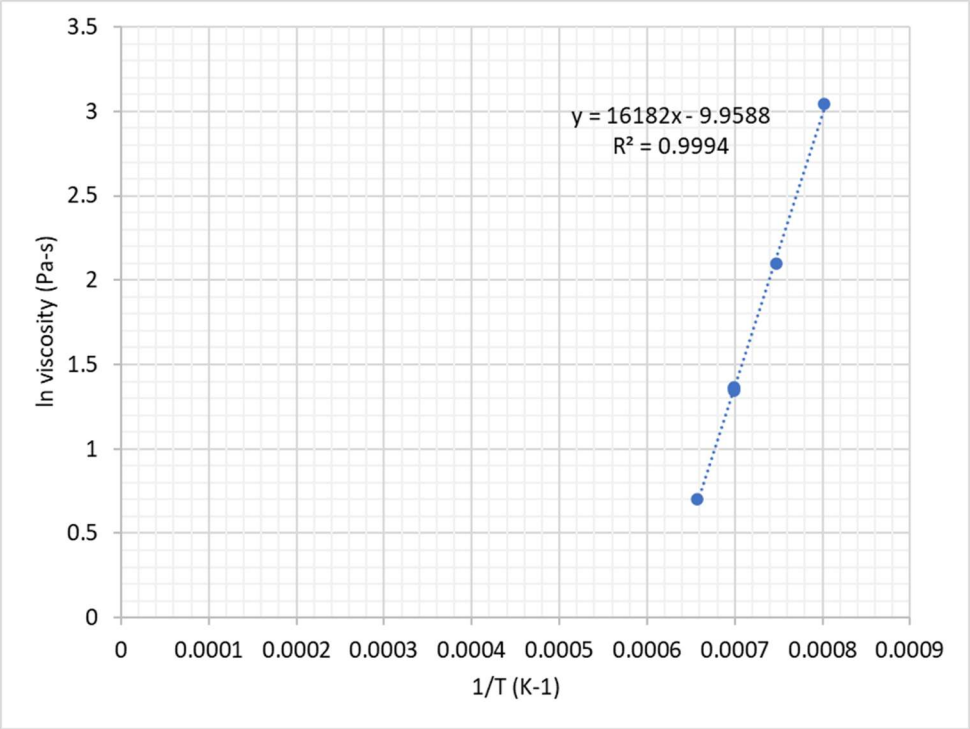


Figure G.13. Viscosity-temperature data and Arrhenius equation fit for APPS2-13.

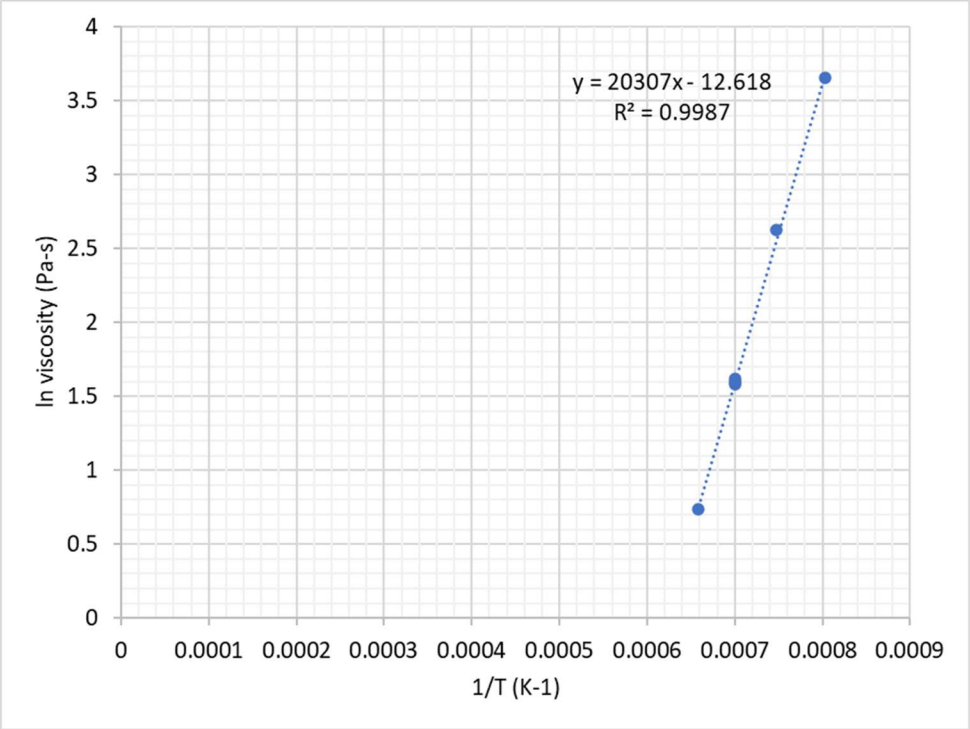


Figure G.14. Viscosity-temperature data and Arrhenius equation fit for APPS2-14-1.

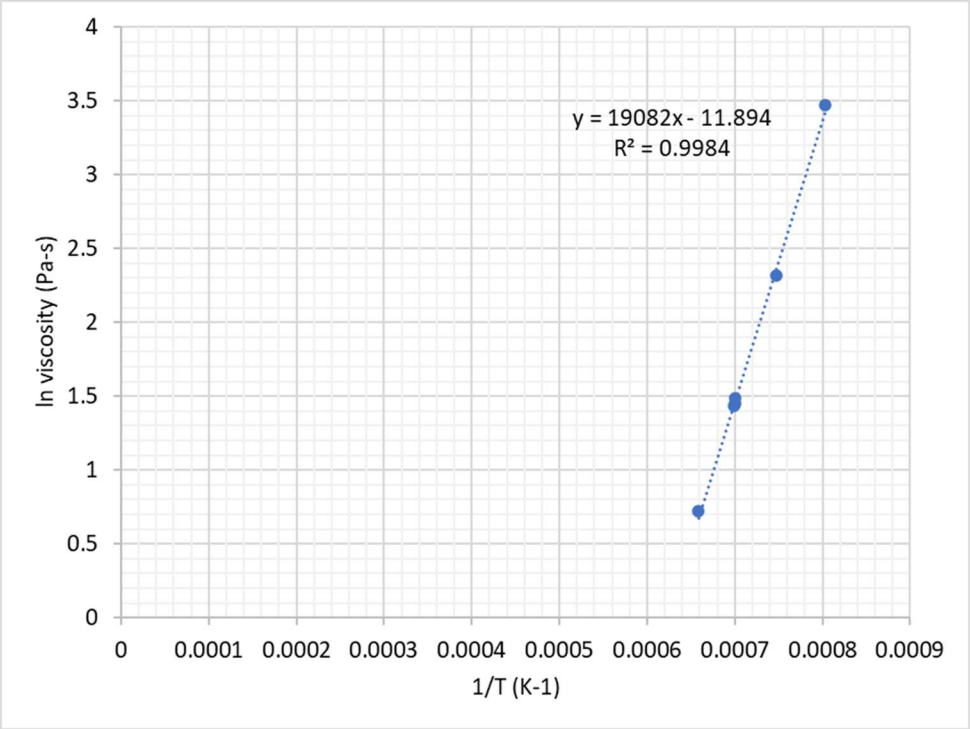


Figure G.15. Viscosity-temperature data and Arrhenius equation fit for APPS2-15.

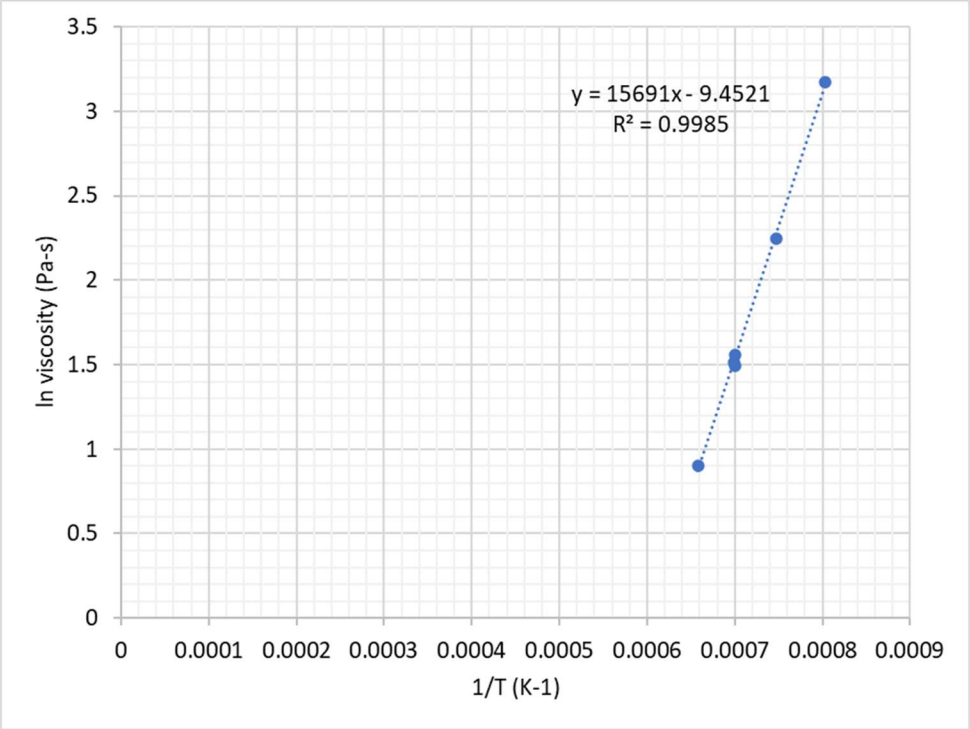


Figure G.16. Viscosity-temperature data and Arrhenius equation fit for APPS2-16.

# Appendix H – Electrical Conductivity Data

This appendix presents the measured electrical conductivity data for each of the glasses in this matrix following Section 2.10 of the main report.

The plots shown in this appendix are fitted to the Arrhenius equation, which is shown below:

$$\ln(\varepsilon) = A + B/T_K \qquad \text{H.1}$$

where $A$ and $B$ are independent of temperature and temperature ($T_K$) is in K (T(°C) + 273.15).

The main intent of the figures and Arrhenius equation fits shown in this appendix is to assess trends in the data and provide observations about whether there may be sufficient curvature in the data to consider Vogel-Fulcher-Tammann (VFT) fits in the subsequent work that will decide between fitting the data to the Arrhenius or VFT equations for the electrical conductivity-temperature data for each glass that is being made.

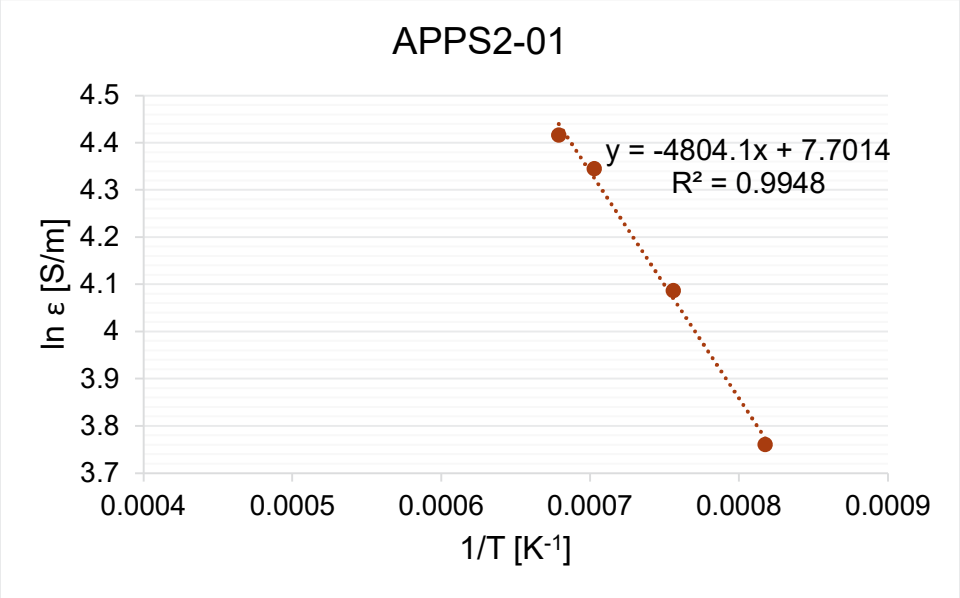


Figure H.1. Electrical conductivity-temperature data and Arrhenius equation fit for glass APPS2-01.

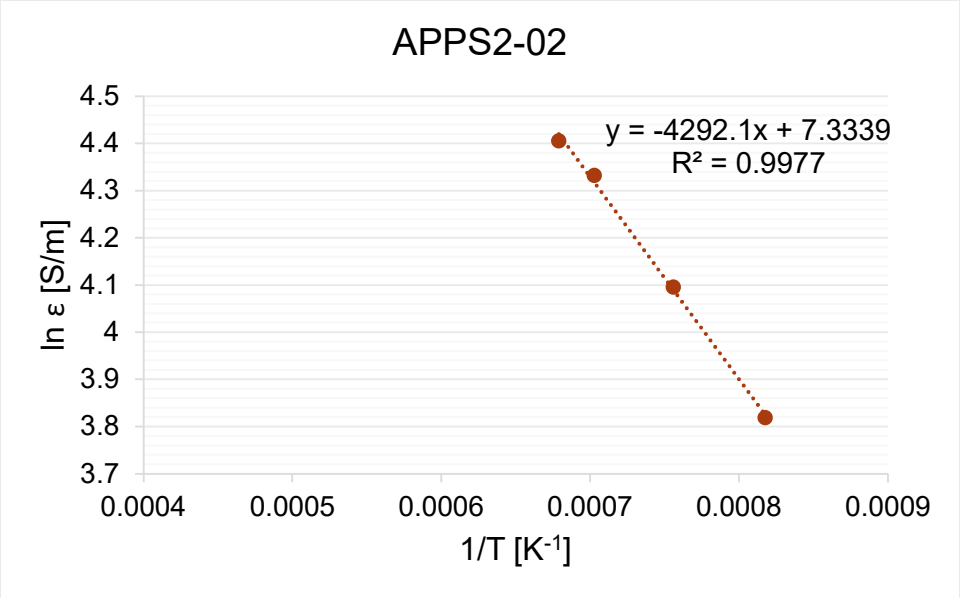


Figure H.2. Electrical conductivity-temperature data and Arrhenius equation fit for glass APPS2-02.

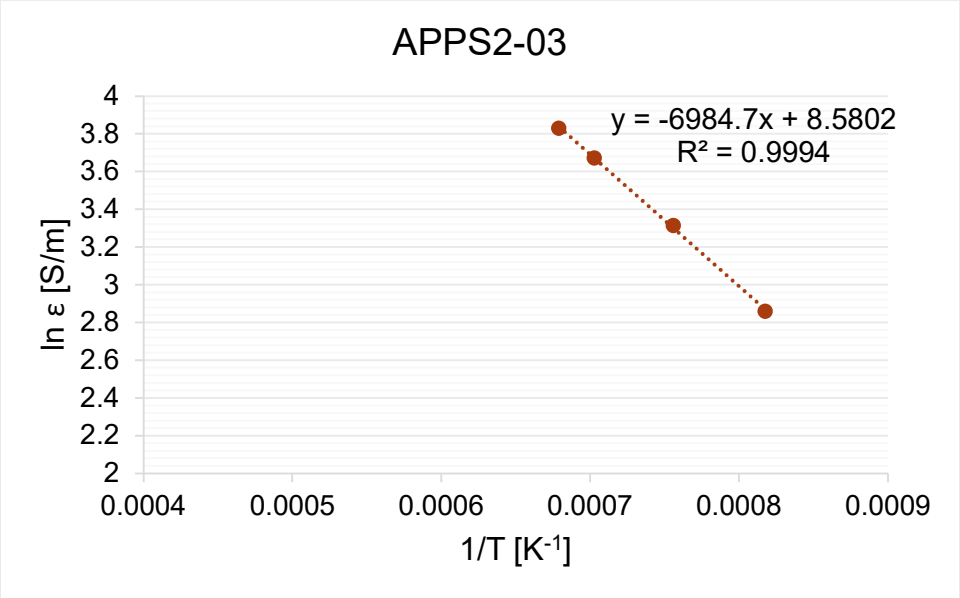


Figure H.3. Electrical conductivity-temperature data and Arrhenius equation fit for glass APPS2-03.

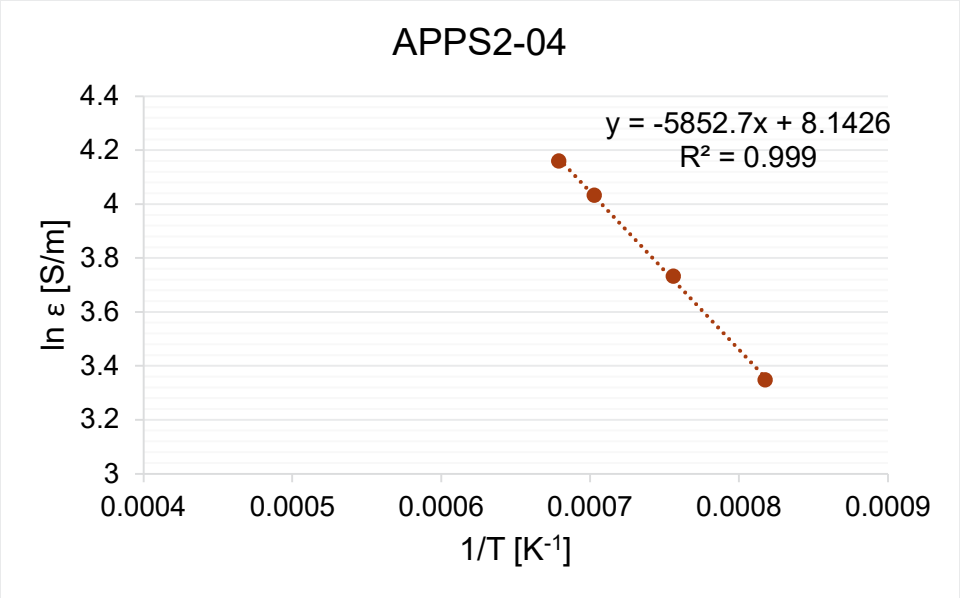


Figure H.4. Electrical conductivity-temperature data and Arrhenius equation fit for glass APPS2-04.

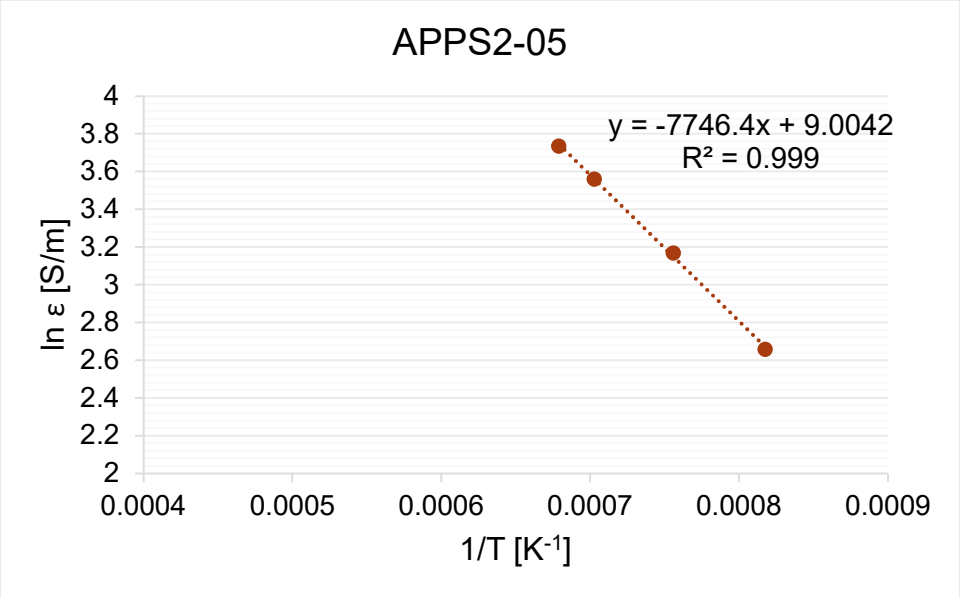


Figure H.5. Electrical conductivity-temperature data and Arrhenius equation fit for glass APPS2-05.

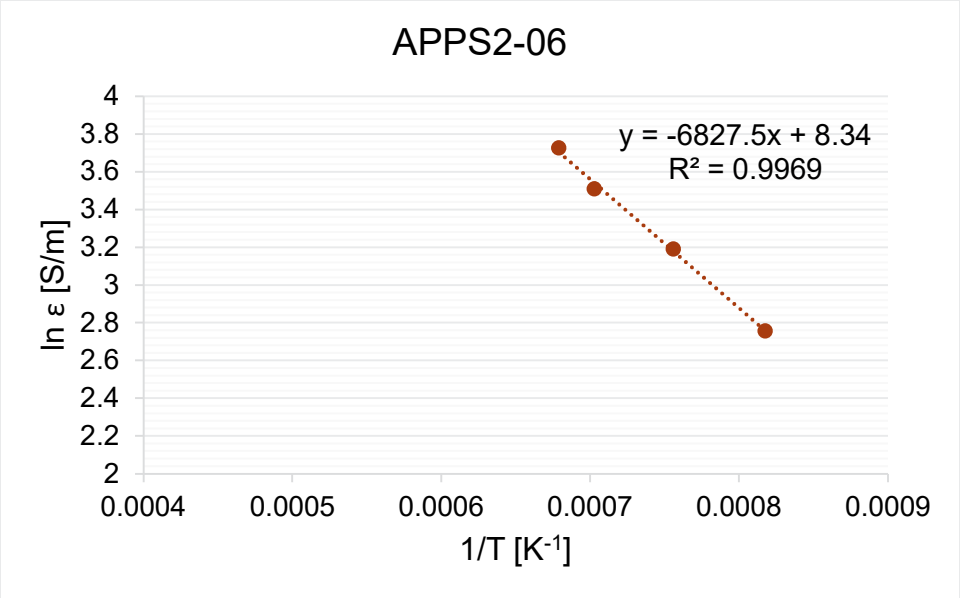


Figure H.6. Electrical conductivity-temperature data and Arrhenius equation fit for glass APPS2-06.

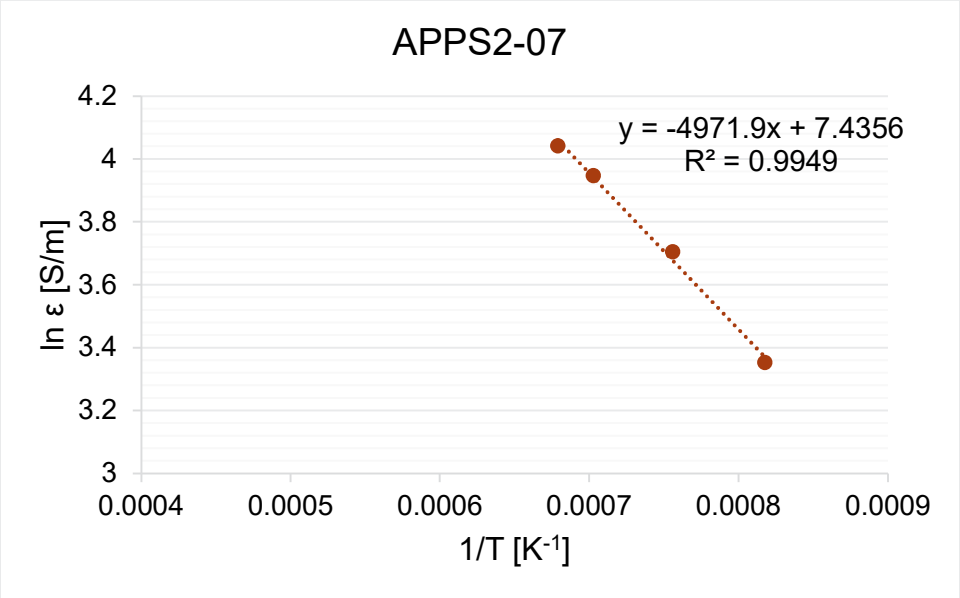


Figure H.7. Electrical conductivity-temperature data and Arrhenius equation fit for glass APPS2-07.

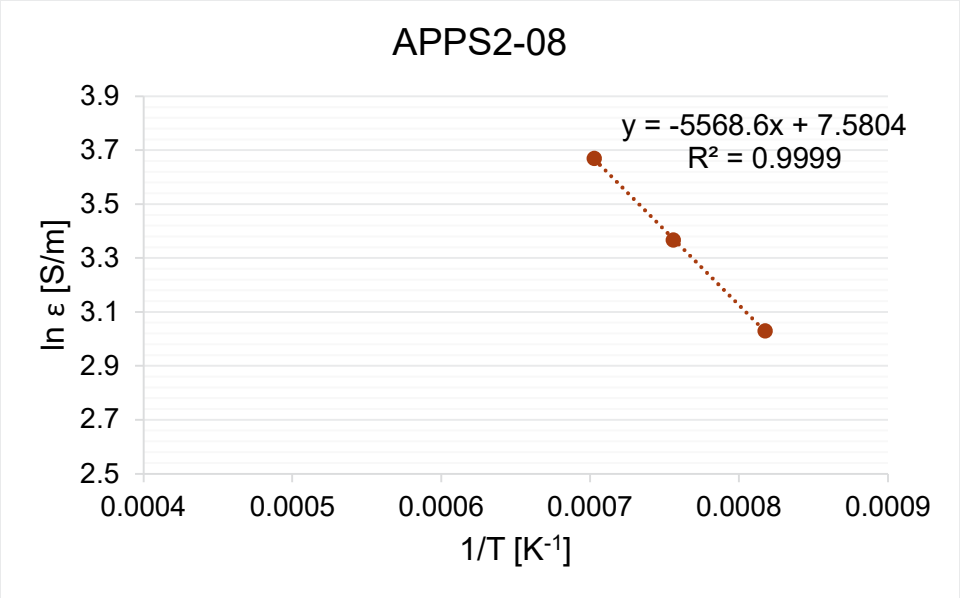


Figure H.8. Electrical conductivity-temperature data and Arrhenius equation fit for glass APPS2-08.

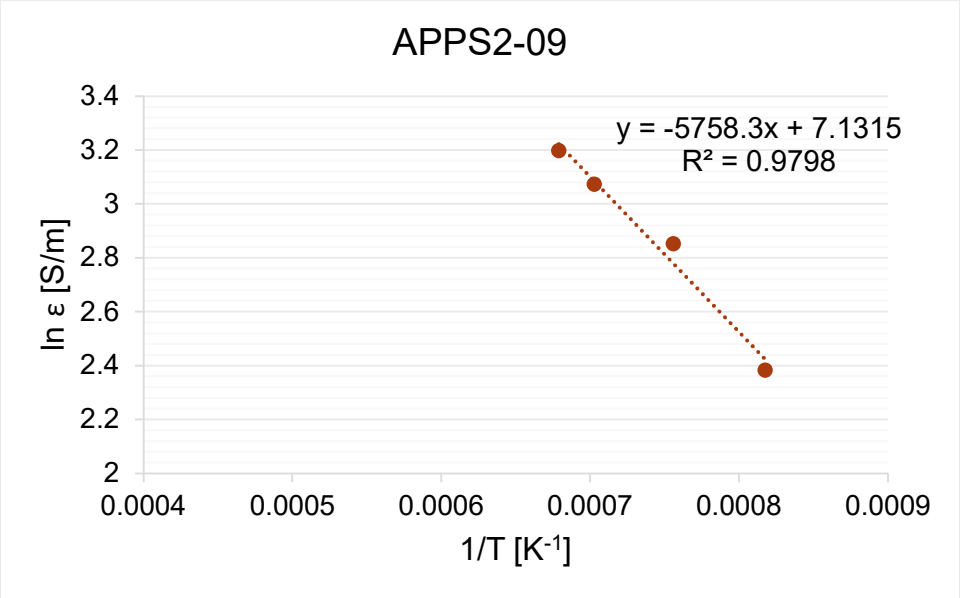


Figure H.9. Electrical conductivity-temperature data and Arrhenius equation fit for glass APPS2-09.

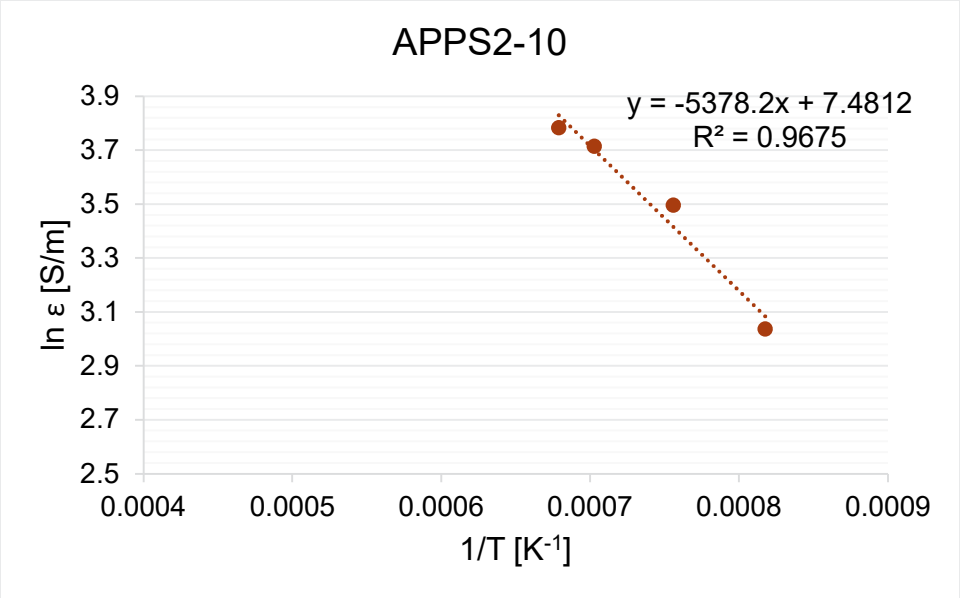


Figure H.10. Electrical conductivity-temperature data and Arrhenius equation fit for glass APPS2-10.

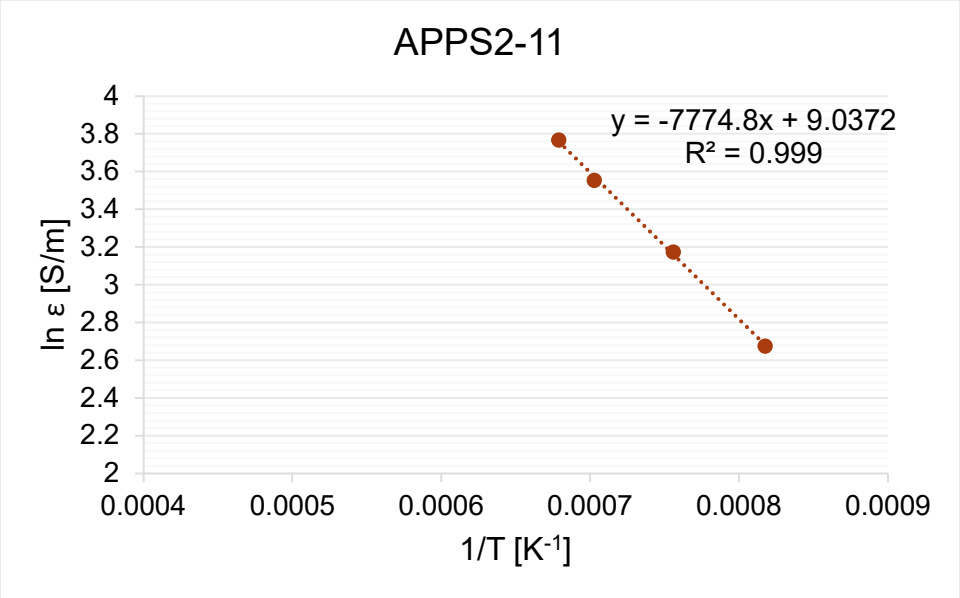


Figure H.11. Electrical conductivity-temperature data and Arrhenius equation fit for glass APPS2-11.

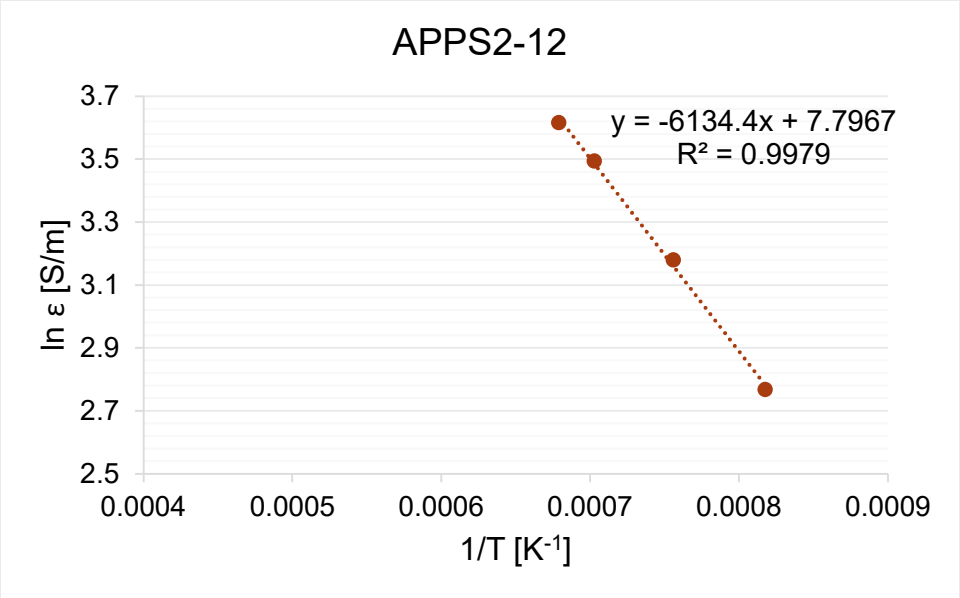


Figure H.12. Electrical conductivity-temperature data and Arrhenius equation fit for glass APPS2-12.

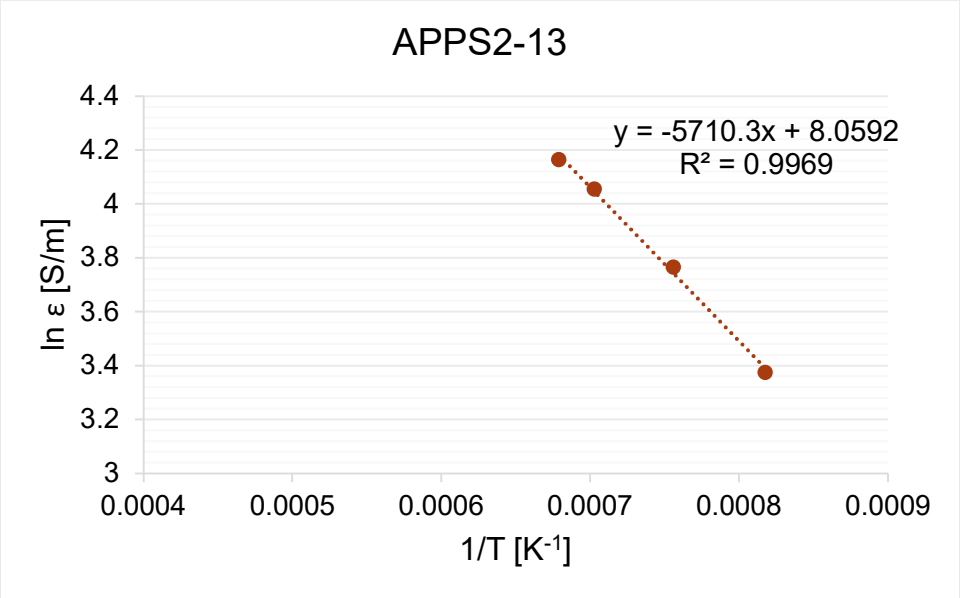


Figure H.13. Electrical conductivity-temperature data and Arrhenius equation fit for glass APPS2-13.

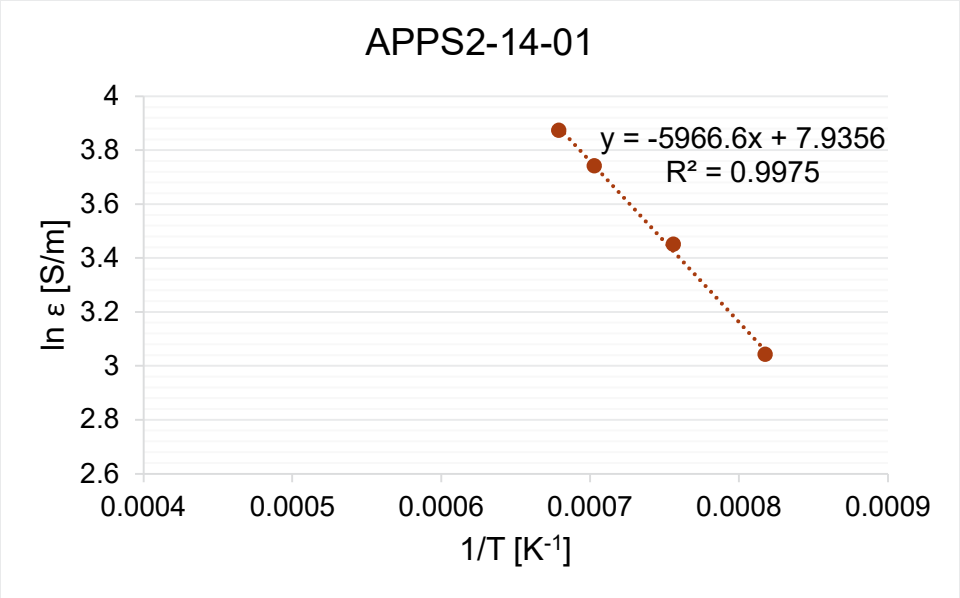


Figure H.14. Electrical conductivity-temperature data and Arrhenius equation fit for glass APPS2-14-1.

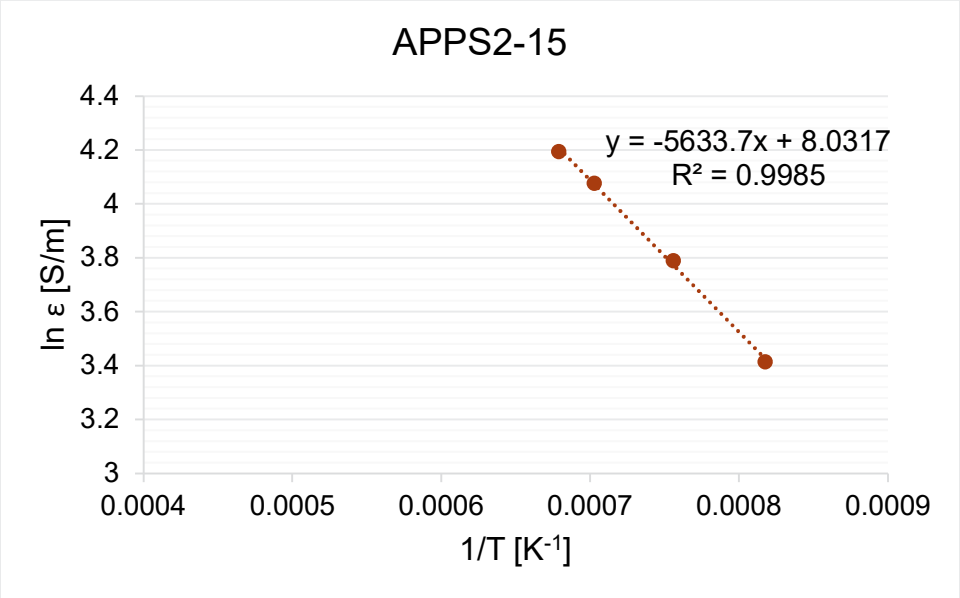


Figure H.15. Electrical conductivity-temperature data and Arrhenius equation fit for glass APPS2-15.

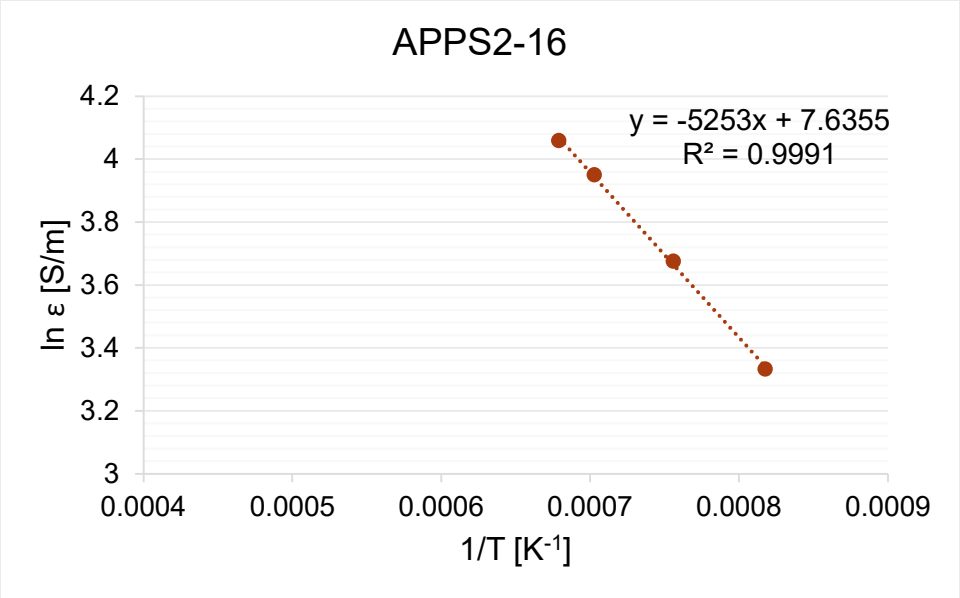


Figure H.16. Electrical conductivity-temperature data and Arrhenius equation fit for glass APPS2-16.

# Appendix I – PCT Full Results

This appendix presents the complete list of PCT results in a manner that enables easy comparison of quenched and CCC glasses.

Table I.1. PCT normalized concentrations (g/L) of B, Si, Na, and Li for Q and CCC APPS2 glasses. N/A = not applicable as the glass does not contain Li.

| | Normalized Concentrations ($NC_i$) in g/L | | | |
|---|---|---|---|---|
| Sample ID | Boron | Silicon | Sodium | Lithium |
| APPS2-01-Q-PCT-A | 6.66 | 1.28 | 5.25 | (a) |
| APPS2-01-Q-PCT-B | 6.66 | 1.29 | 5.25 | (a) |
| APPS2-01-Q-PCT-C | 6.55 | 1.28 | 5.19 | (a) |
| APPS2-01-CCC-PCT-A | 4.17 | 0.88 | 3.47 | (a) |
| APPS2-01-CCC-PCT-B | 4.16 | 0.91 | 3.43 | (a) |
| APPS2-01-CCC-PCT-C | 4.11 | 1.00 | 3.37 | (a) |
| APPS2-02-Q-PCT-A | 10.05 | 0.59 | 6.86 | 13.67(b) |
| APPS2-02-Q-PCT-B | 9.94 | 0.58 | 6.75 | 13.69(b) |
| APPS2-02-Q-PCT-C | 10.09 | 0.59 | 6.86 | 13.65(b) |
| APPS2-02-CCC-PCT-A | 8.98 | 0.55 | 6.16 | 13.69(b) |
| APPS2-02-CCC-PCT-B | 8.88 | 0.54 | 6.05 | 13.66(b) |
| APPS2-02-CCC-PCT-C | 8.85 | 0.54 | 6.10 | 13.72(b) |
| APPS2-03-Q-PCT-A | 4.38 | 0.24 | 2.78 | 3.74 |
| APPS2-03-Q-PCT-B | 4.17 | 0.25 | 2.65 | 3.55 |
| APPS2-03-Q-PCT-C | 4.20 | 0.25 | 2.65 | 3.56 |
| APPS2-03-CCC-PCT-A | 4.77 | 0.26 | 2.85 | 3.91 |
| APPS2-03-CCC-PCT-B | 4.80 | 0.26 | 2.85 | 3.91 |
| APPS2-03-CCC-PCT-C | 4.71 | 0.26 | 2.82 | 3.85 |
| APPS2-04-Q-PCT-A | 1.55 | 0.61 | 1.92 | (a) |
| APPS2-04-Q-PCT-B | 1.51 | 0.60 | 1.92 | (a) |
| APPS2-04-Q-PCT-C | 1.49 | 0.59 | 1.91 | (a) |
| APPS2-04-CCC-PCT-A | 0.91 | 0.43 | 1.25 | (a) |
| APPS2-04-CCC-PCT-B | 0.87 | 0.42 | 1.24 | (a) |
| APPS2-04-CCC-PCT-C | 0.83 | 0.42 | 1.21 | (a) |
| APPS2-05-Q-PCT-A | 1.84 | 0.37 | 1.64 | 1.32 |
| APPS2-05-Q-PCT-B | 1.90 | 0.38 | 1.69 | 1.39 |

| | Normalized Concentrations ($NC_i$) in g/L | | | |
|---|---|---|---|---|
| Sample ID | Boron | Silicon | Sodium | Lithium |
| APPS2-05-Q-PCT-C | 1.91 | 0.38 | 1.68 | 1.40 |
| APPS2-05-CCC-PCT-A | 1.81 | 0.41 | 1.60 | 1.59 |
| APPS2-05-CCC-PCT-B | 1.80 | 0.41 | 1.59 | 1.56 |
| APPS2-05-CCC-PCT-C | 1.75 | 0.41 | 1.56 | 1.54 |
| APPS2-06-Q-PCT-A | 1.13 | 0.25 | 1.10 | 0.81 |
| APPS2-06-Q-PCT-B | 1.11 | 0.25 | 1.07 | 0.78 |
| APPS2-06-Q-PCT-C | 1.10 | 0.25 | 1.06 | 0.77 |
| APPS2-06-CCC-PCT-A | 0.44 | 0.20 | 0.58 | 0.46 |
| APPS2-06-CCC-PCT-B | 0.42 | 0.20 | 0.57 | 0.45 |
| APPS2-06-CCC-PCT-C | 0.43 | 0.20 | 0.56 | 0.44 |
| APPS2-07-Q-PCT-A | 1.02 | 0.69 | 1.75 | (a) |
| APPS2-07-Q-PCT-B | 1.01 | 0.69 | 1.74 | (a) |
| APPS2-07-Q-PCT-C | 1.00 | 0.68 | 1.73 | (a) |
| APPS2-07-CCC-PCT-A | 0.81 | 0.63 | 1.44 | (a) |
| APPS2-07-CCC-PCT-B | 0.80 | 0.62 | 1.44 | (a) |
| APPS2-07-CCC-PCT-C | 0.81 | 0.64 | 1.45 | (a) |
| APPS2-08-Q-PCT-A | 1.77 | 0.29 | 1.01 | 1.49 |
| APPS2-08-Q-PCT-B | 1.67 | 0.28 | 0.96 | 1.40 |
| APPS2-08-Q-PCT-C | 1.65 | 0.28 | 0.95 | 1.38 |
| APPS2-08-CCC-PCT-A | 5.27 | 0.26 | 1.95 | 2.83 |
| APPS2-08-CCC-PCT-B | 5.15 | 0.25 | 1.91 | 2.78 |
| APPS2-08-CCC-PCT-C | 5.29 | 0.28 | 1.97 | 2.83 |
| APPS2-09-Q-PCT-A | 3.06 | 0.25 | 1.88 | 2.67 |
| APPS2-09-Q-PCT-B | 2.92 | 0.23 | 1.80 | 2.56 |
| APPS2-09-Q-PCT-C | 2.86 | 0.23 | 1.78 | 2.52 |
| APPS2-09-CCC-PCT-A | 6.00 | 0.25 | 2.97 | 4.49 |
| APPS2-09-CCC-PCT-B | 5.97 | 0.24 | 2.94 | 4.44 |
| APPS2-09-CCC-PCT-C | 5.92 | 0.25 | 2.91 | 4.38 |
| APPS2-10-Q-PCT-A | 12.91 | 0.15 | 6.94 | 10.34(b) |
| APPS2-10-Q-PCT-B | 12.75 | 0.15 | 6.87 | 10.05(b) |
| APPS2-10-Q-PCT-C | 12.68 | 0.16 | 6.81 | 9.87(b) |
| APPS2-10-CCC-PCT-A | 46.32 | 0.16 | 23.48 | 39.20(b) |
| APPS2-10-CCC-PCT-B | 46.46 | 0.16 | 23.28 | 39.00(b) |

| | Normalized Concentrations ($NC_i$) in g/L | | | |
|---|---|---|---|---|
| Sample ID | Boron | Silicon | Sodium | Lithium |
| APPS2-10-CCC-PCT-C | 46.31 | 0.16 | 23.47 | 39.29(b) |
| APPS2-11-Q-PCT-A | 2.09 | 0.62 | 2.24 | 1.83 |
| APPS2-11-Q-PCT-B | 2.11 | 0.57 | 2.25 | 1.83 |
| APPS2-11-Q-PCT-C | 2.10 | 0.62 | 2.24 | 1.82 |
| APPS2-11-CCC-PCT-A | 1.70 | 0.57 | 1.80 | 1.70 |
| APPS2-11-CCC-PCT-B | 1.66 | 0.57 | 1.77 | 1.68 |
| APPS2-11-CCC-PCT-C | 1.68 | 0.57 | 1.79 | 1.69 |
| APPS2-12-Q-PCT-A | 10.02 | 0.23 | 4.92 | 7.52 |
| APPS2-12-Q-PCT-B | 10.06 | 0.24 | 4.93 | 7.49 |
| APPS2-12-Q-PCT-C | 9.74 | 0.23 | 4.78 | 7.30 |
| APPS2-12-CCC-PCT-A | 11.04 | 0.23 | 5.09 | 7.84 |
| APPS2-12-CCC-PCT-B | 10.92 | 0.22 | 5.05 | 7.87 |
| APPS2-12-CCC-PCT-C | 11.01 | 0.23 | 5.06 | 7.87 |
| APPS2-13-Q-PCT-A | 0.68 | 0.37 | 1.24 | 0.90 |
| APPS2-13-Q-PCT-B | 0.64 | 0.37 | 1.24 | 0.91 |
| APPS2-13-Q-PCT-C | 0.57 | 0.35 | 1.19 | 0.86 |
| APPS2-13-CCC-PCT-A | 0.46 | 0.27 | 0.86 | 0.74 |
| APPS2-13-CCC-PCT-B | 0.39 | 0.27 | 0.84 | 0.73 |
| APPS2-13-CCC-PCT-C | 0.35 | 0.27 | 0.83 | 0.72 |
| APPS2-14-1-Q-PCT-A | 4.93 | 0.14 | 2.86 | 3.44 |
| APPS2-14-1-Q-PCT-B | 4.86 | 0.14 | 2.82 | 3.39 |
| APPS2-14-1-Q-PCT-C | 4.74 | 0.14 | 2.81 | 3.32 |
| APPS2-14-1-CCC-PCT-A | 6.09 | 0.16 | 3.41 | 4.55 |
| APPS2-14-1-CCC-PCT-B | 6.07 | 0.16 | 3.43 | 4.60 |
| APPS2-14-1-CCC-PCT-C | 6.05 | 0.16 | 3.39 | 4.51 |
| APPS2-15-Q-PCT-A | 6.09 | 0.32 | 3.78 | 32.70(b) |
| APPS2-15-Q-PCT-B | 6.06 | 0.32 | 3.79 | 32.76(b) |
| APPS2-15-Q-PCT-C | 6.05 | 0.32 | 3.79 | 32.74(b) |
| APPS2-15-CCC-PCT-A | 4.45 | 0.28 | 2.77 | 32.73(b) |
| APPS2-15-CCC-PCT-B | 4.43 | 0.29 | 2.79 | 32.83(b) |
| APPS2-15-CCC-PCT-C | 4.40 | 0.28 | 2.78 | 32.74(b) |
| APPS2-16-Q-PCT-A | 7.33 | 0.64 | 5.32 | 10.22(b) |
| APPS2-16-Q-PCT-B | 7.37 | 0.64 | 5.34 | 10.22(b) |

| | Normalized Concentrations ($NC_i$) in g/L | | | |
|---|---|---|---|---|
| Sample ID | Boron | Silicon | Sodium | Lithium |
| APPS2-16-Q-PCT-C | 7.40 | 0.65 | 5.30 | 10.23(b) |
| APPS2-16-CCC-PCT-A | 6.60 | 0.59 | 4.71 | 10.25(b) |
| APPS2-16-CCC-PCT-B | 6.62 | 0.59 | 4.73 | 10.23(b) |
| APPS2-16-CCC-PCT-C | 6.65 | 0.61 | 4.72 | 11.14(b) |

(a) The glass does not contain lithium so no $NC_{Li}$ value is reported.
(b) The $Li_2O$ wt% in this glass is less than 0.05. Low concentrations can cause large uncertainties in $f_i$ (see Section 2.8) and thus these values should be treated with caution.

# Appendix J – TCLP Full Results

This appendix presents the complete list of toxicity characteristic leaching procedure (TCLP) results.

Table J.1. TCLP leachate concentrations of B, Cr, Ni, Pb, V, and Zn for Q and CCC APPS2 glasses in $mg \cdot L^{-1}$. The delisting limits for the constituents of concern in $mg \cdot L^{-1}$ are provided as a reference. Values represented by detection limits are provided in red font/cells.

| | Element | | | | | |
|---|---|---|---|---|---|---|
| Sample ID | B | Cr | Ni | Pb | V | Zn |
| Delisting Limits | N/A | 4.95 | 22.6 | 5.00 | 16.9 | 225 |
| APPS2-01-Q | **≤2.51** | **≤0.12** | **≤0.19** | **≤0.25** | 0.69 ± 0.01 | 0.51 ± 0.03 |
| APPS2-02-Q | 12.65 ± 2.19 | **≤0.13** | **≤0.19** | **≤0.25** | **≤0.13** | **≤0.38** |
| APPS2-03-Q | 15 ± 0.14 | **≤0.13** | 0.36 ± 0.05 | **≤0.25** | **≤0.13** | 7.15 ± 0.01 |
| APPS2-04-Q | **≤2.51** | **≤0.13** | **≤0.19** | **≤0.25** | 0.5 ± 0.01 | **≤0.38** |
| APPS2-05-Q | 2.65 ± 0.02 | **≤0.13** | **≤0.19** | **≤0.25** | **≤0.13** | 0.89 ± 0.04 |
| APPS2-06-Q | 3.37 ± 0.02 | **≤0.13** | **≤0.19** | **≤0.25** | 2.49 ± 0.01 | **≤0.38** |
| APPS2-07-Q | **≤2.52** | **≤0.13** | **≤0.19** | **≤0.25** | **≤0.13** | 0.92 ± 0.19 |
| APPS2-08-Q | **≤2.53** | **≤0.13** | **≤0.19** | **≤0.25** | 0.7 ± 0.01 | **≤0.38** |
| APPS2-09-Q | 5.33 ± 0.14 | **≤0.13** | 0.56 ± 0.01 | **≤0.25** | **≤0.13** | **≤0.38** |
| APPS2-10-Q | 9.42 ± 0.28 | 0.14 ± 0 | **≤0.19** | **≤0.25** | **≤0.13** | **≤0.38** |
| APPS2-11-Q | **≤2.51** | **≤0.13** | **≤0.19** | **≤0.25** | **≤0.13** | **≤0.38** |
| APPS2-12-Q | 13.24 ± 0.06 | **≤0.13** | **≤0.19** | **≤0.25** | 4.18 ± 0.05 | 6 ± 0.09 |
| APPS2-13-Q | **≤2.52** | **≤0.13** | **≤0.19** | **≤0.25** | 0.55 ± 0 | **≤0.38** |
| APPS2-14-Q | 2.9 ± 0.12 | **≤0.12** | 0.22 ± 0 | **≤0.25** | 0.23 ± 0 | **≤0.38** |
| APPS2-15-Q | **≤2.51** | **≤0.13** | **≤0.19** | **≤0.25** | **≤0.13** | 1.01 ± 0.14 |
| APPS2-16-Q | 7.68 ± 1.65 | 0.21 ± 0.02 | **≤0.19** | **≤0.25** | **≤0.13** | 2.06 ± 0.4 |
| APPS2-01-CCC | **≤2.51** | 0.46 ± 0.03 | **≤0.19** | **≤0.25** | 1.95 ± 0.09 | 0.61 ± 0 |
| APPS2-02-CCC | 12.59 ± 0.69 | **≤0.13** | **≤0.19** | **≤0.25** | **≤0.13** | **≤0.38** |
| APPS2-03-CCC | 21.19 ± 0.3 | **≤0.13** | **≤0.19** | **≤0.25** | **≤0.13** | 5.66 ± 0.05 |
| APPS2-04-CCC | **≤2.52** | 1.01 ± 0.23 | **≤0.19** | **≤0.25** | 0.97 ± 0.04 | **≤0.38** |
| APPS2-05-CCC | **≤2.51** | **≤0.13** | **≤0.19** | **≤0.25** | **≤0.13** | 0.83 ± 0.01 |
| APPS2-06-CCC | 2.61 ± 0.03 | **≤0.13** | **≤0.19** | **≤0.25** | 3.32 ± 0.04 | **≤0.38** |
| APPS2-07-CCC | **≤2.51** | 0.41 ± 0.06 | **≤0.19** | **≤0.25** | **≤0.13** | 0.8 ± 0.01 |
| APPS2-08-CCC | **≤2.52** | **≤0.13** | **≤0.19** | **≤0.25** | 0.99 ± 0.05 | **≤0.38** |
| APPS2-09-CCC | 9.25 ± 0.35 | **≤0.13** | **≤0.19** | 0.41 ± 0 | **≤0.13** | **≤0.38** |
| APPS2-10-CCC | 182.81 ± 9.63 | 1.35 ± 0.05 | 0.72 ± 0 | **≤0.25** | 0.16 ± 0.01 | **≤0.38** |
| APPS2-11-CCC | 2.88 ± 0.23 | 0.94 ± 0.01 | **≤0.19** | **≤0.25** | **≤0.12** | **≤0.38** |
| APPS2-12-CCC | 19.99 ± 1.41 | **≤0.12** | **≤0.19** | **≤0.25** | 6.09 ± 0.39 | 5.28 ± 0.35 |
| APPS2-13-CCC | **≤2.5** | **≤0.13** | **≤0.19** | **≤0.25** | 0.57 ± 0 | **≤0.38** |

| | Element | | | | | |
|---|---|---|---|---|---|---|
| Sample ID | B | Cr | Ni | Pb | V | Zn |
| Delisting Limits | N/A | 4.95 | 22.6 | 5.00 | 16.9 | 225 |
| APPS2-14-CCC | 5.48 ± 0.05 | **≤0.13** | **≤0.19** | **≤0.25** | 0.53 ± 0.03 | **≤0.38** |
| APPS2-15-CCC | **≤2.51** | 0.52 ± 0 | **≤0.19** | **≤0.25** | **≤0.13** | 0.87 ± 0.02 |
| APPS2-16-CCC | 6.92 ± 0.32 | 0.28 ± 0 | **≤0.19** | **≤0.25** | **≤0.13** | 1.83 ± 0.09 |

# Appendix K – K-3 Coupons after Refractory Corrosion Test

The photographs in this appendix show the K-3 refractory coupons after corrosion testing with APPS2 glasses under various conditions.

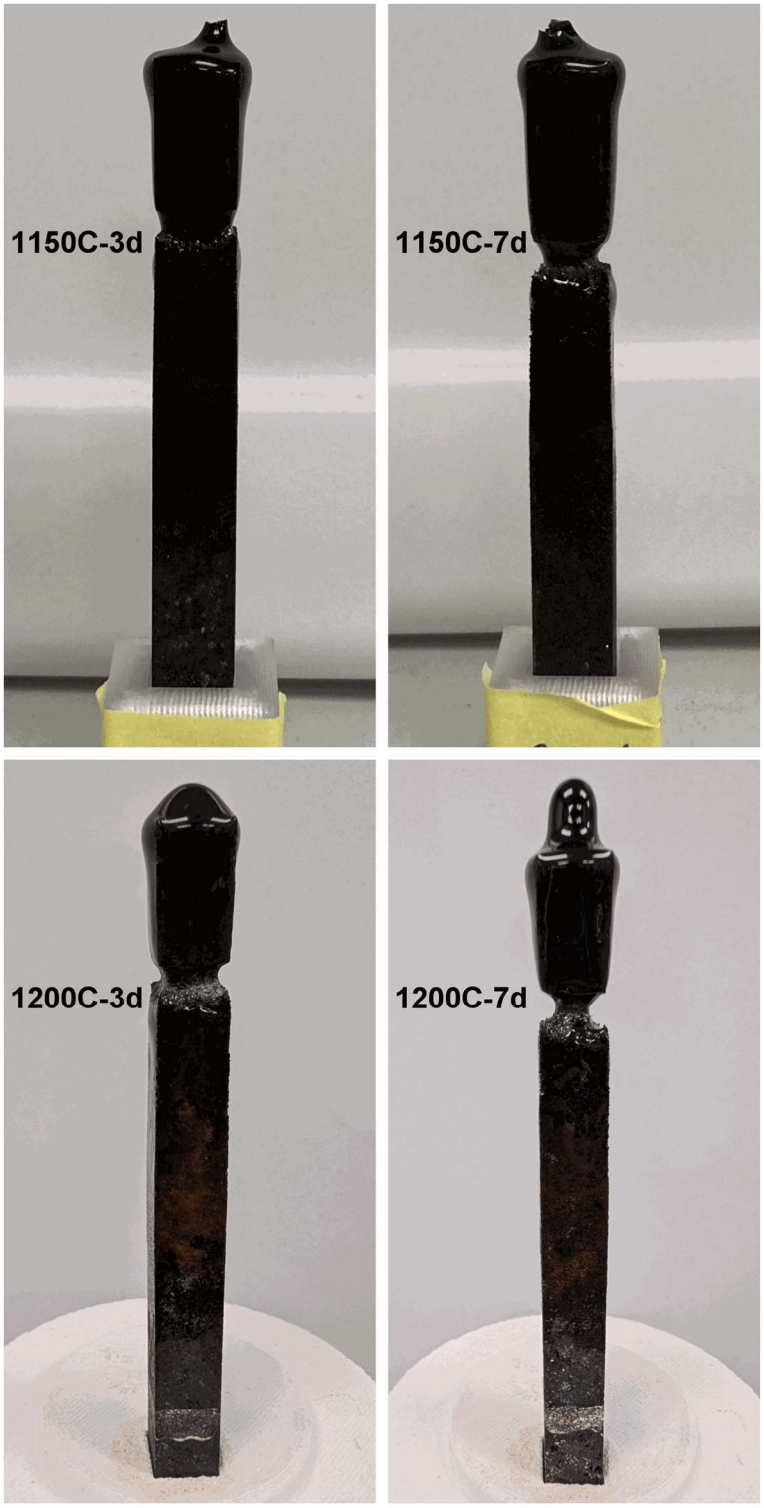


Figure K.1. K-3 coupons after refractory corrosion test, APPS2-01.

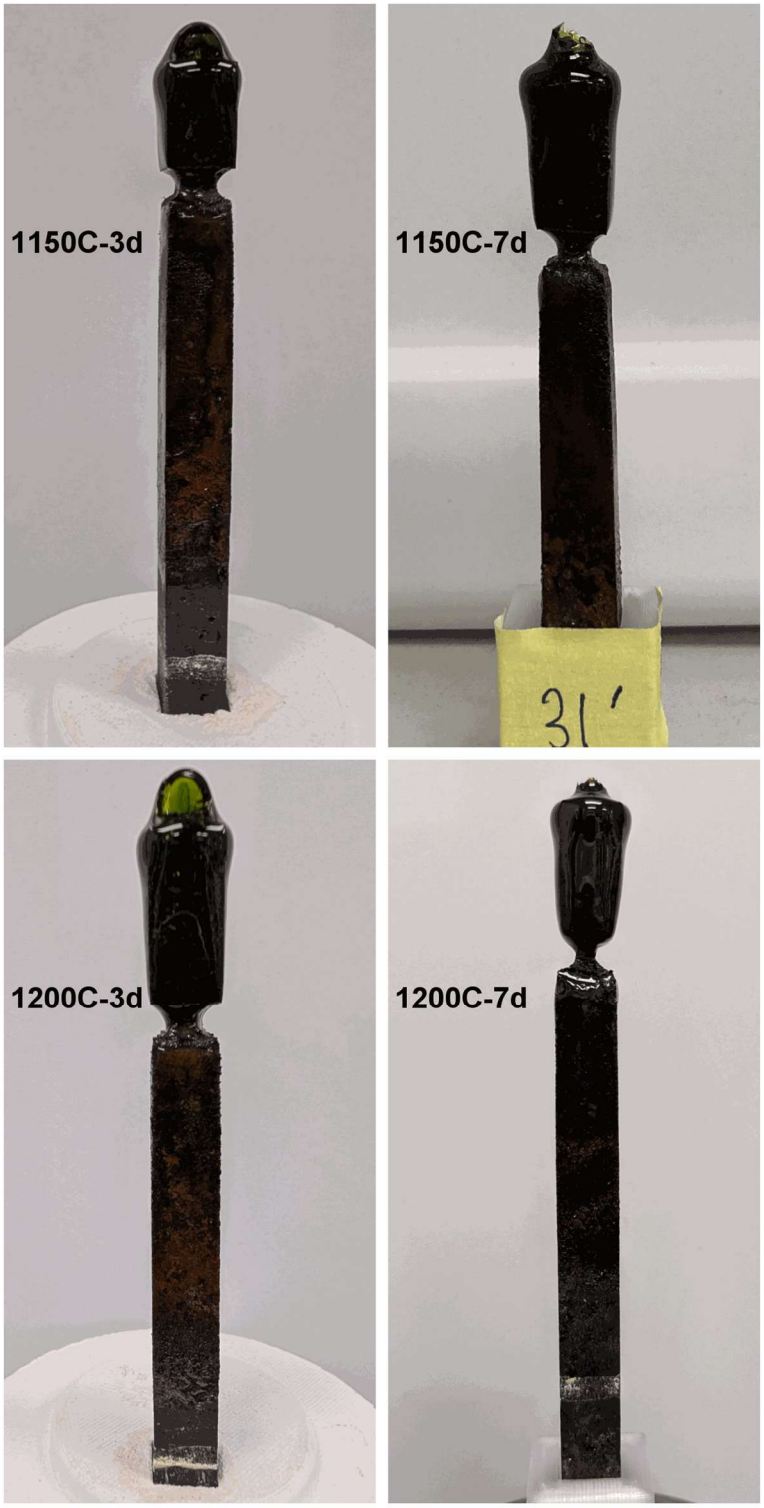


Figure K.2. K-3 coupons after refractory corrosion test, APPS2-02.

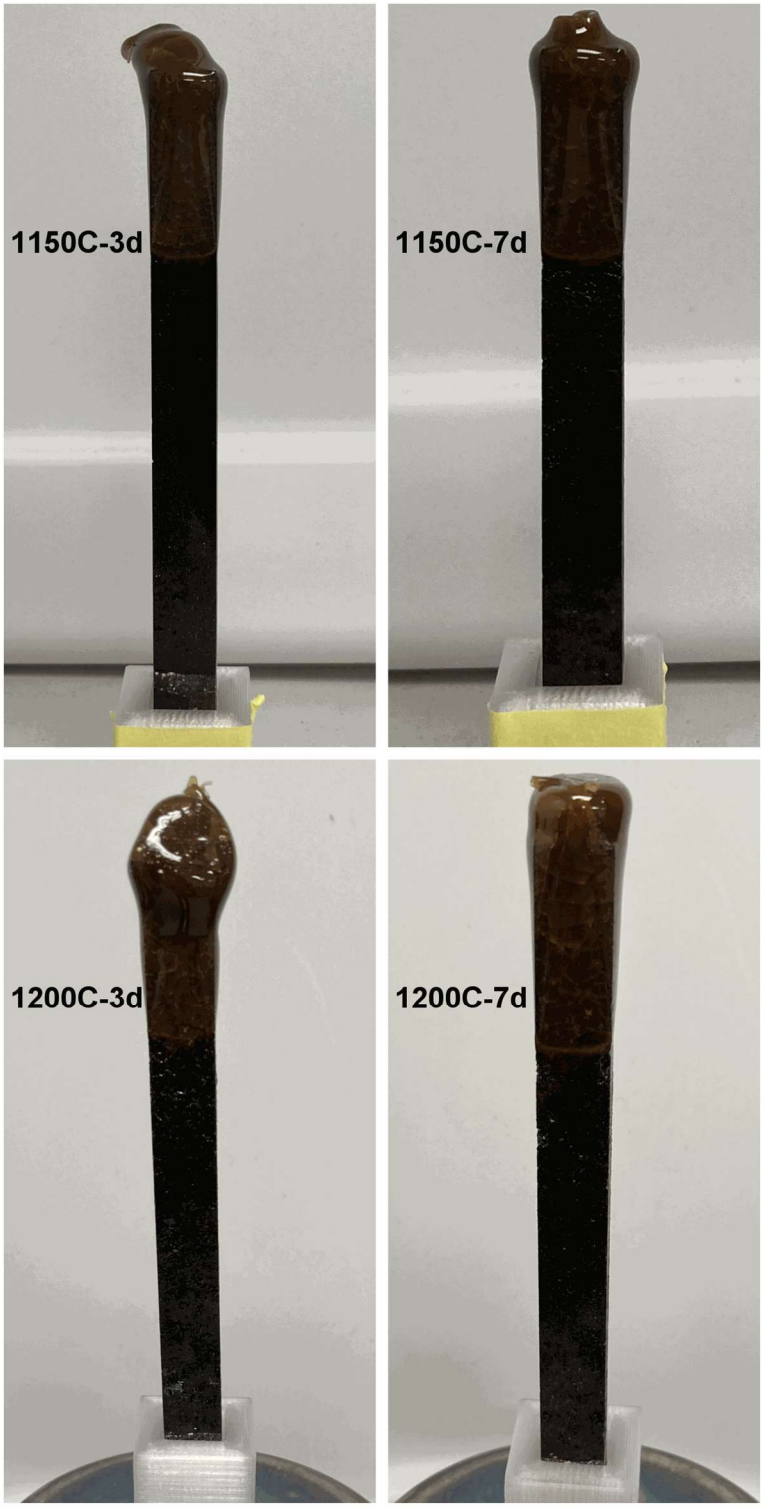


Figure K.3. K-3 coupons after refractory corrosion test, APPS2-03.

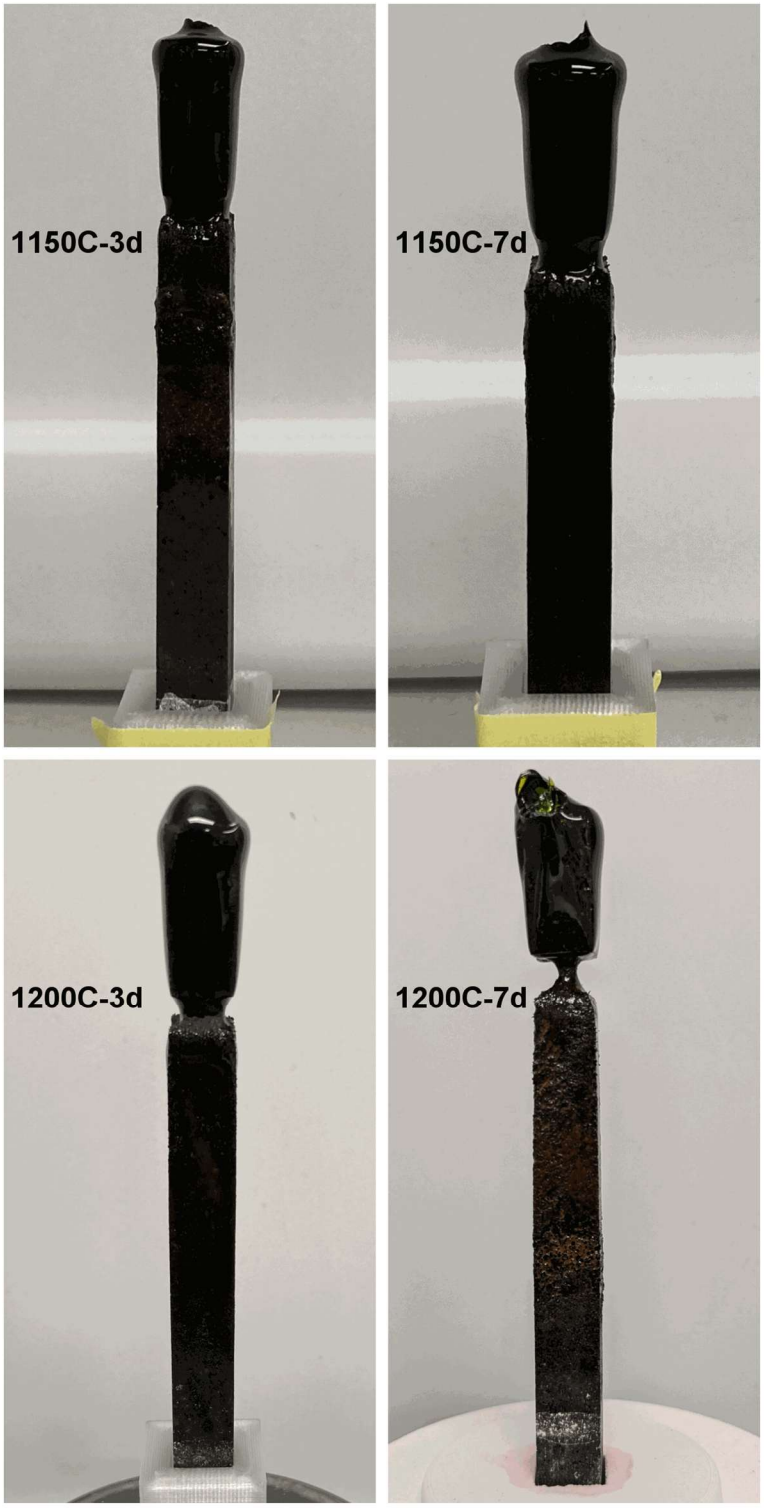


Figure K.4. K-3 coupons after refractory corrosion test, APPS2-04.

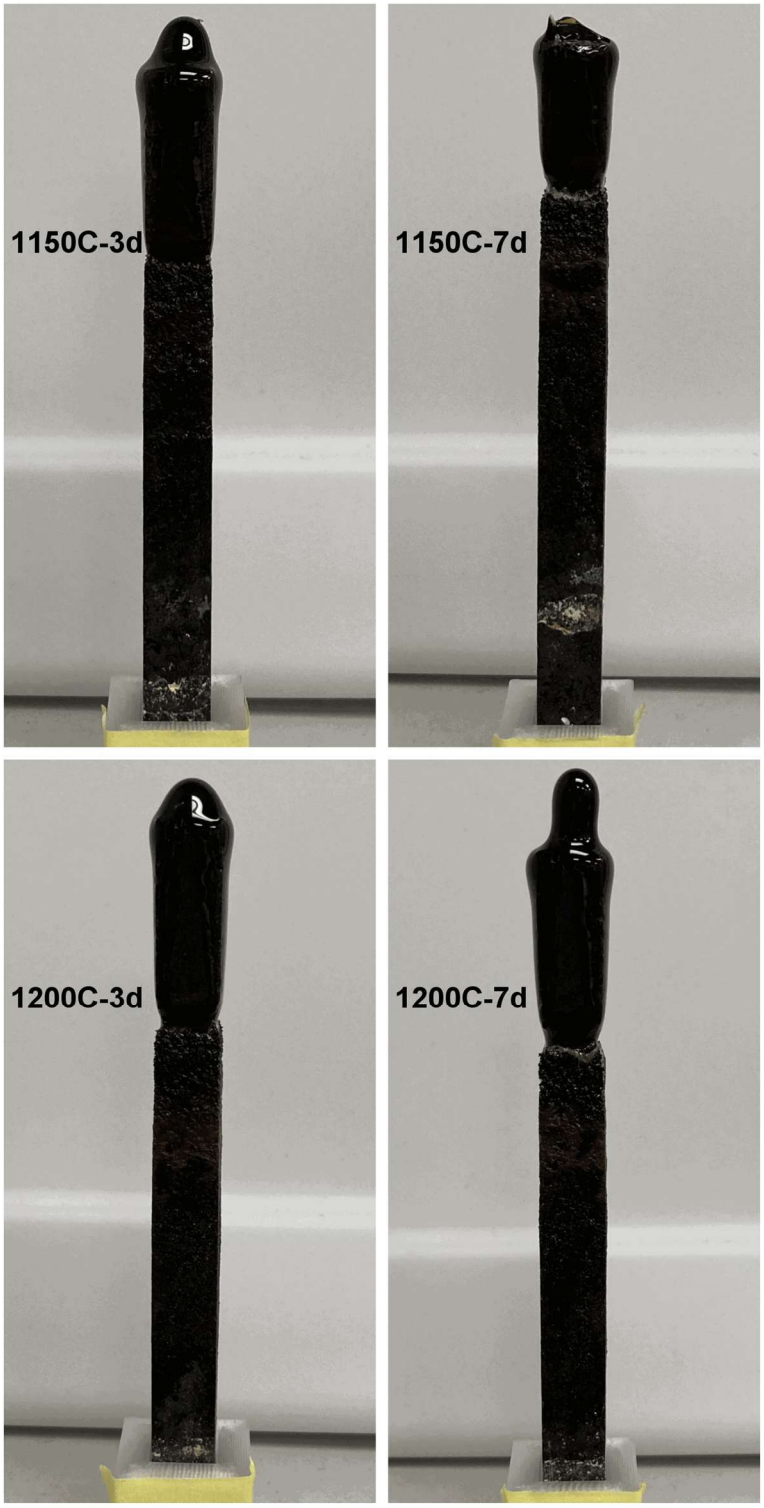


Figure K.5. K-3 coupons after refractory corrosion test, APPS2-05-1.

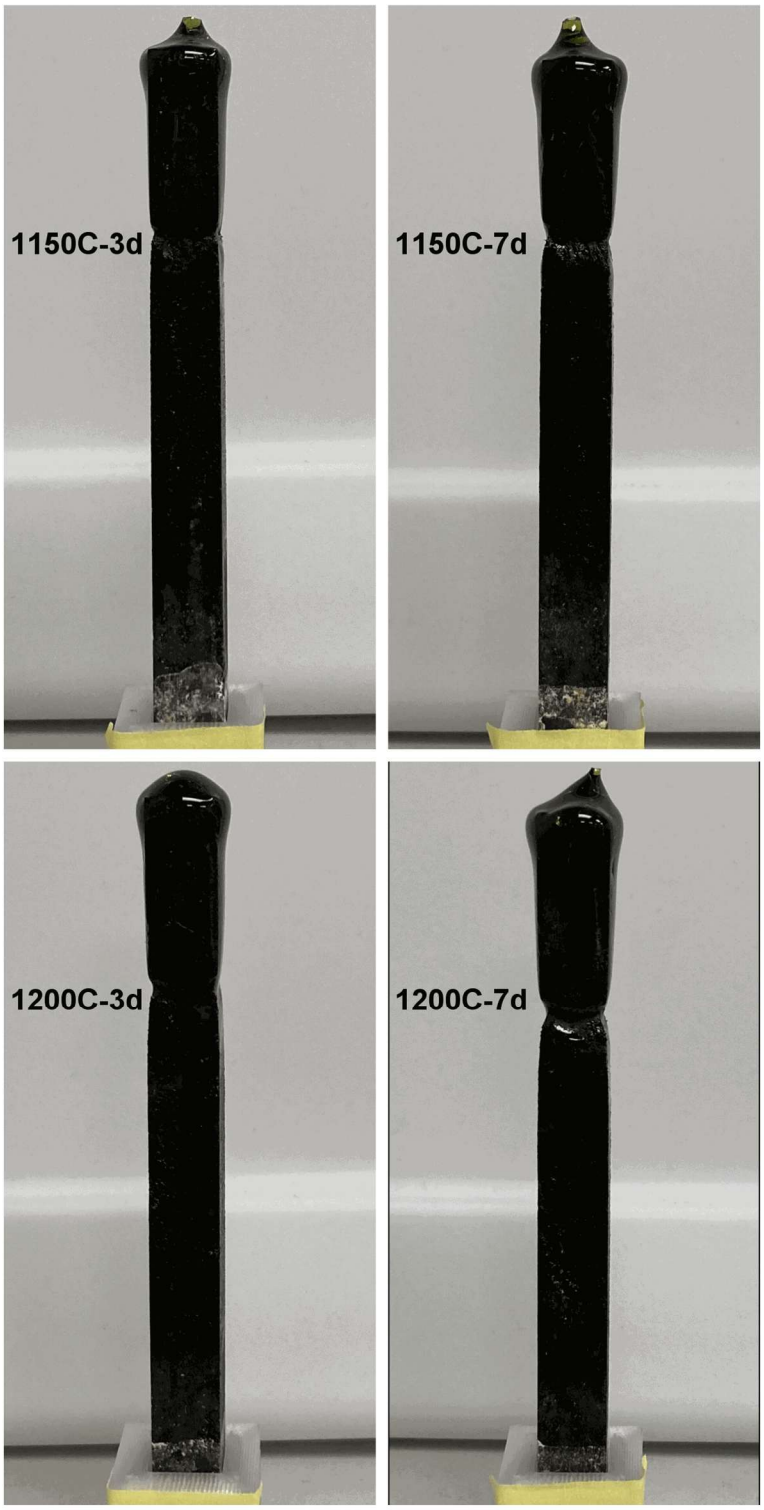


Figure K.6. K-3 coupons after refractory corrosion test, APPS2-06-1.

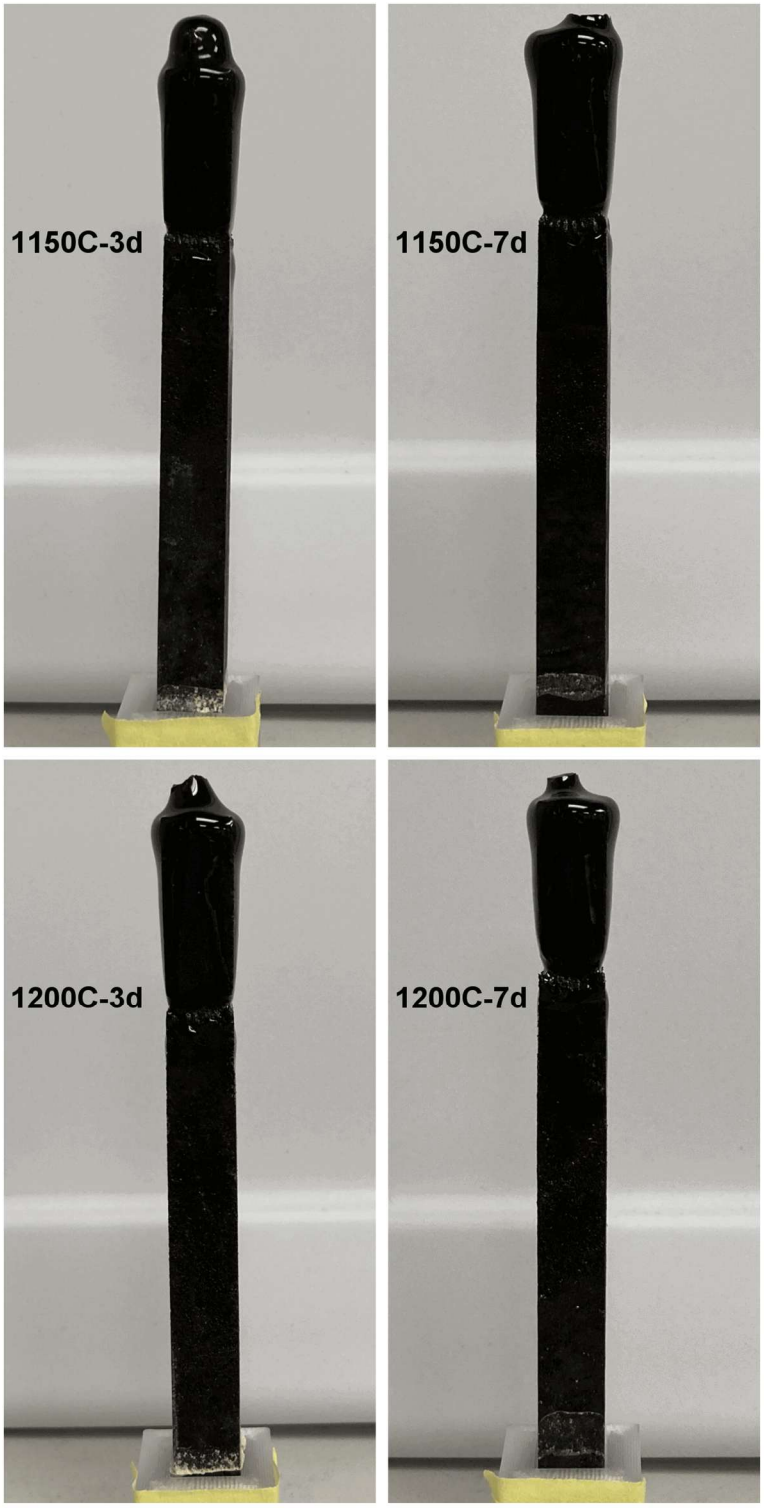


Figure K.7. K-3 coupons after refractory corrosion test, APPS2-07.

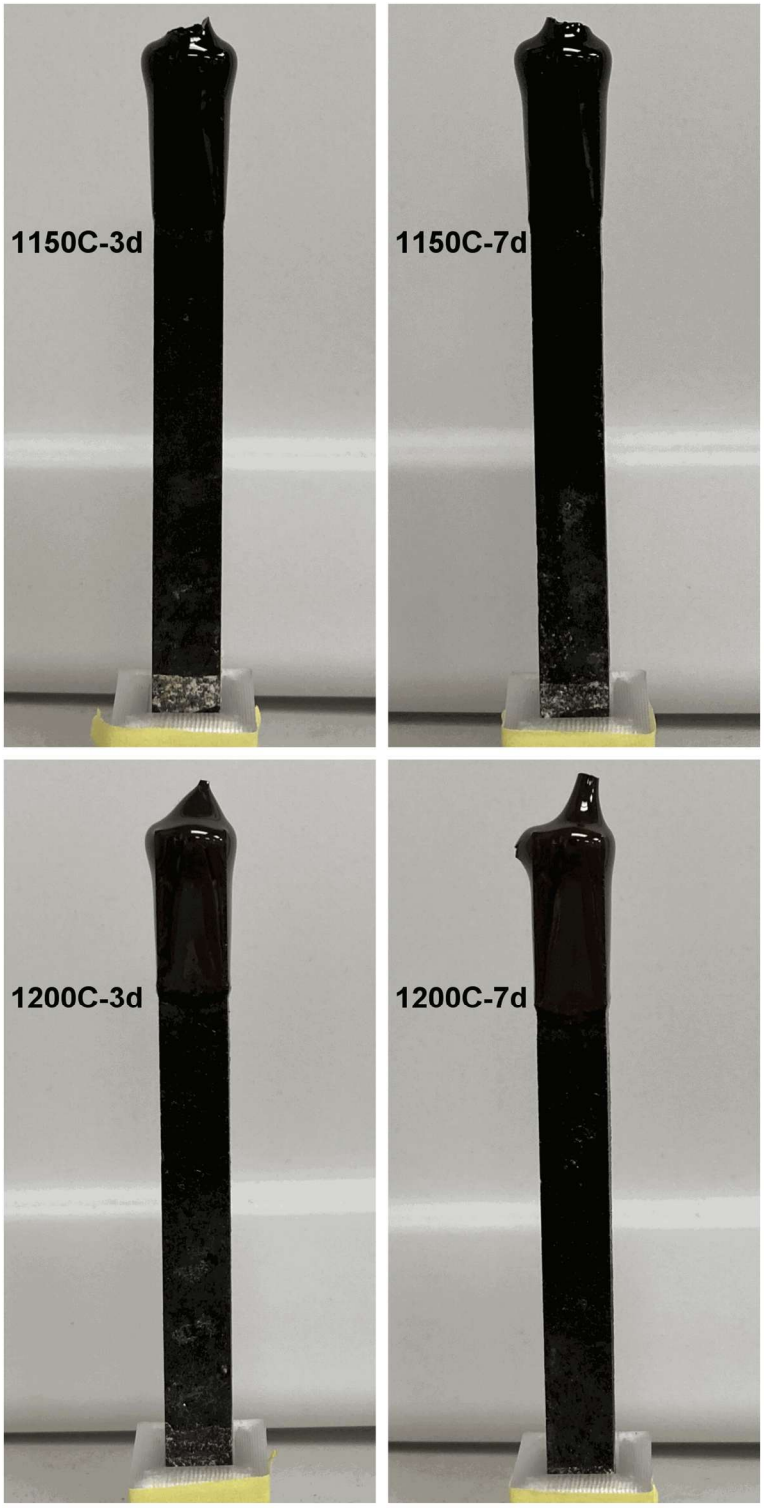


Figure K.8. K-3 coupons after refractory corrosion test, APPS2-08.

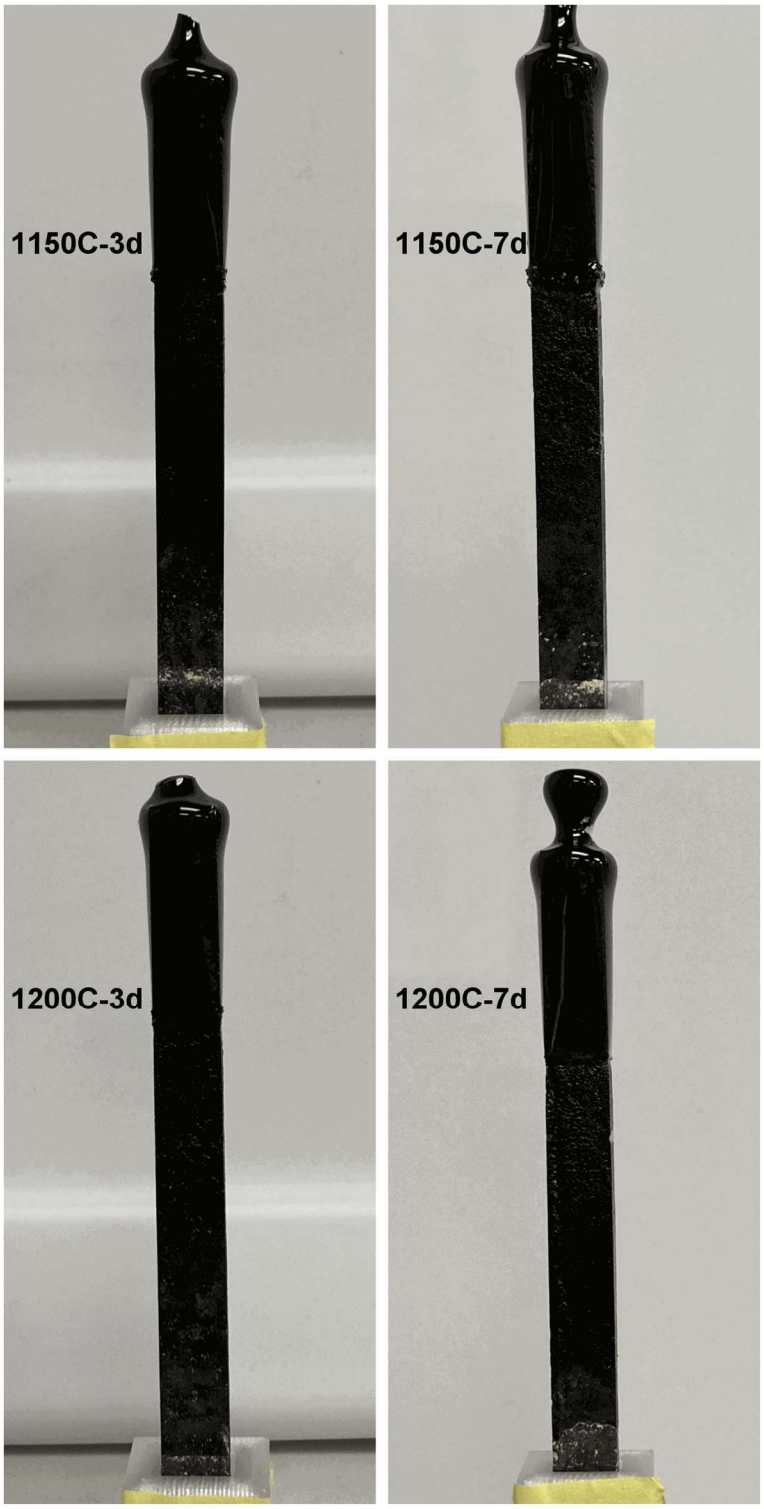


Figure K.9. K-3 coupons after refractory corrosion test, APPS2-09.

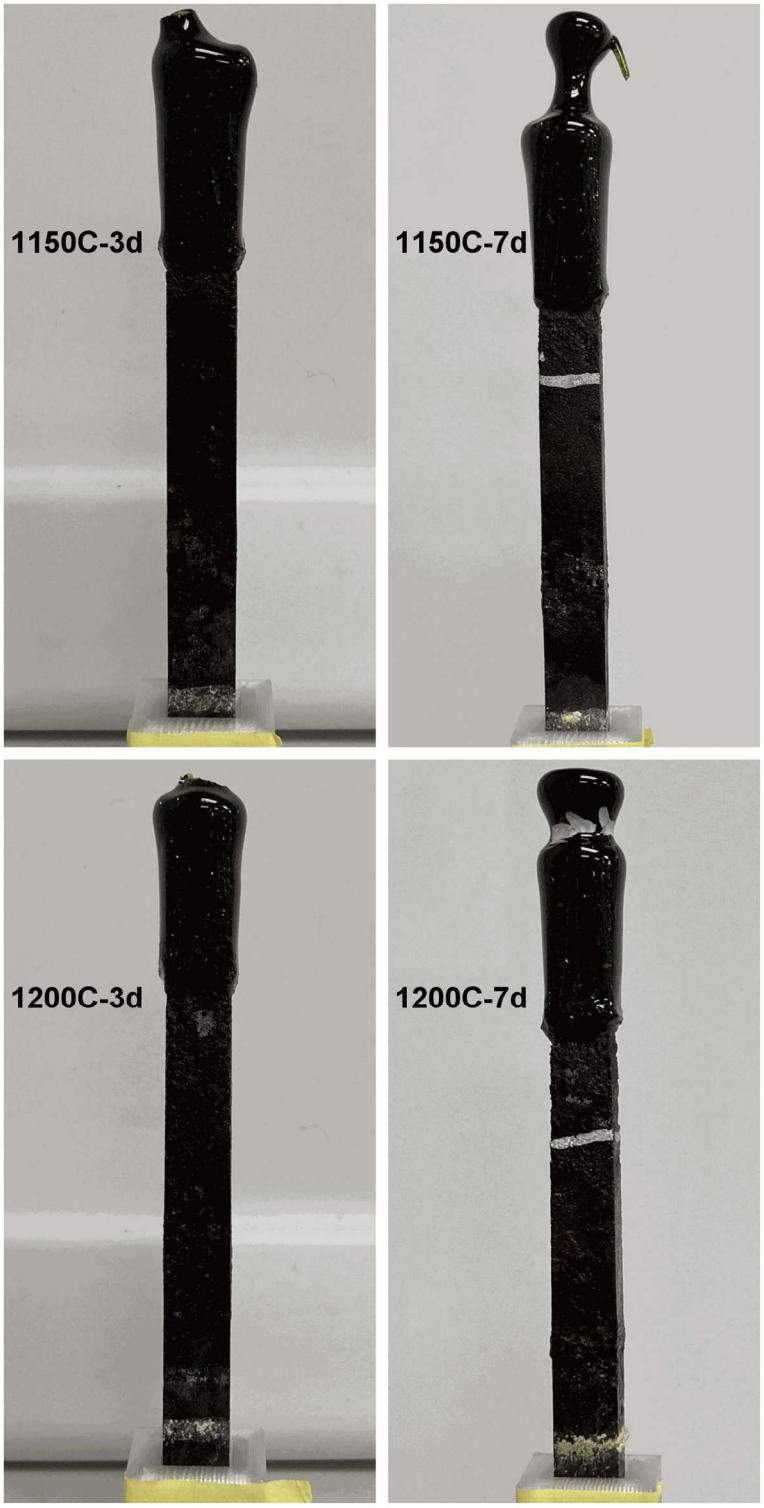


Figure K.10. K-3 coupons after refractory corrosion test, APPS2-10.

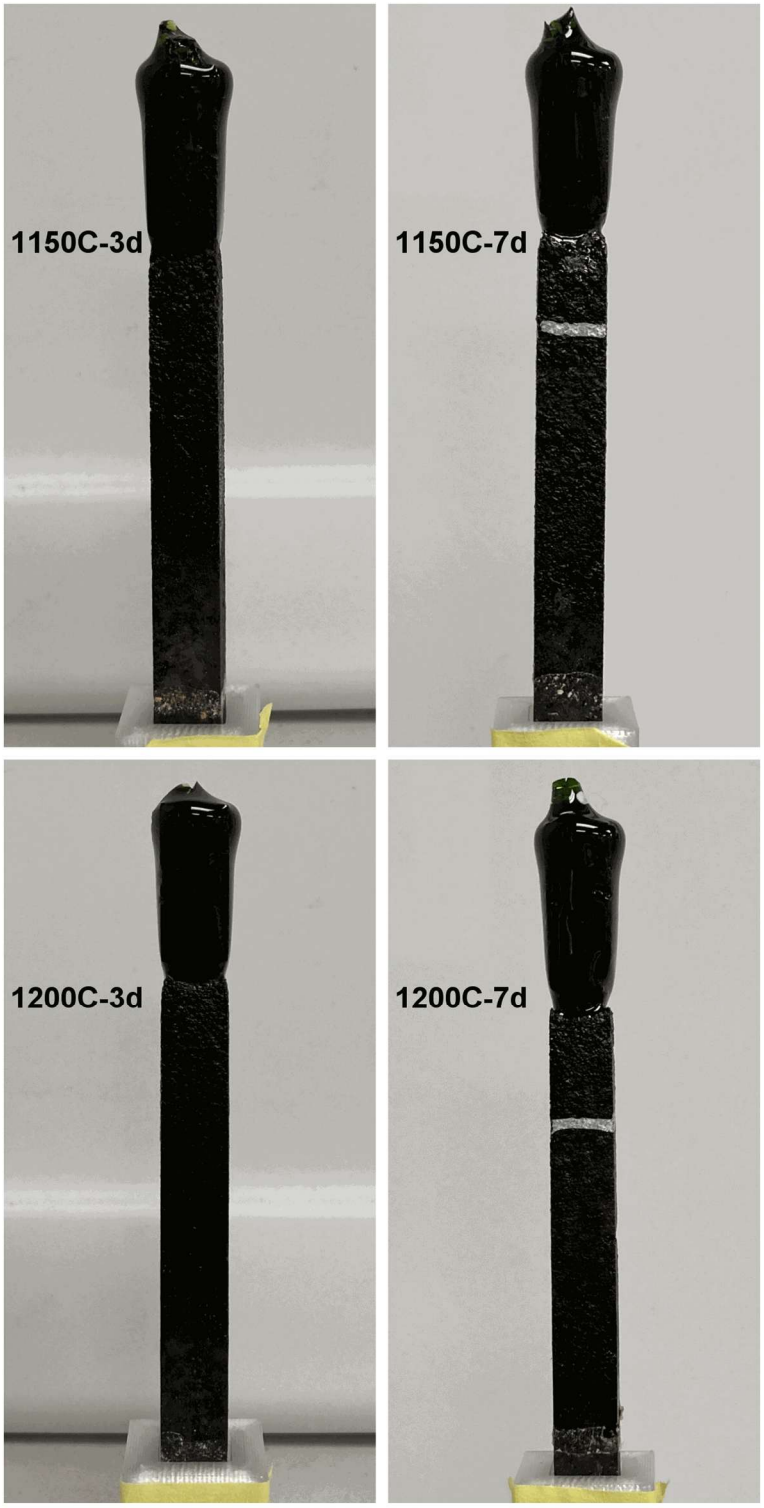


Figure K.11. K-3 coupons after refractory corrosion test, APPS2-11.

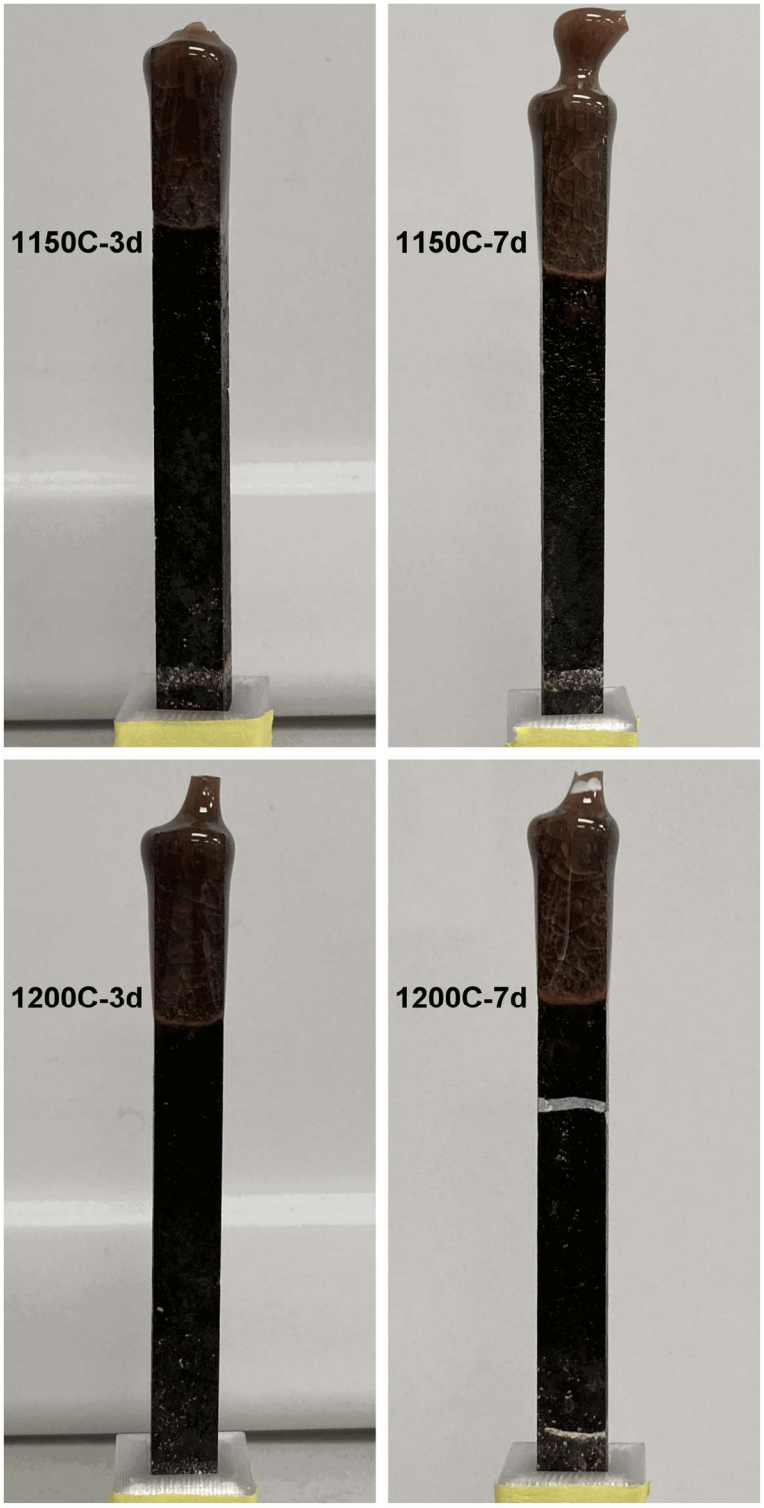


Figure K.12. K-3 coupons after refractory corrosion test, APPS2-12.

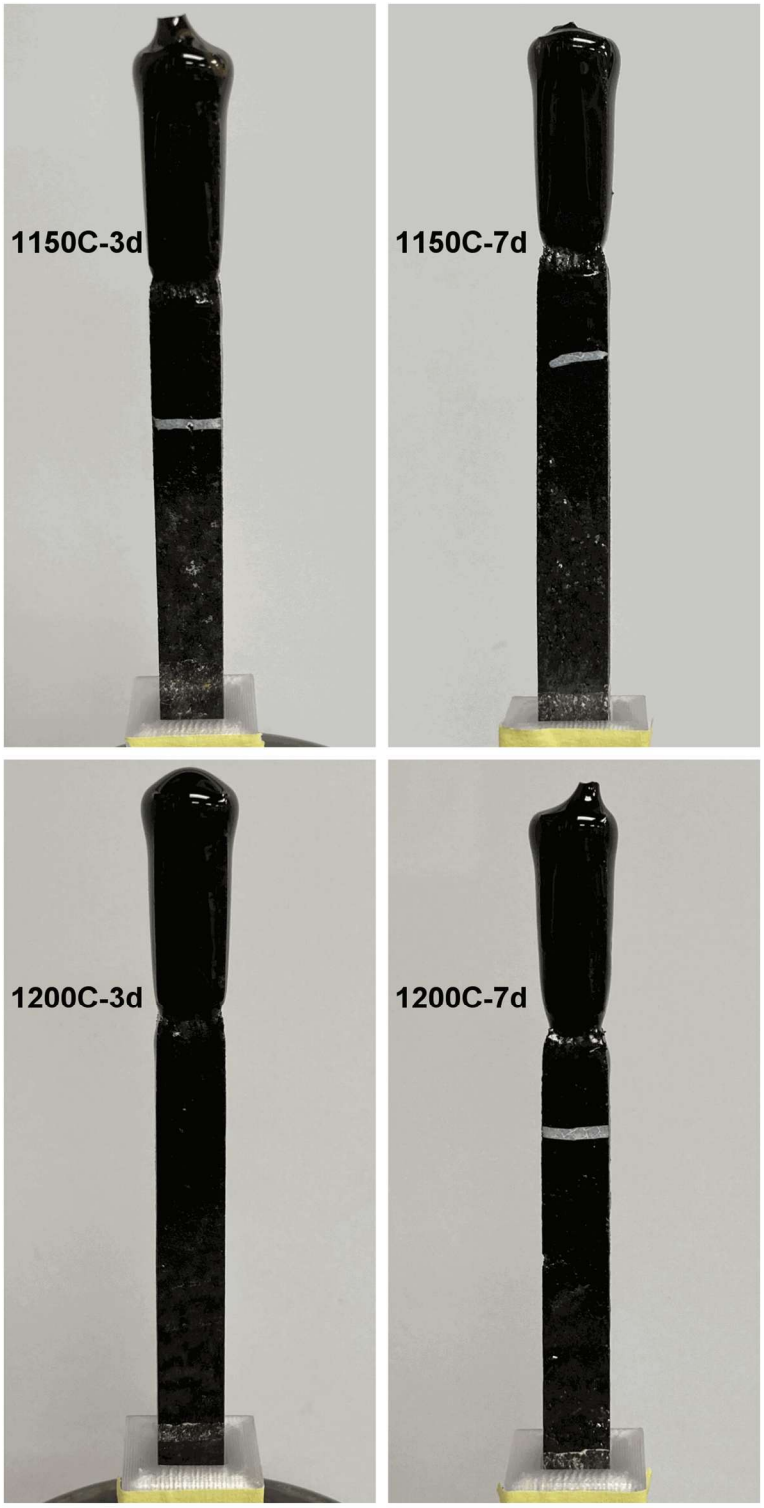


Figure K.13. K-3 coupons after refractory corrosion test, APPS2-13.

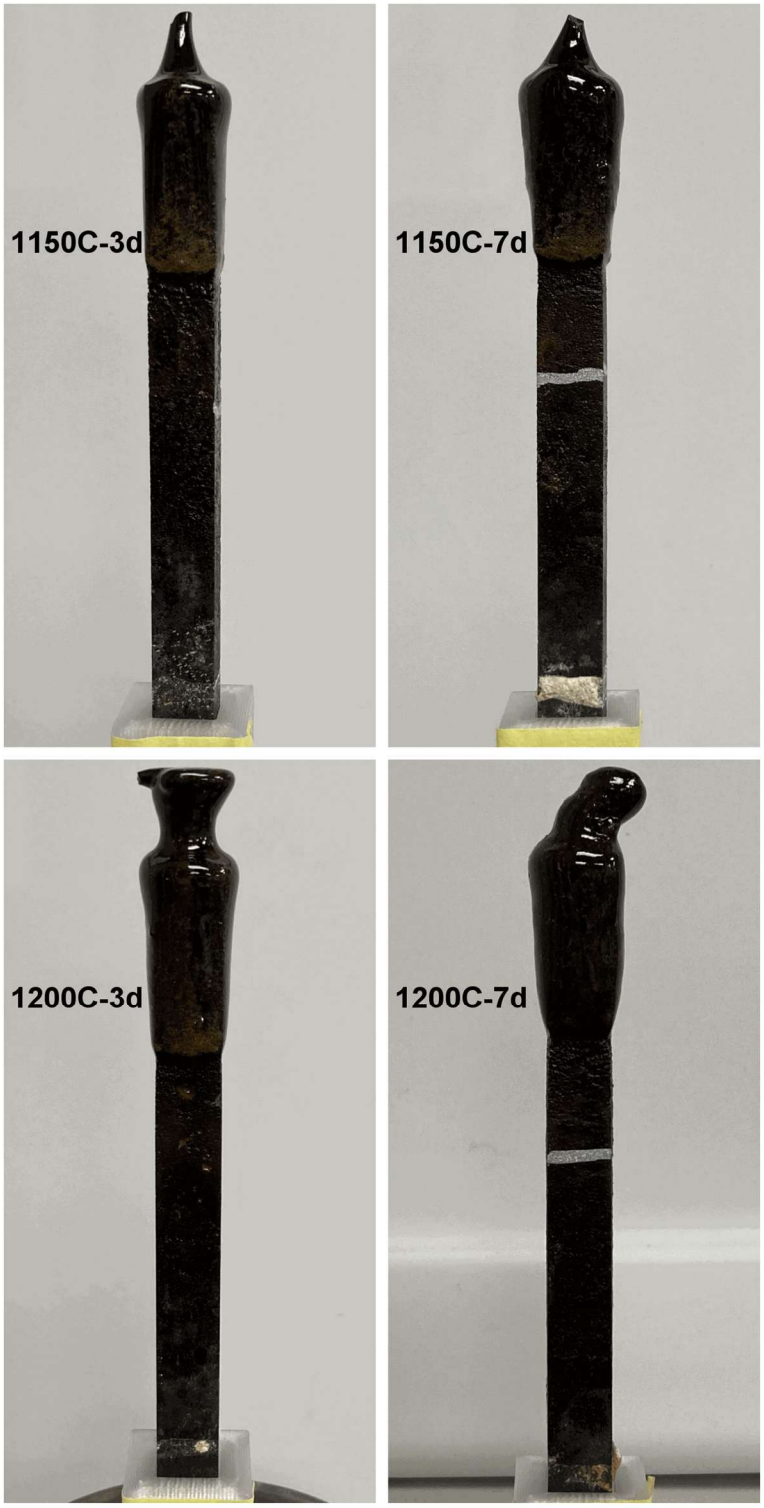


Figure K.14. K-3 coupons after refractory corrosion test, APPS2-14.

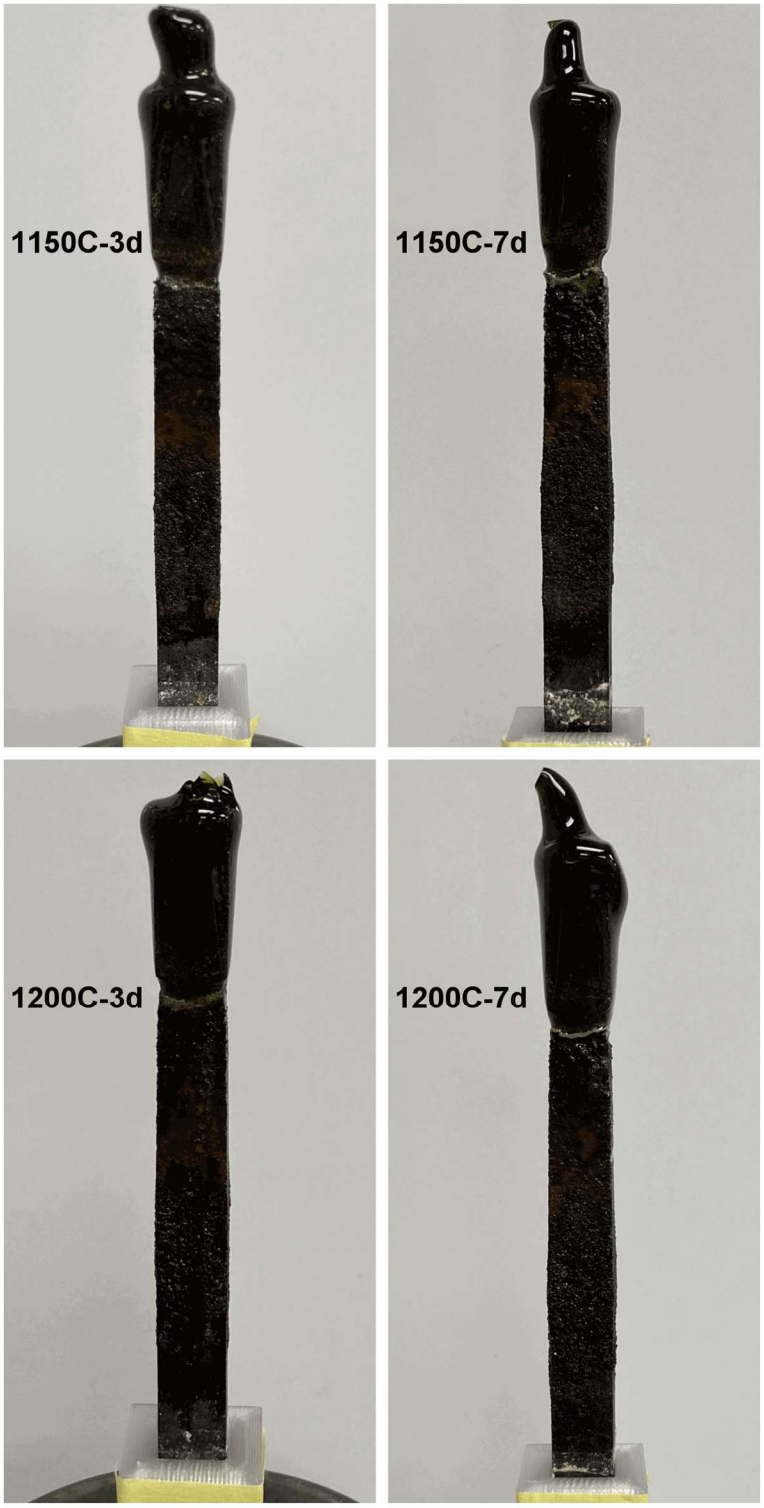


Figure K.15. K-3 coupons after refractory corrosion test, APPS2-15.

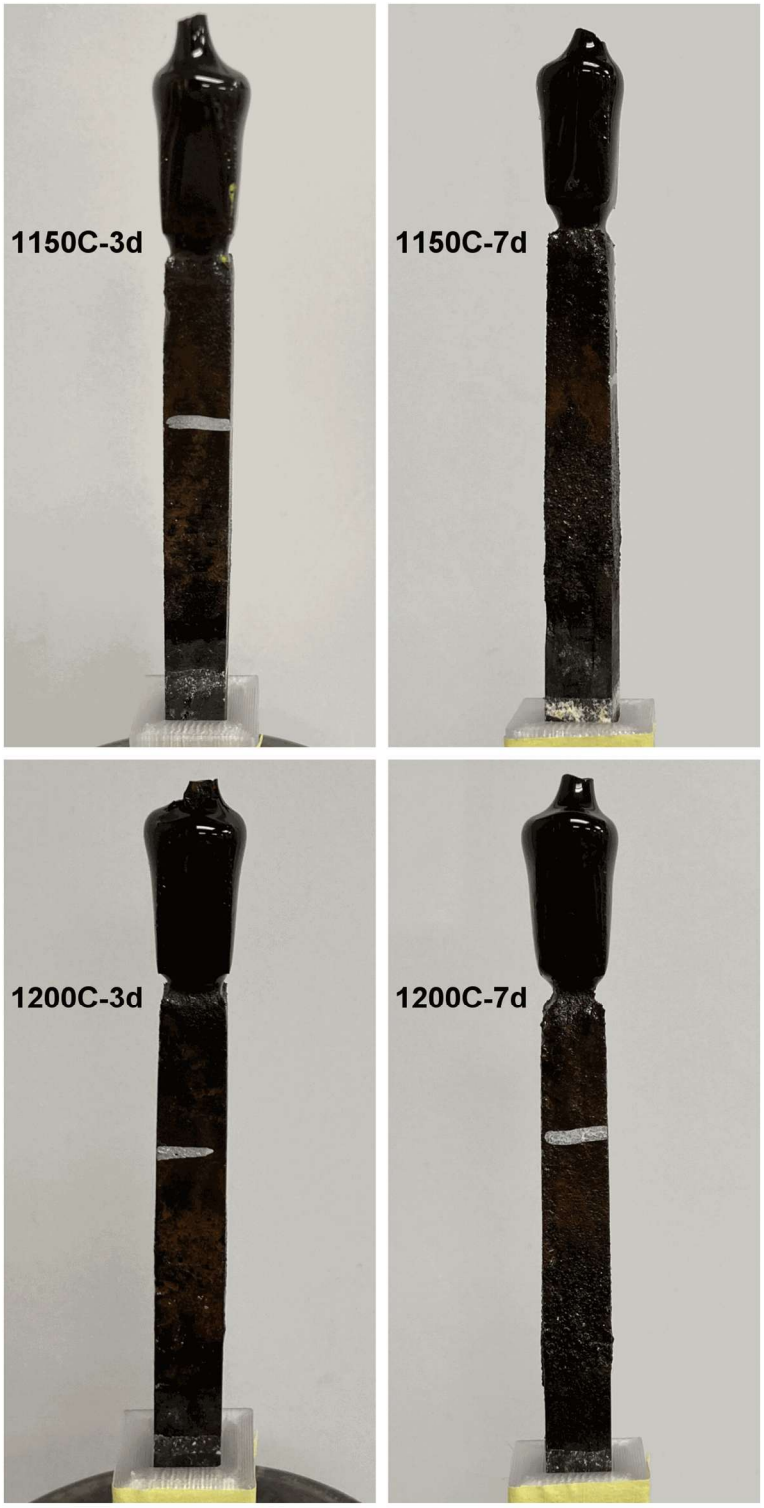


Figure K.16. K-3 coupons after refractory corrosion test, APPS2-16.

# Appendix L – Micro-CT Results of K-3 Refractory Corrosion Test

This appendix presents the X-ray images used for the dimension measurements of the K-3 refractory coupons tested for corrosion with the APPS2 glasses. Each figure shows the results of one test coupon, including cross-section view images, top-view images with outlines and bounding rectangles, and a plot of corrosion depth measured based on the bounding rectangles. For each figure, (a) shows the cross-section view of the post-test coupon at the center from both the A-A and B-B directions with the neck marked by red arrows. A plot of corrosion depth along the coupon is also shown. The neck is expected in the region of 20 to 35 mm from the bottom of the coupon, which is highlighted in the neck plot. In each figure, (b) shows the top-view slices at the neck location with the pre-test image outlined in cyan and post-test image outlined in red. For the same coupon, neck corrosion depth and neck locations measured from the A-A and B-B directions are not exactly the same because, since the K-3 is not homogeneous, the pores and uneven distribution of the different phases can affect the corrosion damage on different faces.

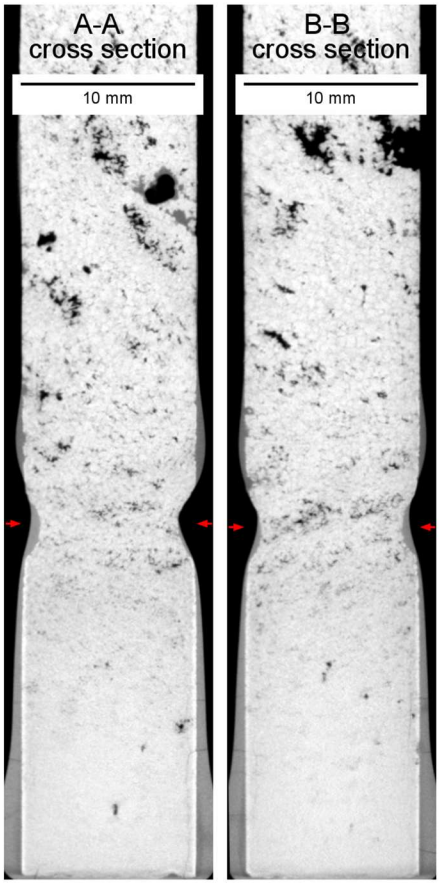


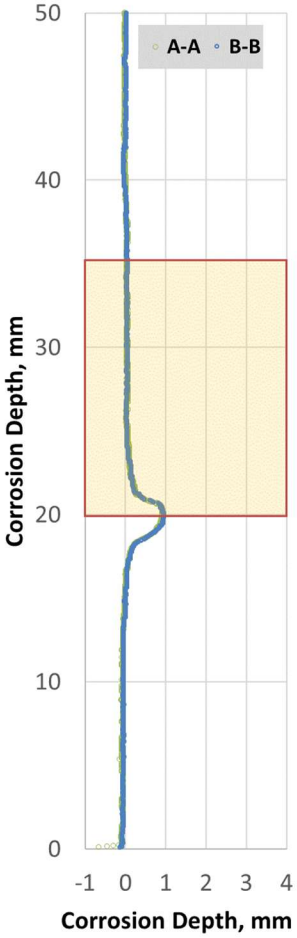


(a)

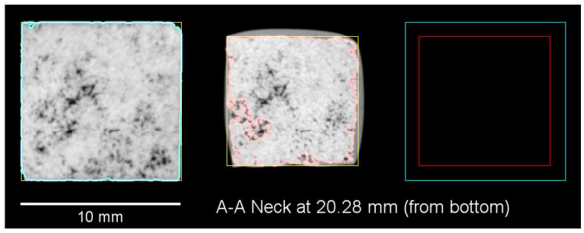


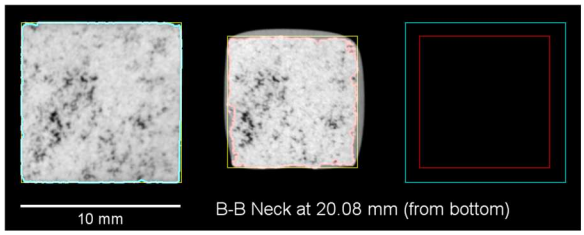


(b)

| Neck Depth, mm | |
|---|---|
| A-A | 0.94 |
| B-B | 0.96 |
| Average | 0.95 |
| Standard deviation | 0.014 |
| | |

Figure L.1. Micro-CT results of K-3 refractory corrosion test, APP2-01 1150 °C-3d.

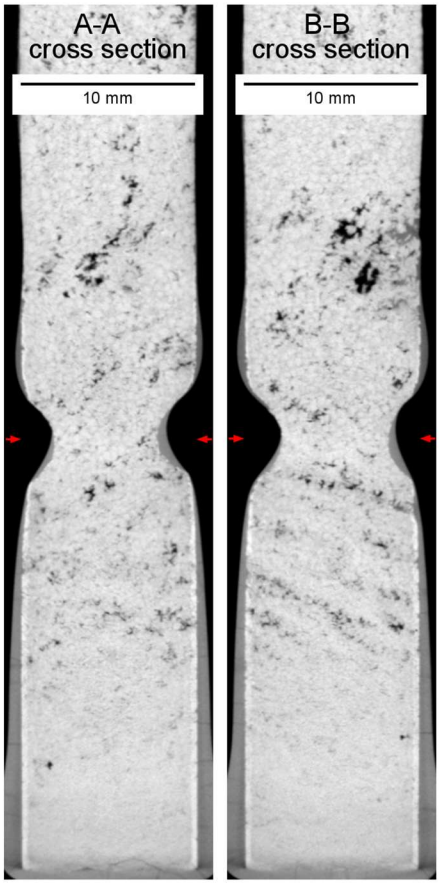


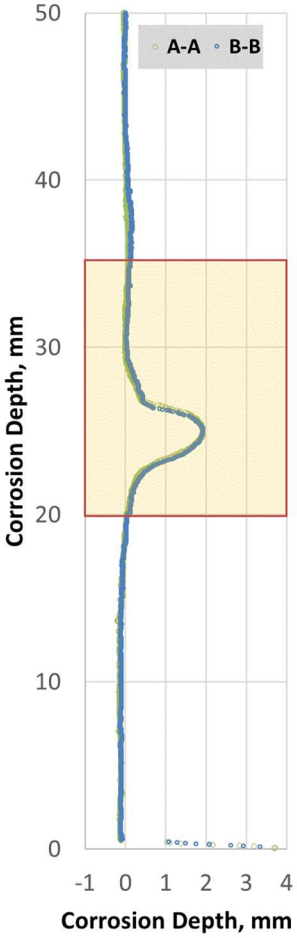


(a)

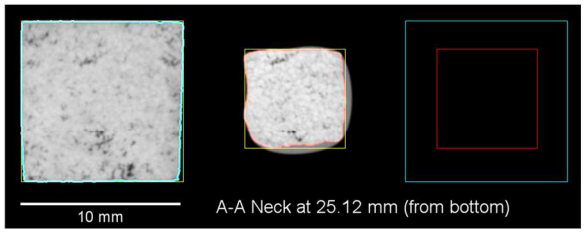


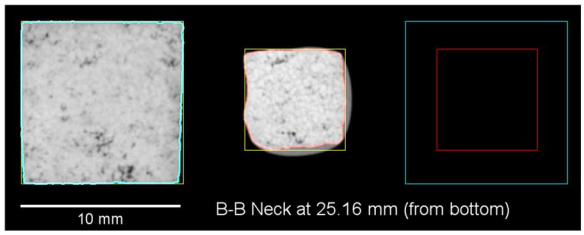


(b)

| Neck Depth, mm | |
|---|---|
| A-A | 1.92 |
| B-B | 1.92 |
| Average | 1.92 |
| Standard deviation | 0.000 |
| | |

Figure L.2. Micro-CT results of K-3 refractory corrosion test, APP2-01 1150 °C-7d.

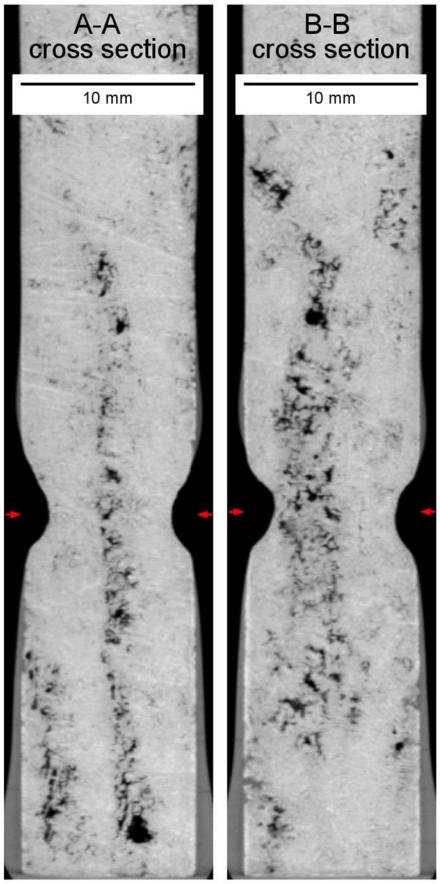


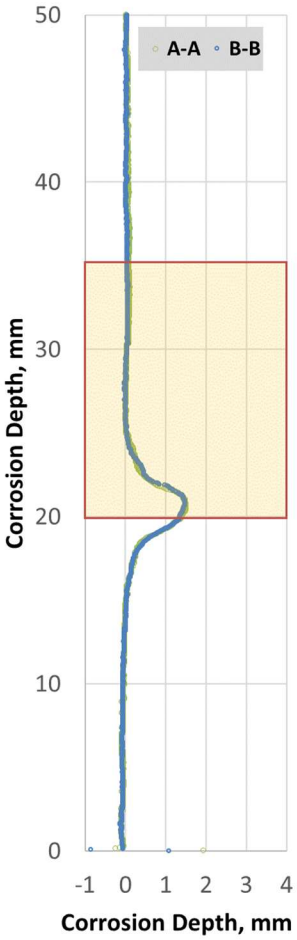


(a)

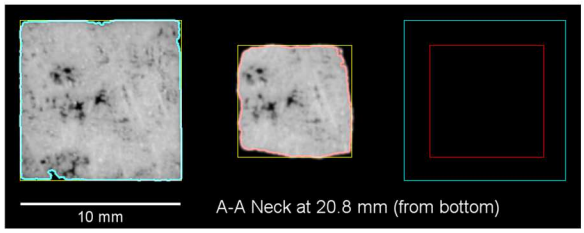


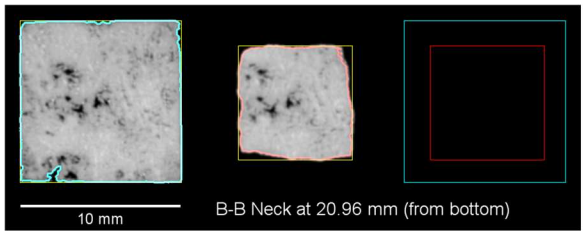


(b)

| Neck Depth, mm | |
|---|---|
| A-A | 1.50 |
| B-B | 1.48 |
| Average | 1.49 |
| Standard deviation | 0.014 |
| | |

Figure L.3. Micro-CT results of K-3 refractory corrosion test, APP2-01 1200 °C-3d.

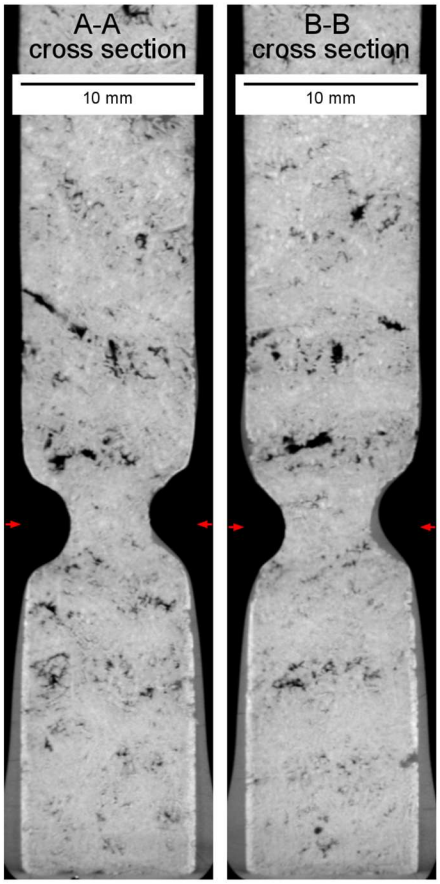


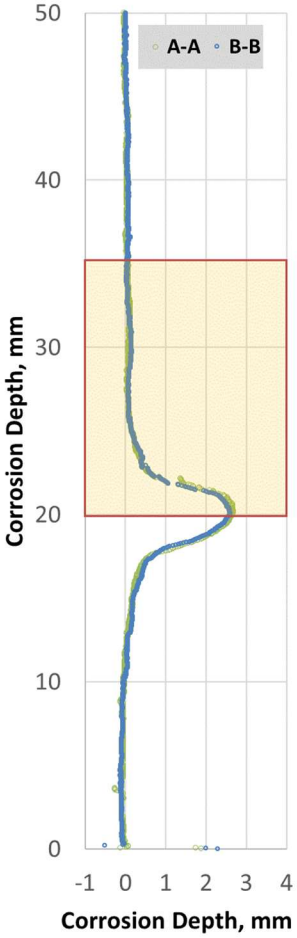


(a)

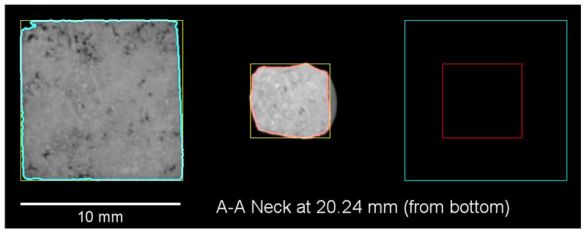


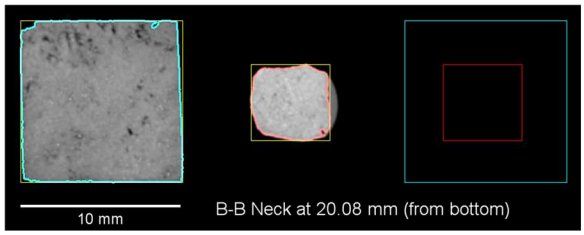


(b)

| Neck Depth, mm | |
|---|---|
| A-A | 2.68 |
| B-B | 2.60 |
| Average | 2.64 |
| Standard deviation | 0.057 |
| | |

Figure L.4. Micro-CT results of K-3 refractory corrosion test, APP2-01 1200 °C-7d.

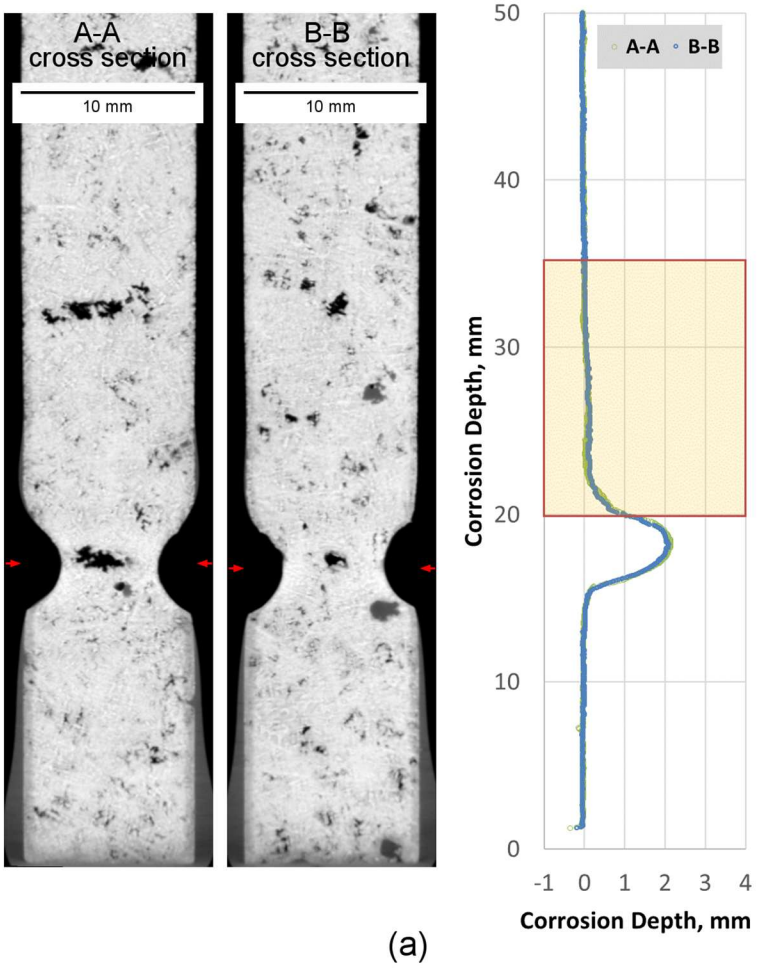


(a)

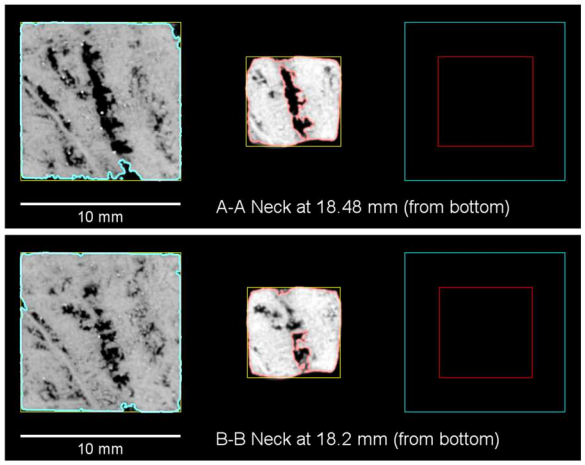


(b)

| Neck Depth, mm | |
|---|---|
| A-A | 2.14 |
| B-B | 2.10 |
| Average | 2.12 |
| Standard deviation | 0.028 |
| Note: Neck is at a lower position (< 20 mm from bottom). This is because a deeper crucible was used for this repeated test. | |

Figure L.5. Micro-CT results of K-3 refractory corrosion test, APP2-02 1150 °C-3d_01.

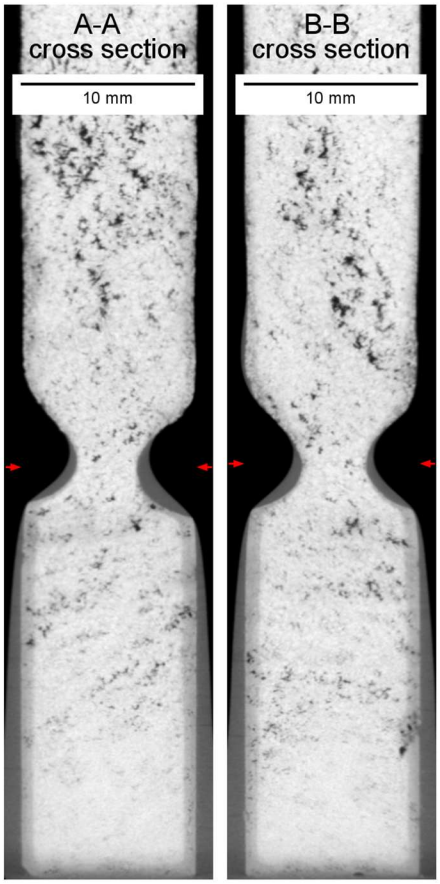



(a)

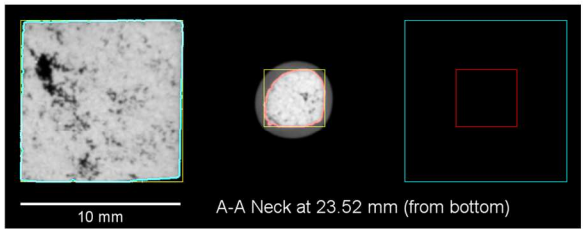


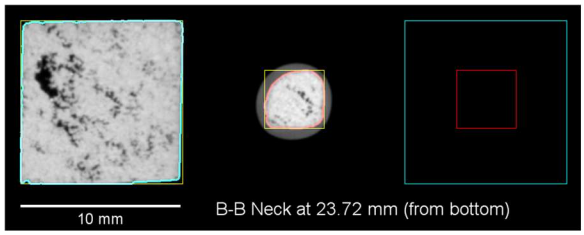


(b)

| Neck Depth, mm | |
|---|---|
| A-A | 3.28 |
| B-B | 3.20 |
| Average | 3.24 |
| Standard deviation | 0.057 |
| | |

Figure L.6. Micro-CT results of K-3 refractory corrosion test, APP2-02 1150 °C-7d.

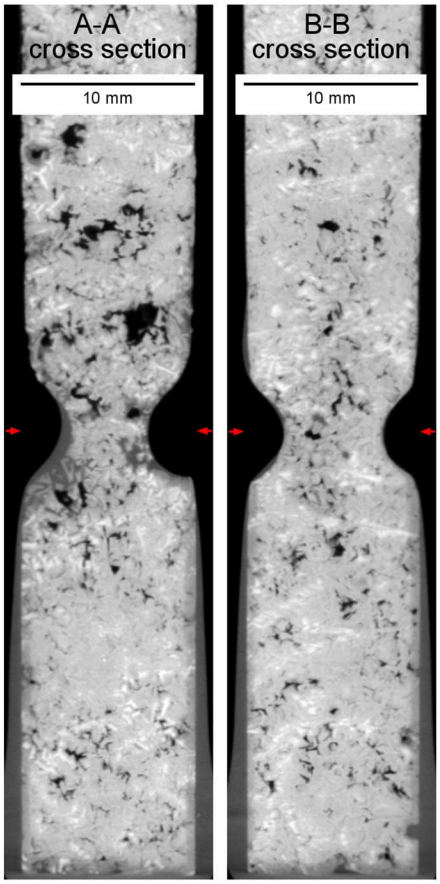


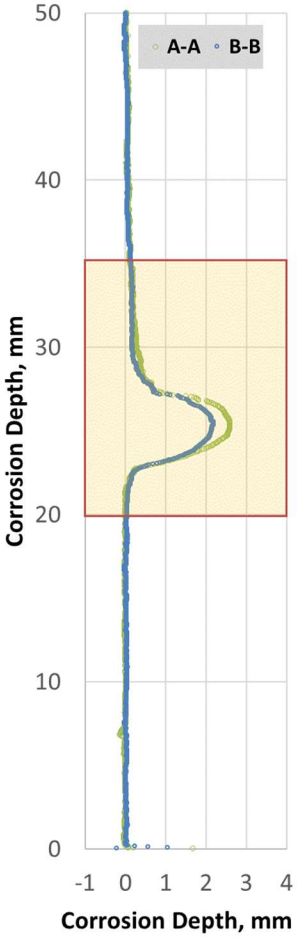


(a)

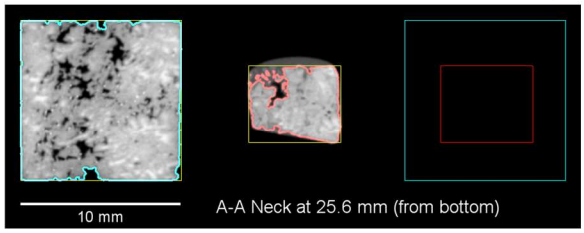


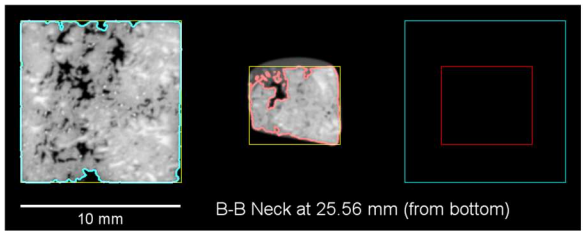


(b)

| Neck Depth, mm | |
|---|---|
| A-A | 2.60 |
| B-B | 2.18 |
| Average | 2.39 |
| Standard deviation | 0.297 |
| | |

Figure L.7. Micro-CT results of K-3 refractory corrosion test, APP2-02 1200 °C-3d.

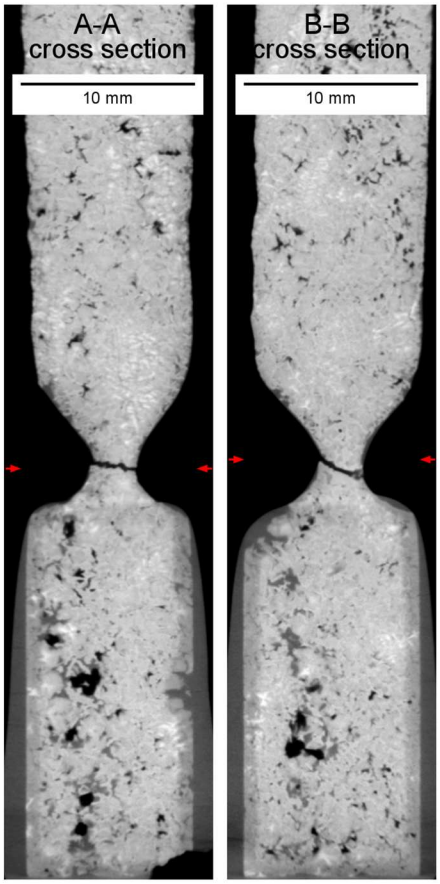


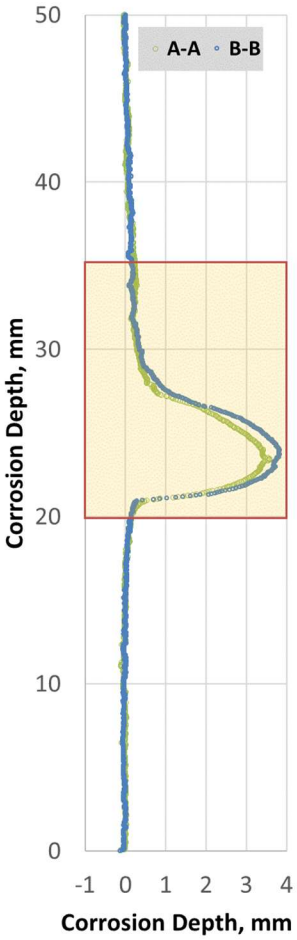


(a)

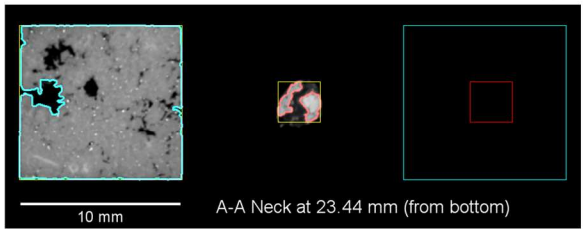


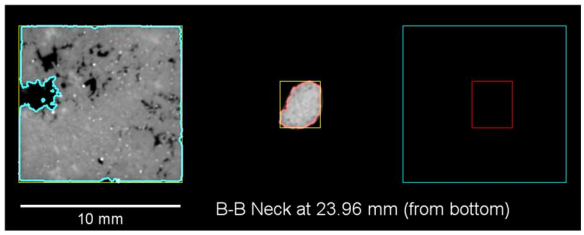


(b)

| Neck Depth, mm | |
|---|---|
| A-A | 3.58 |
| B-B | 3.84 |
| Average | 3.71 |
| Standard deviation | 0.184 |
| Note: Coupon broke before micro-CT scan. Neck measurement is OK. | |

Figure L.8. Micro-CT results of K-3 refractory corrosion test, APP2-02 1200 °C-7d.

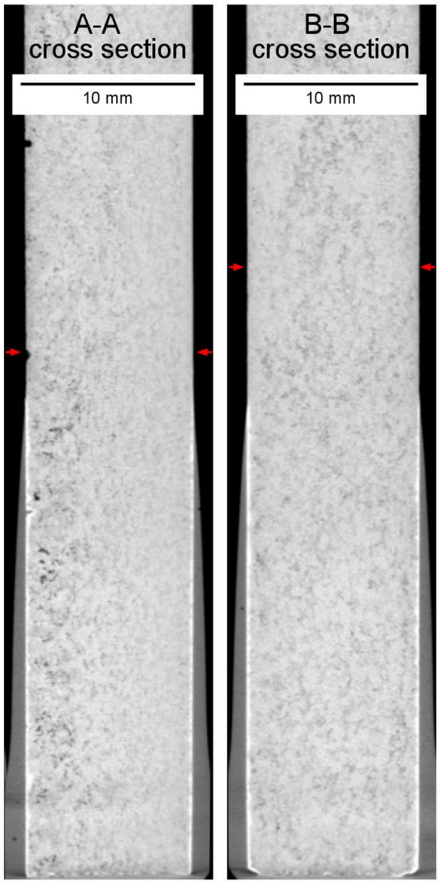


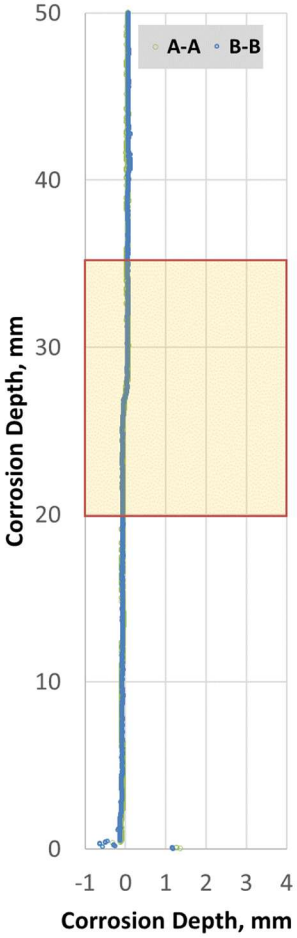


(a)

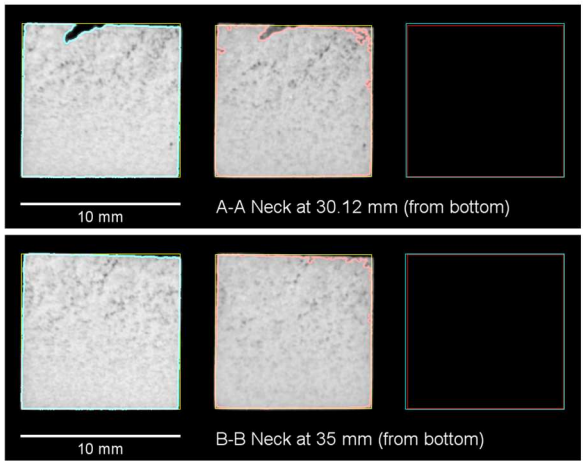


(b)

| Neck Depth, mm | |
|---|---|
| A-A | 0.08 |
| B-B | 0.08 |
| Average | 0.08 |
| Standard deviation | 0.000 |
| | |

Figure L.9. Micro-CT results of K-3 refractory corrosion test, APP2-03 1150 °C-3d.

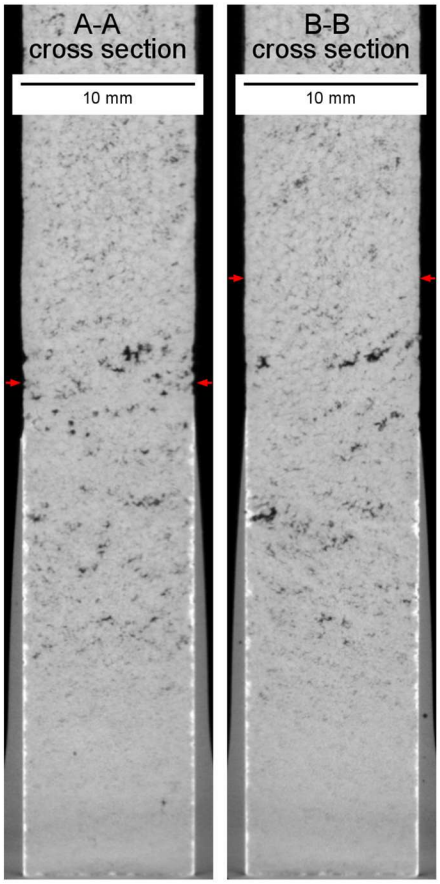


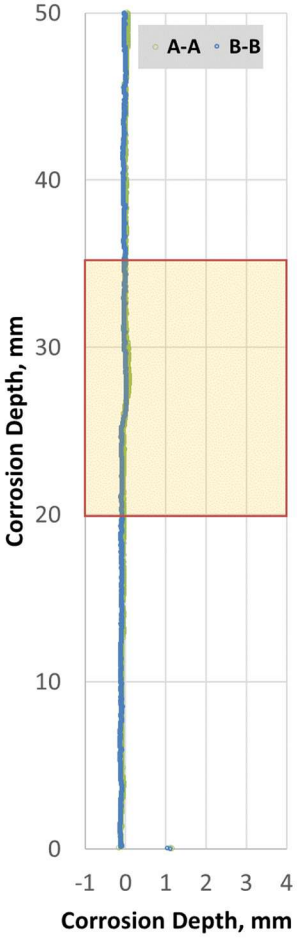


(a)

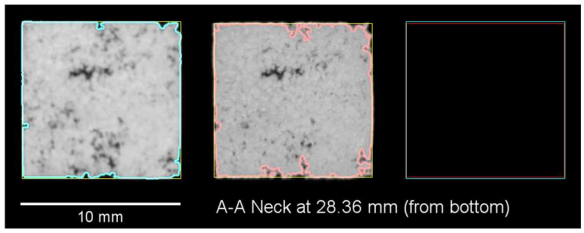


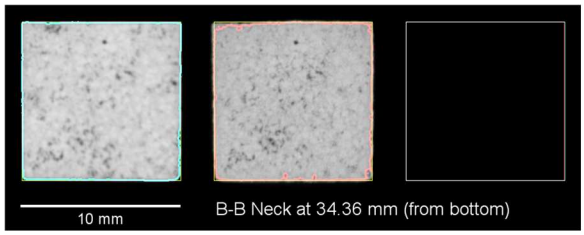


(b)

| Neck Depth, mm | |
|---|---|
| A-A | 0.10 |
| B-B | 0.02 |
| Average | 0.06 |
| Standard deviation | 0.057 |
| | |

Figure L.10. Micro-CT results of K-3 refractory corrosion test, APP2-03 1150 °C-7d.

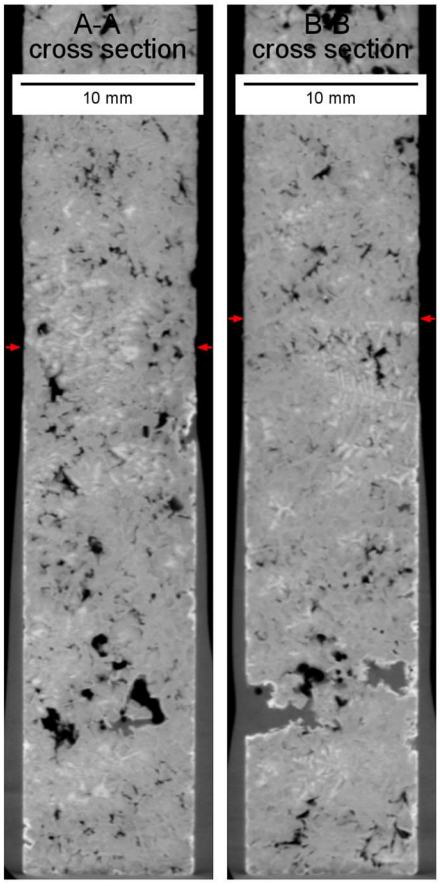


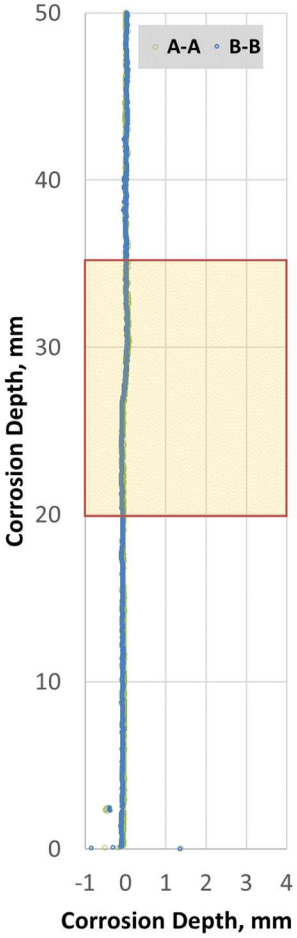


(a)

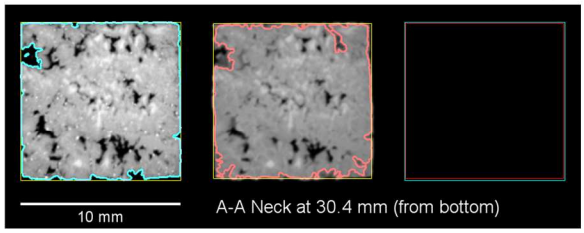


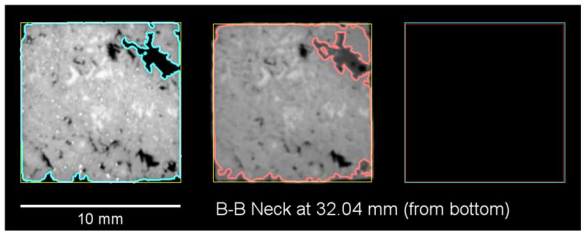


(b)

| Neck Depth, mm | |
|---|---|
| A-A | 0.10 |
| B-B | 0.06 |
| Average | 0.08 |
| Standard deviation | 0.028 |
| | |

Figure L.11. Micro-CT results of K-3 refractory corrosion test, APP2-03 1200 °C-3d.

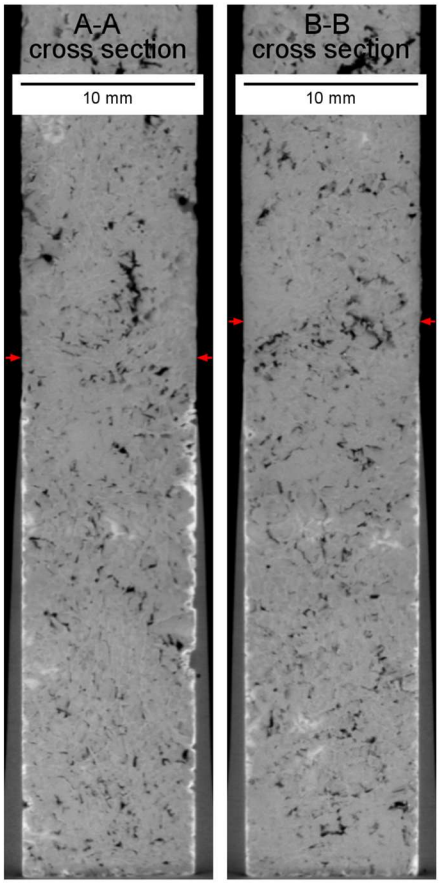


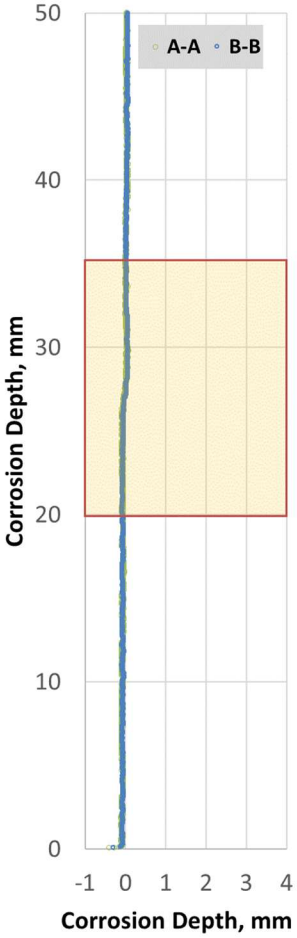


(a)

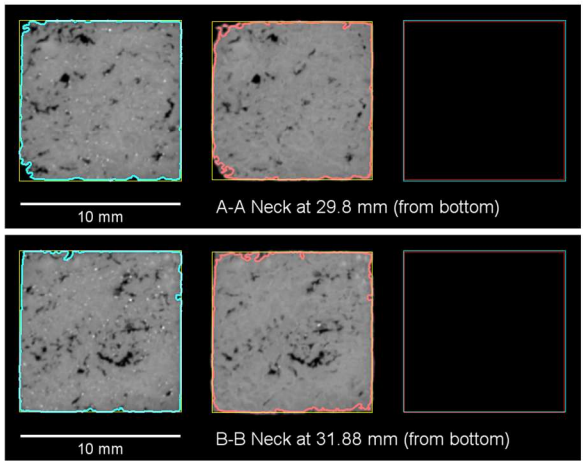


(b)

| Neck Depth, mm | |
|---|---|
| A-A | 0.08 |
| B-B | 0.06 |
| Average | 0.07 |
| Standard deviation | 0.014 |
| | |

Figure L.12. Micro-CT results of K-3 refractory corrosion test, APP2-03 1200 °C-7d.

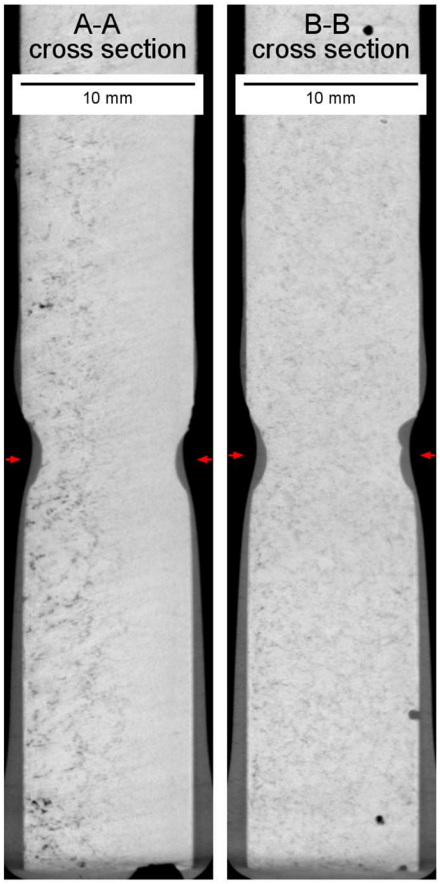


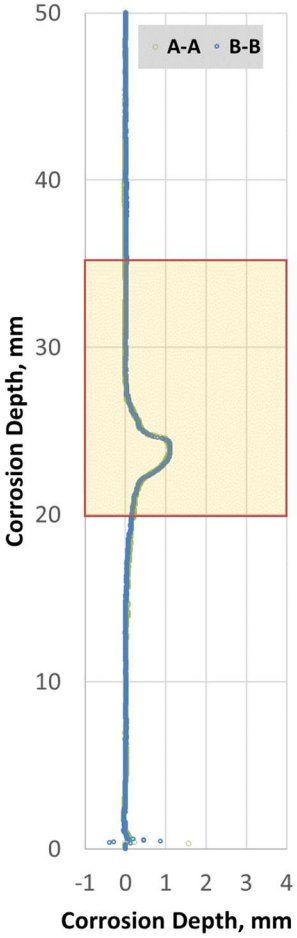


(a)

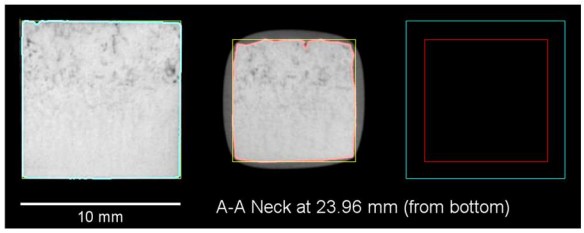


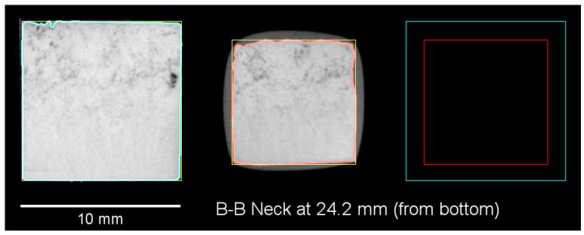


(b)

| Neck Depth, mm | |
|---|---|
| A-A | 1.10 |
| B-B | 1.12 |
| Average | 1.11 |
| Standard deviation | 0.014 |
| | |

Figure L.13. Micro-CT results of K-3 refractory corrosion test, APP2-04 1150 °C-3d.

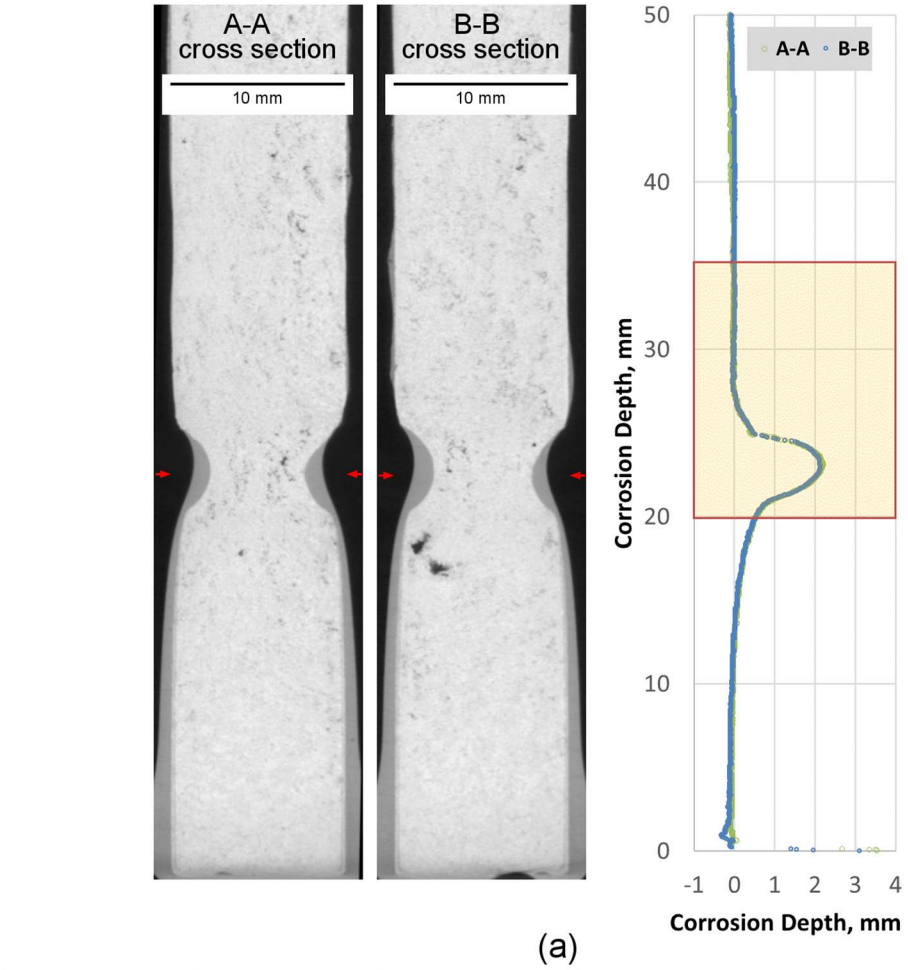


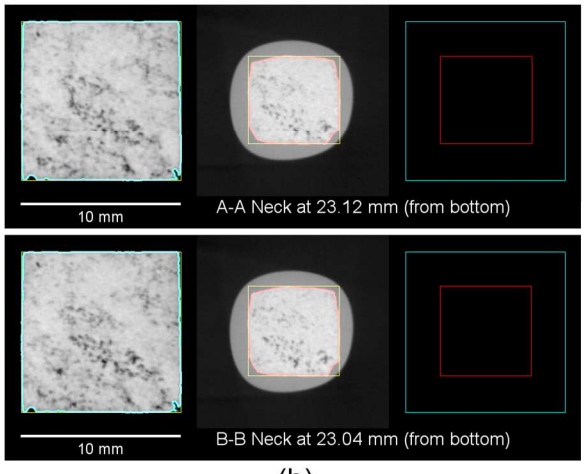


| Neck Depth, mm | |
|---|---|
| A-A | 2.22 |
| B-B | 2.14 |
| Average | 2.18 |
| Standard deviation | 0.057 |
| | |

Figure L.14. Micro-CT results of K-3 refractory corrosion test, APP2-04 1150 °C-7d.

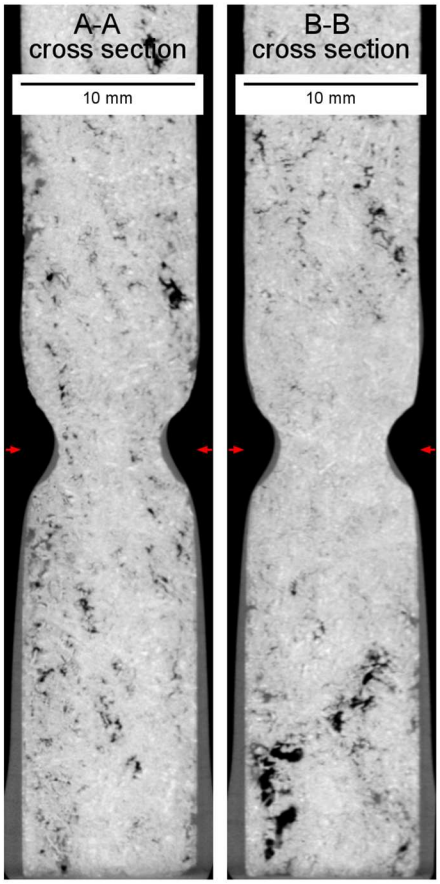


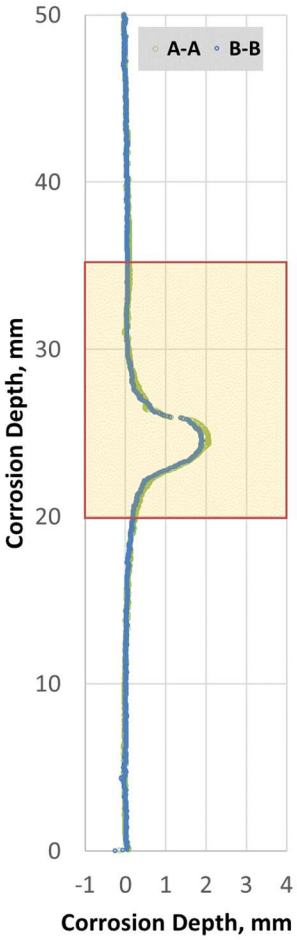


(a)

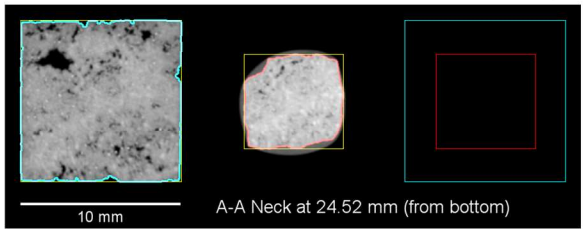


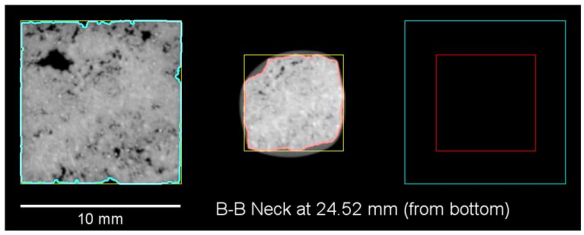


(b)

| Neck Depth, mm | |
|---|---|
| A-A | 2.08 |
| B-B | 1.92 |
| Average | 2.00 |
| Standard deviation | 0.113 |
| | |

Figure L.15. Micro-CT results of K-3 refractory corrosion test, APP2-04 1200 °C-3d.

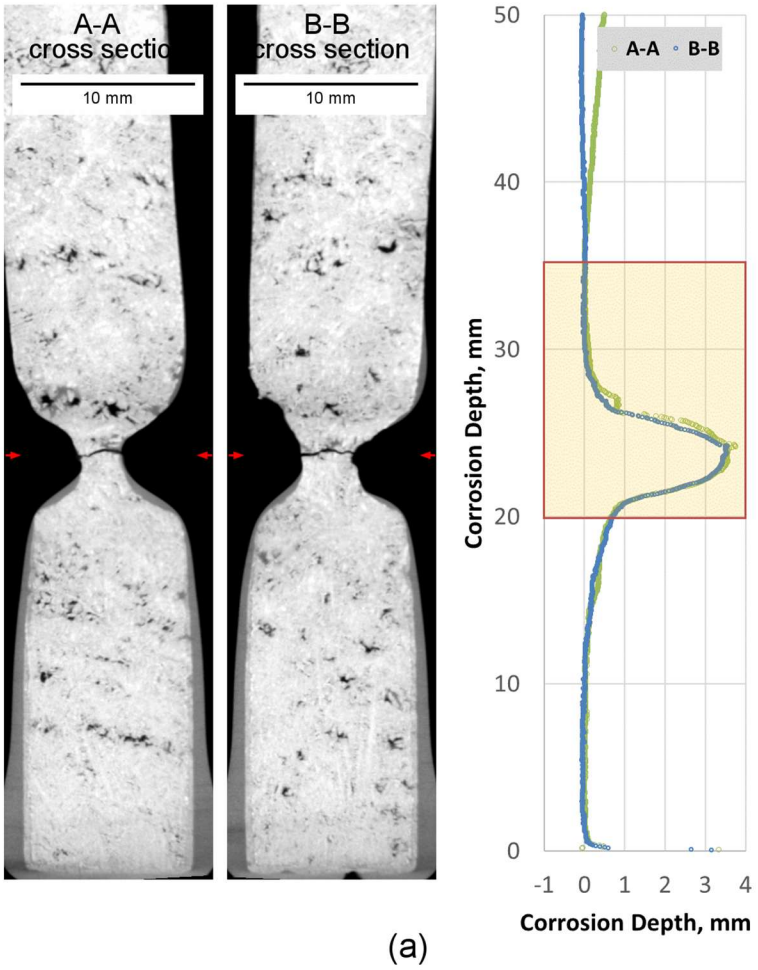


(a)

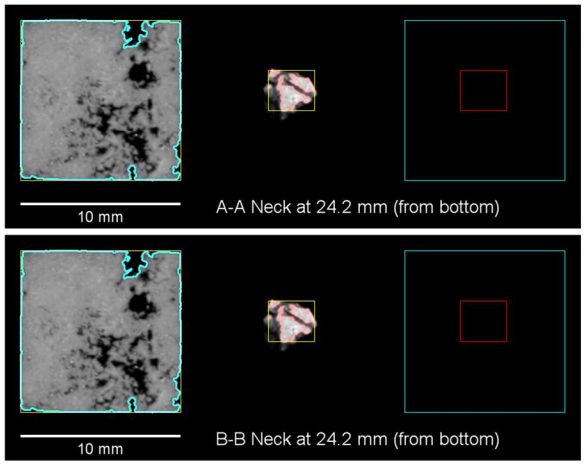


(b)

| Neck Depth, mm | |
|---|---|
| A-A | 3.76 |
| B-B | 3.56 |
| Average | 3.66 |
| Standard deviation | 0.141 |
| Note: Coupon broke before micro-CT scan. Neck measurement is OK. | |

Figure L.16. Micro-CT results of K-3 refractory corrosion test, APP2-04 1200 °C-7d.

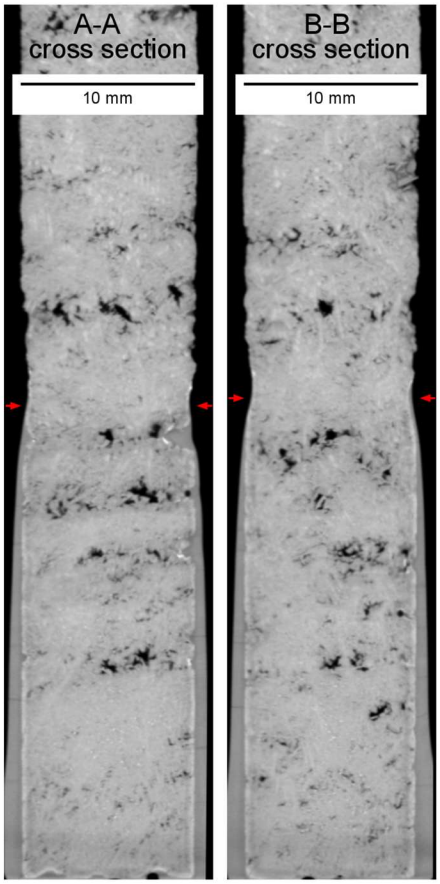


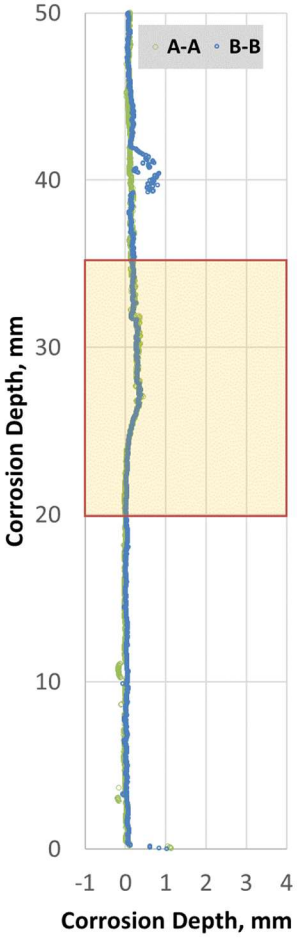


(a)

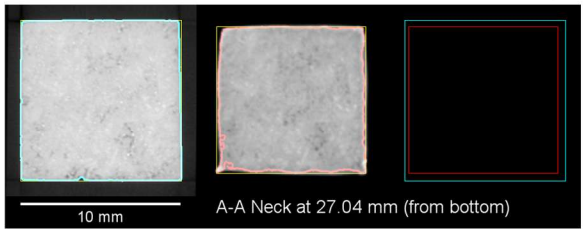


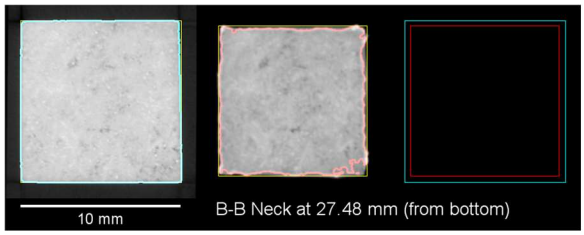


(b)

| Neck Depth, mm | |
|---|---|
| A-A | 0.44 |
| B-B | 0.38 |
| Average | 0.41 |
| Standard deviation | 0.042 |
| | |

Figure L.17. Micro-CT results of K-3 refractory corrosion test, APP2-05 1150 °C-3d.

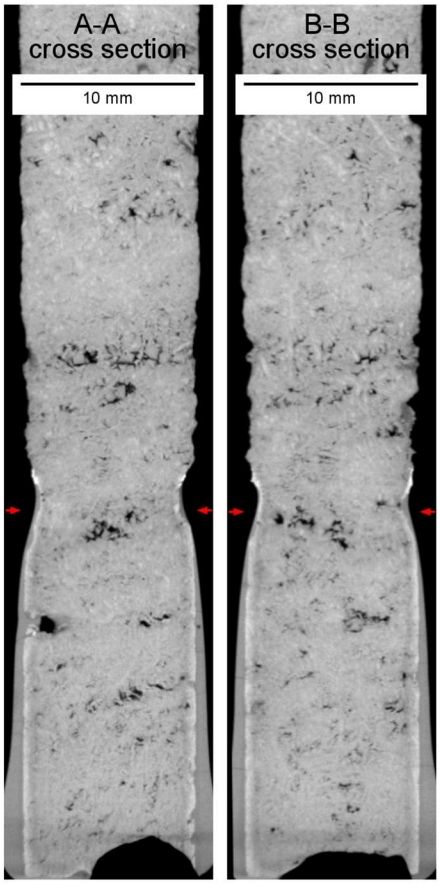


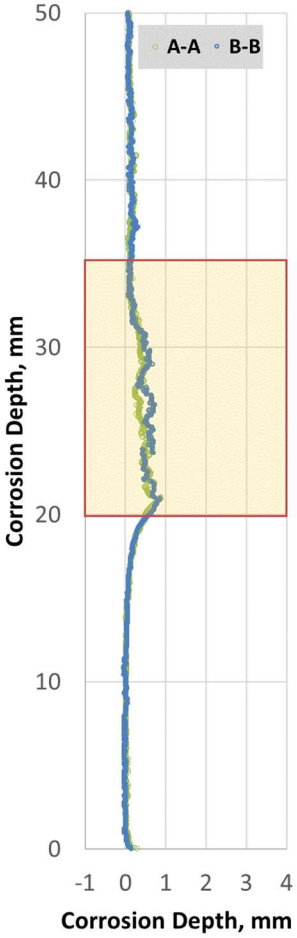


(a)

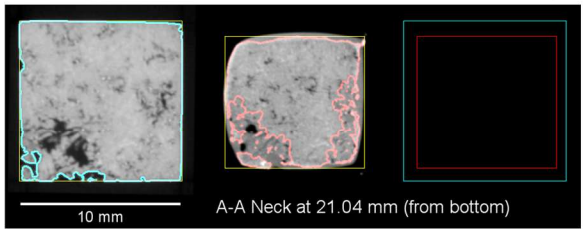


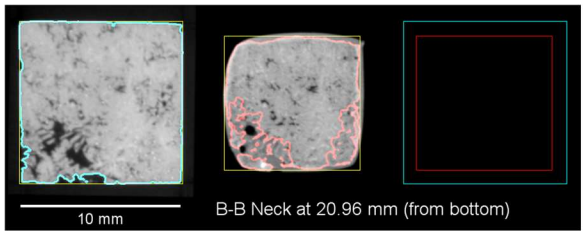


(b)

| Neck Depth, mm | |
|---|---|
| A-A | 0.88 |
| B-B | 0.86 |
| Average | 0.87 |
| Standard deviation | 0.014 |
| | |

Figure L.18. Micro-CT results of K-3 refractory corrosion test, APP2-05 1150 °C-7d.

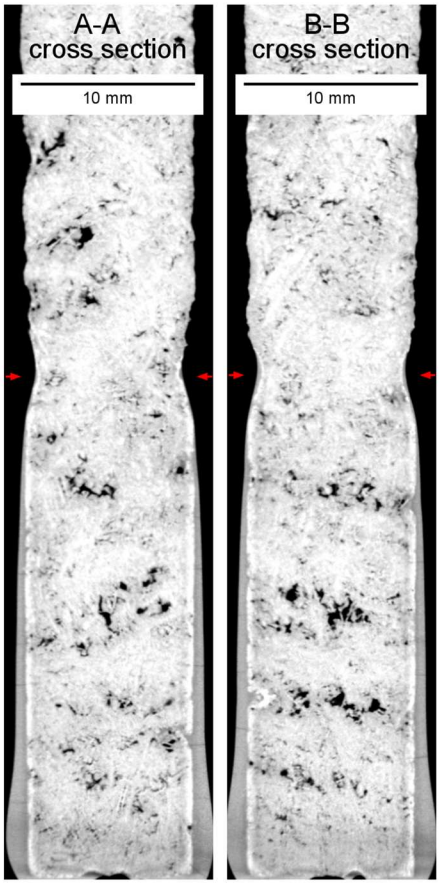


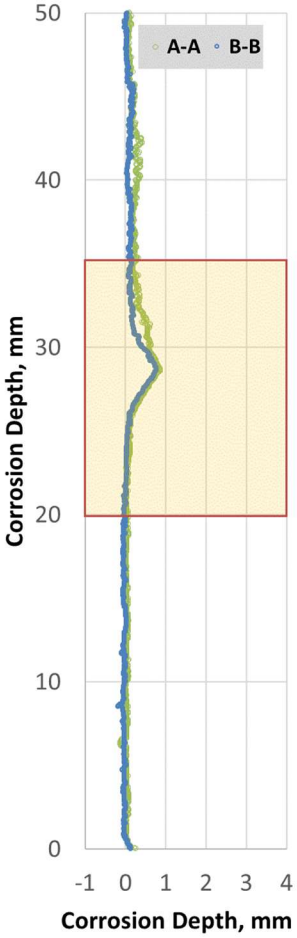


(a)

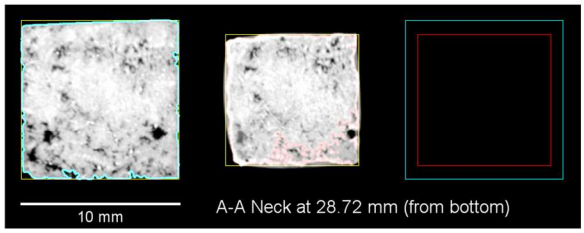


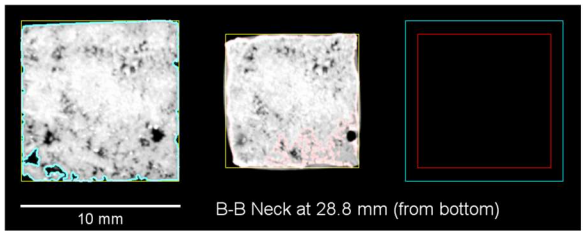


(b)

| Neck Depth, mm | |
|---|---|
| A-A | 0.86 |
| B-B | 0.76 |
| Average | 0.81 |
| Standard deviation | 0.071 |
| | |

Figure L.19. Micro-CT results of K-3 refractory corrosion test, APP2-05 1200 °C-3d.

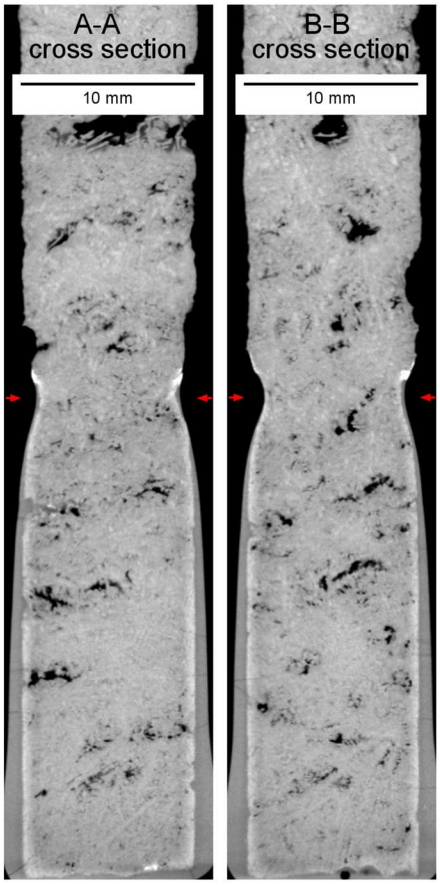


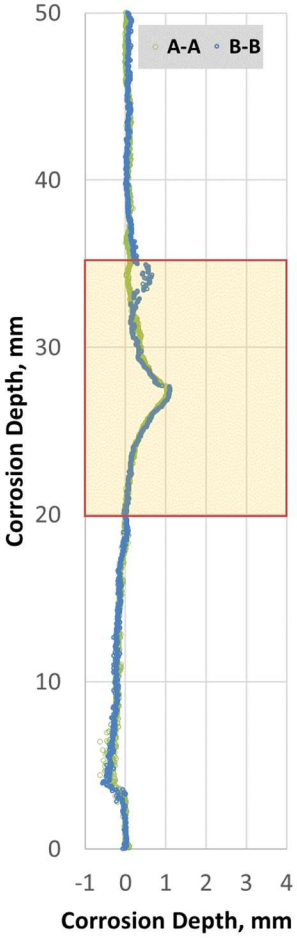


(a)

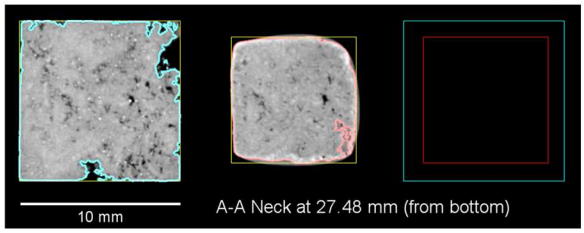


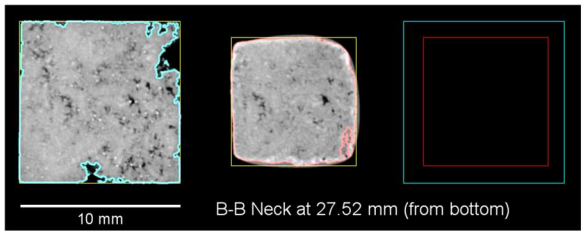


(b)

| Neck Depth, mm | |
|---|---|
| A-A | 1.06 |
| B-B | 1.12 |
| Average | 1.09 |
| Standard deviation | 0.042 |
| | |

Figure L.20. Micro-CT results of K-3 refractory corrosion test, APP2-05 1200 °C-7d.

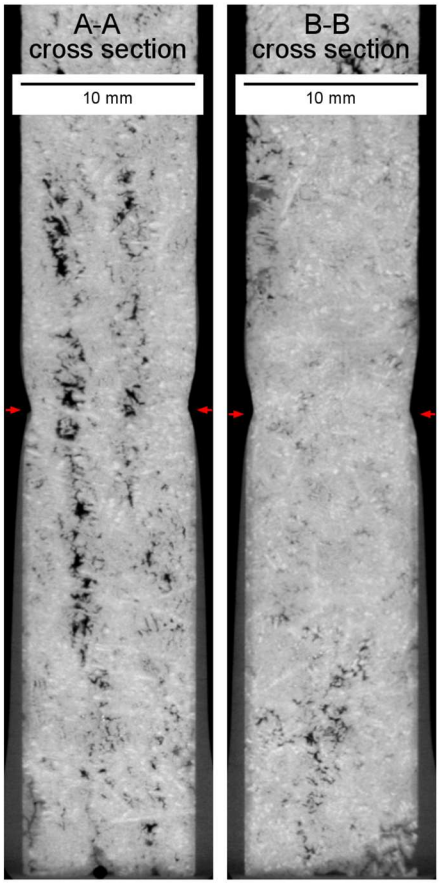


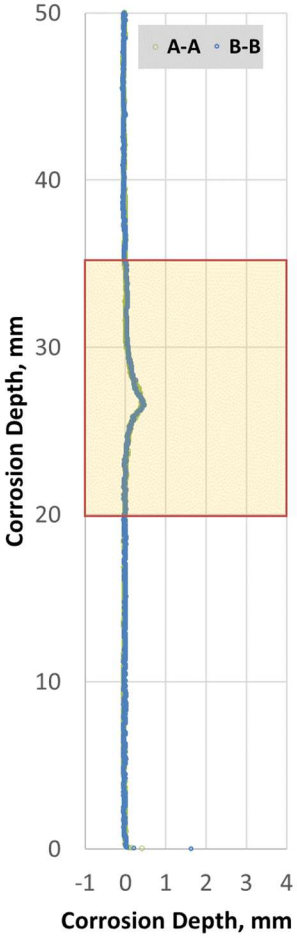


(a)

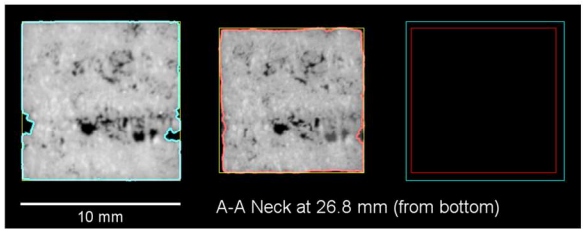


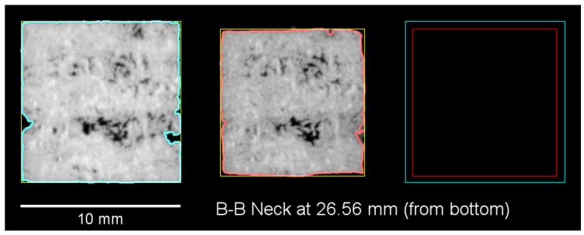


(b)

| Neck Depth, mm | |
|---|---|
| A-A | 0.44 |
| B-B | 0.48 |
| Average | 0.46 |
| Standard deviation | 0.028 |
| | |

Figure L.21. Micro-CT results of K-3 refractory corrosion test, APP2-06 1150 °C-3d.

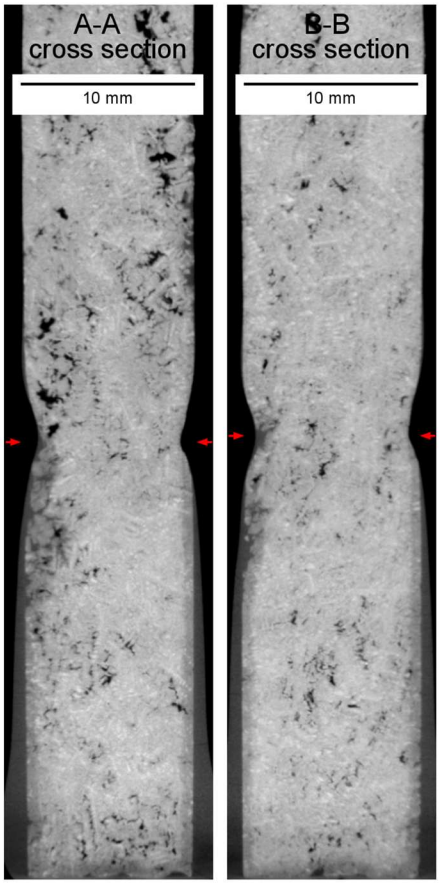


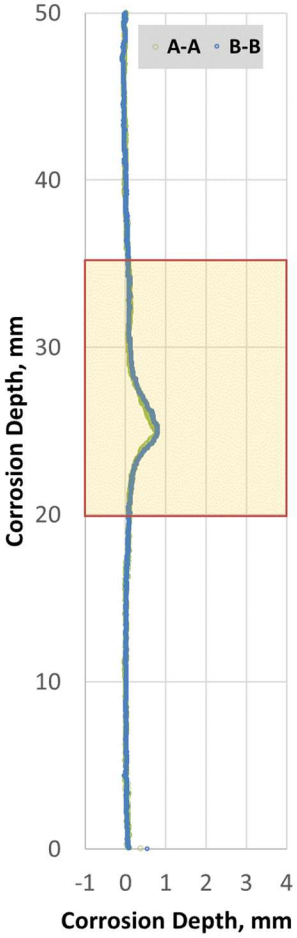


(a)

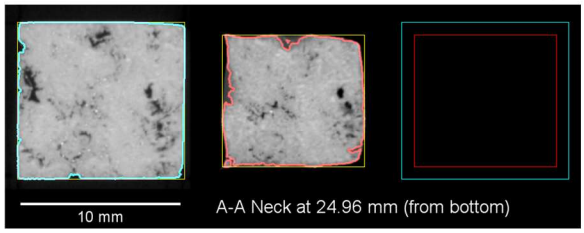


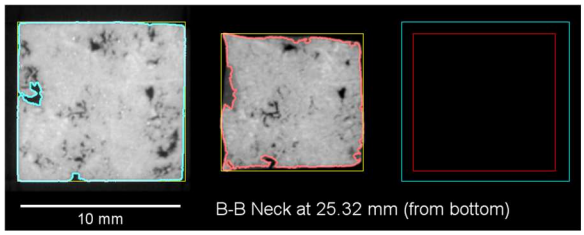


(b)

| Neck Depth, mm | |
|---|---|
| A-A | 0.78 |
| B-B | 0.80 |
| Average | 0.79 |
| Standard deviation | 0.014 |
| | |

Figure L.22. Micro-CT results of K-3 refractory corrosion test, APP2-06 1150 °C-7d.

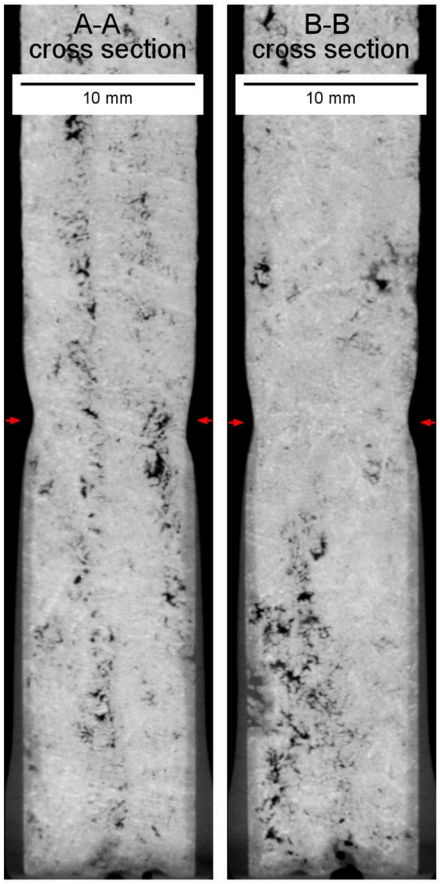


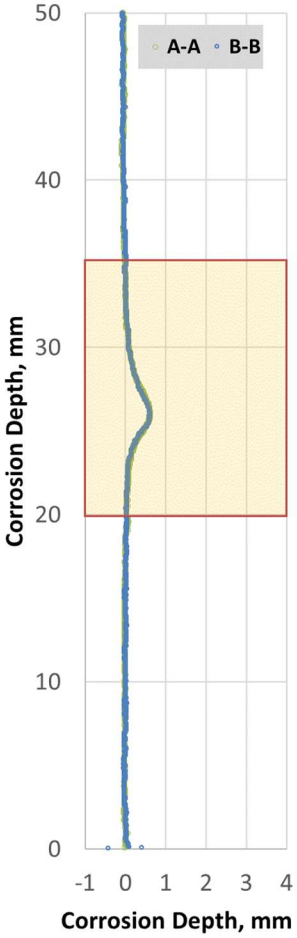


(a)

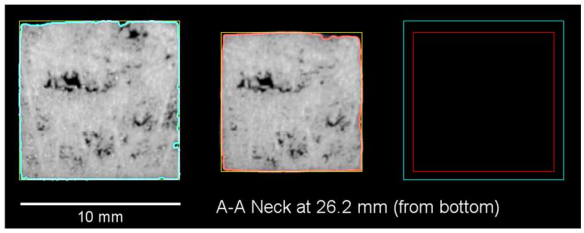


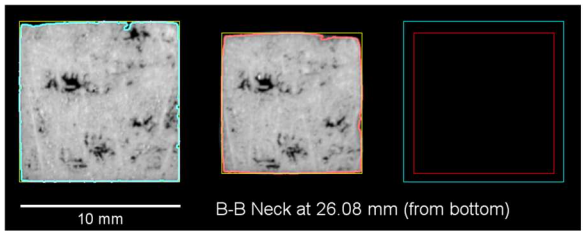


(b)

| Neck Depth, mm | |
|---|---|
| A-A | 0.62 |
| B-B | 0.62 |
| Average | 0.62 |
| Standard deviation | 0.000 |
| | |

Figure L.23. Micro-CT results of K-3 refractory corrosion test, APP2-06 1200 °C-3d.

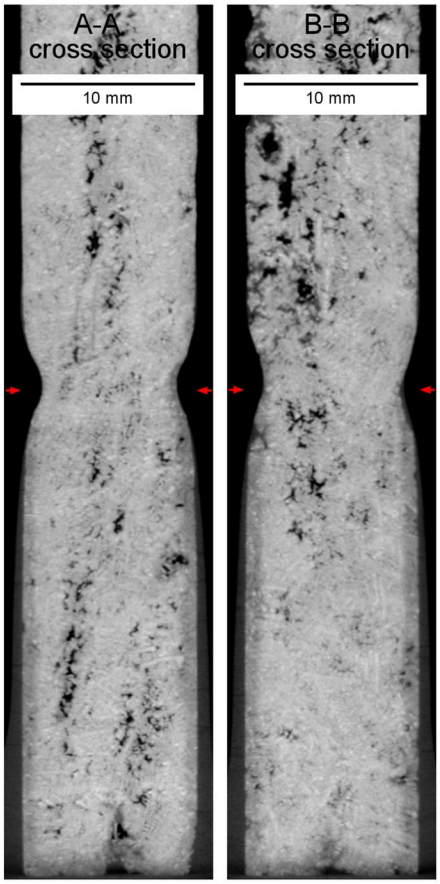


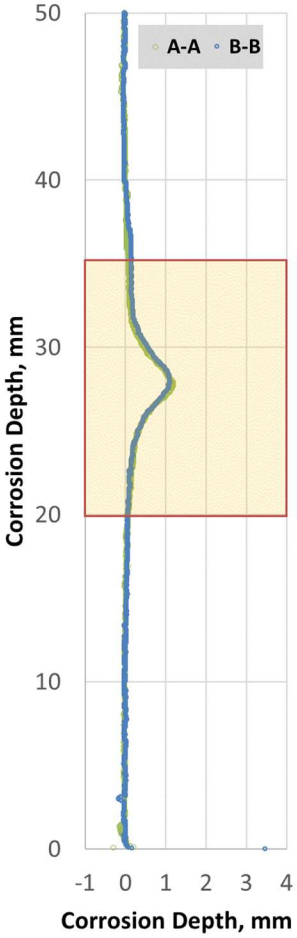


(a)

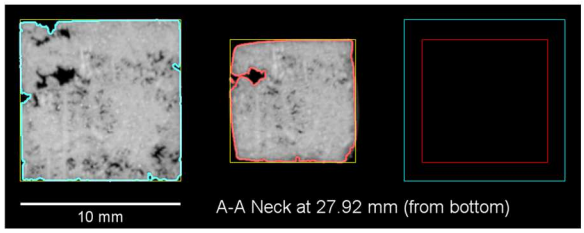


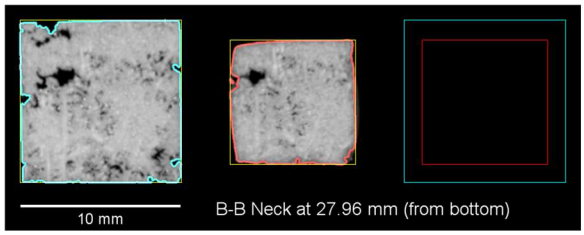


(b)

| Neck Depth, mm | |
|---|---|
| A-A | 1.20 |
| B-B | 1.12 |
| Average | 1.16 |
| Standard deviation | 0.057 |
| | |

Figure L.24. Micro-CT results of K-3 refractory corrosion test, APP2-06 1200 °C-7d.

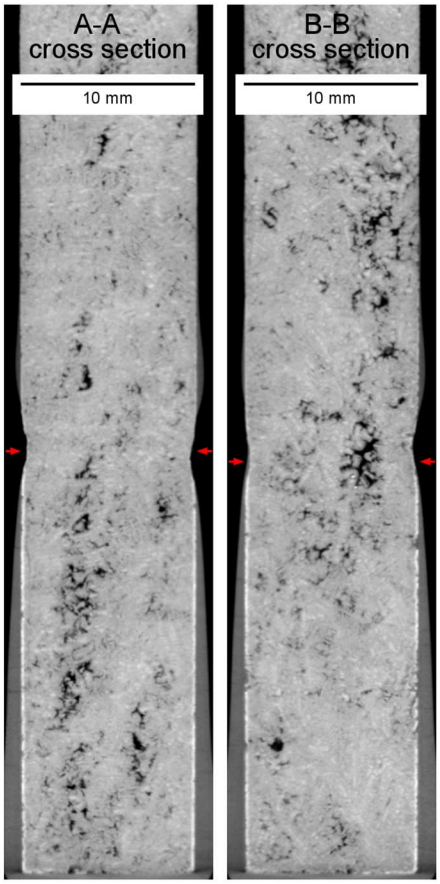


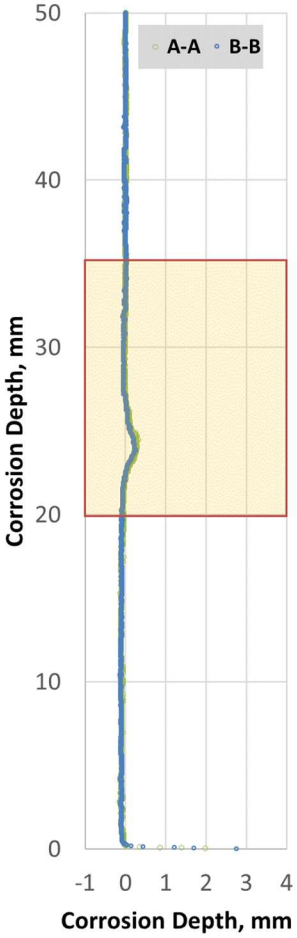


(a)

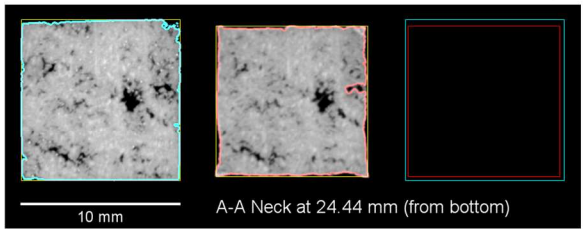


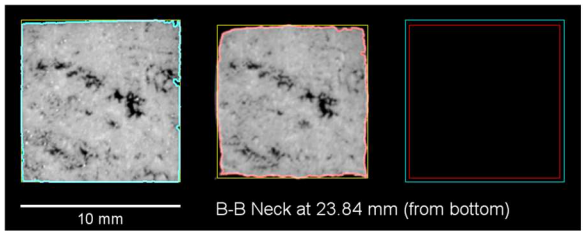


(b)

| Neck Depth, mm | |
|---|---|
| A-A | 0.32 |
| B-B | 0.26 |
| Average | 0.29 |
| Standard deviation | 0.042 |
| | |

Figure L.25. Micro-CT results of K-3 refractory corrosion test, APP2-07 1150 °C-3d.

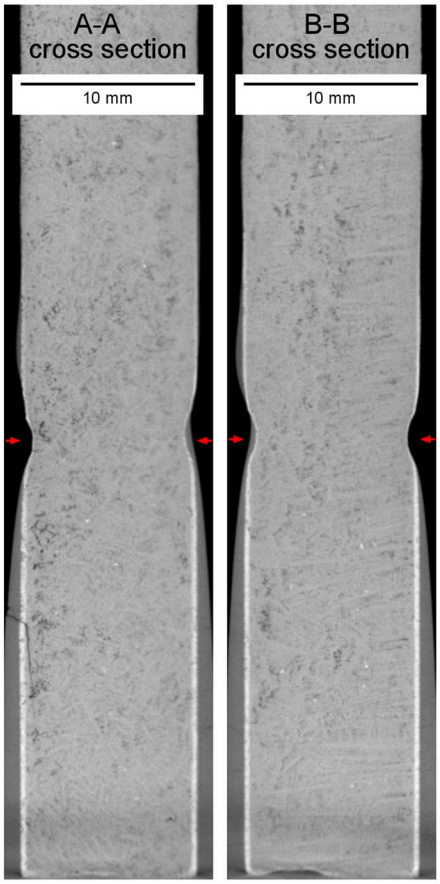


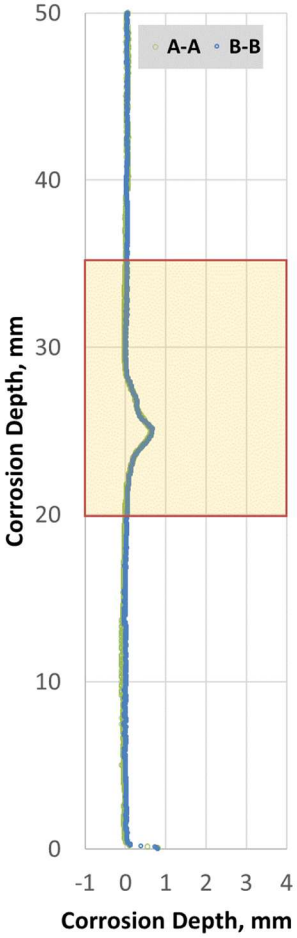


(a)

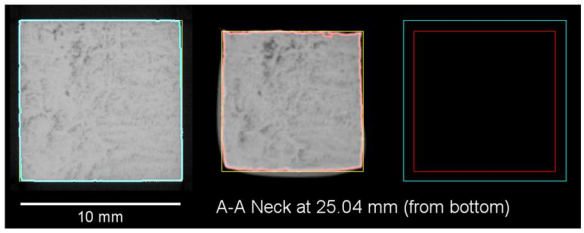


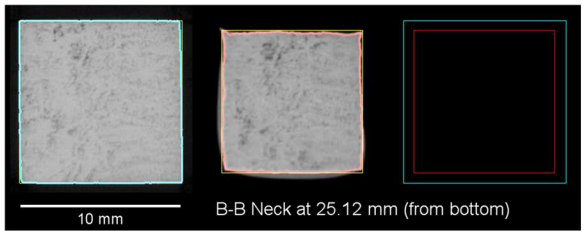


(b)

| Neck Depth, mm | |
|---|---|
| A-A | 0.64 |
| B-B | 0.68 |
| Average | 0.66 |
| Standard deviation | 0.028 |
| | |

Figure L.26. Micro-CT results of K-3 refractory corrosion test, APP2-07 1150 °C-7d.

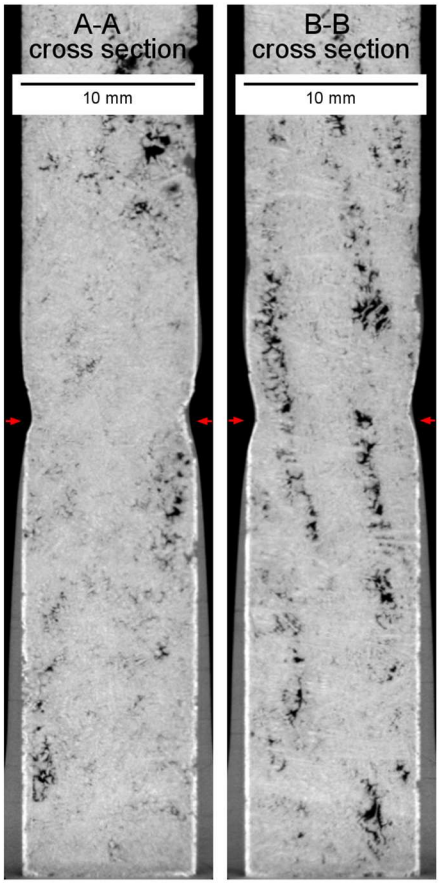


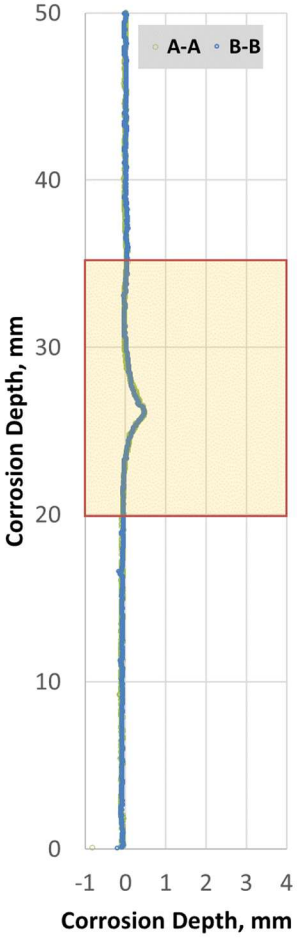


(a)

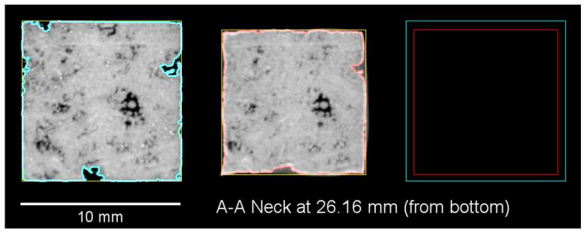


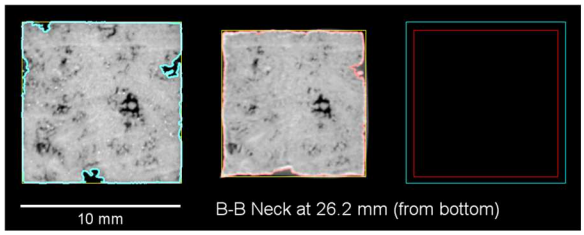


(b)

| Neck Depth, mm | |
|---|---|
| A-A | 0.48 |
| B-B | 0.48 |
| Average | 0.48 |
| Standard deviation | 0.000 |
| | |

Figure L.27. Micro-CT results of K-3 refractory corrosion test, APP2-07 1200 °C-3d.

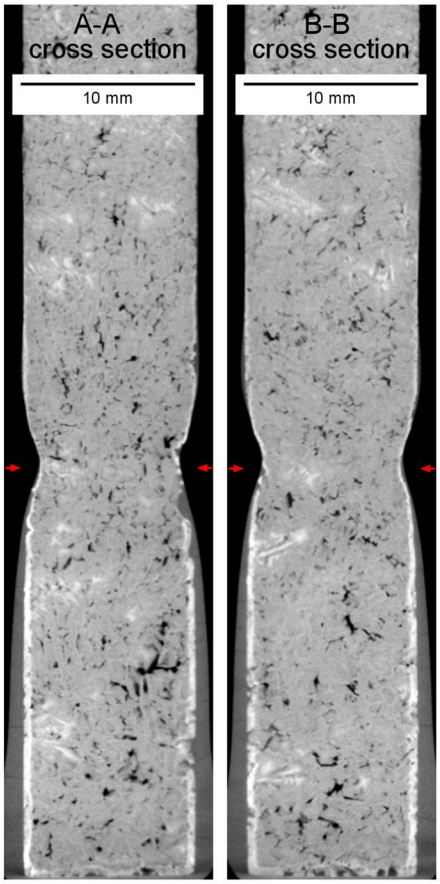


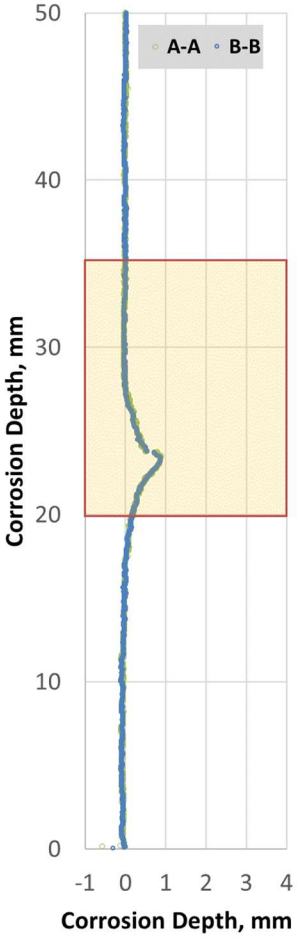


(a)

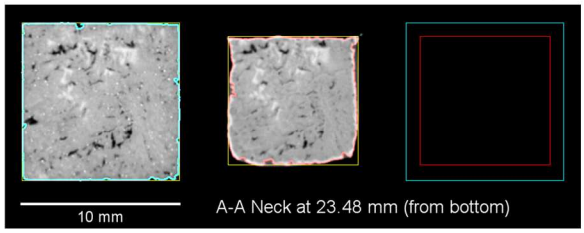


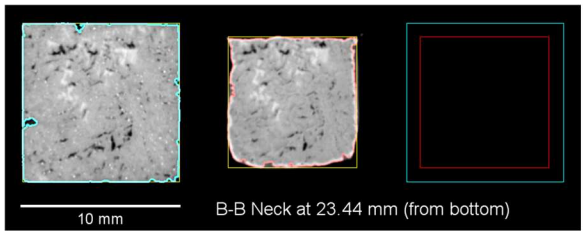


(b)

| Neck Depth, mm | |
|---|---|
| A-A | 0.90 |
| B-B | 0.88 |
| Average | 0.89 |
| Standard deviation | 0.014 |
| | |

Figure L.28. Micro-CT results of K-3 refractory corrosion test, APP2-07 1200 °C-7d.

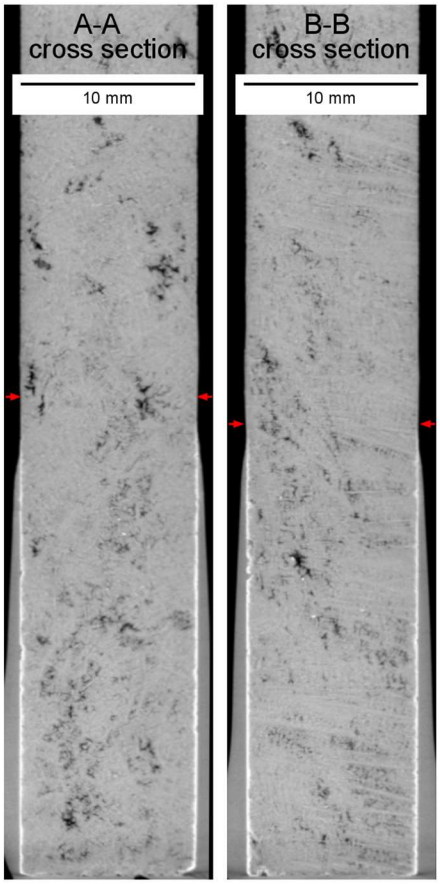


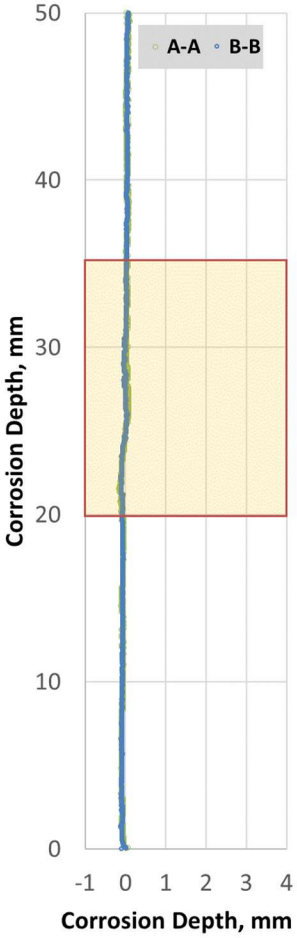


(a)

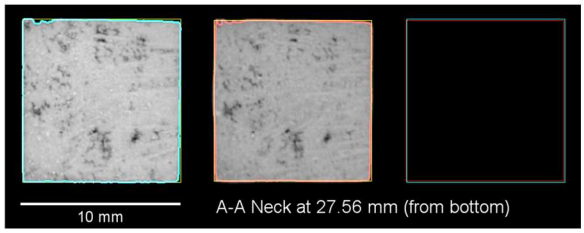


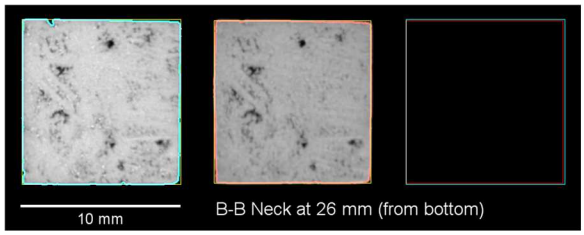


(b)

| Neck Depth, mm | |
|---|---|
| A-A | 0.08 |
| B-B | 0.06 |
| Average | 0.07 |
| Standard deviation | 0.014 |
| | |

Figure L.29. Micro-CT results of K-3 refractory corrosion test, APP2-08 1150 °C-3d.

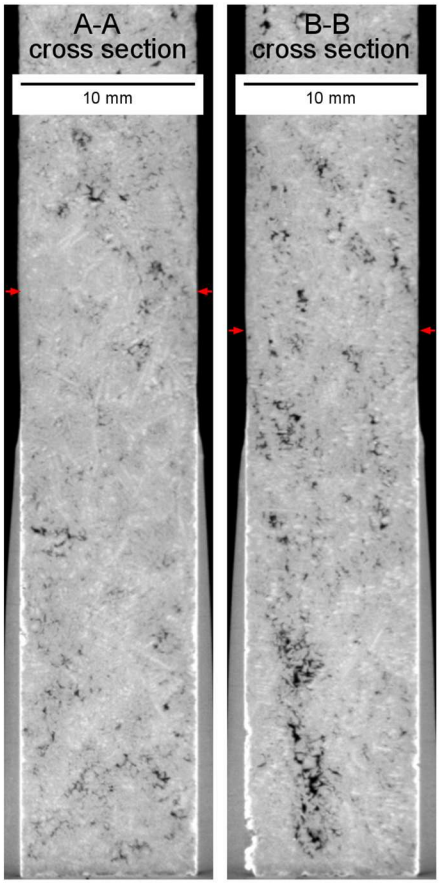


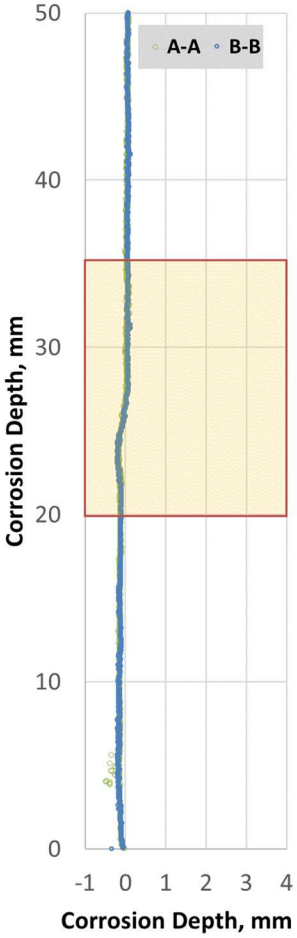


(a)

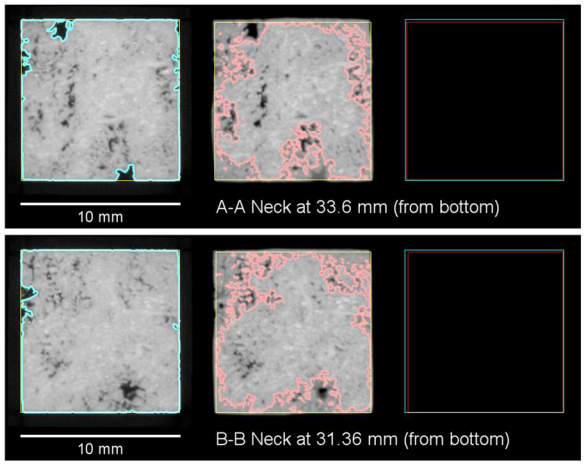


(b)

| Neck Depth, mm | |
|---|---|
| A-A | 0.10 |
| B-B | 0.12 |
| Average | 0.11 |
| Standard deviation | 0.014 |
| Note: Outlines are slightly off due to the low contrast glass vs. K-3. Bounding rectangles are OK for measurement. | |

Figure L.30. Micro-CT results of K-3 refractory corrosion test, APP2-08 1150 °C-7d.

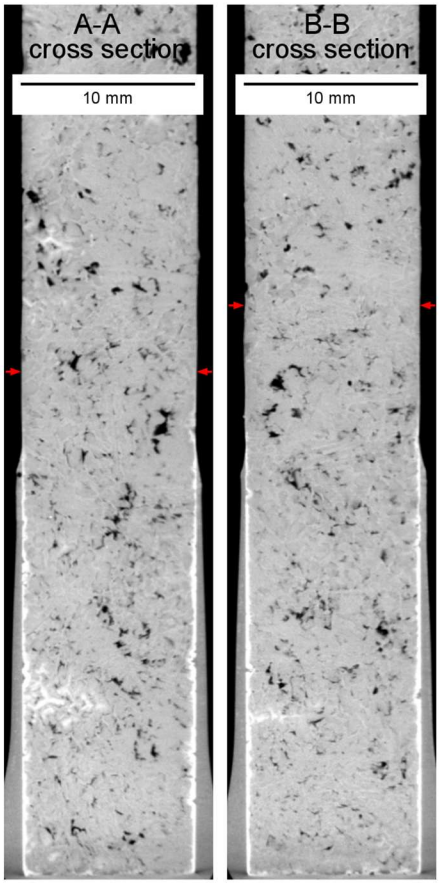


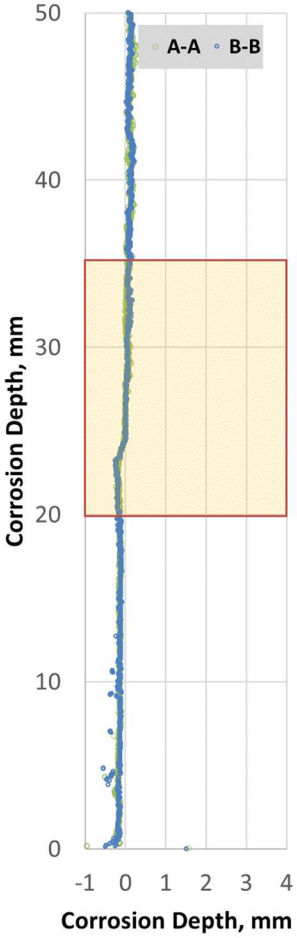


(a)

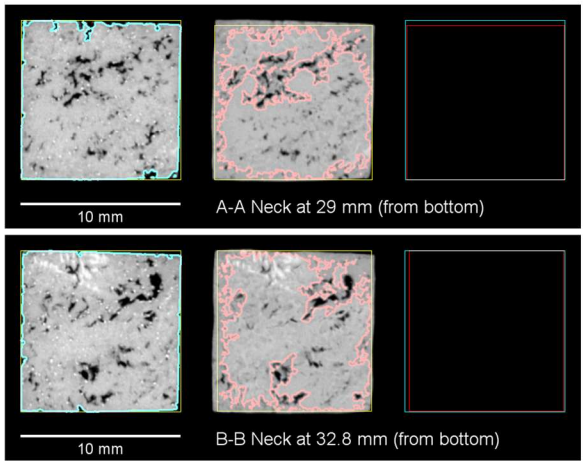


(b)

| Neck Depth, mm | |
|---|---|
| A-A | 0.16 |
| B-B | 0.18 |
| Average | 0.17 |
| Standard deviation | 0.014 |
| Note: Outlines are slightly off due to the low contrast glass vs. K-3. Bounding rectangles are slightly smaller, which can cause measured neck depth values slightly larger. | |

Figure L.31. Micro-CT results of K-3 refractory corrosion test, APP2-08 1200 °C-3d.

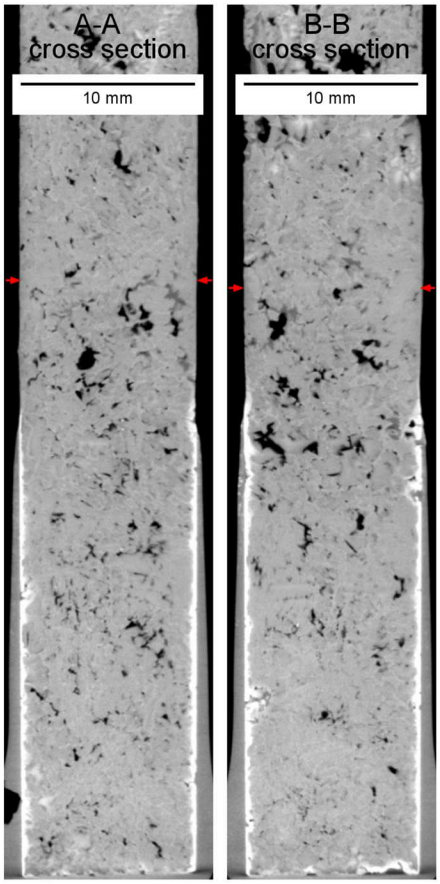


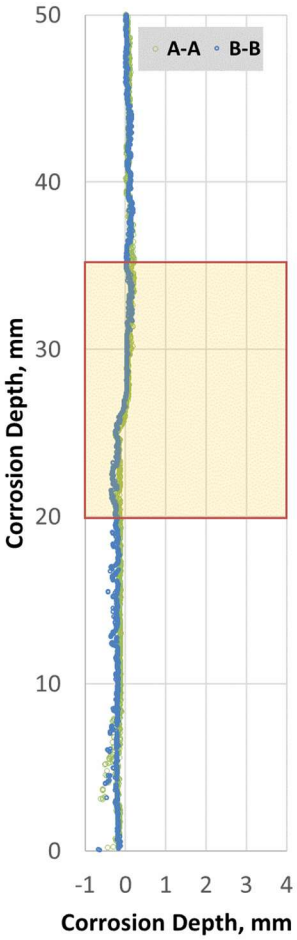


(a)

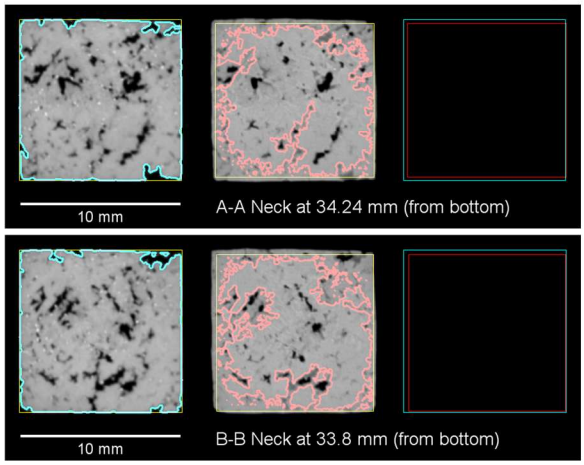


(b)

| Neck Depth, mm | |
|---|---|
| A-A | 0.22 |
| B-B | 0.18 |
| Average | 0.20 |
| Standard deviation | 0.028 |
| Note: Outlines are slightly off due to the low contrast glass vs. K-3. Bounding rectangles are slightly smaller, which can cause measured neck depth values slightly larger. | |

Figure L.32. Micro-CT results of K-3 refractory corrosion test, APP2-08 1200 °C-7d.

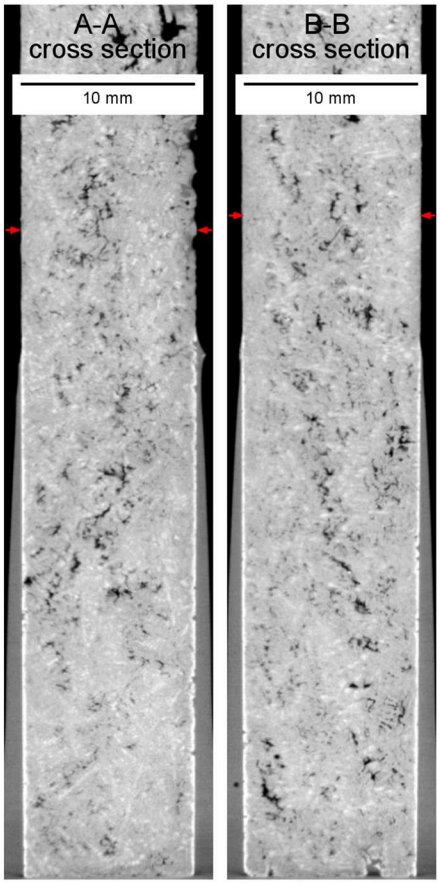


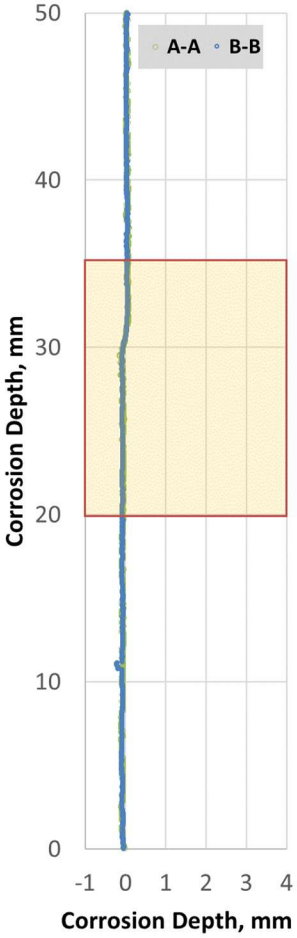


(a)

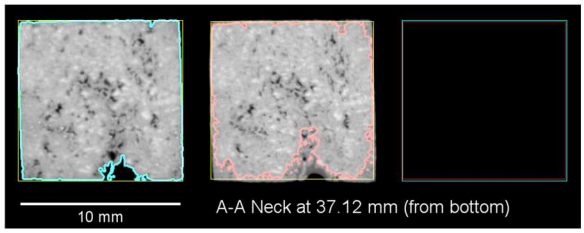


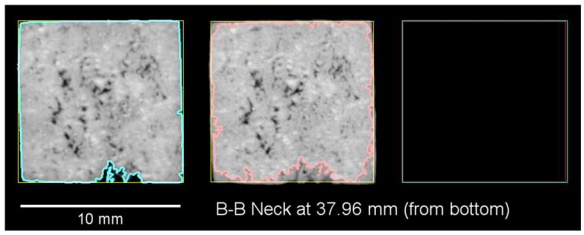


(b)

| Neck Depth, mm | |
|---|---|
| A-A | 0.10 |
| B-B | 0.08 |
| Average | 0.09 |
| Standard deviation | 0.014 |
| Note: Neck is not clear. Glass rose higher than melt line. | |

Figure L.33. Micro-CT results of K-3 refractory corrosion test, APP2-09 1150 °C-3d.

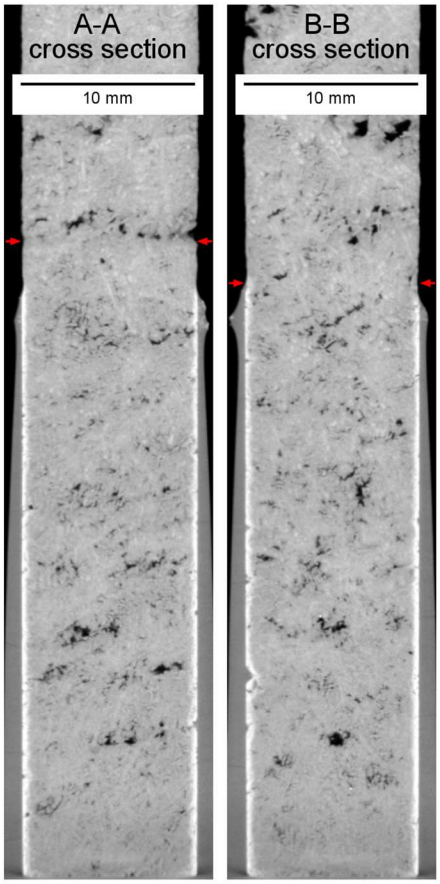


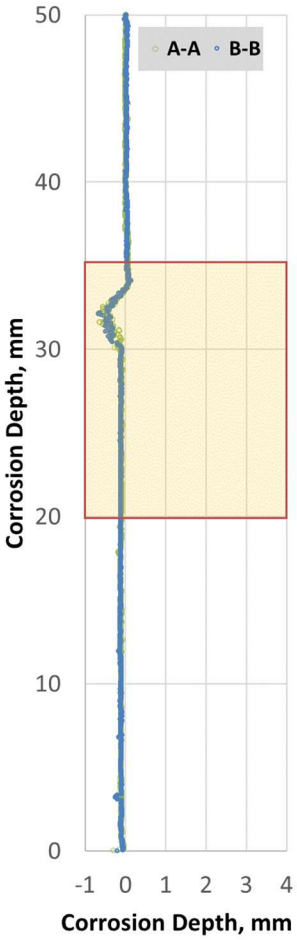


(a)

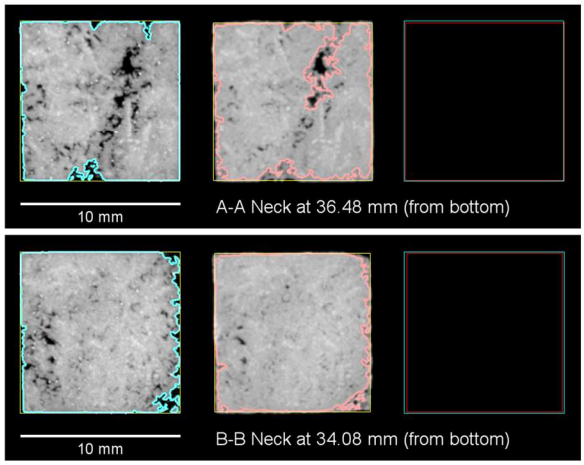


(b)

| Neck Depth, mm | |
|---|---|
| A-A | 0.08 |
| B-B | 0.14 |
| Average | 0.11 |
| Standard deviation | 0.042 |
| Note: Glass rose higher than melt line. A negative dimension loss (expansion) at ~ 32 mm should be cause by reaction layer. | |

Figure L.34. Micro-CT results of K-3 refractory corrosion test, APP2-09 1150 °C-7d.

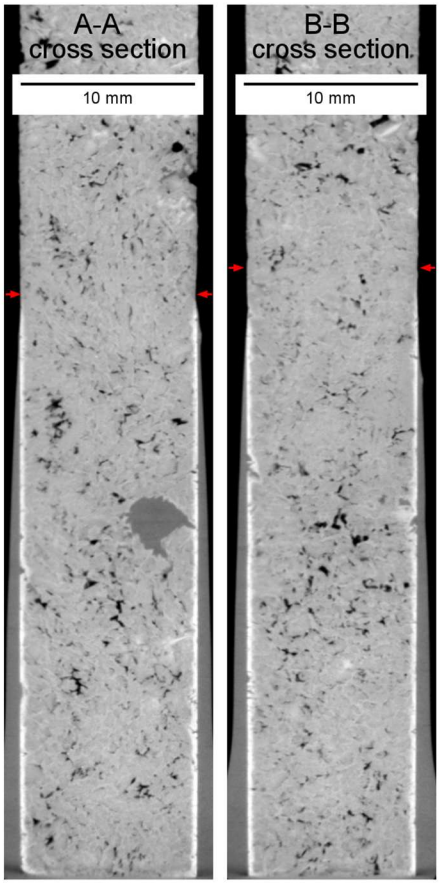


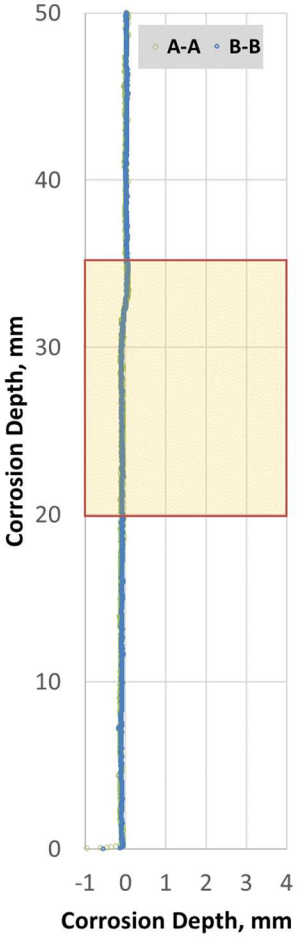


(a)

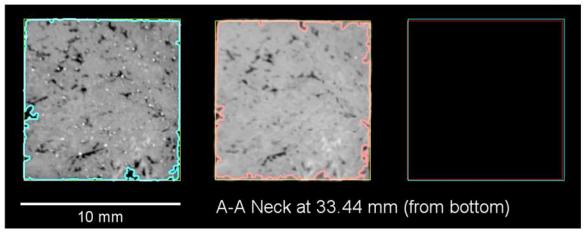


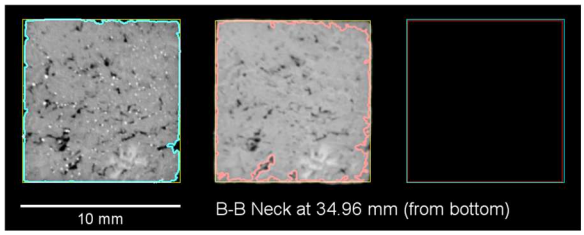


(b)

| Neck Depth, mm | |
|---|---|
| A-A | 0.08 |
| B-B | 0.08 |
| Average | 0.08 |
| Standard deviation | 0.000 |
| Note: Glass rose higher than melt line. | |

Figure L.35. Micro-CT results of K-3 refractory corrosion test, APP2-09 1200 °C-3d.

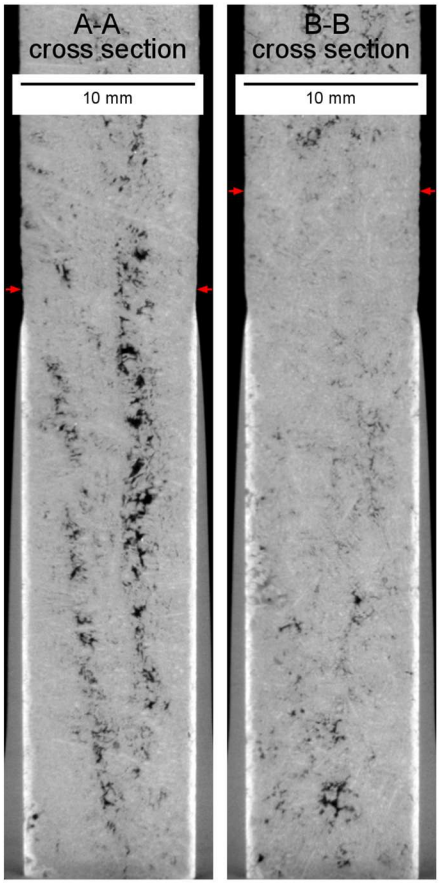


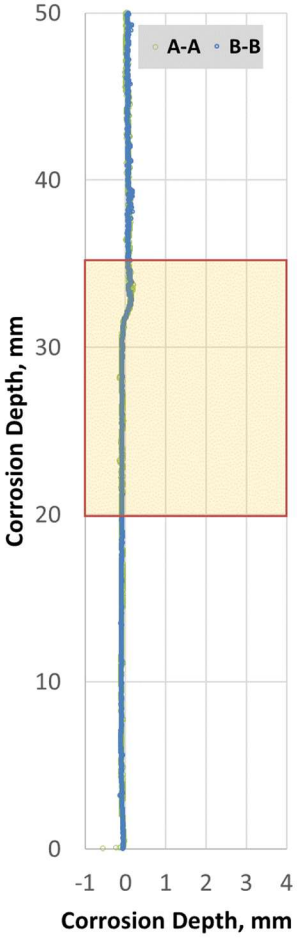


(a)

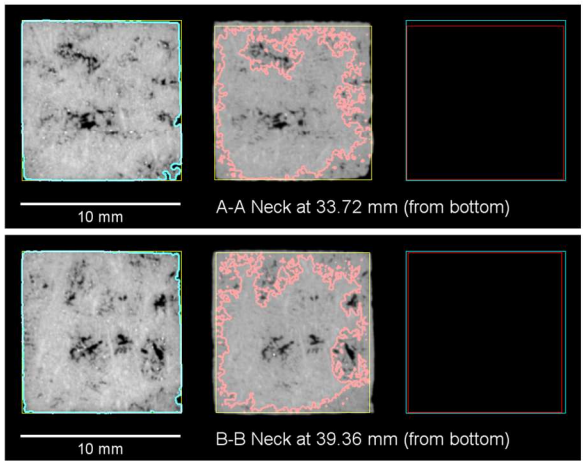


(b)

| Neck Depth, mm | |
|---|---|
| A-A | 0.20 |
| B-B | 0.18 |
| Average | 0.19 |
| Standard deviation | 0.014 |

Note: Outlines are slightly off due to the low contrast glass vs. K-3. Bounding rectangles are slightly smaller, which can cause measured neck depth values slightly larger. Glass rose higher than melt line.

Figure L.36. Micro-CT results of K-3 refractory corrosion test, APP2-09 1200 °C-7d.

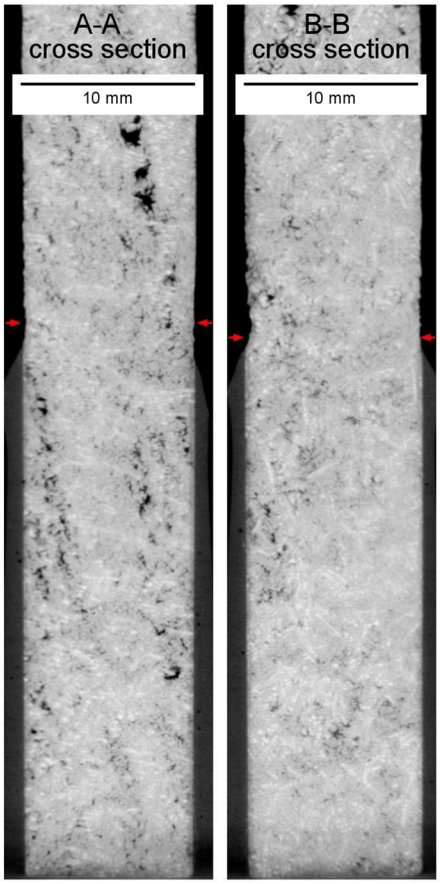


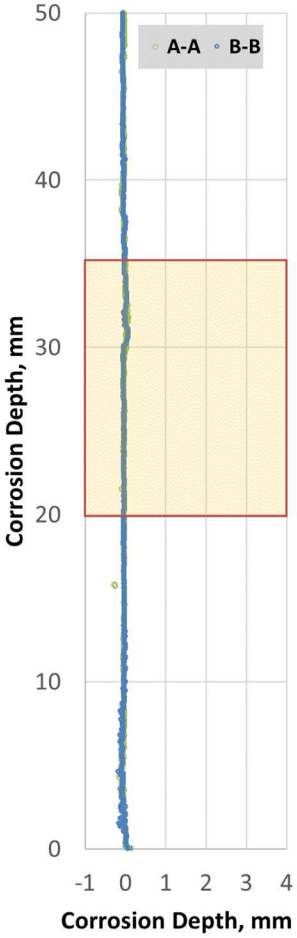


(a)

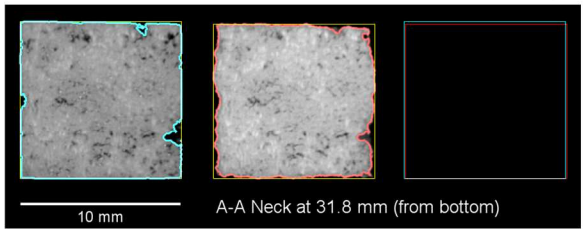


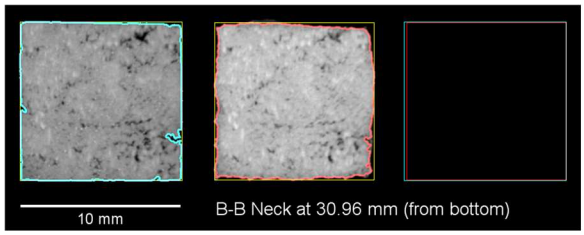


(b)

| Neck Depth, mm | |
|---|---|
| A-A | 0.08 |
| B-B | 0.08 |
| Average | 0.08 |
| Standard deviation | 0.000 |
| | |

Figure L.37. Micro-CT results of K-3 refractory corrosion test, APP2-10 1150 °C-3d.

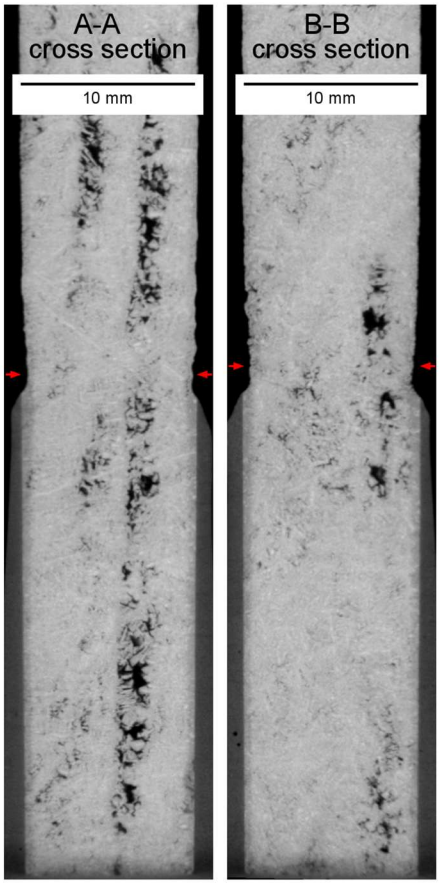


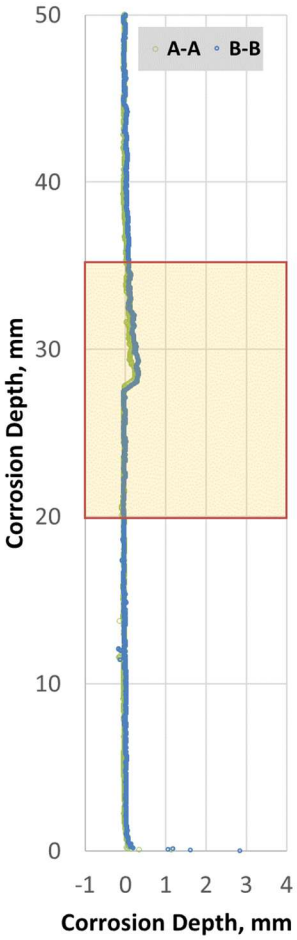


(a)

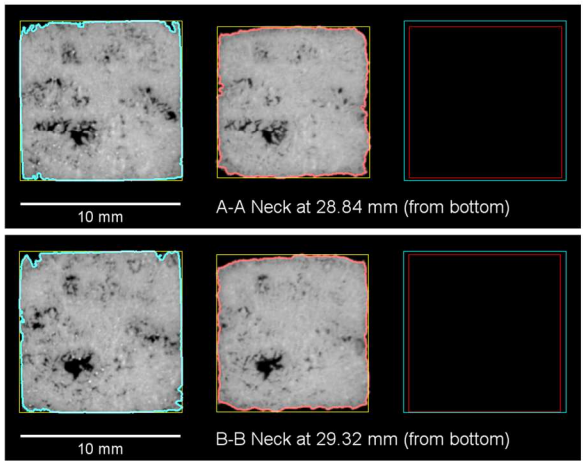


(b)

| Neck Depth, mm | |
|---|---|
| A-A | 0.26 |
| B-B | 0.34 |
| Average | 0.30 |
| Standard deviation | 0.057 |
| | |

Figure L.38. Micro-CT results of K-3 refractory corrosion test, APP2-10 1150 °C-7d.

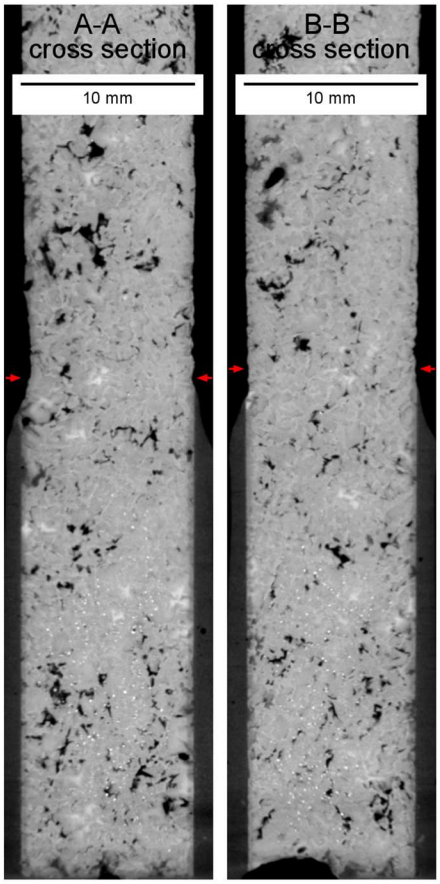


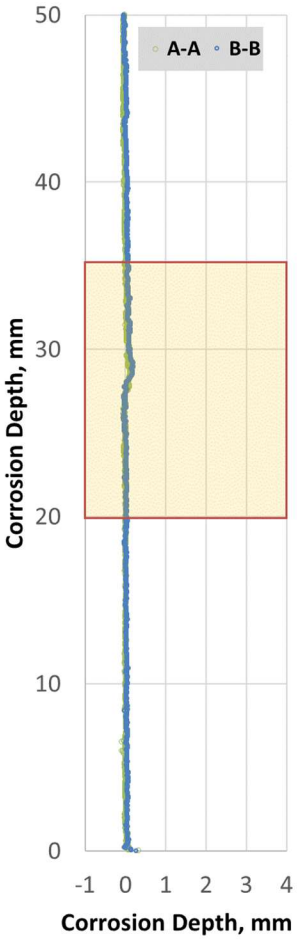


(a)

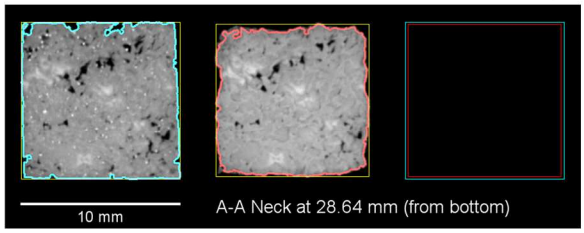


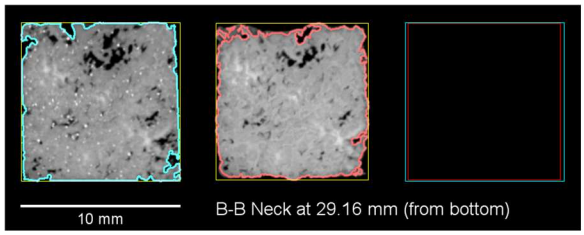


(b)

| Neck Depth, mm | |
|---|---|
| A-A | 0.14 |
| B-B | 0.20 |
| Average | 0.17 |
| Standard deviation | 0.042 |
| | |

Figure L.39. Micro-CT results of K-3 refractory corrosion test, APP2-10 1200 °C-3d.

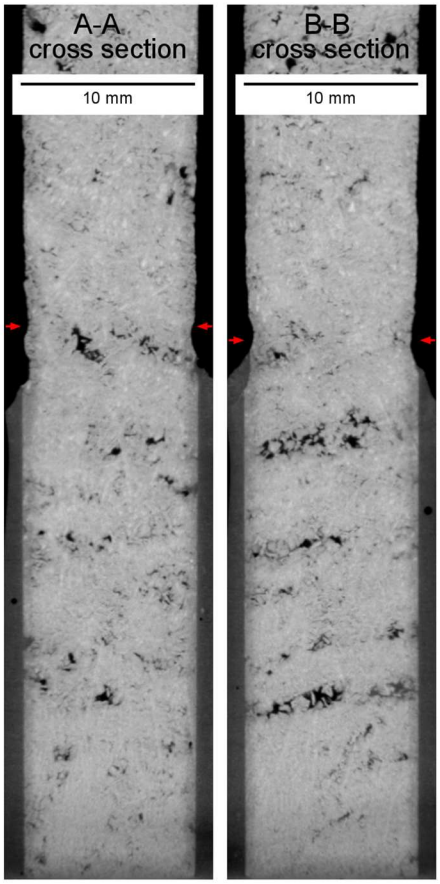


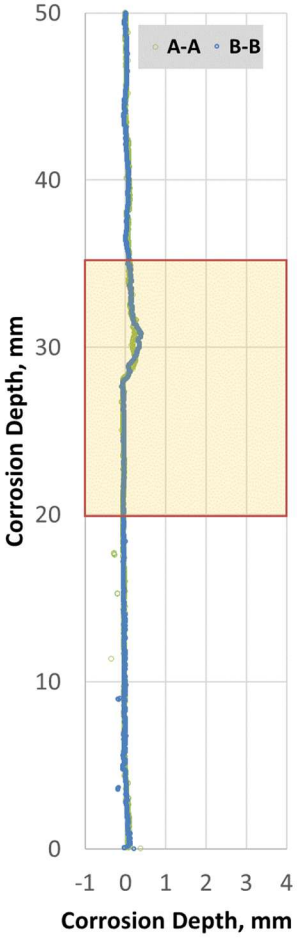


(a)

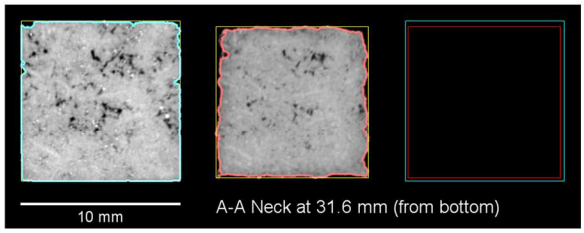


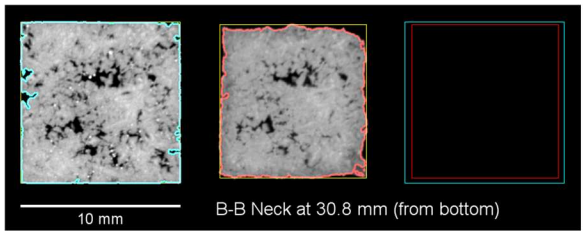


(b)

| Neck Depth, mm | |
|---|---|
| A-A | 0.28 |
| B-B | 0.40 |
| Average | 0.34 |
| Standard deviation | 0.085 |
| | |

Figure L.40. Micro-CT results of K-3 refractory corrosion test, APP2-10 1200 °C-7d.

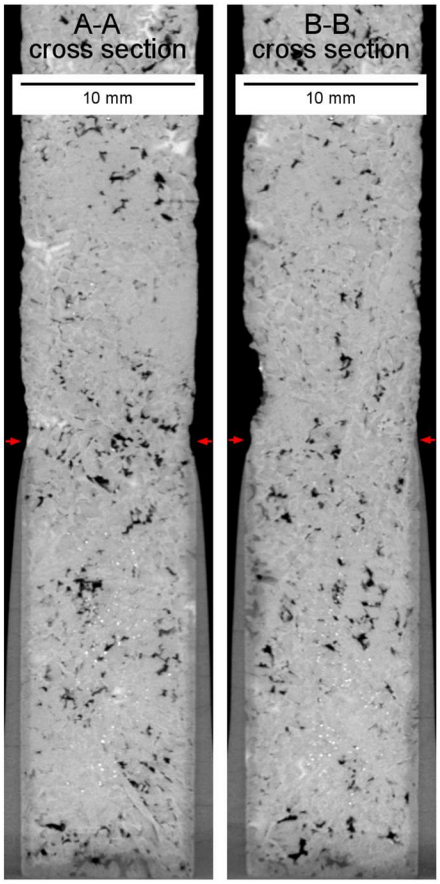


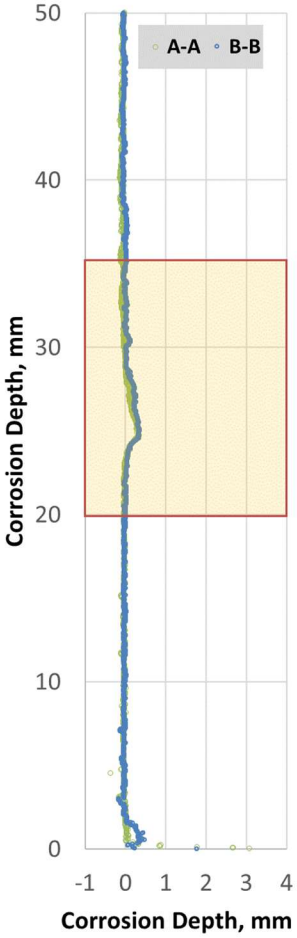


(a)

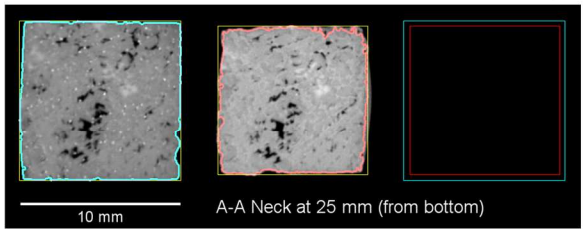


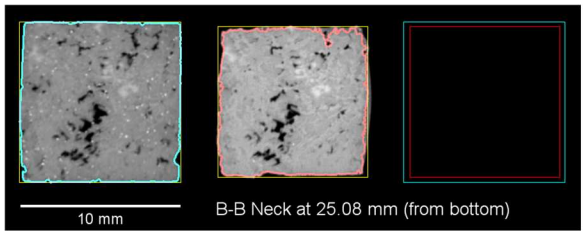


(b)

| Neck Depth, mm | |
|---|---|
| A-A | 0.34 |
| B-B | 0.36 |
| Average | 0.35 |
| Standard deviation | 0.014 |
| | |

Figure L.41. Micro-CT results of K-3 refractory corrosion test, APP2-11 1150 °C-3d.

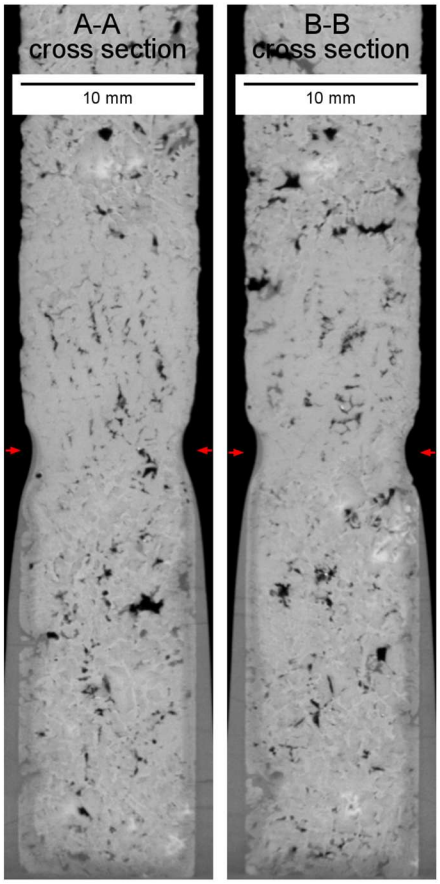


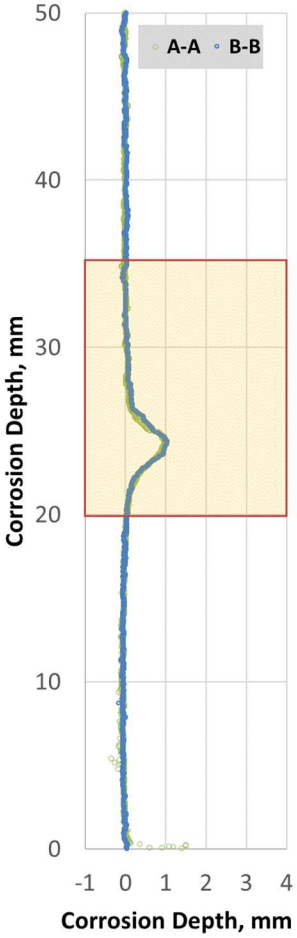


(a)

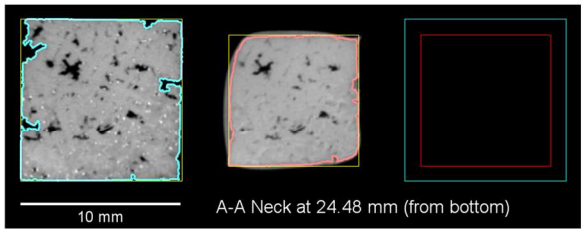


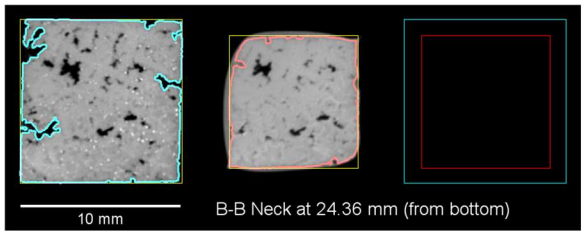


(b)

| Neck Depth, mm | |
|---|---|
| A-A | 0.96 |
| B-B | 1.04 |
| Average | 1.00 |
| Standard deviation | 0.057 |
| | |

Figure L.42. Micro-CT results of K-3 refractory corrosion test, APP2-11 1150 °C-7d.

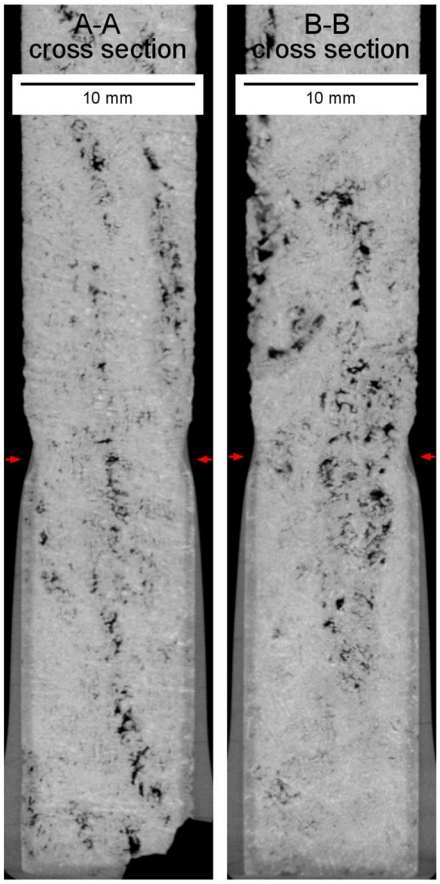


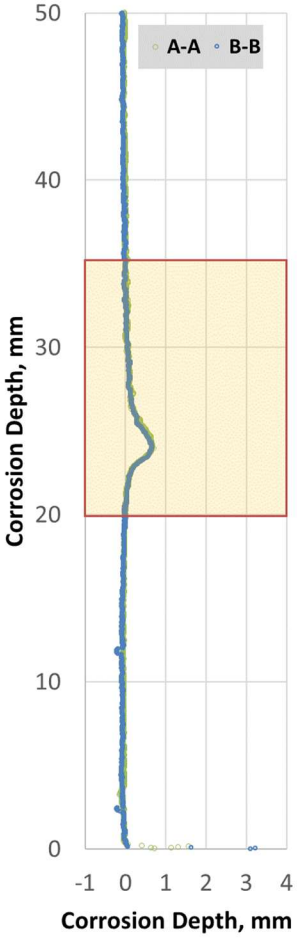


(a)

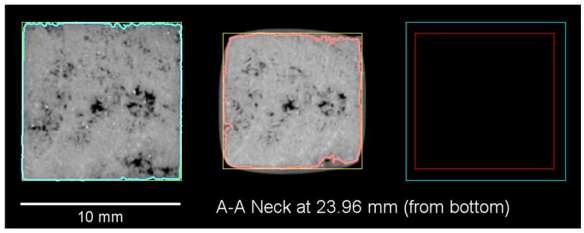


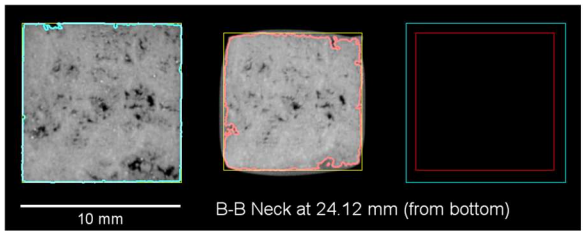


(b)

| Neck Depth, mm | |
|---|---|
| A-A | 0.70 |
| B-B | 0.66 |
| Average | 0.68 |
| Standard deviation | 0.028 |
| | |

Figure L.43. Micro-CT results of K-3 refractory corrosion test, APP2-11 1200 °C-3d.

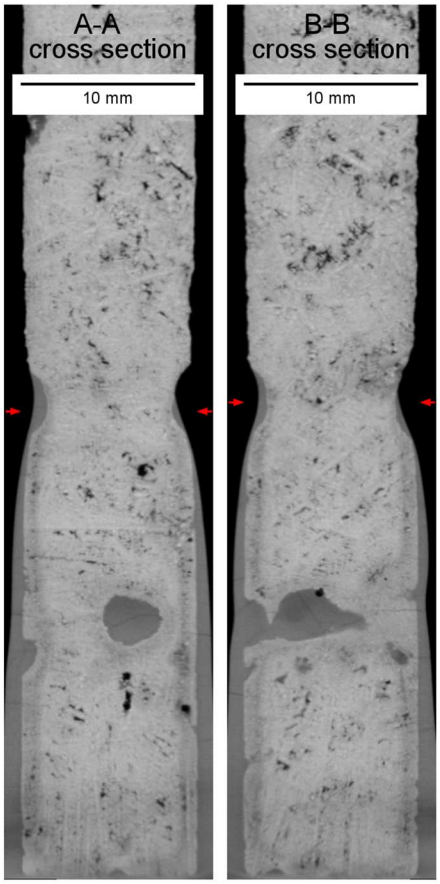


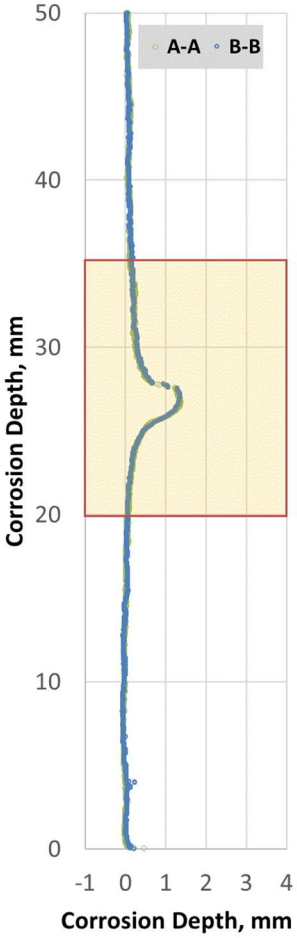


(a)

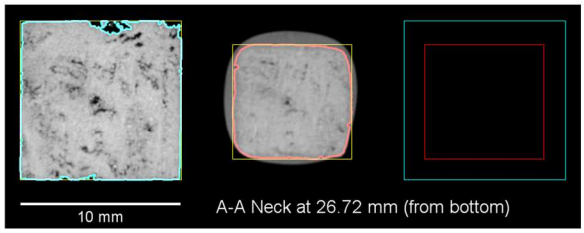


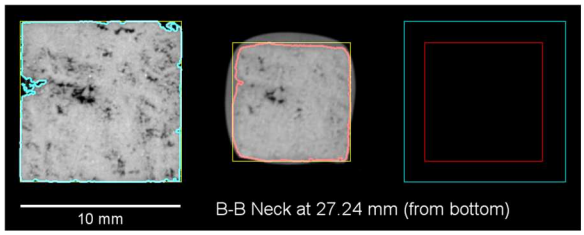


(b)

| Neck Depth, mm | |
|---|---|
| A-A | 1.38 |
| B-B | 1.36 |
| Average | 1.37 |
| Standard deviation | 0.014 |
| | |

Figure L.44. Micro-CT results of K-3 refractory corrosion test, APP2-11 1200 °C-7d.

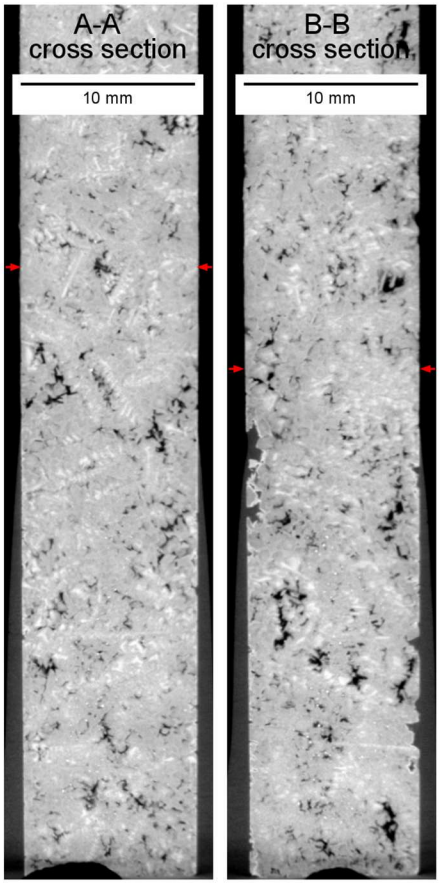


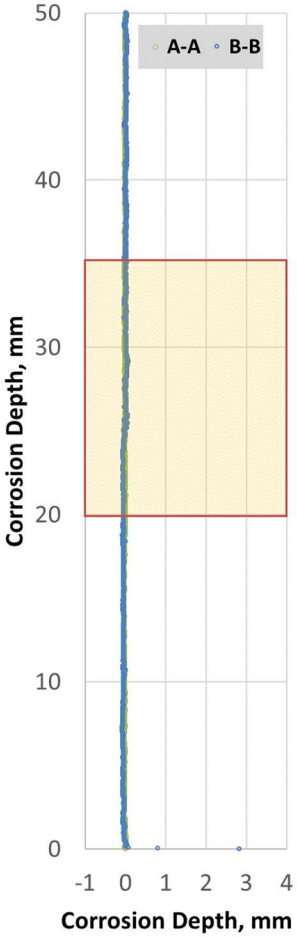


(a)

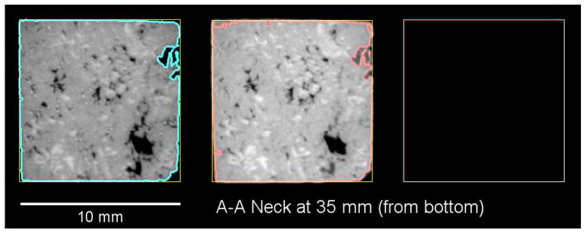


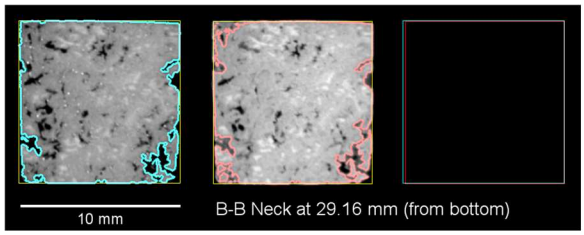


(b)

| Neck Depth, mm | |
|---|---|
| A-A | 0.02 |
| B-B | 0.08 |
| Average | 0.05 |
| Standard deviation | 0.042 |
| Note: No clear neck | |

Figure L.45. Micro-CT results of K-3 refractory corrosion test, APP2-12 1150 °C-3d.

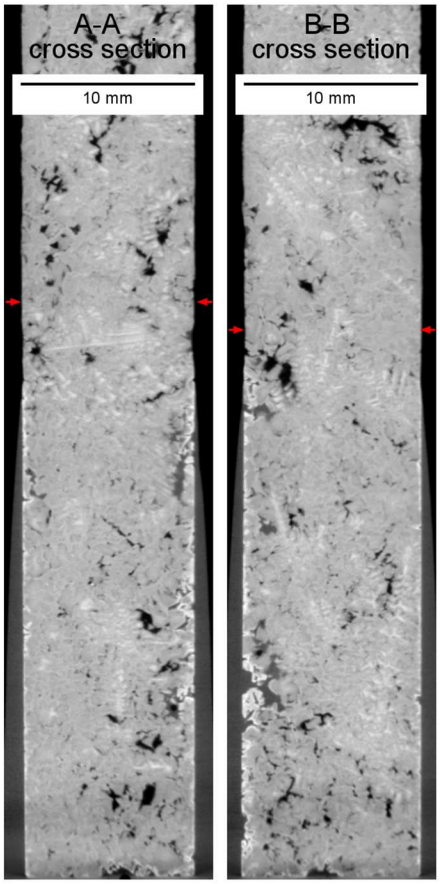


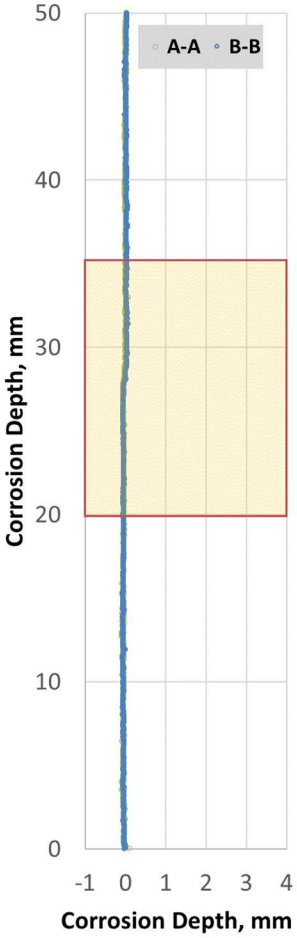


(a)

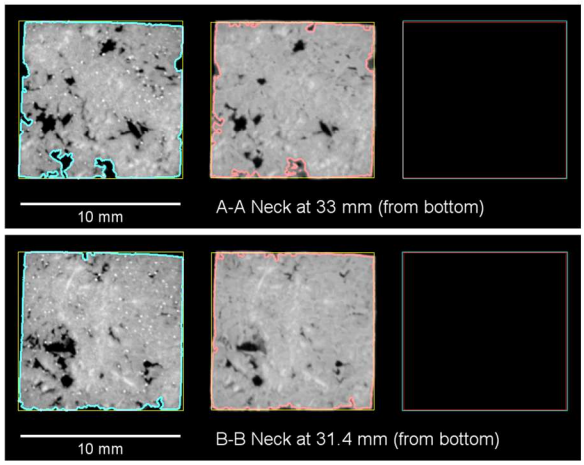


(b)

| Neck Depth, mm | |
|---|---|
| A-A | 0.06 |
| B-B | 0.08 |
| Average | 0.07 |
| Standard deviation | 0.014 |
| Note: No clear neck | |

Figure L.46. Micro-CT results of K-3 refractory corrosion test, APP2-12 1150 °C-7d.

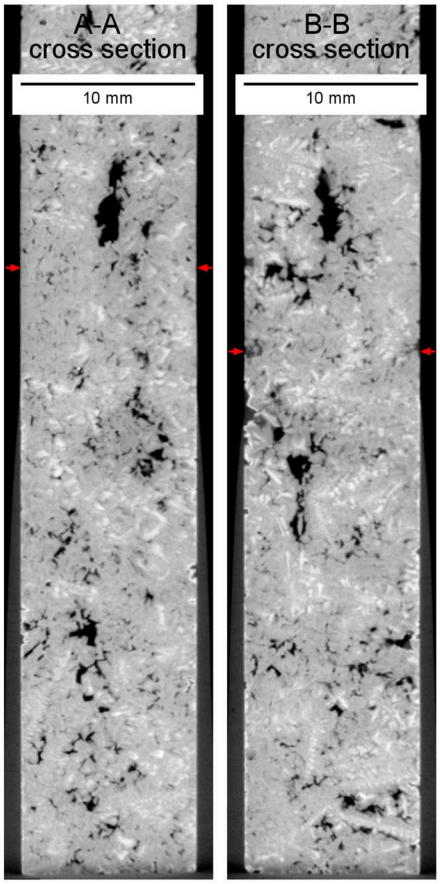


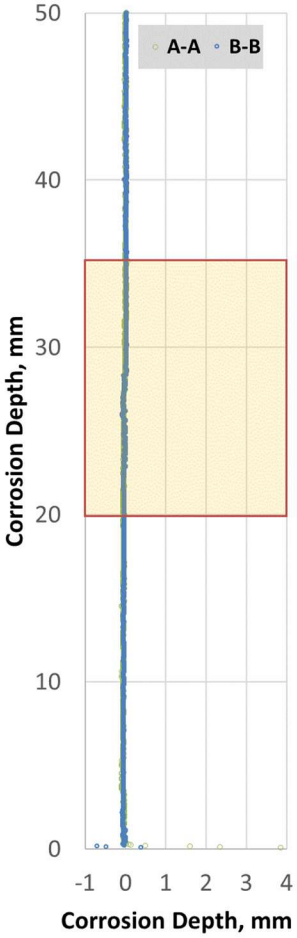


(a)

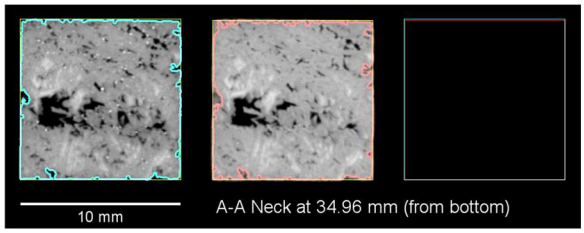


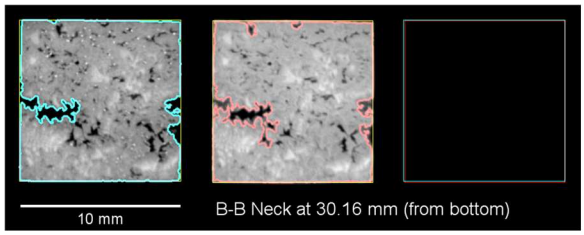


(b)

| Neck Depth, mm | |
|---|---|
| A-A | 0.04 |
| B-B | 0.04 |
| Average | 0.04 |
| Standard deviation | 0.000 |
| Note: No clear neck | |

Figure L.47. Micro-CT results of K-3 refractory corrosion test, APP2-12 1200 °C-3d.

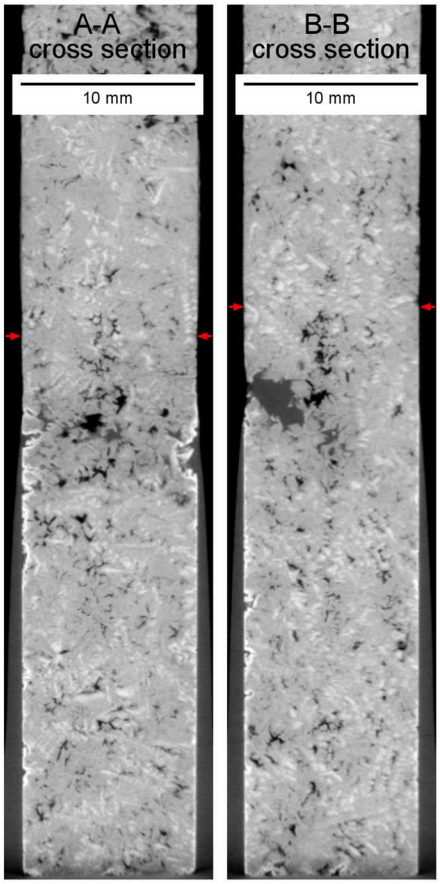


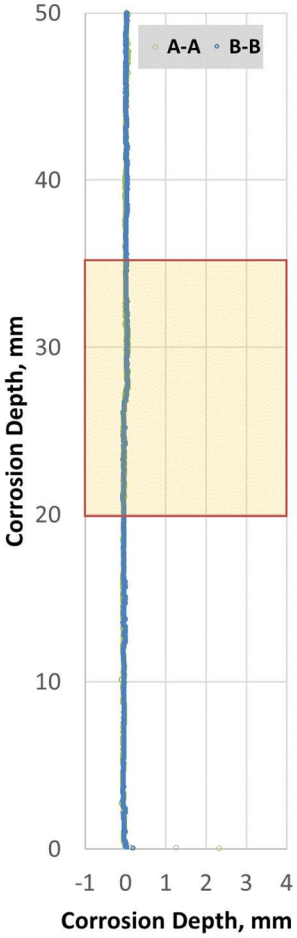


(a)

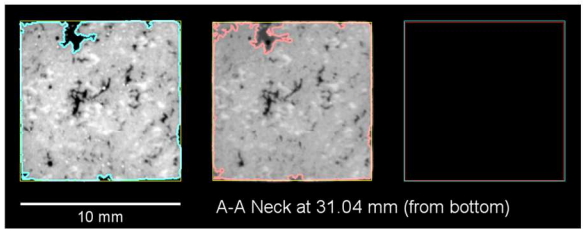


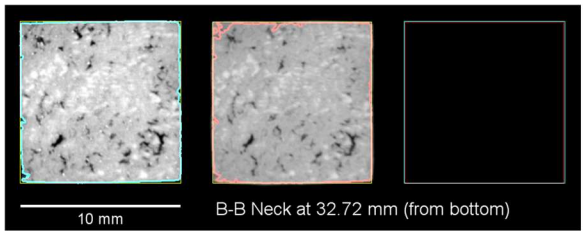


(b)

| Neck Depth, mm | |
|---|---|
| A-A | 0.06 |
| B-B | 0.06 |
| Average | 0.06 |
| Standard deviation | 0.000 |
| Note: No clear neck | |

Figure L.48. Micro-CT results of K-3 refractory corrosion test, APP2-12 1200 °C-7d.

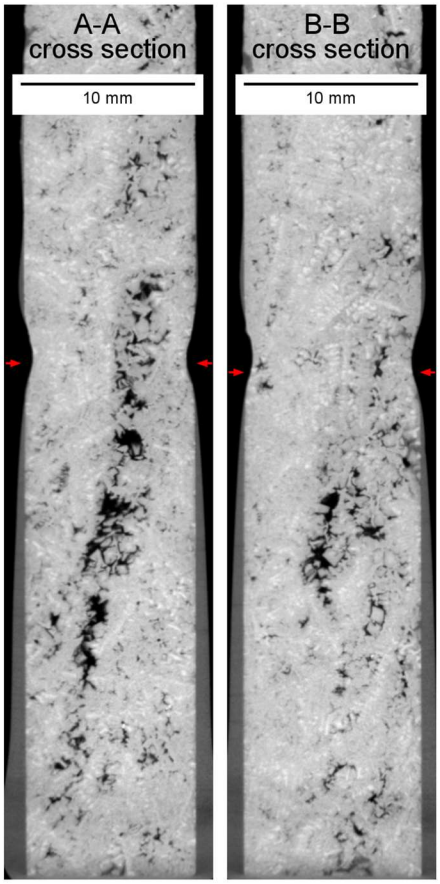


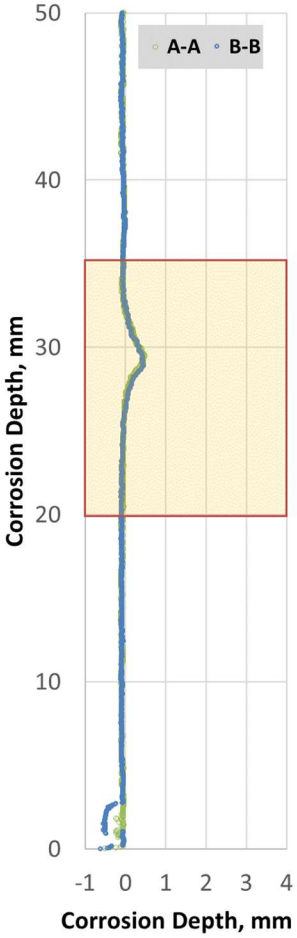


(a)

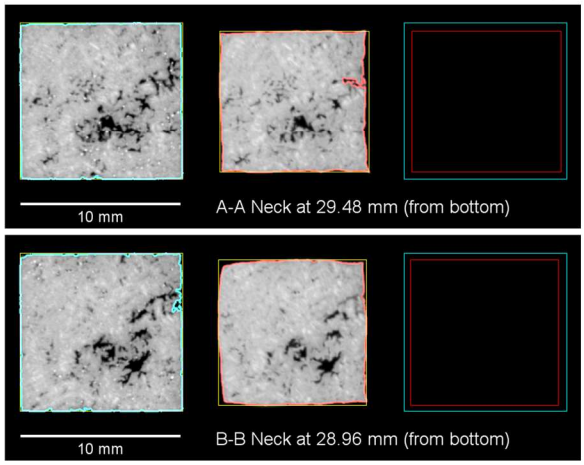


(b)

| Neck Depth, mm | |
|---|---|
| A-A | 0.48 |
| B-B | 0.46 |
| Average | 0.47 |
| Standard deviation | 0.014 |
| | |

Figure L.49. Micro-CT results of K-3 refractory corrosion test, APP2-13 1150 °C-3d.

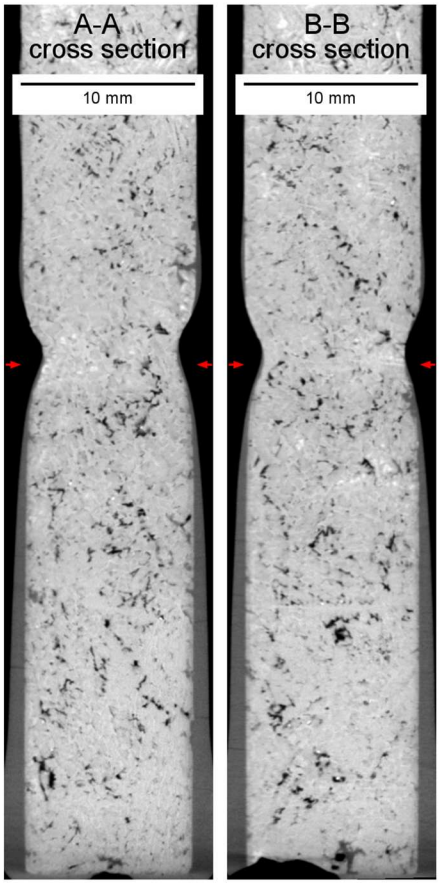


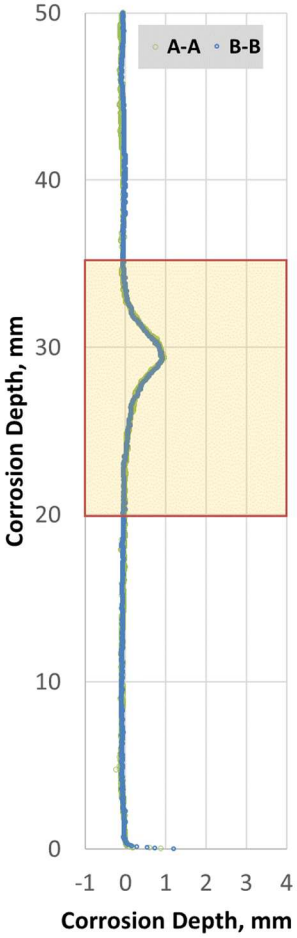


(a)

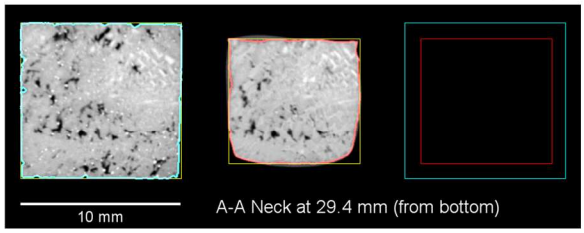


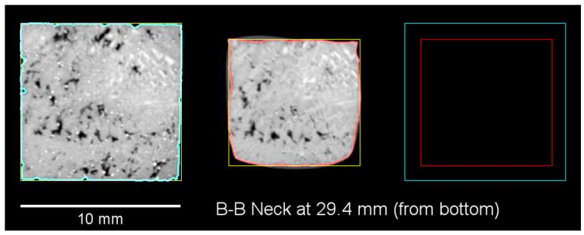


(b)

| Neck Depth, mm | |
|---|---|
| A-A | 0.96 |
| B-B | 0.92 |
| Average | 0.94 |
| Standard deviation | 0.028 |
| | |

Figure L.50. Micro-CT results of K-3 refractory corrosion test, APP2-13 1150 °C-7d.

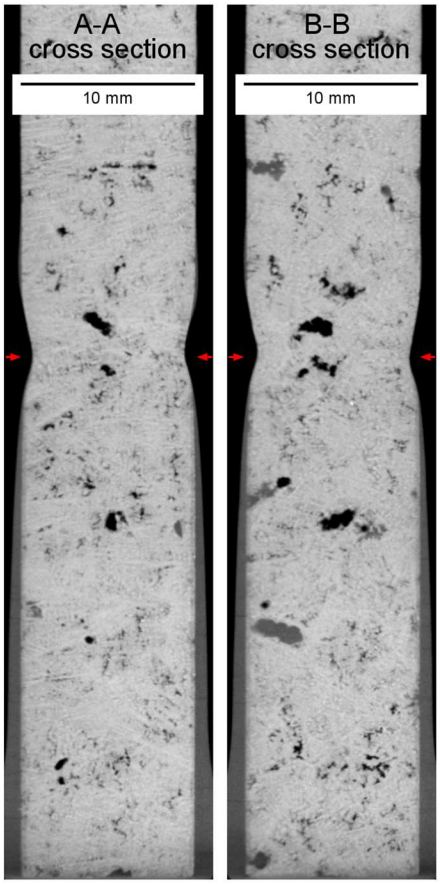


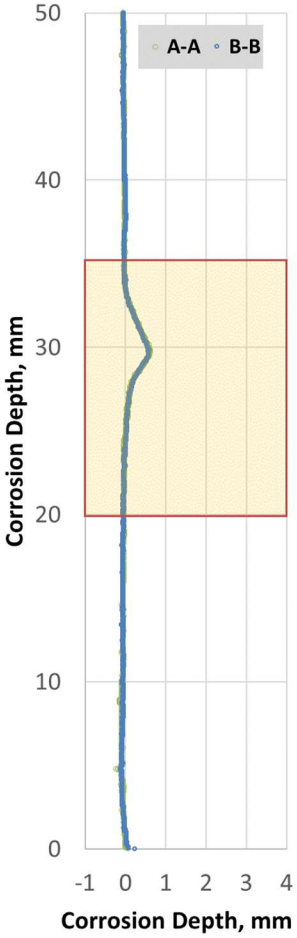


(a)

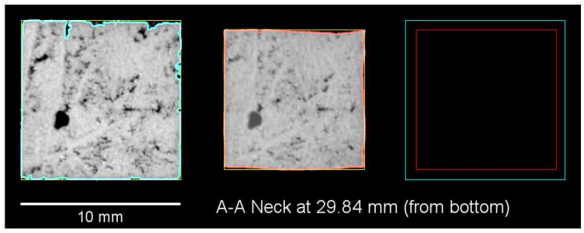


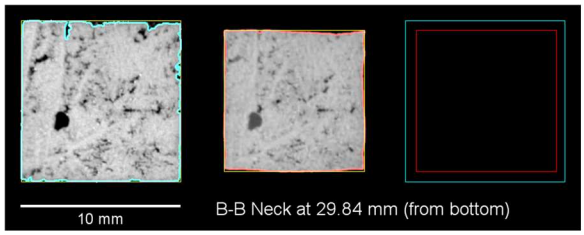


(b)

| Neck Depth, mm | |
|---|---|
| A-A | 0.62 |
| B-B | 0.60 |
| Average | 0.61 |
| Standard deviation | 0.014 |
| | |

Figure L.51. Micro-CT results of K-3 refractory corrosion test, APP2-13 1200 °C-3d.

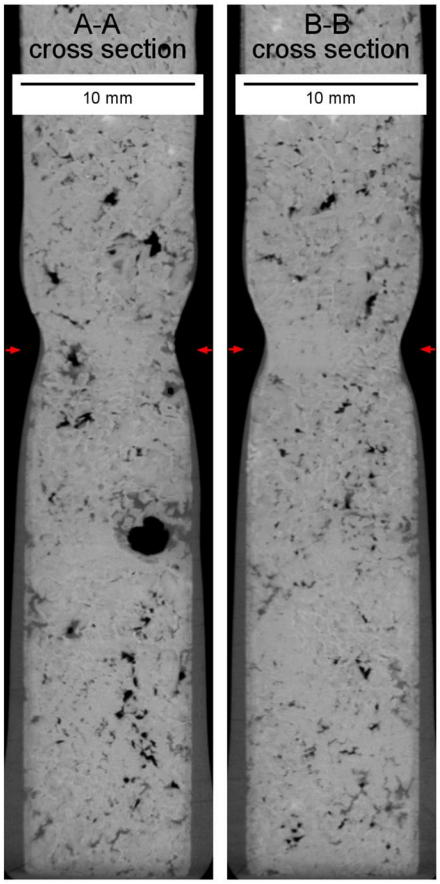


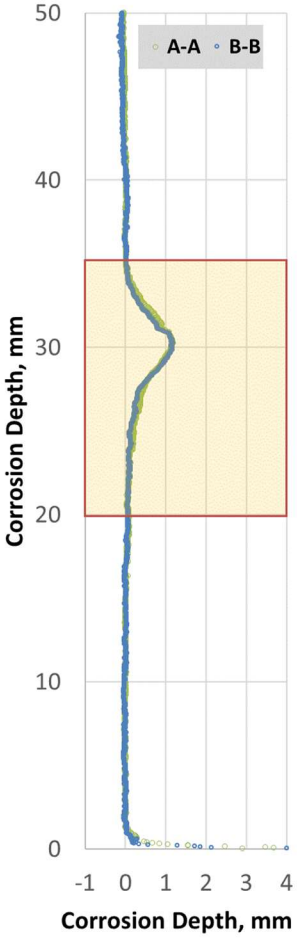


(a)

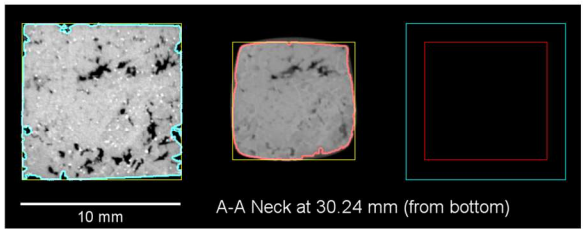


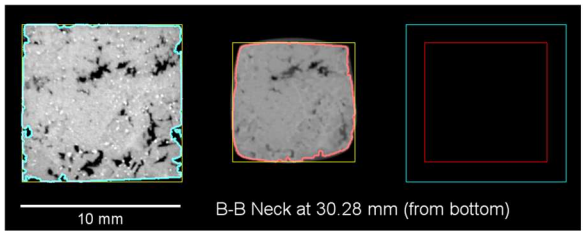


(b)

| Neck Depth, mm | |
|---|---|
| A-A | 1.20 |
| B-B | 1.18 |
| Average | 1.19 |
| Standard deviation | 0.014 |
| | |

Figure L.52. Micro-CT results of K-3 refractory corrosion test, APP2-13 1200 °C-7d.

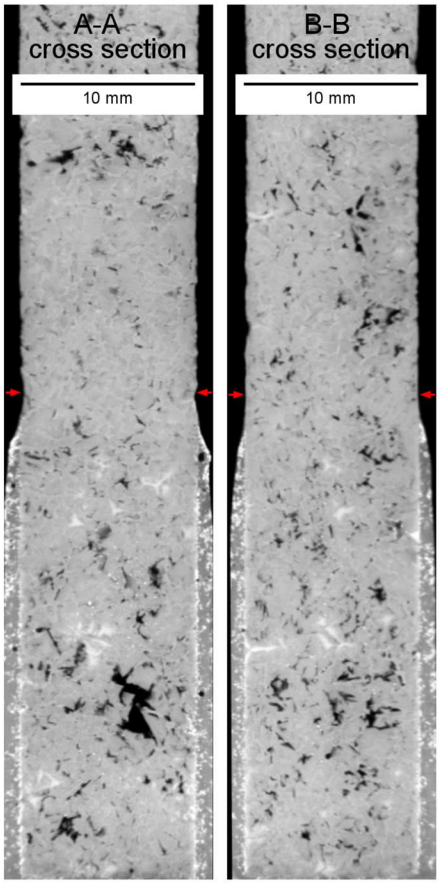


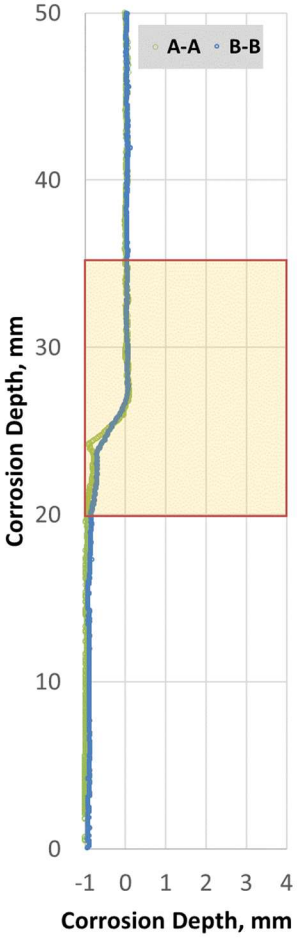


(a)

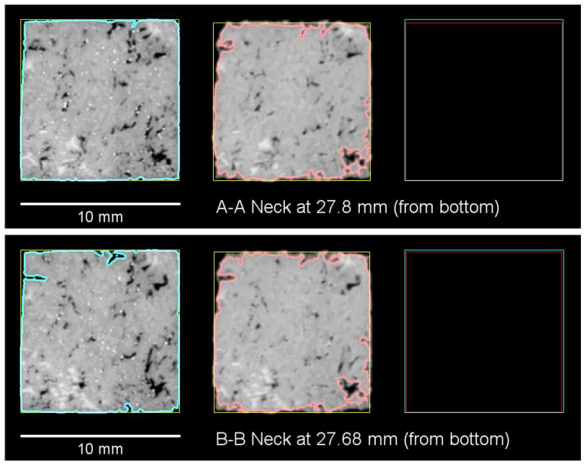


(b)

| Neck Depth, mm | |
|---|---|
| A-A | 0.10 |
| B-B | 0.10 |
| Average | 0.10 |
| Standard deviation | 0.000 |
| Note: Crystals in glass make it difficult to outline the K-3 phase. However, the neck is clear. | |

Figure L.53. Micro-CT results of K-3 refractory corrosion test, APP2-14 1150 °C-3d.

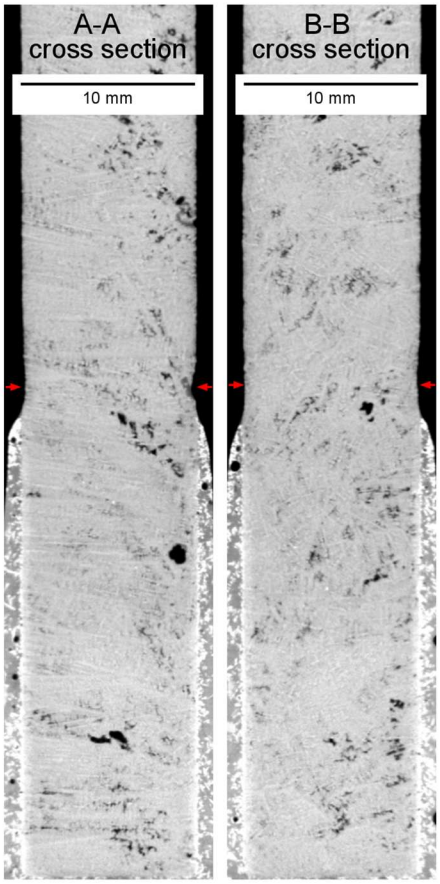


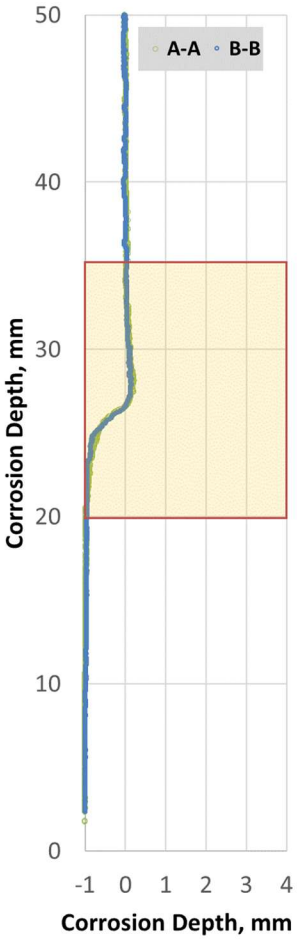


(a)

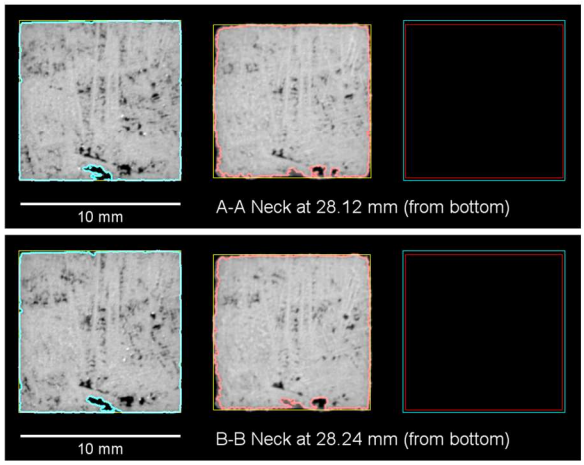


(b)

| Neck Depth, mm | |
|---|---|
| A-A | 0.22 |
| B-B | 0.16 |
| Average | 0.19 |
| Standard deviation | 0.042 |
| Note: Crystals in glass make it difficult to outline the K-3 phase. However, the neck is clear. | |

Figure L.54. Micro-CT results of K-3 refractory corrosion test, APP2-14 1150 °C-7d.

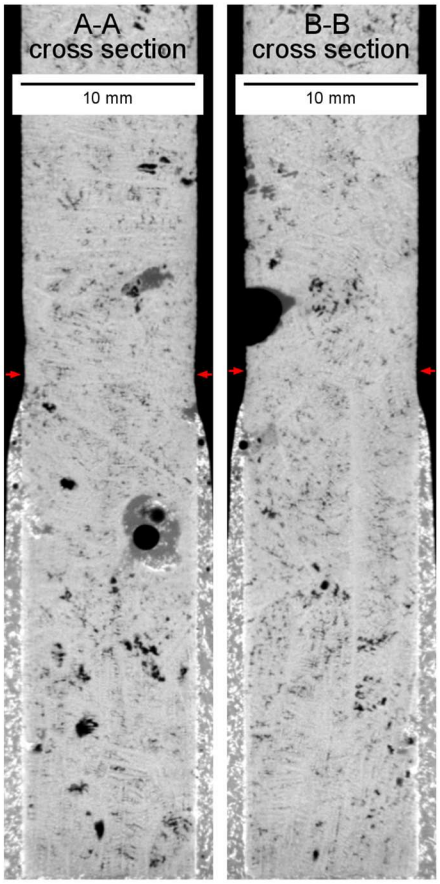


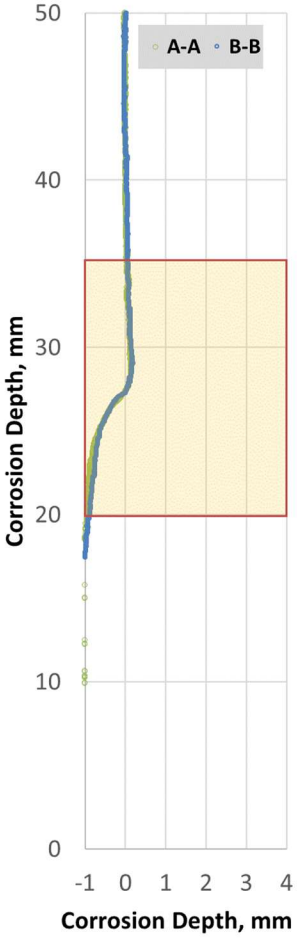


(a)

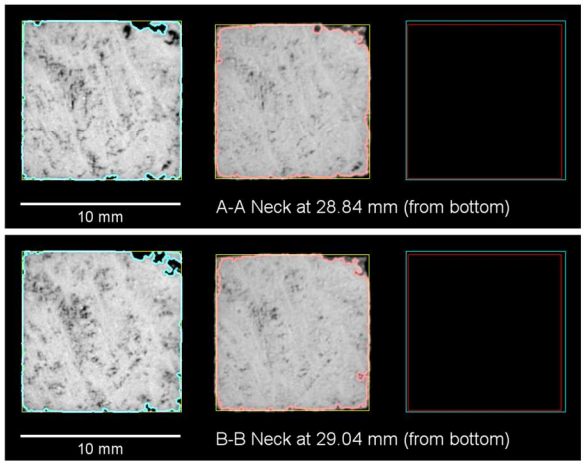


(b)

| Neck Depth, mm | |
|---|---|
| A-A | 0.16 |
| B-B | 0.20 |
| Average | 0.18 |
| Standard deviation | 0.028 |
| Note: Crystals in glass make it difficult to outline the K-3 phase. However, the neck is clear. | |

Figure L.55. Micro-CT results of K-3 refractory corrosion test, APP2-14 1200 °C-3d.

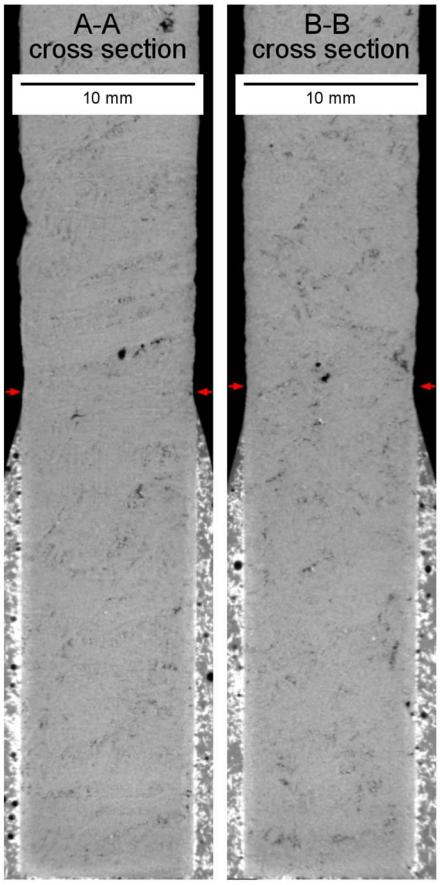


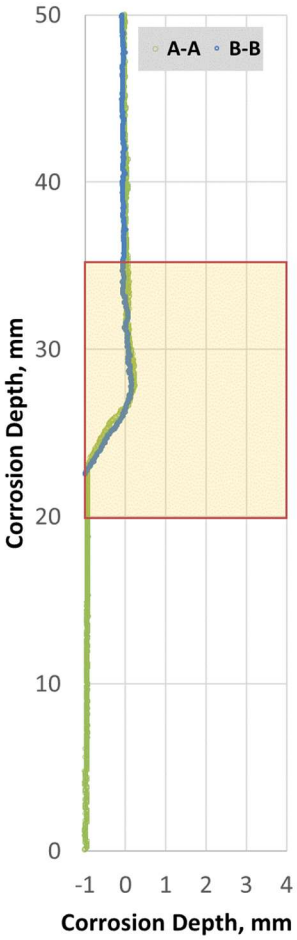


(a)

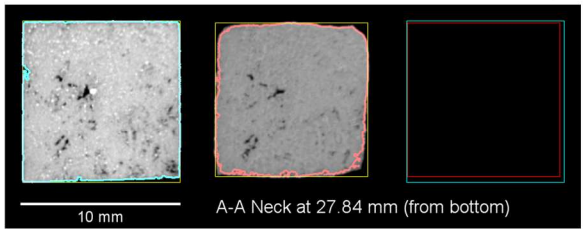


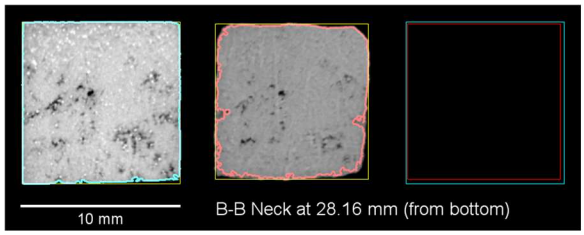


(b)

| Neck Depth, mm | |
|---|---|
| A-A | 0.24 |
| B-B | 0.16 |
| Average | 0.20 |
| Standard deviation | 0.057 |
| Note: Crystals in glass make it difficult to outline the K-3 phase. However, the neck is clear. | |

Figure L.56. Micro-CT results of K-3 refractory corrosion test, APP2-14 1200 °C-7d.

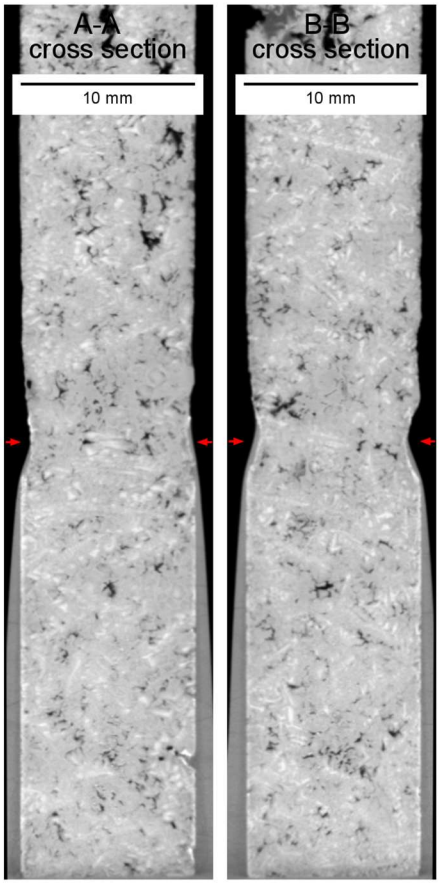


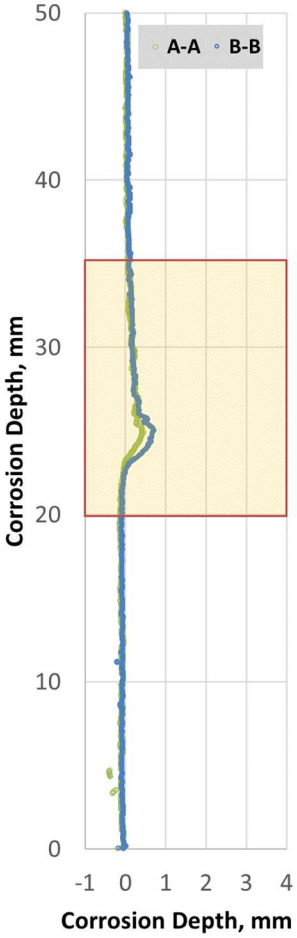


(a)

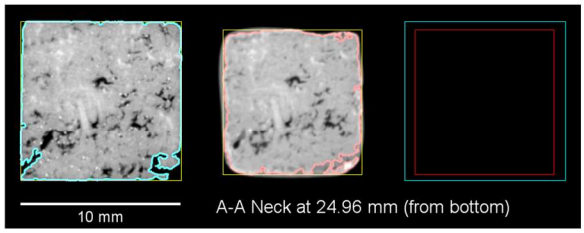


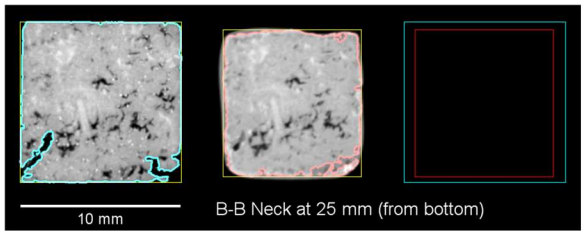


(b)

| Neck Depth, mm | |
|---|---|
| A-A | 0.44 |
| B-B | 0.72 |
| Average | 0.58 |
| Standard deviation | 0.198 |
| | |

Figure L.57. Micro-CT results of K-3 refractory corrosion test, APP2-15 1150 °C-3d.

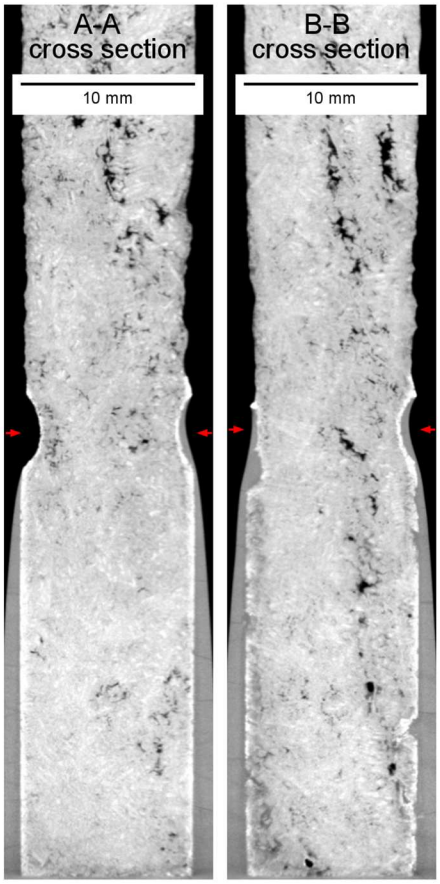


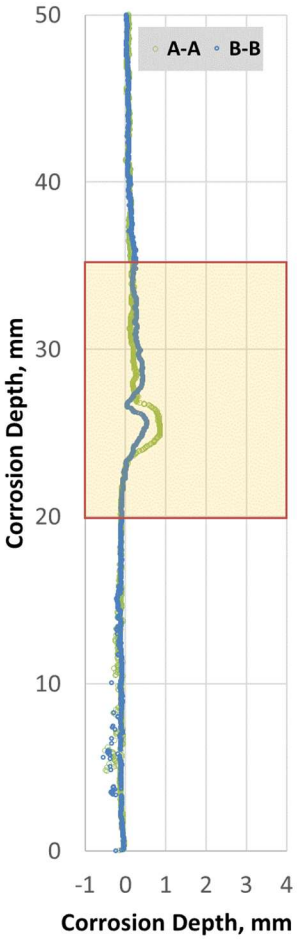


(a)

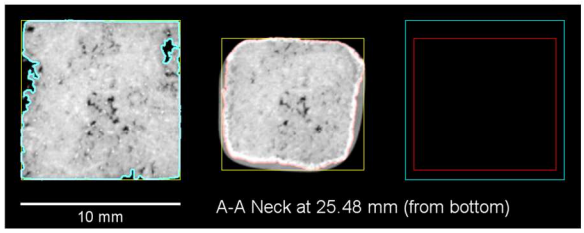


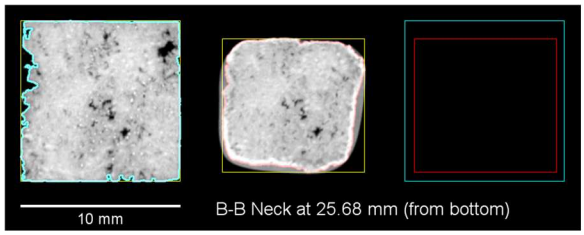


(b)

| Neck Depth, mm | |
|---|---|
| A-A | 0.86 |
| B-B | 0.54 |
| Average | 0.70 |
| Standard deviation | 0.226 |
| | |

Figure L.58. Micro-CT results of K-3 refractory corrosion test, APP2-15 1150 °C-7d.

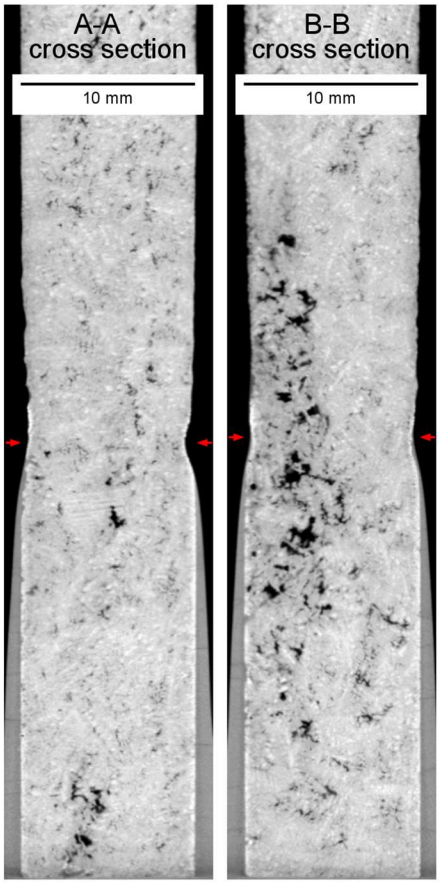


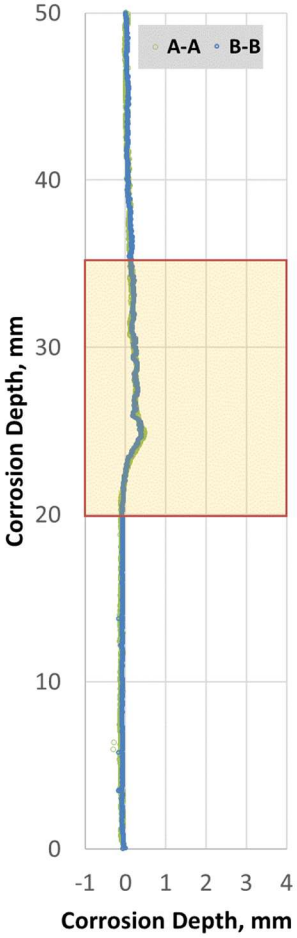


(a)

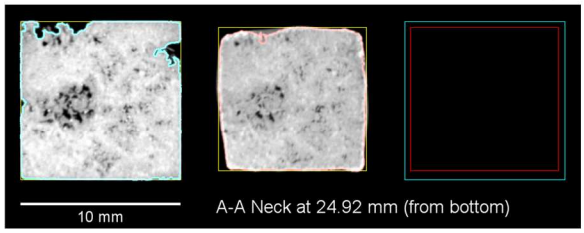


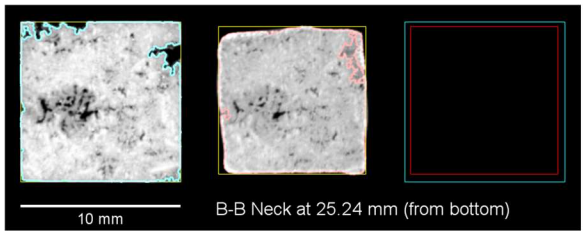


(b)

| Neck Depth, mm | |
|---|---|
| A-A | 0.48 |
| B-B | 0.40 |
| Average | 0.44 |
| Standard deviation | 0.057 |
| | |

Figure L.59. Micro-CT results of K-3 refractory corrosion test, APP2-15 1200 °C-3d.

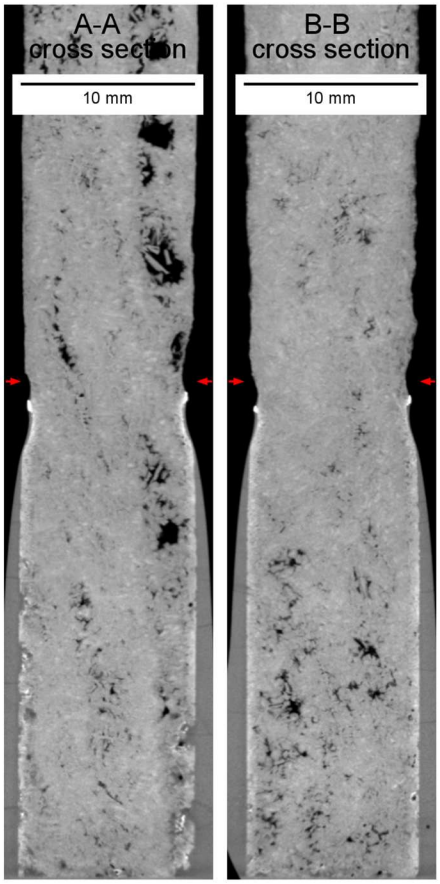


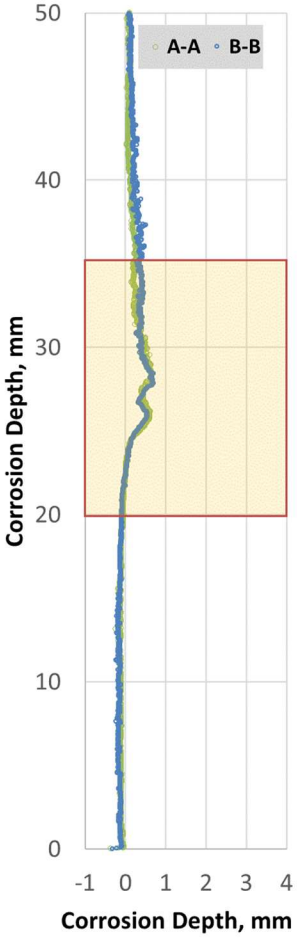


(a)

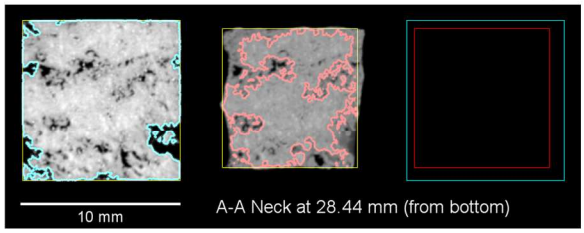


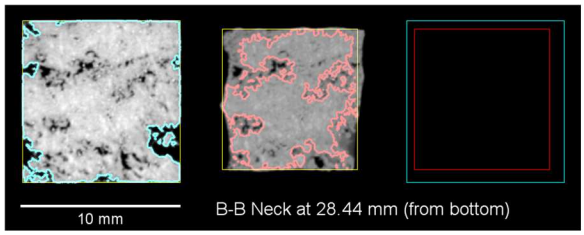


(b)

| Neck Depth, mm | |
|---|---|
| A-A | 0.68 |
| B-B | 0.74 |
| Average | 0.71 |
| Standard deviation | 0.042 |

Note: Reaction layer at the neck region may affect the neck measurement. Outlines and bounding rectangles are slightly smaller, which can cause measured neck depth values slightly larger.

Figure L.60. Micro-CT results of K-3 refractory corrosion test, APP2-15 1200 °C-7d.

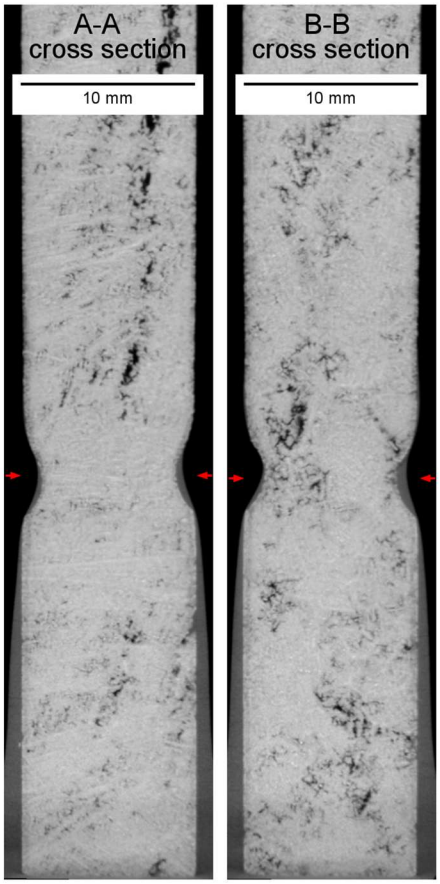


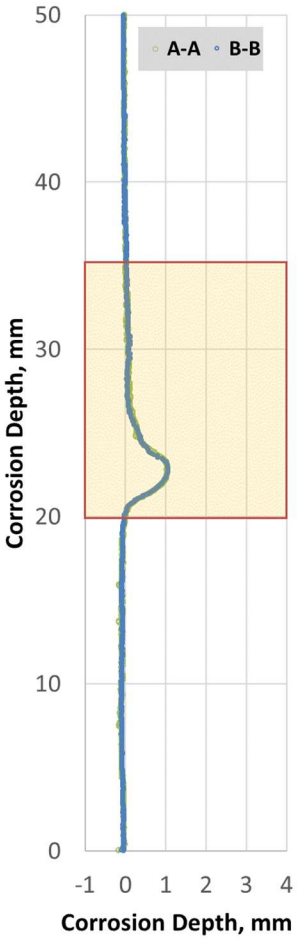


(a)

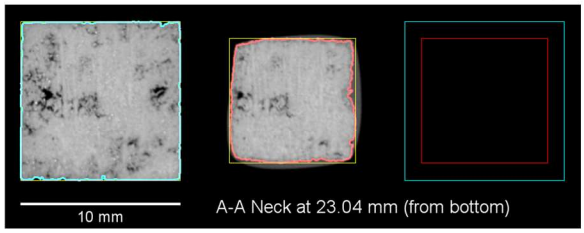


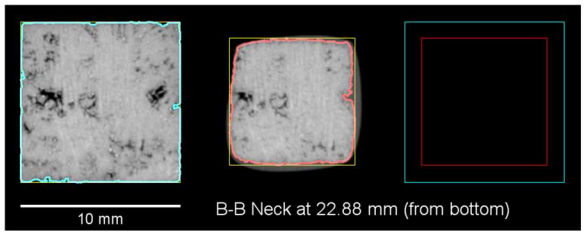


(b)

| Neck Depth, mm | |
|---|---|
| A-A | 1.06 |
| B-B | 1.06 |
| Average | 1.06 |
| Standard deviation | 0.000 |
| | |

Figure L.61. Micro-CT results of K-3 refractory corrosion test, APP2-16 1150 °C-3d.

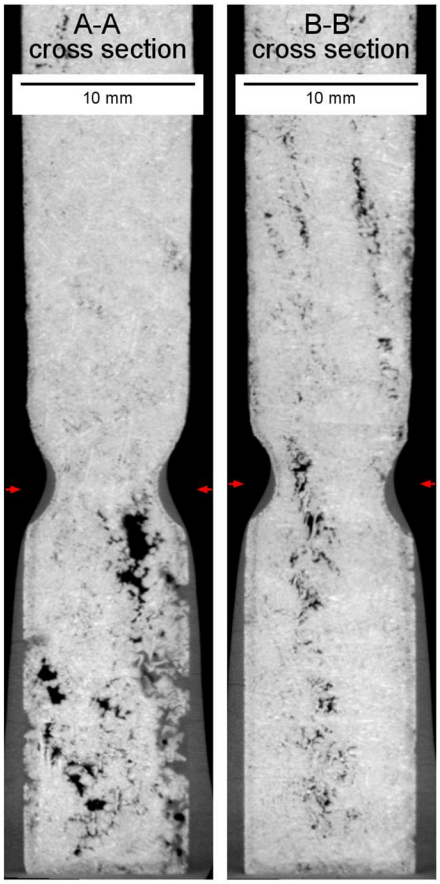


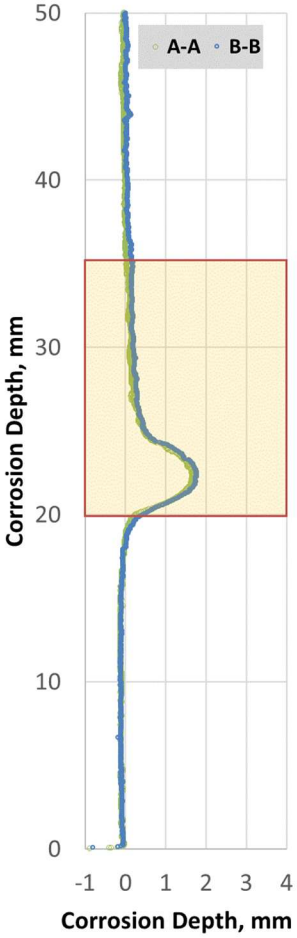


(a)

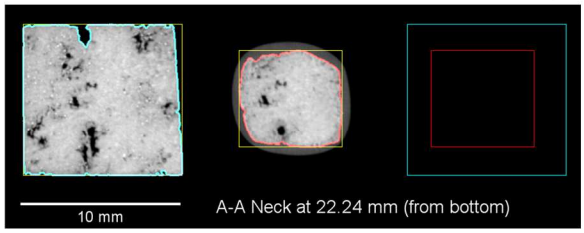


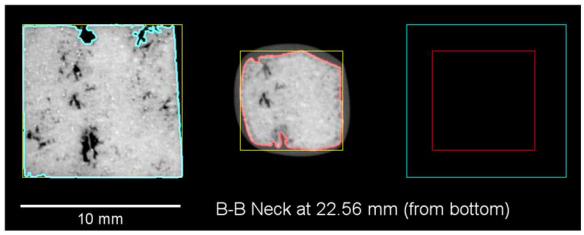


(b)

| Neck Depth, mm | |
|---|---|
| A-A | 1.70 |
| B-B | 1.78 |
| Average | 1.74 |
| Standard deviation | 0.057 |
| | |

Figure L.62. Micro-CT results of K-3 refractory corrosion test, APP2-16 1150 °C-7d.

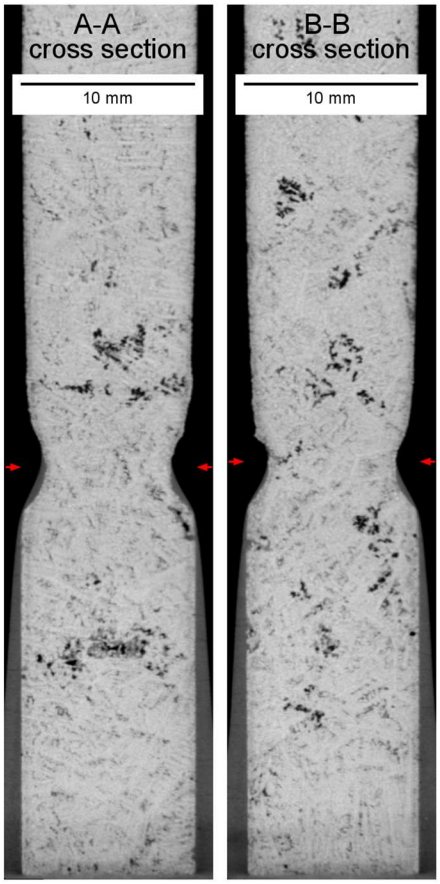


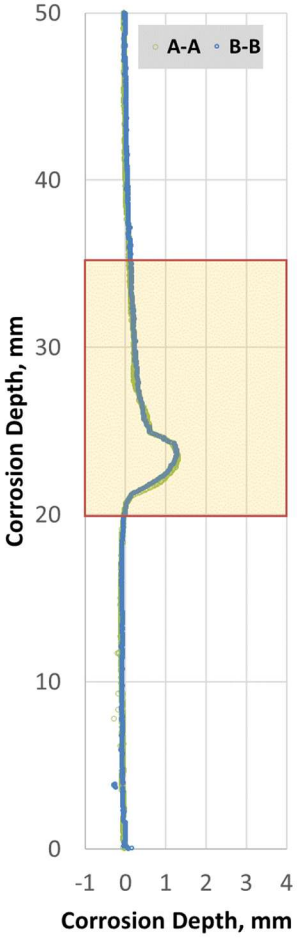


(a)

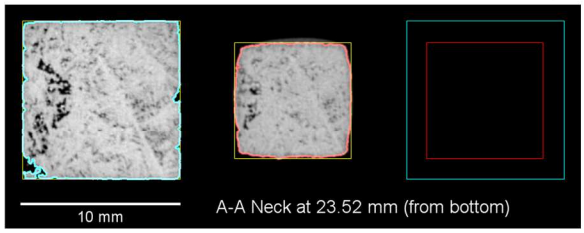


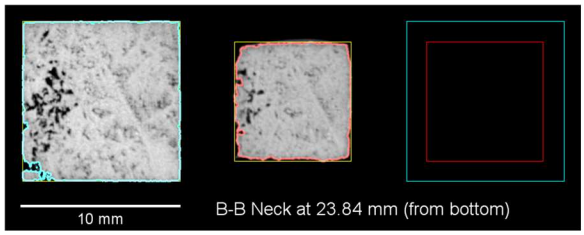


(b)

| Neck Depth, mm | |
|---|---|
| A-A | 1.32 |
| B-B | 1.28 |
| Average | 1.30 |
| Standard deviation | 0.028 |
| | |

Figure L.63. Micro-CT results of K-3 refractory corrosion test, APP2-16 1200 °C-3d.

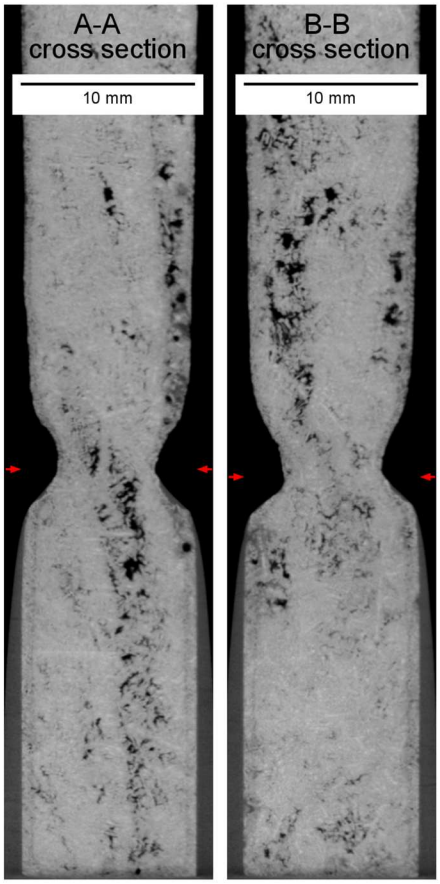


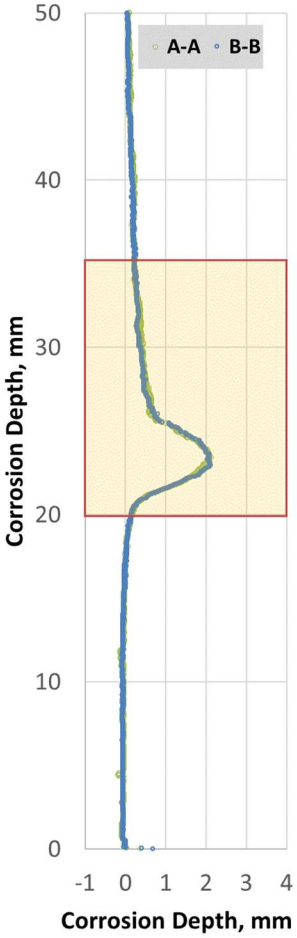


(a)

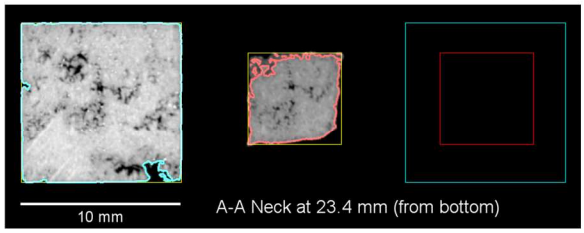


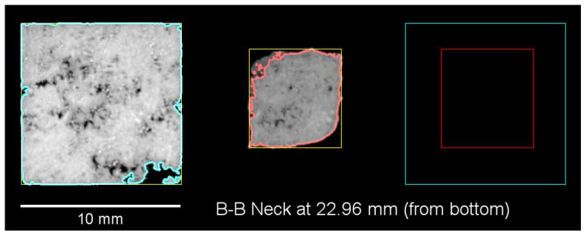


(b)

| Neck Depth, mm | |
|---|---|
| A-A | 2.12 |
| B-B | 2.12 |
| Average | 2.12 |
| Standard deviation | 0.000 |
| | |

Figure L.64. Micro-CT results of K-3 refractory corrosion test, APP2-16 1200 °C-7d.

# Pacific Northwest National Laboratory

902 Battelle Boulevard
P.O. Box 999
Richland, WA 99354
1-888-375-PNNL (7665)

***www.pnnl.gov***